Experimental Study of the Effect of Dilution Jets on Film Cooling Flow in a Gas Turbine Combustor

Joseph J. Scrittore

Dissertation submitted to the faculty of
Virginia Polytechnic Institute and State University
in partial fulfillment of the requirements for the degree of

Doctor of Philosophy
In
Mechanical Engineering

Dr. Karen A. Thole, Advisor and Chair
Dr. Wing Fai Ng
Dr. Thomas E. Diller
Dr. Pavlos P. Vlachos
Dr. Steven W. Burd

June 27, 2008
Blacksburg, Virginia Tech

Keywords: Gas Turbine, Combustor, Film Cooling

Experimental Study of the Effect of Dilution Jets on Film Cooling Flow in a Gas Turbine Combustor

Joseph J. Scrittore

Abstract

Cooling combustor chambers for gas turbine engines is challenging because of the complex flow fields inherent to this engine component. This complexity, in part, arises from the interaction of high momentum dilution jets required to mix the fuel with effusion film cooling jets that are intended to cool the combustor walls. The dilution and film cooling flow have different performance criteria, often resulting in conflicting flow mechanisms.

The purpose of this study is to evaluate the influence that the dilution jets have on the film cooling effectiveness and how the flow and thermal patterns in the cooling layer are affected by both the dilution flow and the closely spaced film cooling holes. This study also intends to characterize the development of the flow field created by effusion cooling injection without dilution injection. This work is unique because it allows insight into how the full-coverage discrete film cooling layer is interrupted by high momentum dilution jets and how the surface cooling is affected.

The film cooling flow was disrupted along the combustor walls in the vicinity of the high momentum dilution jets and the surface cooling effectiveness was reduced with increased dilution jet momentum. This was due to the secondary flows that were intensified by the increased jet momentum. High turbulence levels were generated at the dilution jet shear layer resulting in efficient mixing. The film cooling flow field was affected by the freestream turbulence and complex flow fields created by the combined dilution and effusion cooling flows both in the near dilution jet region as well as downstream of the jets. Effusion cooling holes inclined at 20˚ created lower coolant layer turbulence levels and higher surface cooling effectiveness than 30˚ cooling holes. Results showed an insensitivity of the coolant penetration height to the diameter and angle of the cooling hole in the region downstream of the dilution mixing jets.

When high momentum dilution jets were injected into crossflow, a localized region in the flow of high vorticity and high streamwise velocity was created. When film cooling air was injected the inlet flow field and the dilution jet wake were fundamentally changed and the vortex diminished significantly. The temperature field downstream of the dilution jet showed evidence of a hot region which was moderated appreciably by film cooling flow. Differences in the temperature fields were nominal compared to the large mass flow increase of the coolant.

A study of streamwise oriented effusion film cooling flow without dilution injection revealed unique and scaleable velocity profiles created by the closely spaced effusion holes. The effusion cooling considered in these tests resulted in streamwise velocity and turbulence level profiles that scaled well with blowing ratio which is a finding that allows the profile shape and magnitude to be readily determined at these test conditions. Results from a study of compound angle effusion cooling injection showed significant differences between the flow field created with and without crossflow. It was found from the angle of the flow field velocity vectors that the cooling film layer grew nearly linearly in the streamwise direction. The absence of crossflow resulted in higher turbulence levels because there was a larger shear stress due to a larger velocity difference between the coolant and crossflow. The penetration height of the coolant was relatively independent of the film cooling momentum flux ratio for both streamwise oriented and compound angle cooling jets.

Preface

This dissertation is composed of five papers that were written to better understand the complex flows in a gas turbine combustor and the implication on surface cooling effectiveness. This research was purely experimental and was meant to fill gaps in knowledge regarding the behavior of effusion film cooling and how effective it is in the presence of dilution jet flow. Major areas of research that lacked sufficient attention in the literature were addressed by this research including the following: high resolution measurements of adiabatic cooling effectiveness on a combustor liner surface at the near-region of a dilution jet, highly resolved measurements of flow and thermal fields created by effusion film cooling holes aligned with the crossflow and at a compound angle, measurements to identify sensitivities of the velocity and temperature profiles to different film cooling hole patterns and cooling and dilution flow rates, and investigation of the effect of film cooling on the flow structures created by a high momentum dilution jet injecting into crossflow that affect surface cooling performance.

An evaluation of the effect of dilution jets on film cooling surface cooling effectiveness is presented in the first paper. This paper was presented at the International Gas Turbine Institute (IGTI) conference in 2005 in Reno, NV. The second paper presented measurements of how the turbulence and flow field produced by high momentum dilution injection affected the far-field film cooling behavior. The third paper offered a systematic analysis of the mechanism by which effusion film cooling altered the flow and thermal fields created by dilution jet injection into crossflow. The kinematics of the flow field was also presented in the third paper examining the effect on the vortical flows that developed near the dilution jet. The fourth paper evaluated the velocity and turbulence profiles developed by effusion cooling holes at multiple streamwise locations and blowing ratios and used the blowing ratio to successfully scale the velocity and turbulence level profiles. The fourth paper was presented at the International Gas Turbine Institute (IGTI) conference in 2006 in Barcelona, Spain, and was accepted for publication in the *Journal of Turbomachinery*. The fifth and final paper examined the flow and thermal fields created by compound angle effusion film cooling injection without dilution jets. These measurements offered a comparison of the penetration height of the coolant with and without crossflow. A summary is included of the significant results from this research, as well as suggesting several topics for additional investigation into this research area.

Acknowledgments

There are many people without whom my completion of this degree would not have been possible. My advisor, Dr. Karen Thole, guided me and was always accessible and very generous with her time. She gave me the opportunity to do exciting research and to travel to share it with colleagues in Europe and America. I am forever indebted to her. I also would like to thank my committee members, Dr. Diller, Dr. Ng, Dr. Vlachos, and Dr. Burd for their support.

I really enjoyed my time at Virginia Tech and it has been quite a journey getting to know everyone I've worked with at VTExCCL. Andrew Gratton, Sundar Narayan, Will Colban, Dan Knost, Eric Couch, Jesse Christophel, Erik Hohlfeld, William Ranson, Chris Ebeling, Nick Cardwell, Paul Sanders, Mike Barringer, Scott Walsh, Jeff Prausa, Erin Elder, Scott Brumbaugh, Mike Lawson, Steve Lynch, Andrew Duggleby, Satoshi Hada, Alan Thrift, Seth Lawson, Cam Land, Angela Morris, Eric Lyall, Jeff Carullo and Markus Schwänen. Many of these friendships will last for a lifetime. The many other friends that I have met in Randolph Hall and in Blacksburg have made my experience here truly wonderful and you all have made me felt at home at Virginia Tech.

I would also like to thank Pratt & Whitney for making my project financially possible and for giving the research relevance and direction, and I am extremely grateful to them. I would like to particularly thank Dr. Steven Burd for making this a positive research experience.

Most importantly, I have to thank my family whose support and love were unconditional and ubiquitous. I would not have been able to complete this degree without Mom, Dad, Tara, and Brian reminding me to keep perspective and to remember what the important things are in my life. I love and appreciate you guys more than you probably know.

Attribution

Several colleagues and coworkers aided in the writing and research behind several of the chapters of this dissertation. A brief description of their background and their contributions are included here.

Prof. Karen A. Thole - Ph.D. (Department of Mechanical and Nuclear Engineering, Pennsylvania State University) is the primary Advisor and Committee Chair. Prof. Thole provided support throughout the duration of this research. Furthermore, Prof. Thole also contributed to all aspects of the experimental designs, results, and analyses of this research.

Paper 1: Experimental Characterization of Film Cooling Effectiveness Near Combustor Dilution Holes

Steven W. Burd - Ph.D. (Department of Mechanical Engineering, University of Minnesota) is employed by Pratt & Whitney and worked in collaboration with the authors on a project supported by Pratt & Whitney. Steven contributed to the experimental design and helped guide the experimental test program. His mentorship also aided in making the analysis more relevant to gas turbine design.

Paper 4: Investigation of Velocity Profiles for Effusion Cooling of a Combustor Liner

Steven W. Burd - Ph.D. (Department of Mechanical Engineering, University of Minnesota) is employed by Pratt & Whitney and worked in collaboration with the authors on a project supported by Pratt & Whitney. Steven assisted in the experimental design and contributed to the discussion of the results of this study while increasing the applicability of the results to combustor design.

Table of Contents

Abstract ii

Preface iv

Acknowledgements v

Attribution vi

Table of Contents vii

List of Figures x

List of Tables xv

Paper 1: Experimental Characterization of Film Cooling Effectiveness Near Combustor Dilution Holes 1
- Abstract 1
- Introduction 2
- Past Studies 3
- Experimental Facilities and Measurement Methods 5
  - Test Section Design 5
  - Combustor Liner Design 7
  - Measurement Methods and Uncertainty 9
- Experimental Results 12
  - Adiabatic Effectiveness Measurements 12
  - Flow and Thermal Field Measurements 16
- Conclusions 20
- Acknowledgments 21
- Nomenclature 21
- References 23

Paper 2: Effect of Dilution Jets on the Downstream Effusion Flow and Thermal Fields in a Combustor Simulator 25
- Abstract 25
- Introduction 26
- Past Studies 27
- Experimental Facilities and Measurement Methods 29
  - Experimental Test Section Design 29
  - Effusion and Dilution Hole Liner Design and Test Conditions 30
  - Measurement Methods and Uncertainty 33
- Experimental Results 34
  - Inlet Flow Conditions 35
  - Static Pressure Measurements 36
  - Flow Field Results 38
  - Thermal Field Results 45
- Conclusions 48
- Acknowledgments 49

Nomenclature 49
References 50

Paper 3: The Effect of a Film Cooling Layer on the Flow and Thermal Fields in the Near-Region of an Array of Staggered Opposed Dilution Jets 53
Abstract 53
Introduction 54
Past Studies 55
Experimental Facilities and Measurement Methods 57
Experimental Test Section Design 57
Film Cooling and Dilution Hole Liner Design and Test Conditions 58
Measurement Methods and Uncertainty 61
Experimental Results 62
Inlet and Coolant Flow Conditions 62
Static Pressure Measurements 64
Flow Field Results 67
Thermal Field and Adiabatic Cooling Effectiveness Results 76
Conclusions 78
Acknowledgments 79
Nomenclature 80
References 81

Paper 4: Investigation of Velocity Profiles for Effusion Cooling of a Combustor Liner 84
Abstract 84
Introduction 85
Past Studies 85
Experimental Facilities and Measurement Methods 87
Experimental Facilities 87
Measurement Methods and Uncertainty 90
Experimental Results 92
Inlet and Cooling Flow Conditions 92
Development of the Velocity Profiles 94
Cooling Effectiveness Results 105
Conclusions 107
Acknowledgments 108
Nomenclature 108
References 109

Paper 5: Investigation of the Velocity and Thermal Development of Cooling Film Created by Compound Angle Effusion Holes 112
Abstract 112
Introduction 113
Past Studies 114
Experimental Facilities and Measurement Methods 117
Experimental Facilities 117
Effusion Plate Design and Measurement Locations 118

Discharge Coefficient Measurements 121
Measurement Methods and Uncertainty 122
Experimental Results 124
Static Pressure Measurements 124
Determination of Measurement Locations 125
Flow Field Results 126
Effusion Injection With Crossflow 126
Effusion Injection Without Crossflow 133
Thermal Field Results 136
Conclusions 138
Acknowledgments 139
Nomenclature 139
References 141

Summary and Recommendations for Future Work 143
Recommendations for Future Work 145

List of Figures

Paper 1: Experimental Characterization of Film Cooling Effectiveness Near Combustor Dilution Holes

Figure 1.1 Illustration of the wind tunnel facility used for combustor simulator experiments 6

Figure 1.2 Layout and measurement planes for the combustor simulator 7

Figure 1.3 Illustration and description of cooling hole arrangement on liners 8

Figure 1.4 Adiabatic effectiveness contours for cases a) 1, b) 2, c) 3, and d) 4 13

Figure 1.5 Lateral average of adiabatic effectiveness for all cooling cases 15

Figure 1.6 Adiabatic effectiveness profiles at the dilution center-line for all four film cooling flow rates 16

Figure 1.7 Thermal field measurements in plane 1p for cases (a) 1 and (b) 3 17

Figure 1.8 Thermal field measurements for plane 2p for cases (a) 1 and (b) 3. The black rectangle denotes where the flow field of Figure 1.9 was measured 18

Figure 1.9 Vectors show $v/U_{\infty,in}$ and $w/U_{\infty,in}$ velocity components for case 4. (a) Flow field at plane 2p with contours showing $u/U_{\infty,in}$ values. (b) Contour of turbulence level at plane 2p. Note 4x enlargement of scale. 18

Figure 1.10 (a) Flow field at plane 1s for case 4. Vectors show $u/U_{\infty,in}$ and $w/U_{\infty,in}$ velocity components and contours show $u/U_{\infty,in}$ values. (b) Flow field vectors and contours of turbulence level at plane 1s for case 4 19

Figure 1.11 Thermal field measurements in plane 3p for cases (a) 1, (b) 3, and (c) 4 20

Paper 2: Effect of Dilution Jets on the Downstream Effusion Flow and Thermal Fields in a Combustor Simulator

Figure 2.1 Illustration of the wind tunnel facility used for experiments 30

Figure 2.2 Illustration of the geometry and hole spacing of effusion liners 1 - 3 31

Figure 2.3 Illustration of the test plate where the dotted black circles signify locations of the opposing dilution holes on the top of the test section. The red and blue dots signify the measured profile location 33

Figure 2.4 Streamwise velocity and turbulence level profiles measured at the liner leading edge $X/D_L = 2.1$ upstream of the dilution jet row 35

Figure 2.5 Streamwise and pitchwise velocity profiles measured at the dilution jet exit plane 36

Figure 2.6 Film cooling momentum flux ratios calculated using measured surface static pressures for all liners and flow cases. Red and blue dots indicate centerline and dilution mid-pitch measurement locations, respectively 37

Figure 2.7 Streamwise development of streamwise velocity, turbulence level, and Reynolds shear stress at the cooling hole exit at location DL for $I_{fc,in}$ = 25, I_D = 60, α = 30˚, d = 0.46 cm 39

Figure 2.8 Comparison of velocity, turbulence level and Reynolds shear stress for locations US and DS on test liner 1 for all flow cases 41

Figure 2.9 Streamwise velocity components at locations UM and DM for I_D = 100 and $I_{fc,in}$ = 12 (left) and $I_{fc,in}$ = 25 (right) for all liners 42

Figure 2.10 Nondimensional Reynolds shear stresses at locations US and DS for $I_{fc,in}$ = 25 and for I_D = 60 (left) and I_D = 100 (right) for all liners.....43

Figure 2.11 Turbulence level profiles at locations UM and DM for I_D = 60 and $I_{fc,in}$ = 12 (left) and $I_{fc,in}$ = 25 (right) 44

Figure 2.12 Temperature profiles on liner 1 at locations a) US and b) DS for all flow cases 46

Figure 2.13 Temperature profiles for all liners at locations US and DS for $I_{fc,in}$ = 25 and I_D = 60 (left) and I_D = 100 (right) 47

Paper 3: The Effect of a Film Cooling Layer on the Flow and Thermal Fields in the Near-Region of an Array of Staggered Opposed Dilution Jets

Figure 3.1 Illustration of the wind tunnel facility used for experiments 58

Figure 3.2 Illustration of the film cooling holes detailing the layout and geometric parameters 59

Figure 3.3 Illustration of the test plates highlighting the measurement planes 60

Figure 3.4 Flow velocity at center of the channel upstream of I_D = 100 jet injection.....63

Figure 3.5 a) Spanwise velocity and turbulence level profiles and b) spanwise and pitchwise temperature profiles at the mid-pitch and mid-span, respectively. Measurements were made at X/D = -5 for I_D = 100 64

Figure 3.6 a) Streamwise and b) pitchwise profiles of the dilution jet velocity measured at the dilution jet exit plane for I_D = 100 65

Figure 3.7 Local film cooling momentum flux ratios for I_D = 100 66

Figure 3.8 Pressure coefficient measured without film cooling as a function of a) the angular coordinate, φ, and b) the streamwise coordinate for I_D = 100. Red dots indicate static tap locations 66

Figure 3.9 Streamwise and pitchwise flow planes showing flow velocity vectors and streamwise velocity component contours for a dilution momentum flux

ratio of 100 67

Figure 3.10 Streamwise and pitchwise flow planes showing flow velocity vectors and turbulence level contours for a dilution momentum flux ratio of 100 68

Figure 3.11 Pitchwise flow planes of velocity vectors and streamwise velocity contours for I_D = 100 without film cooling. Inset graphs identify a vortex centered at Y/D, Z/D = 0.57, 0.23, respectively 69

Figure 3.12 Pitchwise plane for I_D = 100 showing contours of a) rotation rate, b) rate of angular fluid distortion about an axis parallel to the x-axis and c) rate of change of streamwise velocity 70

Figure 3.13 Comparison of streamwise velocity in the pitchwise flow plane for I_D = 100 a) without film cooling and b) with film cooling ($I_{fc,in}$ = 25) 71

Figure 3.14 Comparison of turbulence level in the pitchwise flow plane for I_D = 100 a) without film cooling and b) with film cooling ($I_{fc,in}$ = 25) 72

Figure 3.15 Spanwise velocity component profiles with and without film cooling flow at three streamwise locations upstream of the dilution hole for I_D = 100. For cases with film cooling $I_{fc,in}$ = 25 73

Figure 3.16 Comparison of turbulence level and flow vectors near the dilution hole leading edge (X/D = -0.5) for I_D = 100 a) without film cooling and b) with film cooling ($I_{fc,in}$ = 25) 74

Figure 3.17 Comparison of turbulence level and flow vectors near the dilution hole trailing edge (X/D = 0.5) for I_D = 100 a) without film cooling and b) with film cooling ($I_{fc,in}$ = 25) 75

Figure 3.18 Comparison of temperature planes showing non-dimensional temperature contours for I_D = 100 a) without film cooling and b) with film cooling ($I_{fc,in}$ = 25) 76

Figure 3.19 Streamwise temperature planes showing non-dimensional temperature contours at the dilution injection location for I_D = 100 in the presence of film cooling at a) $I_{fc,in}$ = 12 and b) $I_{fc,in}$ = 25 77

Figure 3.20 Adiabatic surface temperature measurements made on film cooling liner at flow conditions $I_{fc,in}$ = 25 and I_D = 100 78

Paper 4: Investigation of Velocity Profiles for Effusion Cooling of a Combustor Liner

Figure 4.1 Illustration of the wind tunnel facility used for film cooling experiments 88

Figure 4.2 Illustration of the test plate showing the surface temperature measurement region and velocity profile measurement locations 89

Figure 4.3 Inlet flow conditions measured at mid-pitch and quarter-pitch 93

Figure 4.4 Streamwise dependence on the local film cooling momentum flux ratios 94

Figure 4.5 Streamwise velocity profiles measured for I = 10.6 95

Figure 4.6 Streamwise velocity profiles measured for I = 25.5 96

Figure 4.7 Turbulence level profiles for I = 10.6 97

Figure 4.8 Turbulence level profiles for I = 25.5 98

Figure 4.9 Streamwise velocity profiles measured one row downstream of rows 1, 5, and 10 for I = 10.6 and 25.5 using the blowing ratio, M, to normalize the profiles 98

Figure 4.10 Turbulence level profiles measured one row downstream of rows 1, 5, and 10 for I = 10.6 and I = 25.5. Profiles normalized to blowing ratio, M 99

Figure 4.11 Streamwise velocity profiles measured one row downstream of row 20 100

Figure 4.12 Turbulence level profiles measured one row downstream of row 20 100

Figure 4.13 Streamwise velocity profiles measured one row downstream of row 20. Profiles normalized to blowing ratio, M 101

Figure 4.14 Turbulence level profiles measured one row downstream of row 20. Profiles normalized to blowing ratio, M 102

Figure 4.15 Streamwise velocity contours downstream of row fifteen for I = 25.5. Vectors show streamwise and wall-normal velocity components. Arrow indicates row 15 cooling hole 103

Figure 4.16 Turbulence levels with flow field vectors for I = 25.5 showing streamwise and wall-normal velocity components. Arrow indicates row 15 cooling hole.....104

Figure 4.17 Cross-sectional plane X/d = 3 downstream of row 15 showing (a) streamwise velocity, $u/U_{\infty,in}$, (b) wall-normal velocity, $w/U_{\infty,in}$, and (c) turbulence levels. Solid arrows indicate row 15 hole location and dashed arrows indicate row 14 hole location. 105

Figure 4.18 Adiabatic effectiveness contours of the effusion panel from row 1 to 20 for (a) I = 10.6 and (b) I = 25.5 106

Figure 4.19 Lateral average of adiabatic effectiveness of the effusion panel from row 1 to 20 for I = 10.6 and I = 25.5. Note that $X/S_S = 0$ is the leading edge of the first hole row 107

Paper 5: Investigation of the Velocity and Thermal Development of Cooling Film Created by Compound Angle Effusion Holes

Figure 5.1 Illustration of the wind tunnel facility used for experiments.....117

Figure 5.2 Illustration of the effusion liner and measurement locations.....119

Figure 5.3 Illustration of the effusion hole geometry and tabulated parameters.....120

Figure 5.4 Discharge coefficients of the compound angle effusion holes based on absolute pressure ratio.....121

Figure 5.5 a) Local effusion jet momentum flux ratio normalized to the momentum flux ratio of the first row of jets and b) the local film cooling Reynolds numbers with and without crossflow.....124

Figure 5.6 Pitchwise measurements showing a) three components of velocity and b) non-dimensional temperature at the positions X/S_S = -1, 19, and 35 for I = 1.0.....126

Figure 5.7 Profiles of the streamwise velocity components with crossflow for a) I = 1.0, b) I = 15.3, and c) I = 25.1 measured at the streamwise positions shown.....127

Figure 5.8 Profiles of the pitchwise velocity components with crossflow for a) I = 1.0, b) I = 15.3, and c) I = 25.1.....128

Figure 5.9 Profiles of the spanwise velocity components with crossflow for a) I = 1.0, b) I = 15.3, and c) I = 25.1.....129

Figure 5.10 Profiles of the XY-plane flow angle, φ, with crossflow for a) I = 1.0, b) I = 15.3, and c) I = 25.1.....130

Figure 5.11 Turbulence level profiles (normalized by U_∞) with crossflow for a) I = 1.0, b) I = 15.3, and c) I = 25.1.....131

Figure 5.12 Profiles of the streamwise velocity for Re_j = 3199 (a) with crossflow and (b) without crossflow and Re_j = 4088 (c) with crossflow and (d) without crossflow.....133

Figure 5.13 Profiles of the pitchwise velocity for Re_j = 3199 (a) with crossflow and (b) without crossflow and Re_j = 4088 (c) with crossflow and (d) without crossflow.....134

Figure 5.14 Profiles of the spanwise velocity for Re_j = 3199 (a) with crossflow and (b) without crossflow and for Re_j = 4088 (c) with crossflow and (d) without crossflow.....135

Figure 5.15 Turbulence level profiles (normalized to U_j) of Re_j = 3199 (a) with crossflow and (b) without crossflow and Re_j = 4088 (c) with crossflow and (d) without crossflow.....136

Figure 5.16 Profiles of the non-dimensional temperature, θ, with crossflow for a) I = 1.0 and b) I = 25.1.....137

List of Tables

Paper 1: Experimental Characterization of Film Cooling Effectiveness Near Combustor Dilution Holes

Table 1.1 Film Cooling and Dilution Flow Settings 12

Paper 2: Effect of Dilution Jets on the Downstream Effusion Flow and Thermal Fields in a Combustor Simulator

Table 2.1 Description of effusion plate geometries 32

Paper 4: Investigation of Velocity Profiles for Effusion Cooling of a Combustor Liner

Table 4.1 Description of effusion plate geometry 90

Paper 1:
Experimental Characterization of Film Cooling Effectiveness Near Combustor Dilution Holes

Accepted at the 2005 *ASME Turbo Expo**

Abstract

Cooling combustor chambers for gas turbine engines is challenging, given the complex flow and thermal fields inherent to these modules. This complexity, in part, arises from the interaction of high-momentum dilution jets required to mix the fuel with film cooling jets that are intended to cool the combustor walls.

This paper discusses the experimental results from a combustor simulator tested in a low-speed wind tunnel that includes both the dilution jets and film cooling jets. The specific purpose of this study is to evaluate the influence that the dilution jets has on the film cooling effectiveness. Infrared thermography was used to measure surface temperatures along a low thermal conductivity plate to quantify the adiabatic effectiveness from an array of film cooling holes with the presence of dilution holes. To further understand the flow phenomena, thermocouple probes and laser Doppler velocimetry were used to measure the thermal and flow fields, respectively. Parametric experiments indicate that the film cooling flow is disrupted along the combustor walls in the vicinity of the high-momentum dilution jets. In fact, a significant penalty in cooling effectiveness of the combustor is observed with increased dilution jet penetration.

*Co-authors: Dr. Karen A. Thole, Mechanical and Nuclear Engineering Department, Pennsylvania State University
Dr. Steven W. Burd, Pratt & Whitney

Introduction

Firing temperatures of gas turbine combustors are higher than ever as the demand for higher output gas temperatures increase. The ability to effectively cool the chamber walls of gas turbine combustors is important to insure a stable combustion system and the required durability. As such, it is important to identify hot-spots that may occur along the combustor walls. It is also essential to identify flow features that reduce the cooling effectiveness of the combustor liner.

The flow and thermal fields in a gas-turbine combustor are some of the most important and complex physical processes in a gas-turbine engine. A typical gas turbine aero-engine employs an annular combustor with dilution holes and film cooling holes. The dilution jets serve to increase mixing of the fuel and air and insure that there is efficient combustion and quality of the combustion gases exiting the combustor. As such, high jet penetration may be desired to promote high levels of turbulence to assist in the mixing process. The introduction of cooling air along the combustor chamber walls serve to isolate the walls from the hot combustor gases and provide the heat transfer required to cool the walls. Low film cooling jet penetration with little mixing is beneficial. Regardless of these objectives, the dilution and cooling flows are constrained by the overall coolant air budget, making it important to understand these trade-offs.

To evaluate the cooling that might be expected in a typical combustor of an aero-engine, a large-scale facility was developed to simulate typical combustor flows. The study presented in this paper does not include the reacting flow thereby effects attributed to the heat release due to combustion are not represented in this study. From these large scale tests, however, it is possible to understand the effects on combustor liner cooling.

The objective for the work reported in this paper was to quantify the film cooling effectiveness in the vicinity of dilution jets for different conditions. Typically, combustors have multi-row film cooling holes that are closely spaced. Moreover, the film cooling blowing ratios are typically higher than those presented in most of the open literature. This study is unique because it simulates the combined film cooling and dilution jets and was completed for realistic blowing ratios. After describing the development of the combustor simulator facility, this paper describes measured adiabatic wall temperatures to quantify cooling effectiveness. Flow and thermal fields were measured near the dilution jets to gain better understanding of how the flow is behaving in this region. This paper concentrates on how the liner cooling and the flow and thermal fields are sensitive to the blowing ratios of these different jets.

Past Studies

Many experimental studies have been reported in the open literature documenting both experimental and computational data for model combustor flows. The large number prevents a full discussion of all of the results in our paper, but rather a small subset will be discussed that is relevant to cooling methods for combustor liners. Cooling methods for combustor liners consist of the following: film cooling (also referred to as effusion cooling), slot cooling, backside impingement, and backside pin fin cooling. Both the film cooling and slot cooling are highly susceptible to any effects that the dilution jets may cause such as increased mixing and interruption of the cooling flow along the liner.

Most combustor film cooling patterns consist of a closely spaced array of holes, also known as full-coverage film cooling, which has been studied by a number of investigators. Sasaki et al. [2] examined if it were possible to use a superposition method with full-coverage film cooling. They found that, in fact, there was an additive nature of multi-row film cooling that allowed the use of the superposition method. A series of papers by Andrews et al. [3 and 4] have compared the influence of cooling hole size and pitch through a number of experimental studies. In combustor designs, the amount of coolant flow per surface area must be considered in the design of the cooling hole diameter to insure that the hole loss is of similar levels as the pressure loss across the combustor. From this study, larger pressure losses generally occur for smaller cooling holes than for larger cooling holes at a given cooling flux. The discharge coefficients of any hole pattern, however, are a function of the hole geometry and the aerodynamics to which the holes are exposed. It is necessary to supply the flow at an adequate pressure drop and quantity to prevent any ingestion of hot gas into the cooling holes. Barringer et al. [5] found that film cooling hole discharge coefficients depend on the coolant to freestream density ratio and the number of rows of holes in the array. Their results indicated that increasing the number of rows slightly increased the discharge coefficient due to the increased film layer causing a reduction in the resistance to the film cooling flow. Gritsch et al. [6] found that for a 30° inclined, cylindrical film cooling hole, the overall discharge coefficient of any flow configuration can be predicted if the pressure ratio across the hole and the hole jet-to-internal and external crossflow momentum flux ratios are known. These results show the influence of external crossflow on discharge coefficients. Andrews et al. [4] found that for the same hole pitch and coolant flow, cooling effectiveness increased nearly linearly with cooling hole diameter and the heat transfer

coefficients decreased nearly linearly with cooling hole diameter.

Three studies have looked at a disruption of a film cooling layer by a larger normal jet that include Odgers and Son [7], Button [8], and Martiny et al. [9]. Odgers and Son [7] found that when a normal jet, such as a dilution jet, was injected into a film cooling layer at $I_D < 20$, the net effect on the film cooling efficiency depended upon the dynamic pressure ratio of the jet relative to the hot mainstream gas (note this is analogous to momentum flux ratio). If the dynamic pressure ratio was below unity, there was a net benefit on film cooling efficiency. If, however, the ratio was larger than unity, as most combustors are designed, there was a net reduction on effectiveness.

Button [8] evaluated the effectiveness for a slot alone, a jet alone (I_D = 0.25 to 4), and the combined slot and jet. In all of the cases they considered, the combined slot and jet indicated lower effectiveness levels as compared to the slot alone. Martiny, et al. [9] performed experiments whereby slot film cooling was interrupted by a single large dilution jet at I_D = 7 and 10. They also determined that the film cooling lifted off the wall just downstream of the dilution jet leading to weaker film cooling coverage and increased heat transfer coefficients in this area. Their measurements indicated a reduction in the adiabatic effectiveness levels by as much as 25% in the area just downstream of the jet injection location. Similar to Odgers and Son, they found that the effect was more dramatic with higher jet momentum flux ratios.

As others have shown, the turbulence levels in a combustor resulting from the dilution jet injection are relatively high. In a related paper with a geometry similar to that reported in our paper, Vakil and Thole [10] reported measured turbulence levels that were extremely high throughout the combustor as well as highly anisotropic. Moreover, the thermal field measurements of the film cooling layer downstream of the dilution jet injection indicated a much thicker layer relative to upstream of the dilution jets. This vertical spreading of the coolant into the hot gas path was attributed to the mixing caused by the very high turbulence levels.

In summary, there is little data presented in the literature with a realistic cooling configuration for a gas turbine combustor. While there is an abundance of film cooling literature, much of this data is not applicable because of the high blowing ratios required for most aero-engine combustors, the densely spaced cooling holes and the interaction that the cooling has with the large dilution jets. Our study presents data that is of interest to designers and modelers who develop combustor cooling methods.

Experimental Facilities and Measurement Methods

The focus of this study was to obtain highly resolved surface measurements of adiabatic effectiveness for a realistic combustor cooling design. To achieve good spatial resolution, it is beneficial to use large scale models while matching the relevant non-dimensional parameters. The primary measurement techniques used was an infrared camera, in which surface temperatures could be deduced, a laser Doppler velocimeter to quantify the flow field, and a thermocouple rake to quantify the thermal field. This section describes the experimental facility used to achieve these measurements as well as the instrumentation that was used followed by estimates of measurement uncertainty.

Test Section Design

The development of the combustor simulator used in our study was previously described by Barringer et al. [5] and Vakil and Thole [10]. The geometric scaling factor for the combustor was 9X, which permitted good measurement resolution in the experiments, and was matched to that of a linear turbine vane cascade that was pre-existing. Other than performing the measurements in an actual operating engine, it is not feasible to have a measurement environment with representative turbine engine conditions. In designing this combustor simulator, the parameters chosen for a prototypical combustor for aircraft applications included the following: i) a combustor exit velocity that insured the needed inlet Reynolds number for the downstream turbine section; ii) coolant-to-mainstream momentum flux ratios of the liner cooling holes and the dilution holes; and iii) scaled geometric features of a combustor including the film cooling staggered hole pattern and dilution hole size and placement. Note that the parameters for the prototypical engine combustor are for actual running (hot) operating conditions. The air loading parameter (ALP defined in the nomenclature) for the wind tunnel design was 0.40×10^{-4}. Figure 1.1 illustrates the wind tunnel containing the combustor simulator and turbine vane test sections. Downstream of a primary heat exchanger is a transition section that divides the flow into three channels that include a heated primary channel, representing the main gas path (center arrows), and two symmetric secondary channels (outer arrows), representing the coolant flow path.

Within the transition section of the primary channel, the flow immediately passes through a perforated plate that provides the necessary pressure drop to control the flow splits between the

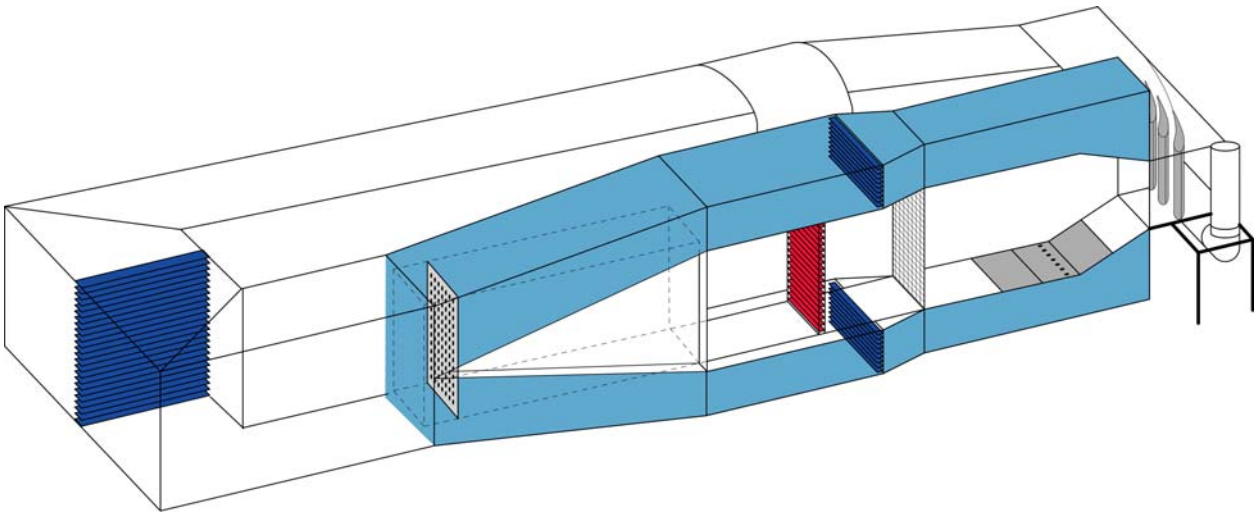

Figure 1.1. Illustration of the wind tunnel facilities used for combustor simulator experiments.

primary and secondary passages. At a distance 2 m downstream of the perforated plate, the flow passes through a bank of heaters followed by a series of screens and flow straighteners. The heater section comprises three individually controlled banks of electrically powered, finned bars supplying a maximum total heat addition of 55 kW. Downstream of the flow straighteners, the heated primary flow enters the combustor simulator. In the combustor simulator, secondary coolant flow is injected into the primary flow passage through cooling panels for the combustor liner and through dilution holes. In addition, the flow is accelerated prior to entering the turbine section. In addition to heat being removed from the flow by a primary heat exchanger, the flow in the secondary passages must go through a second heat exchanger to further reduce the coolant flow temperature. The flow in the secondary passages is then directed into a large plenum that supplies combustor liner coolant and dilution flow.

The combustor simulator begins at the start of the first panel, as illustrated in Figure 1.2**.** The cross-sectional area of the simulator at this location is 1 m in height (H_{in} = 1 m) and 1.1 m in width (W = 1.1 m). At the exit of the simulator, the cross-sectional area is H = 0.55 m in height and remained W = 1.1 m in width giving an inlet to exit area ratio of 1.8. The width was to allow for a dimension that was slightly greater than a turbine sector while the height was matched to that of the radial extent of a first vane. The area ratio was matched to a non-dimensional acceleration parameter through an aeroengine combustor.

Combustor Liner Design

The cooling hole pattern in the panels is illustrated in Figures 1.2 and 1.3. To ensure representative coolant flow splits among the three liner panels and dilution row, separate supply chambers with adjustable shutters were used. The mass flow exiting the film cooling holes was set by applying the appropriate pressure ratio between the supply plenum and the exit static pressure. Using previously documented discharge coefficients for this particular cooling hole configuration (Barringer et al. [5]), the mass flows through the panels were determined. The dilution holes were spaced two hole diameters apart. The mass flows exiting the dilution holes were set by directly measuring the velocity through the use of a pitot probe installed at the exit of the dilution hole.

The liners for the combustor simulator were a streamwise series of three film cooled panels that started 2.7 vane chords (1.6 m) upstream of the turbine test section. The lengths of the first two panels were 39 cm and 41 cm while the third panel was 37 cm. The panels extended across the full width of the test section (111.7 cm), which was slightly greater than a scaled turbine

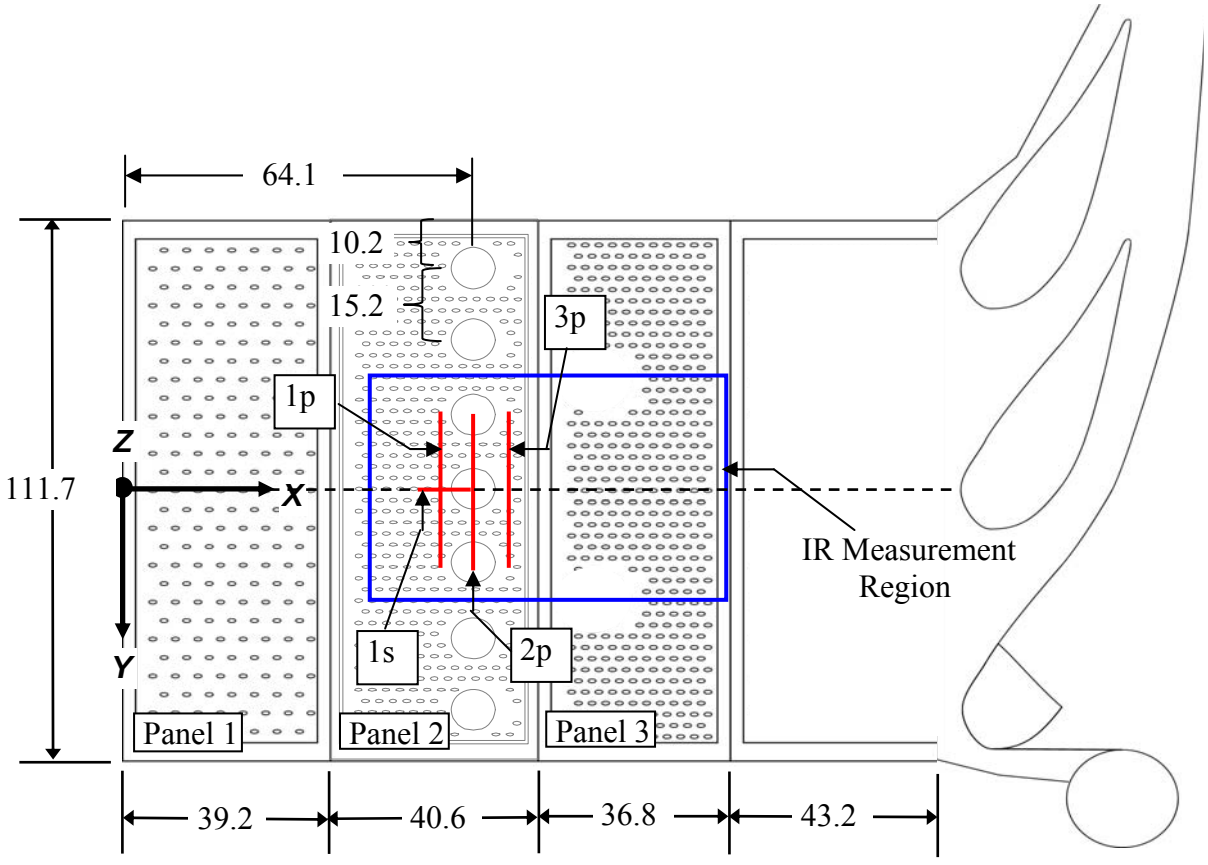

Figure 1.2. Layout and measurements planes for the combustor simulator (dimensions in cm).

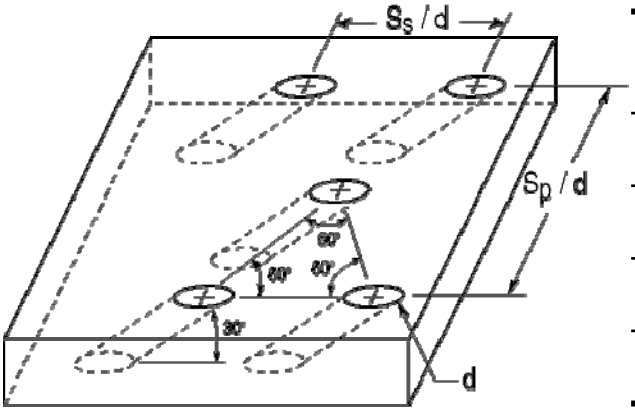

	Diameter (cm)	S_p/d	S_s/d
Panel 1	0.76	10.1	5.8
Panel 2	0.76	6.1	3.5
Panel 3	0.76	6.1	3.5
Dilution	7.6	20 (2D)	-

Figure 1.3. Illustration and description of cooling hole arrangement on liners.

sector. The first two panels were flat to maintain a constant cross-sectional area while the following two panels were inclined at 15.7° to give the required area contraction. As shown in Figure 1.2, there is a region on the third panel in which there were no film cooling holes. Previously, there was a second row of dilution holes, but in this study second row of dilution holes was sealed off to isolate the effects on cooling by a single row, to prevent communication between rows and to eliminate the blockage effects of the aft row. Moreover, given facility flow-loss capacity, the limitation of the open dilution flow to one row allowed a dilution ratio I_D = 125 to be achieved and investigated in this study. In addition, the first dilution row was fabricated in the second panel to which a developed, fairly uninterrupted cooling flow was provided. Measurements were also facilitated by the fact that the combustor walls were parallel to the opposing walls in this section of the combustor simulator. The panels were constructed of 1.27 cm thick urethane foam with a low thermal conductivity (k = 0.037 W/mK) to allow for adiabatic surface temperature measurements. The dense matrix of film cooling and dilution holes was cut into the urethane foam using a water jet.

One parameter that is not representative is the coolant-to-mainstream density ratios, which are typically quite high. Typical operating conditions for the wind tunnel tests consisted of a flow temperature just downstream of the heater of 50˚C and a coolant flow temperature of 20˚C. Although the density ratios were not matched, the jet-to-mainstream momentum flux ratios and percentage of mass flow addition by both the film cooling and dilution holes was representative. The momentum flux ratio is the parameter that most affects mixing characteristics of jets in cross-flow at high momentum flux ratios. Holdeman [11] simulated a non-reacting gas turbine

combustion chamber by conducting computations and experiments on the mixing of single, double, and opposed rows of dilution jets with an isothermal or variable temperature mainstream in a confined subsonic crossflow. The principal finding from the investigation was that the momentum flux ratio of the jets dictated the exit velocity and temperature profiles. The results from the cases involving opposed-rows of jets revealed that for in-line jets the two streams mixed very rapidly and that the effective mixing height was half the duct height for equal momentum flux ratios on both sides. The cooling hole patterns, shown in Figure 1.3, were configured in equilateral triangles and spaced evenly across the surface. The diameter of the cooling holes was 0.76 cm giving an L/d = 3.3.

The dilution hole diameters were designed to ensure the percent mass addition of the dilution fluid and coolant-to-mainstream momentum flux ratios were representative of that in an engine. There are seven dilution holes in a row, evenly spaced with the center hole being aligned with the center of the simulator (and also the vane stagnation). The dilution row is located at 40% of the combustor length (0.64 m or X/D = 8.4) downstream of the start of the panels. The dilution holes have a diameter that is 7.6 cm. The supply chamber for the dilution flow was required to be some distance from the hole exits to ensure uniform jet flow giving an L/D ratio of 5. The combustor simulator is symmetric about the vertical mid-span meaning that for each row the dilution holes were aligned with one another in the pitchwise and streamwise directions.

For the cases presented in this paper, between 38% and 45% of the total flow was directed through the primary passage of the combustor simulator while the remaining flow is directed through the secondary coolant passages for the liner coolant and dilution holes. Of the total cooling flow, 50% is injected through the film cooling holes and 50% is injected through the dilution holes. The density ratio for all of the cases investigated was 1.08 (jet-to-mainstream) while the flow accelerated to nearly 2.5 times the inlet velocity through the combustor simulator as a result of the mass flow addition and contraction ratio. These flow conditions resulted in an exit Reynolds number for the combustor of 2.1×10^5.

Measurement Methods and Uncertainty

A Flir Systems P20 infrared camera was used to take measurements of the combustor liner panels to calculate the adiabatic effectiveness at the liner surface. The camera captured the temperature of the surface at each image pixel location by measuring the total heat flux emitted

from the black painted foam liner panels. Two surface type E thermocouples measuring temperatures at the surface of the panel were used to calibrate the images to assure that the correct surface emissivity and ambient temperatures were being used to report the actual surface temperatures. Five pictures were averaged at each image location to reduce uncertainty in the measurements.

The large scale of the combustor permitted the infrared camera to be mounted in the primary path of the combustor simulator 0.5 m from the liner wall upstream of the dilution holes. The close proximity of the camera to the combustor wall allowed good spatial resolution of less than 1 mm, with a maximum image size of 700 square centimeters. However, the non-orthogonal camera angles and the exposure of the camera to the hot primary flow required additional steps in the infrared image calibration process in which the images were transformed into a correctly dimensioned image.

Thermocouples were used in monitoring inlet and coolant temperatures as well as taking the thermal fields within the combustor. All of the temperature measurements were made using 30-gage, type E thermocouples that were connected to a data acquisition system through 20-gage thermocouple extension wire. All of the thermocouples used in this study were made using an argon-gas thermocouple welder that resulted in spherical beads ranging in diameter from a minimum of approximately 0.8 mm to a maximum of 1 mm. The thermal fields were taken using a twenty-one probe thermocouple rake. The rake spanned a total distance of 10.2 cm with thermocouples evenly spaced every 5.1 mm. Each thermocouple probe on the rake consisted of a 5.1 cm long, 2.5 mm outer diameter aluminum casing that encapsulated the thermocouple wire. The approximate flow blockage was shown to have no effect on the measured thermal field. Each thermocouple bead is fixed approximately 6.4 mm from the end of the aluminum shaft in order to minimize heat conduction effects from the aluminum rod to the thermocouple.

Velocities were measured using a two and a three-component laser Doppler velocimeter (LDV). The flow was seeded with olive oil particles that were nominally 1 μm in diameter. The probability of obtaining a sample was proportional to the speed of the flow; therefore, statistical particle bias corrections were applied to the data by weighting each sample based on the residence time in the probe volume.

In taking flow plane measurements that were aligned with the flow direction, a single fiber optic LDV probe capable of measuring two-components was used. To allow the measurement

volume of the probes to reach mid-pitch of the combustor simulator, data was taken with a 750 mm focusing lens equipped with a 2.6 magnification beam expander. This set-up had a measurement volume of 73 μm in diameter and 1.3 mm in length. The plane was acquired with the probe perpendicular to the outer wall surface. This allowed for the direct measurement of the local streamwise velocity component, u. However, in order to take measurements near the surface of the liner panel, the probe was slightly tilted at 8.8˚, whereby there was little effect on the true vertical component measurements.

For the measurements taken in the cross-stream direction where three-component velocity measurements were made, two separate fiber optic probes were used. This set-up also used a 2.6 magnification beam expander along with a 750 mm focusing lens. Using these two probes, the measurements were conducted through a non-orthogonal set-up requiring the velocity components to be transformed into the true components. Furthermore, as with the single LDV probe measurements, a tilt was applied to both probes to allow for near-wall measurements. To ensure a single beam crossing, both probes were turned 14˚ towards each other in the cross-stream direction while the vertical tilt angle was set to 8.8˚. The nominal sampling time for each measurement location was 20 seconds whereby 10,000 data points were acquired for each component.

The partial derivative and sequential perturbation methods, described by Moffat [12], were used to estimate the uncertainties of the measured values. Precision uncertainties were calculated based on a 95% confidence interval using the deviation of six measurement sets of IR camera images with each set consisting of five images. The precision uncertainty of the measurements was ±0.088°C. The bias uncertainty was ±0.44°C based on the calibration of the image. The bias uncertainty of the thermocouples was ±0.2°C. The total uncertainty was then calculated as ±0.47°C for the images and ±0.22°C for the thermocouples. Uncertainty in effectiveness, η, was found based on the partial derivative of η with respect to each temperature in the definition and the total uncertainty in the measurements. An uncertainty of $\partial\eta = \pm 0.017$ at $\eta = 0.4$ and $\partial\eta = \pm 0.019$ at $\eta = 1.0$ were calculated. The precision uncertainty for the highest streamwise velocities was 0.79% while the bias uncertainty for the mean velocity measurements was 1%. The bias and precision uncertainties of the thermal field values were ±0.2 and ±0.4, respectively, giving an uncertainty of ±0.021 at $\theta = 0.9$ and ±0.020 at $\theta = 0.3$.

Experimental Results

The measurements made in this study included adiabatic wall temperature measurements and flow and thermal fields. The adiabatic wall temperatures were resolved over the entire combustor liner surface. Flow and thermal field measurements were made at four planes near the mid-pitch dilution hole as shown in Figure 1.2. These locations were chosen to illustrate the effect of the dilution and film cooling interaction on the flow and thermal fields and the effects of different momentum flux ratios on cooling effectiveness. It should be noted that the combustor simulator area remains constant at all of the measurement planes in this study. The measurement locations included the following: i) a pitchwise plane 0.75 dilution hole diameters upstream of the mid-pitch dilution hole whereby the film cooling thermal field can be quantified (1p), ii) at the dilution jet centerline to capture effects in the core of the high momentum dilution jet (2p), iii) 0.75 dilution hole diameters downstream of the dilution jet (3p), and iv) a streamwise plane at mid-pitch beginning 1.5 dilution hole diameters upstream of the dilution hole (1s). The flow conditions that were tested are summarized in Table 1.1 for each of the film cooling and dilution flows. Note that two different film cooling flows and two different dilution flows were studied. The momentum flux ratios are defined based on the freestream velocity at the entrance of the combustor simulator. The density ratio for all of the tests was 1.08.

Adiabatic Effectiveness Measurements

Adiabatic surface temperature measurements were made in a region extending one dilution hole pitch on either side of the downstream vane stagnation point. This region extended 28% of the width of the combustor simulator. The streamwise extent of this region was chosen to quantify the development of the film cooling upstream of the dilution jets as well as in the near-jet region. Three dilution jets were included in this region, but it should be noted that there were seven dilution jets across the entire width of the combustor simulator (one vane sector). This

Table 1.1. Film Cooling and Dilution Flow Settings

Case	Film Cooling, I_{fc}	Dilution, I_D
1	12	60
2	12	125
3	25	60
4	25	125

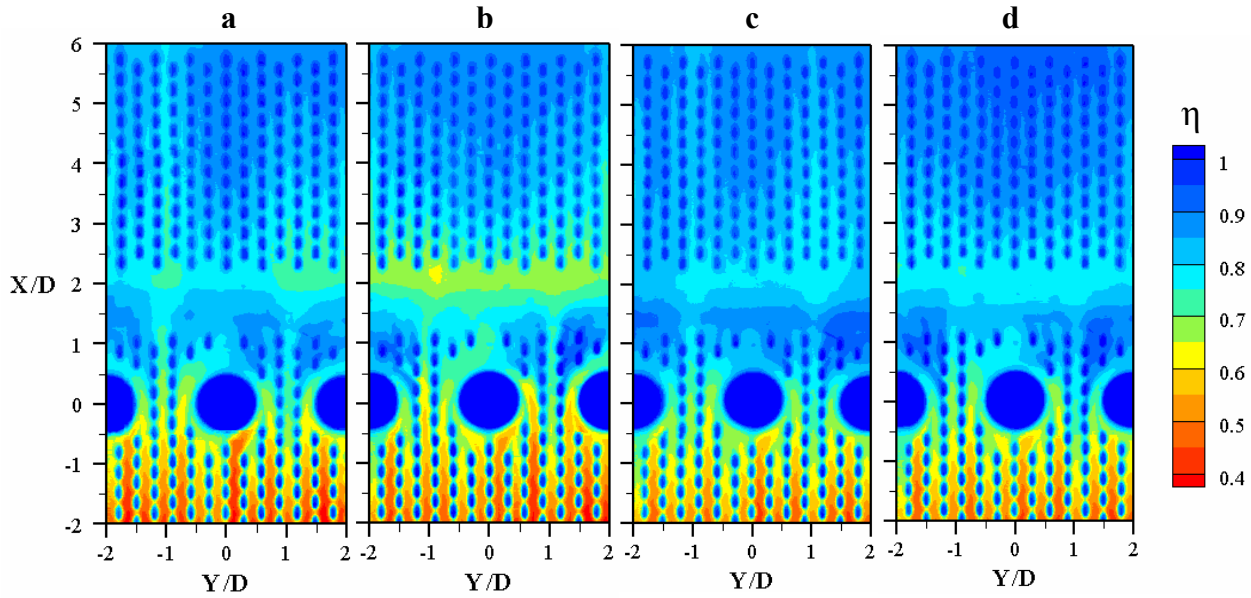

Figure 1.4. Adiabatic effectiveness contours for cases (a) 1, (b) 2, (c) 3, and (d) 4.

was done to show that periodicity had been achieved.

Figure 1.4 shows the adiabatic effectiveness contours for each of the four test cases. For these cases, the nature of the contours showed little difference yet the flow conditions were quite different. Upstream of the dilution jets, it is apparent that there are high temperature streaks between the staggered rows of film cooling holes, indicating values of $\eta = 0.4$. These distinct streaks upstream of the dilution jets were in stark contrast to the surface temperature patterns downstream of the dilution jets where the coolant became more merged indicating nearly an isothermal wall. This downstream phenomenon can be attributed to the high turbulence levels created by the dilution jets. The high turbulence served to mix out the film cooling jets and thereby providing better wall coverage.

The cooling performance depended upon where the rows of film cooling holes intersected the dilution holes. Our results indicate that just upstream of the dilution jet the worst condition occurred at the center hole in which a row of film cooling jets was directly aligned with the centerline of a dilution jet. Hot streaks surrounded the center dilution hole relative to the outer two dilution holes, where for the other two dilution jets the film cooling centerlines were not directly aligned with the centerline of the dilution jets. In all cases, however, it did appear that there is some coolant that surrounded the dilution hole even though the presence of the film cooling holes was quite sparse.

Downstream of the dilution holes, there was an agglomeration of cooler fluid which had been convected around the dilution jets as a result of the vortices that developed. Furthermore, the start of the contraction promoted better cooling just downstream of the dilution holes. On the cooling panel downstream of the dilution holes, it is obvious that there was a lack of cooling where the cooling holes were not present, but there was some effect of the dilution jets impacting the downstream wall as well. This flow behavior and the impact the dilution jets had on cooling are described in more detail in the subsequent sections and paragraphs. Other specific conclusions from Figure 1.4 are that (1) the streaks around the dilution holes were more substantial in surface coverage downstream and between the large holes at the lower cooling momentum flux ratio, (2) cooling effectiveness values were lower downstream of the dilution holes for the higher dilution I_D case and (3) cooling effectiveness was lower at the junction of the second and third liner panels with $I_{fc} = 12$ (as represented by the "green" areas in the contour plots around X/D = 2). The discussion that follows provides more details regarding these observations.

Lateral averages of adiabatic effectiveness for the four cases given in Figure 1.4 are shown in Figure 1.5. Note that the cooling and dilution hole areas were included in the lateral averaging. It was found that the best cooling upstream of the dilution holes occurred for the higher film cooling flow (cases 3 and 4) relative to the lower cooling flow (cases 1 and 2). The film cooling effectiveness trends upstream of the dilution jets were similar at each streamwise location irrespective of the dilution momentum flux ratio. In addition, cooling effectiveness appears to correlate with I_{fc} and, hence, coolant mass. It is also significant to note that the increasing "sawtooth" pattern corroborates the additive nature of cooling rows in a manner consistent with superposition of effectiveness values proposed by other researchers. Downstream of the dilution injection at X/D = 0.5, cases 3 and 4 ($I_{fc} = 25$) resulted in better surface cooling than cases 1 and 2 ($I_{fc} = 12$). The crossflow and film layer accelerated as they passed between adjacent dilution jets at the near-wall due to the flow blockage of the jets. The accelerated flow resulted in an effectively lower local coolant momentum flux ratio causing a cooling effectiveness increase between $0.5 < X/D < 1$. Figure 1.5 highlights cooling effectiveness decay in the region at the junction of panels 2 and 3 ($1 < X/D < 2$). Effectiveness decay should be expected where full-coverage cooling ends and/or is spatially interrupted. This is followed by a cooling increase when the next row is introduced, similar to that found upstream of the dilution hole.

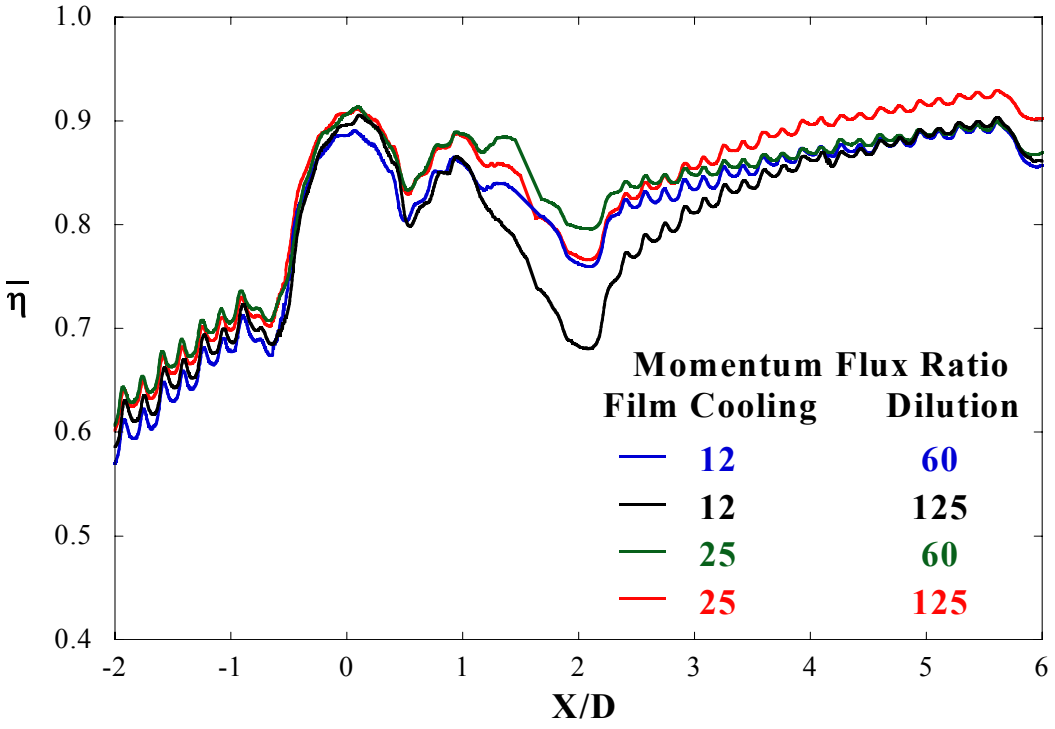

Figure 1.5. Lateral average of adiabatic effectiveness for all cooling cases.

The effects of the dilution jets are present on panel 3, downstream of X/D = 2. In this region, the dilution jets with the higher momentum flux ratios (cases 2 and 4) showed a steeper increase in the cumulative effect of cooling indicated by the adiabatic effectiveness levels, even at different film cooling flows. Moreover, lower local minima of effectiveness were found with the higher I_D cases downstream of the dilution jet injection. In comparison, cases 1 and 3 (lower momentum flux ratio dilution jets) indicate a lower slope in the laterally averaged adiabatic effectiveness values. The lower minima and steeper slopes for cases 2 and 4 were due to the fact that the higher momentum jets were more disruptive to the cooling immediately downstream of the dilution holes but produced more favorable conditions for the cooling further downstream. This phenomenon of film cooling performing better for the cases with the lower momentum dilution jets was most likely due to the less disruptive nature of the low I_D jet with its lower wall-normal momentum and the reduced strength of the three-dimensional flows and turbulence energy inherent to that jet. This result is similar to Odgers and Son [7] who also found that better cooling occurred when the film cooling layer was interrupted by dilution jets with lower momentum flux ratios.

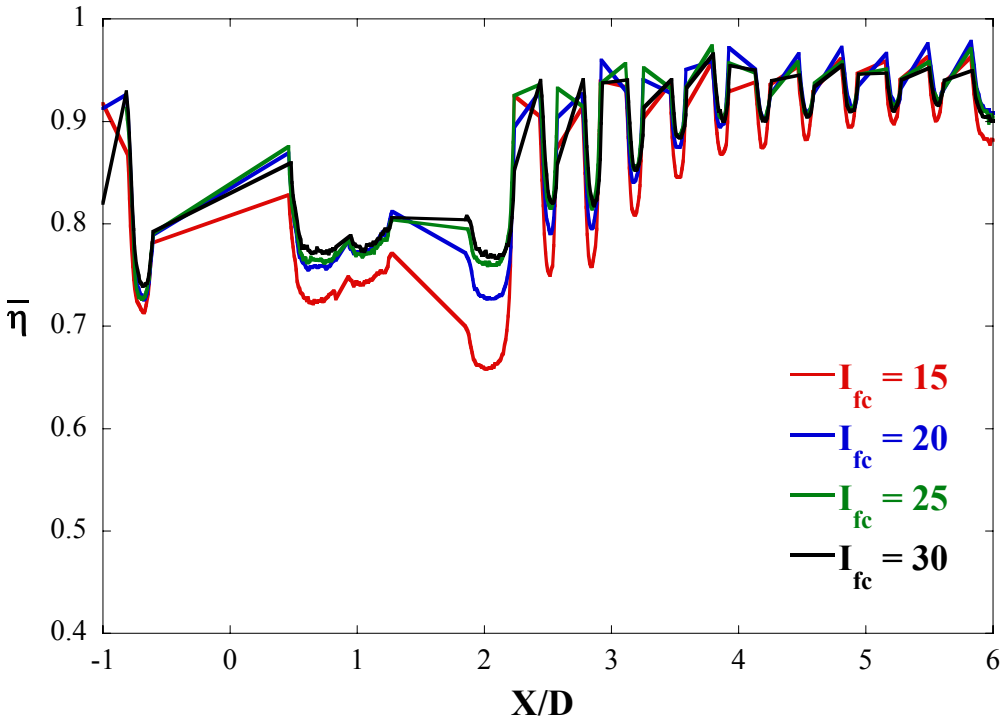

Figure 1.6. Adiabatic effectiveness profiles at the dilution center-line for all four film cooling flow rates.

Because the cooling effectiveness is more dependent on film cooling flow, a study was undertaken where the dilution flow was held constant (I_D = 125) and the film cooling was varied between four different flow rates. Streamwise effectiveness line plots for these cases were generated to determine cooling effects downstream of the dilution hole centerline. From the data shown in Figure 1.6, it can be concluded that the adiabatic effectiveness began approaching an asymptotic value at approximately five dilution jet diameters downstream of the injection. The highest momentum flux ratio (I_{fc} = 30) was found to produce the best cooling effectiveness, but there was a diminishing effectiveness benefit as the blowing ratio was increased.

Flow and Thermal Field Measurements

The thermal fields of three planes were measured in this study for cases 1, 3 and 4. Focus was placed on these three flow configurations because they offered the best cooling and they allowed sufficient variation of the flow parameters. Plane 1p was measured (shown in Figure 1.2) to document the film cooling layer approaching the row of dilution jets. It was found that cases 3 and 4 showed a higher film penetration into the freestream, which is consistent with the higher film cooling momentum flux ratio. It can be seen from the contours in Figure 1.7 that the

coolant accumulated up to a location of Z/d = 13 (Z/H_{in} = 0.1). It should also be noted that upstream of the dilution jet row the streamwise velocity in the coolant layer was 2.75 times the combustor inlet velocity, as will be discussed later in the text. It was observed in the wall effectiveness contours as well as the thermal fields that the jets were discrete allowing for warmer fluid between the hole injection locations.

The thermal fields measured at the dilution center pitchwise location (2p in Figure 1.2) for cases 1 and 3 are shown in Figure 1.8. The penetration distance of the dilution jet core ($\theta = 0.95$) for each case was approximately 9% of the combustor height (or Z/D = 0.7). However, there was a thicker layer of coolant between the dilution jets for case 3, the flows being set at I_{fc} = 25 and I_D = 60.

The flow field measurements, shown in Figure 1.9a, indicate a high streamwise velocity region adjacent to the dilution jets. A bound vortex at the shear layer between the dilution jet and crossflow was generated due to the very high velocity gradients. A high velocity region existed at the center of the bound vortex. Note that the measurement location for the flow field in Figure 1.9a is indicated by the box placed in Figure 1.8a. Turbulence levels were also extracted from the mean and rms velocity measurements and are shown in Figure 1.9b. The peak turbulence level, which occurred in the shear layer between the dilution jet and coolant flow, reached values of two times higher than the inlet velocity (or Tu = 25%). The turbulence intensity of the dilution jet was about 14%. The mid-passage turbulence level was found to be about 30%, based on the combustor inlet velocity. Note that the mass-averaged velocity at this

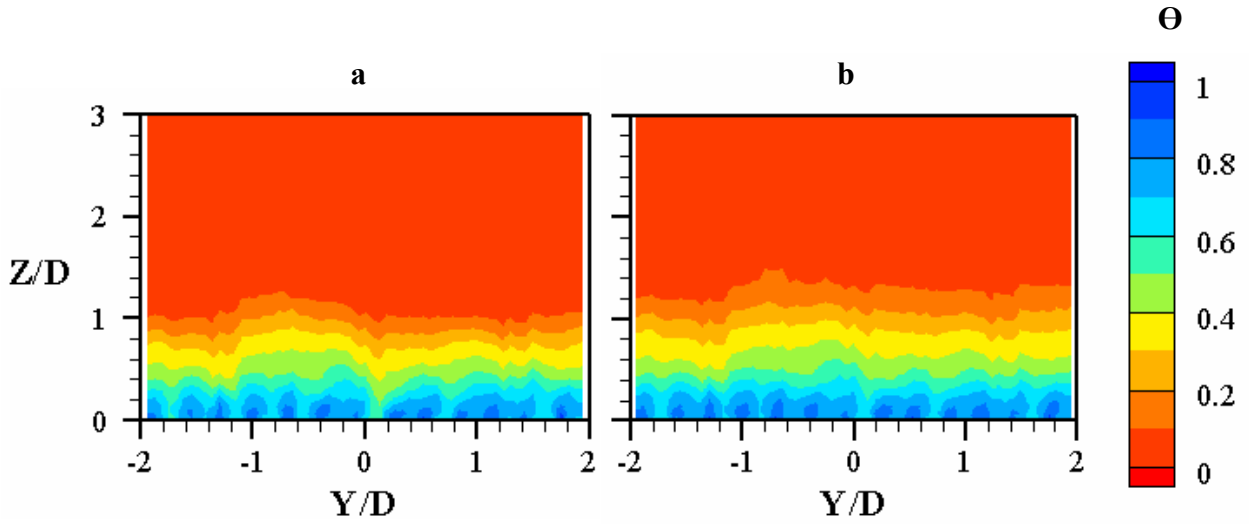

Figure 1.7. Thermal field measurements in plane 1p for cases (a) 1 and (b) 3.

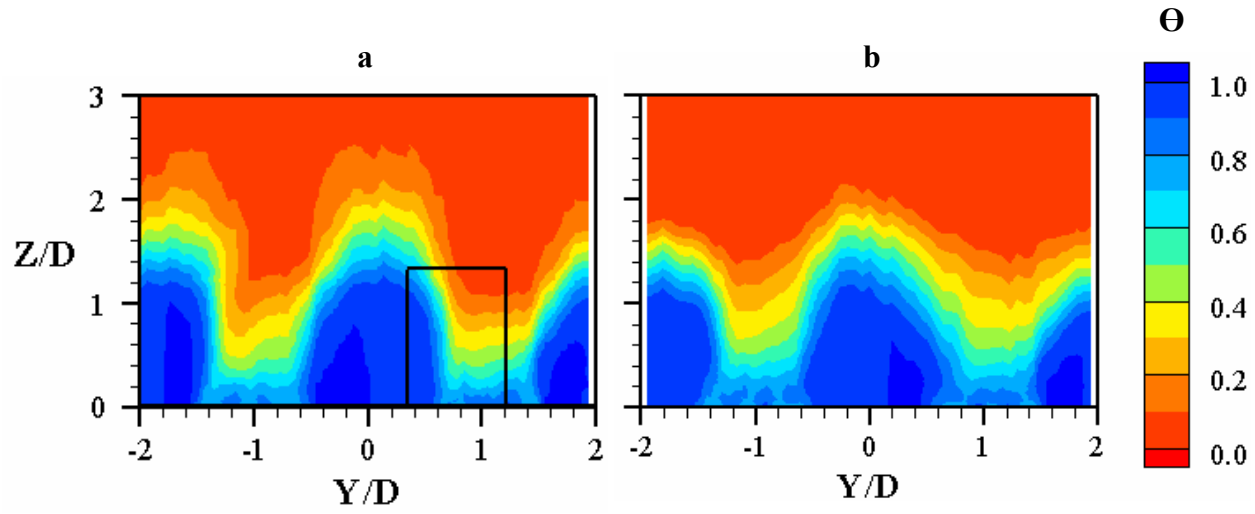

Figure 1.8. Thermal field measurements for plane 2p for cases (a) 1 and (b) 3. The black rectangle denotes where the flow field of Figure 1.9 was measured.

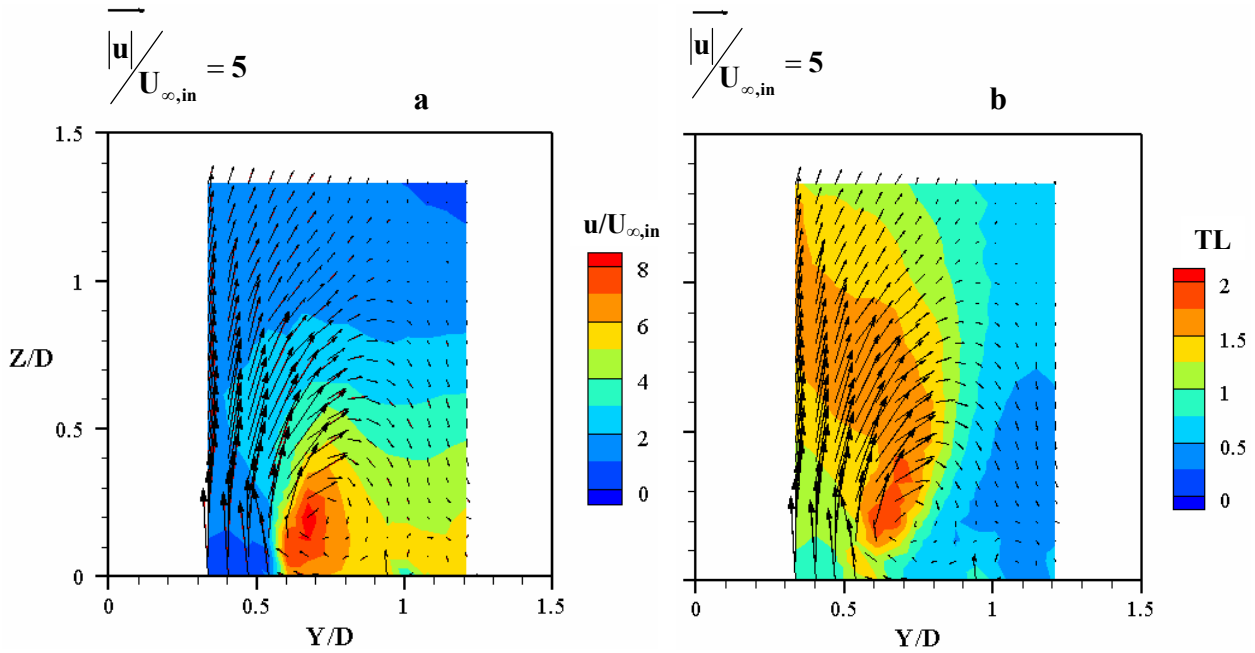

Figure 1.9. Vectors show $v/U_{\infty,in}$ and $w/U_{\infty,in}$ velocity components for case 4. (a) Flow field at plane 2p with contours showing $u/U_{\infty,in}$ values. (b) Contour of turbulence level at plane 2p. Note 4x enlargement of scale.

location was about 14% higher than the inlet velocity.

The velocity and turbulence field approaching the dilution jet (plane 1s) is shown in Figure 1.10. Near the wall, velocities reached 2.5 times the inlet velocity due to the film cooling injection. The crossflow velocity reached a maximum of 1.5 times the inlet velocity as it approached the dilution jet. Near the wall, the film cooling flow stagnated as it approached the dilution jet. Upstream of the dilution jet, the turbulence level of the film cooling layer reached a maximum of about 50%, based on the combustor inlet velocity.

The downstream thermal development of the dilution jets and the film cooling flow for plane 3s is shown in Figure 1.11 for cases 1, 3, and 4. It is clear at this location that the $I_D = 125$ jet had a higher penetration of 25% of the combustor height (based on a temperature of $\theta = 0.8$) relative to 18% of the combustor height for $I_D = 60$. The thermal fields indicate core values that were elliptical shaped resulting from a counter-rotating vortex pair that formed as the jets were bent by the freestream. Vakil and Thole [10] also reported a large recirculation region that

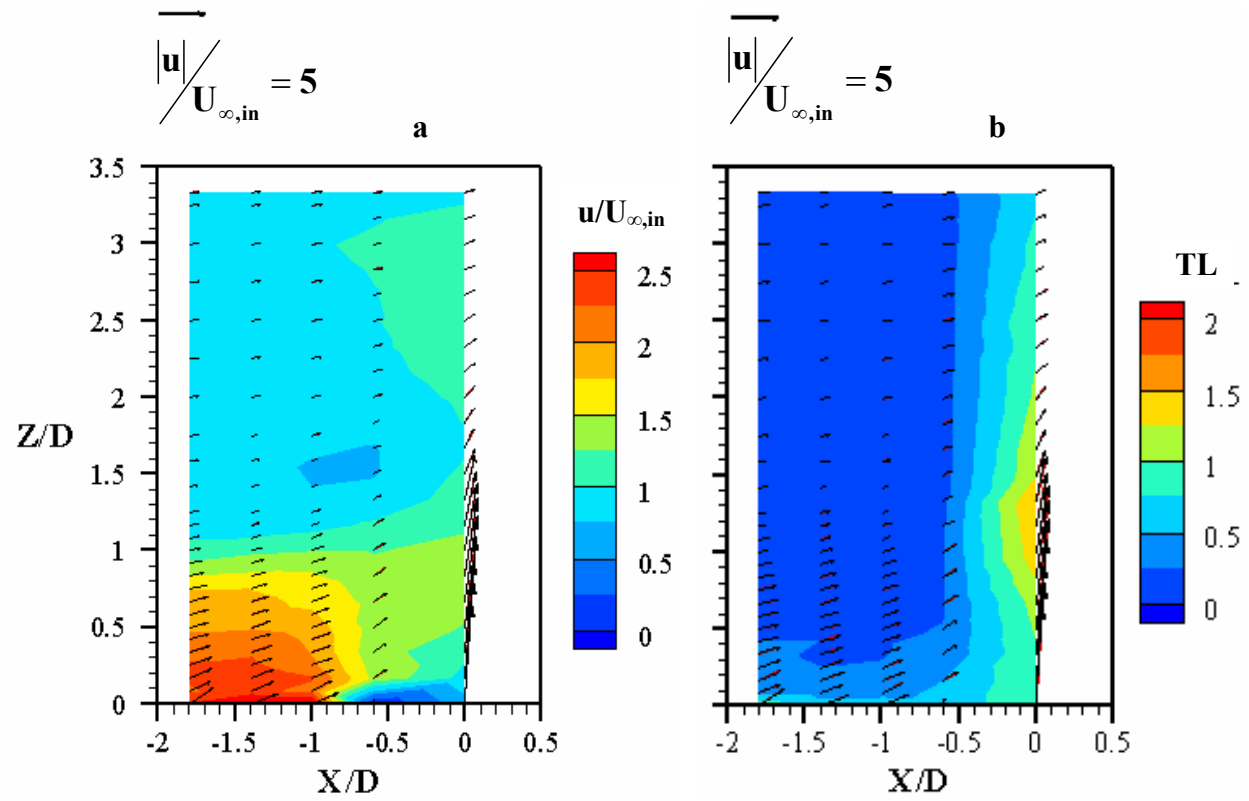

Figure 1.10. (a) Flow field at plane 1s for case 4. Vectors show $u/U_{\infty,in}$ and $w/U_{\infty,in}$ velocity components and contour shows $u/U_{\infty,in}$ values. (b) Flow field vectors and contour of turbulence level at plane 1s for case 4.

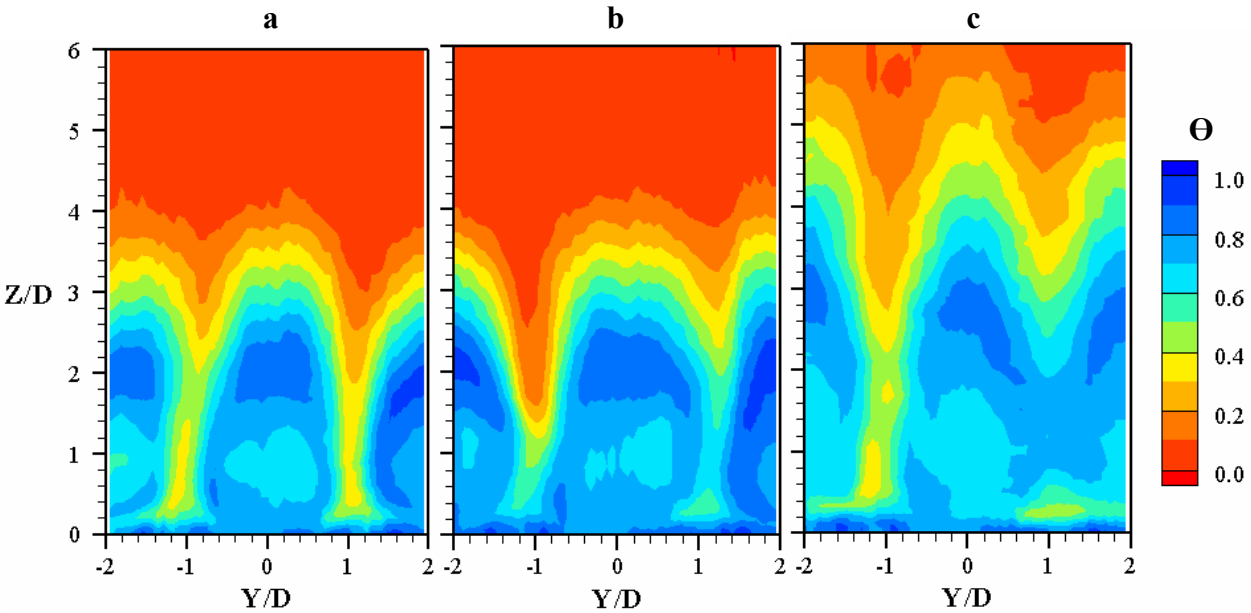

Figure 1.11. Thermal field measurements in plane 3p for cases (a) 1, (b) 3, and (c) 4.

extended two dilution jet diameters downstream of the injection, which served to recirculate warm fluid below the core of the jet.

Comparing cases 1 and 3 (Figure 1.11a and 1.11b), it is evident there was more coolant between the dilution jets below Z/D = 1 with higher film cooling flow injection. This confirms the conclusion that the film cooling flow was entrained by the dilution jets and was carried off the liner wall. However, there was enough film cooling flow at I_{fc} = 25 to ensure that there was an elevated effectiveness level at the liner surface despite the entrainment of cool flow off the wall.

Conclusions

The results of this study indicate that the cooling effectiveness for a realistic combustor wall is dependent on multiple flow mechanisms. It was important in this study to quantify the effect of the dilution jets and cooling flow, which are typical in an aero-gas turbine, on the effectiveness of the coolant at the combustor liner wall. The flow and thermal fields that these flows produced gave insight into how the coolant was transported from the film cooling layer in the near wall region to the freestream and downstream of the dilution jets. Adiabatic effectiveness contours of the combustor wall taken using an infrared camera offer very good spatial resolution and a unique opportunity to identify hot spots and coolant streaks that develop

in a representative combustor simulator.

Surface adiabatic effectiveness measurements along with thermal field measurements indicate the presence of warm fluid between the distinct film cooling jets upstream of the dilution holes. Downstream of the dilution holes, the turbulence levels were quite high resulting in good spreading of the film cooling jets. For the same film cooling flows, there was better surface cooling in the near-dilution region for lower momentum dilution jet injection relative to higher momentum dilution jet injection. The reason for this better cooling was because of the additional cooling resulting from the interaction of the dilution jets with the combustor liner.

The flow fields indicated that the film cooling fluid stagnated as it approached the dilution jets. Further downstream, the film cooling flow was convected around the dilution jets resulting in high streamwise velocities adjacent to the dilution jets. Turbulence measurements indicated localized turbulent regions that developed in the shear layer between the crossflow and dilution jets. These regions partially extended into the jet cores, but remained distinct regions of high turbulence intensity. As such, it would be expected that good mixing would occur at these locations.

Acknowledgments

The authors gratefully acknowledge United Technologies – Pratt & Whitney for their support of this work.

Nomenclature

ALP	air loading parameter, $ALP = P_o^{1.75} A_{ref} D_{ref}^{0.75} e^{T/300} \Big/ \dot{m}$, Lefebvre [1]
A_{ref}	reference combustor area
d	film cooling hole diameter
D	dilution hole diameter
D_{ref}	reference diameter
H	combustor height
I	momentum flux ratio, $I = \rho_c U_c^2 / \rho_\infty U_\infty^2$
L	film cooling/dilution hole length, combustor simulator length

$\dot{m}$	mass flowrate
M	mass flux ratio, $M = \rho_c U_c / \rho_\infty U_\infty$
P	vane pitch
P_o	total pressure
S_s, S_p	streamwise, pitchwise film cooling hole spacing
T	temperature
TL	turbulence level, $TL = \sqrt{0.33\left((u_{rms}^2 + v_{rms}^2 + w_{rms}^2)\right)} / U_{\infty,inlet}$
u, v, w	local, mean velocity components
X, Y, Z	coordinate system shown in Figure 1.1
W	combustor inlet width

Greek

ρ	density
ν	kinematic viscosity
θ	non-dimensional temperature, $\theta = (T_\infty - T)/(T_\infty - T_c)$
η	adiabatic effectiveness, $\eta = (T_\infty - T_{adiabatic})/(T_\infty - T_c)$

Subscripts

ave	spatial average
in	combustor inlet conditions
rms	root mean square
∞	freestream conditions (primary flow)
c	coolant conditions (secondary flow)
D	dilution flow
fc	film cooling flow

Superscripts

$\bar{}$	lateral average

References

[1] Lefebvre, A. H., *Gas Turbine Combustion* (Taylor & Francis: Philadelphia, PA), 1999.

[2] Sasaki, M., Takahara, K., Kumagai, T., and Hamano, M., 1979, "Film Cooling Effectiveness for Injection from Multirow Holes," ASME *Journal of Engineering for Power*, Vol. 101, pp. 101-108.

[3] Andrews, G. E. and Mkpadi, M. C., 1984, "Full Coverage Discrete Hole Wall Cooling: Discharge Coefficients," ASME *Journal of Engineering for Power*, vol. 106, pp. 183-192.

[4] Andrews, G. E., Asere, A. A., Gupta, M. L., and Mkpadi, M.C., "Full Coverage Discrete Hole Film Cooling: The Influence of Hole Size," ASME 85-GT-47.

[5] Barringer, M. D., Richard, O. T., Walter, J. P., Stitzel, S. M., And Thole, K. A., 2002, "Flow Field Simulations of a Gas Turbine Combustor," *Journal of Turbomachinery*, Vol. 124, Pp. 508-516.

[6] Gritsch, M., Shulz, A., and Wittig, S., 1998, "Method for Correlating Discharge Coefficients of Film-Cooling Holes," *AIAA Journal,* vol. 36, pp. 976-980.

[7] Odgers, J. and Son, N. N., "Film Cooling—The Effect of a Cold Jet Normal to the Coolant Layer," Winter Annual Meeting, Houston, Texas, 1975.

[8] Button, B. L., "Effectiveness Measurements for a Cooling Film Disrupted by a Single Jet," 83-GT-250.

[9] Martiny, M., Schulz, A., Wittig, S. and Dilzer, M., "Influence of a Mixing-Jet on Film Cooling," 97-GT-247.

[10] Vakil, S. and Thole, K. A., 2005, "Flow and Thermal Field Measurements in a Combustor Simulator Relevant to a Gas Turbine Aero-Engine," *Journal of Engineering for Gas Turbines and Power*, vol. 127, pp. 1-11.

[11] Moffat, J. R., "Describing the Uncertainties in Experimental Results," *Experimental Thermal and Fluid Science*, Vol. 1, pp. 3-17, 1988.

[12] Holdeman, J. D., "Mixing of Multiple Jets with a Confined Subsonic Crossflow," *Prog. Energy Combust. Sci.*, Vol. 19, pp. 31-70, 1993.

Paper 2:

Effect of Dilution Jets on the Downstream Effusion Flow and Thermal Fields in a Combustor Simulator

Abstract

The flow and temperature fields in a gas turbine combustor are very complex due to the flow processes required in the combustor. Understanding how the dilution jets affect the downstream effusion coolant layer is of critical importance for ensuring sufficient component cooling. Considering the wide range of effusion hole geometries, the present study takes account of how the coolant layer is affected on three different full-coverage cooling hole arrangements by the highly turbulent flow field created on three different full-coverage cooling hole arrangements by a row of dilution jets.

This paper discusses results from a combustor simulator tested in a large-scale low speed wind tunnel with engine representative dilution and film cooling jet momentum flux ratios. Near-wall and mainstream flow velocity and turbulence characteristics were made several dilution hole diameters downstream of one row of staggered vertically opposed normal jets. Three effusion hole designs were tested to compare differences in hole diameter and surface angle while maintaining a constant spacing to diameter ratio. The dilution jets and effusion jets were each tested at two different flow rates, resulting in four test cases.

The results indicate that 20˚ inclined cooling holes in an effusion array create lower coolant layer turbulence levels and higher surface cooling effectiveness than 30˚ cooling holes. It was also found that all three of the cooling hole geometries had comparable velocity coolant layer thicknesses. Results show an insensitivity of the coolant penetration height to the diameter and angle of the cooling hole in the region downstream of the dilution mixing jets. However, temperature profiles indicate differences in the thermal fields of the coolant layer produced by the three effusion liners. When comparing the coolest thermal field temperature for the larger and smaller cooling holes injected at 30˚, the larger cooling holes generate their coolest temperature at a higher vertical distance from the surface. This trend was observed only at the lower dilution jet flow rate.

Introduction

Combustors present one of the greatest component cooling challenges within gas turbine engines. This challenge arises from the extremely high temperatures and very complex flow field that arises within the combustor core flow. The flow complexity is caused in part by the injection of high momentum normal dilution jets required to mix and cool the hot core gases and injection of film cooling flow required to have a low penetration and act as a buffer between the hot core flow and the combustor liner. The coolant is often injected in a full-coverage discrete hole arrangement extending downstream of the row of dilution jets. It is necessary to understand how the velocity and turbulence fields created by the dilution jet injection affect the velocity, turbulence, and temperature fields produced by effusion downstream of the dilution jets.

Experiments were performed in a combustor simulator where the interaction of dilution and film cooling flows were tested featuring engine representative momentum flux ratios. One row of staggered size, vertically opposed, normal dilution jets was injected into the core flow. Three different effusion liners were used to test differences in hole diameter (d = 0.46 cm and 0.57 cm) and surface angle (α = 20° and 30°), maintaining the same spacing to diameter ratio of 4.9 and no compound angle. The dilution jets and effusion jets were each tested at two different flow rates ($I_{fc,in}$ = 12 and 25 for film cooling and I_D = 60 and 100 for dilution) and both were representative of the high momentum jets common in gas turbine combustors.

The objective of the work reported herein was to quantify the downstream velocity and thermal near-wall layer resulting from the interaction of the mixing jets, the approaching crossflow, and the developing layer of coolant air. The velocity and temperature measurements were made at 3.8 and 5.7 dilution jet diameters downstream of the dilution jet injection to measure how the developing flow and turbulence fields affect the velocity and turbulence characteristics of the film layer. Laser Doppler velocimetry was used to make all the velocity and turbulence level measurements. Three cooling hole array geometries were evaluated in this study, paying particular attention to how they affected the shear layer between the film and diluted crossflow. This paper will describe results from the experiments conducted in the simulated combustor after a review of relevant past studies and a description of the test section facility and measurement methods.

Past Studies

Many researchers have studied model combustor flows pertaining to surface coolant coverage and heat transfer as well as to the characterization of the velocity and thermal fields. Combustor surface cooling performance due to the introduction of film flow has also been exhaustively researched. In addition, there have been many papers studying how a high momentum normal jet influences the surface cooling effectiveness of slot injection. These studies have investigated the effect of the normal jets in the vicinity of the jets, with few presenting measurements in the far field region. The effects that the elevated freestream turbulence and altered flow field produced by the dilution jet injection have on the downstream cooling effectiveness are reviewed. Finally, the geometries of the discrete effusion holes that relate to cooling performance are discussed.

In a combustor, dilution jet injection significantly affects the hot crossflow, especially with implications on cooling effectiveness. Odgers et al. [1], Button [2], Martiny et al. [3], Köhler et al. [4], and Gritsch et al. [5] all studied how normal jets injecting into a slot coolant layer affected the surface coolant coverage. The general trend of these studies is that normal jet injection interrupts the slot coolant layer leading to weaker cooling performance and augmented heat transfer, which is exacerbated by increased jet momentum. These studies differ from the data presented in this paper because of the much higher jet momentum flux ratios, a more realistic arrangement of the dilution jet row, discrete full-coverage film cooling injection, and a focus on the velocity behavior of the coolant layer downstream of the jet injection.

The turbulence levels created by the dilution jet injection in a combustor are quite high. Köhler et al. [4] found that a row of jets generates a higher turbulence level than a single jet, and the cooling effectiveness is significantly reduced with closer spaced jets. In two papers with similar experimental geometries Vakil et al. [6] measured the flow and thermal fields and Scrittore et al. [7] measured the surface adiabatic cooling effectiveness due to high momentum dilution jets injecting into an effusion flow. Vakil et al. [6] concluded that the coolant layer was much thicker downstream of the dilution jet injection due to the mixing caused by the elevated turbulence. Scrittore et al. [7] compared the effect of the dilution jet momentum flux ratio and found that the higher momentum jet resulted in lower surface cooling effectiveness downstream of the dilution hole by as much as 10%.

The literature contains many papers on the performance of full-coverage film cooling due to

the effect of variations of all aspects of the hole geometry and spacing. The performance criteria tend to be surface cooling effectiveness and heat transfer coefficient. The relevant geometric variations include hole diameter, hole length, axial/circumferential spacing, surface angle, orientation angle, and the number of rows of holes. The crossflow conditions such as the freestream turbulence and the nature of the internal and external crossflow also affect the coolant issued from the effusion jets. The literature that offers the best comparison includes papers studying the effect of freestream turbulence as well as hole diameter and spacing on the effusion layer velocity and temperature characteristics.

Many studies on the effect of freestream turbulence focus on how the elevated turbulence affects the surface cooling effectiveness, but fail to capture changes to the film layer velocity characteristics. Bons et al. [8] tested single row injection for the range of blowing ratios M = 0.55 to 1.85 and showed that high freestream turbulence decreased effectiveness when the film cooling air was injected at low blowing ratios, but increased effectiveness at high blowing ratios. They reasoned that when a high momentum jet is injected into a high turbulence crossflow, more uniform cooling and higher effectiveness for $x/d > 30$ are produced due to the quicker diffusion of the separated coolant fluid to the wall.

Injection of a high momentum jet into a low turbulence flow field inevitably results in poor cooling due to jet liftoff. Higher freestream turbulence results in better cooling performance because the detached air is mixed and transported toward the surface. Also, there is faster lateral spread of the coolant at elevated freestream turbulence due to increased mixing. In a paper with significantly lower blowing ratios than the current study, Mayhew et al. [9] measured the effect of freestream turbulence on single row film cooling adiabatic effectiveness. These researchers found that elevated freestream turbulence has little effect on effectiveness for a blowing ratio of M = 1.5, and high freestream turbulence makes cooling effectiveness worse for blowing ratios lower than unity.

In a study by Andrews et al. [10], the hole size in a discrete full-coverage film cooling array had a major influence on the overall cooling effectiveness for a constant hole spacing. The relationship between the overall cooling effectiveness and hole size was determined to be approximately linear, whereas the relationship of mean heat transfer coefficient to hole size was inversely linear.

Dilution jets are very important in the aero-turbine combustion process and many papers

have studied how these jets affect the downstream flow field. Several papers have also studied how these jets disrupt an approaching film layer. There have also been many investigations on how cooling effectiveness is affected by high freestream turbulence. However, there is little knowledge on how the complex flow and turbulence fields created by high momentum normal dilution jets affect the downstream near-wall flow field created by full-coverage discrete cooling jet injection.

Experimental Facilities and Measurement Methods

The following section describes the facilities wherein the velocity and temperature measurements were made. This includes a description of the cooling hole liners and flow rates that were used in an effort to attain as realistic flow conditions as possible. Also described are the measurement methods and uncertainty associated with those methods.

Experimental Test Section Design

The measurements reported in this paper were made in a large-scale low speed recirculating facility. The geometric scaling factor for the test section was approximately nine times that of an actual combustor which permitted good experimental measurement resolution. Figure 2.1 illustrates the wind tunnel containing the test section and effusion/dilution jet plate.

The wind tunnel facility had flow and thermal conditioning capabilities suited to attain a uniform thermal and flow field at the inlet of the test section. The thermal conditioning capabilities also served to create a temperature difference between the core and bypass flows, simulating the heat release due to combustion. A 50 hp axial fan supplied flow through a primary heat exchanger to a transition section that divided the flow into three channels including a heated primary channel, representing the main gas path, and two symmetric secondary outer channels, representing the coolant flow paths.

Within the transition section of the primary channel, the flow immediately passed through a perforated plate that provided the necessary pressure drop to control the flow splits between the primary and secondary passages. At a distance 2 m downstream of the perforated plate, the flow passed through a bank of heaters followed by a series of screens and flow straighteners. The heater section was comprised of three individually controlled banks of electrically powered, finned bars supplying a maximum total heat addition of 55 kW. In addition to heat being

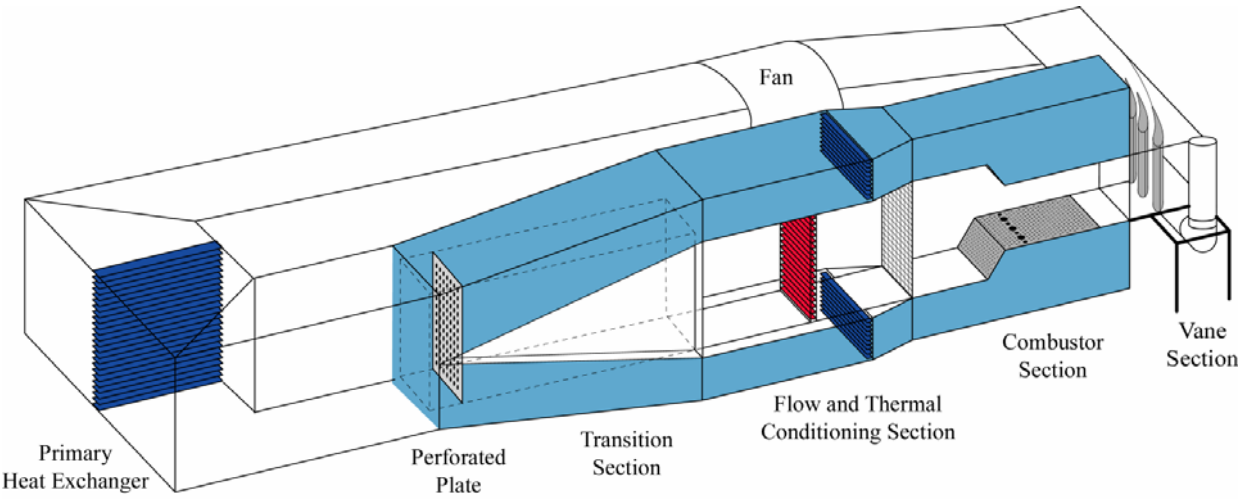

Figure 2.1. Illustration of the wind tunnel facility used for experiments.

removed from the flow by a primary heat exchanger, heat exchangers in the secondary passages further reduced the coolant flow temperature.

The inlet cross-sectional area of the test section was 1 m in height (H_{in}) and 1.1 m in width (W). At a distance of 0.85 m downstream of the flow straighteners, the heated primary flow was accelerated via a 45° contraction to a cross-section measuring 0.55 m in height (4.1 Z/D_L) and 1.1 m in width giving an inlet to exit cross-sectional area ratio of 1.8.

Effusion and Dilution Hole Liner Design and Test Conditions

Full-coverage film cooling flow was injected from the bottom of the test section via two individually controllable plenums. One plenum supplied an upstream effusion plate located on the 45˚ contraction surface. The effusion plate extended 0.3 m in the streamwise direction and had eight rows of holes, amounting to a total of 292 cooling holes inclined 30˚ from the surface. Downstream of the contraction, film cooling flow was also injected through a larger effusion liner on which all of the measurements were made. This liner was located on the bottom wall of the test section and was supplied by a 0.6 m^3 plenum in the secondary passage. An adjustable valve at the plenum inlet was used to ensure the correct coolant flow to the effusion liner. The dilution flow was injected through one row of staggered vertically opposed normal jets which will be described further.

Three different liners were tested in order to determine the sensitivity of the coolant to the cooling hole angle and diameter, maintaining a constant spacing to diameter ratio and no

compound angle. The mass flow exiting the film cooling holes was set by applying the appropriate ratio between the supply plenum total pressure and the exit static pressure. Using the appropriate discharge coefficient for the particular cooling hole and flow configuration based on the required pressure ratio, the mass flows through the test plate were established. Liners 1 and 3 had a 30˚ cooling hole angle, and the discharge coefficients were based on measurements made by Barringer et al. [11]. The effusion holes on liner 2 were oriented at 20˚, but there has been little previous work documenting the discharge coefficients of these types of holes in a full-coverage arrangement. Consequently, the discharge coefficients were measured for liner 2 based on an average of 437 holes arranged in twenty five rows. Illustrations of the effusion liners are given in Figure 2.2.

The effusion plates were constructed of 2.54 cm thick urethane foam with a low thermal conductivity (k = 0.029 W/mK) to allow for adiabatic surface temperature measurements. The dense pattern of 1694 cylindrical film cooling holes for liners 1 and 2 and 1206 holes for liner 3 was cut into the urethane foam liners using a five-axis water jet. The holes were arranged into 43 rows in the streamwise direction for liners 1 and 2 and 35 rows for liner 3. Fewer rows were present on liner 3 due to the larger row spacing. The hole pattern for each test plate is shown schematically in Figure 2.2 and all relevant geometric values are given in Table 2.1.

Velocity and thermal profiles were measured at six locations on the test plates as illustrated in Figure 2.3. These included two different streamwise locations and three different pitchwise locations. The streamwise locations were chosen to gain an understanding of how the flow develops in the axial direction and the pitchwise locations were chosen to understand the effect of the different sized dilution jets on the downstream flow field and coolant layer. For the sake of clarity, U and D denote upstream and downstream measurement locations, respectively, and L, S, and M denote if the measurement was made directly downstream of the large or small dilution jet or at the midpoint between the adjacent jets, respectively.

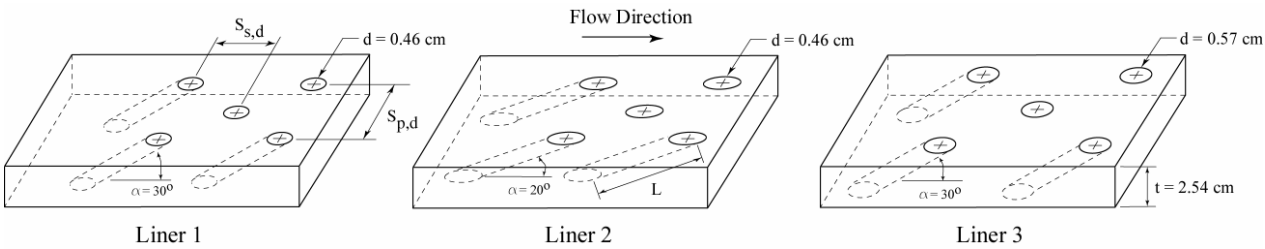

Figure 2.2. Illustration of the geometry and hole spacing of effusion liners 1 - 3.

Table 2.1. Description of effusion plate geometries

Liner	1	2	3
N	1694	1694	1206
d	0.46 cm	0.46 cm	0.57 cm
α	30°	20°	30°
L/d	11.1	16.2	8.9
t/d	5.56	5.56	4.44
$S_{s,d}/d$ $S_{p,d}/d$	4.86		
$S_{p,D}/D_L$	1.07		

There were fourteen total normal dilution jets, including seven injected from the bottom of the test section and seven from the top. The row of jets was arranged in an alternating small and large diameter pattern of 5.1 cm and 13.3 cm, respectively. The bottom row contained three large jets and four small jets, whereas the top had four large jets and three small jets, all injected 2.29 large dilution jet diameters downstream of the contraction. These jets were aligned in a staggered manner, where the small jets on the bottom were aligned with the large jets on the top and vice versa. The pitchwise spacing of adjacent jets was 14.3 cm ($S_{p,D}/D_L$ = 1.07). Note that the coordinate distances in this study were normalized by three parameters: the combustor span, the cooling hole diameter, and the large dilution jet diameter. The flow was controlled through each of the jets with a cone valve and was measured directly using a pitot probe at the center of the jet. Dilution jet flow qualification tests using streamwise and pitchwise profiles through the hole center were measured and are reported in a later section.

For this study, the film cooling characteristics were studied at the two momentum flux ratios of $I_{fc,in}$ = 12 and 25. The dilution jets were injected at the momentum flux ratios of I_D = 60 and 100. One parameter that is not representative is the coolant-to-mainstream density ratio, which is typically quite high in combustors. Typical operating conditions for the film cooling flow tests consisted of a matched coolant and mainstream temperature of 30˚C. For the temperature field measurements, the mainstream temperature was 45˚C and the coolant flow temperature was

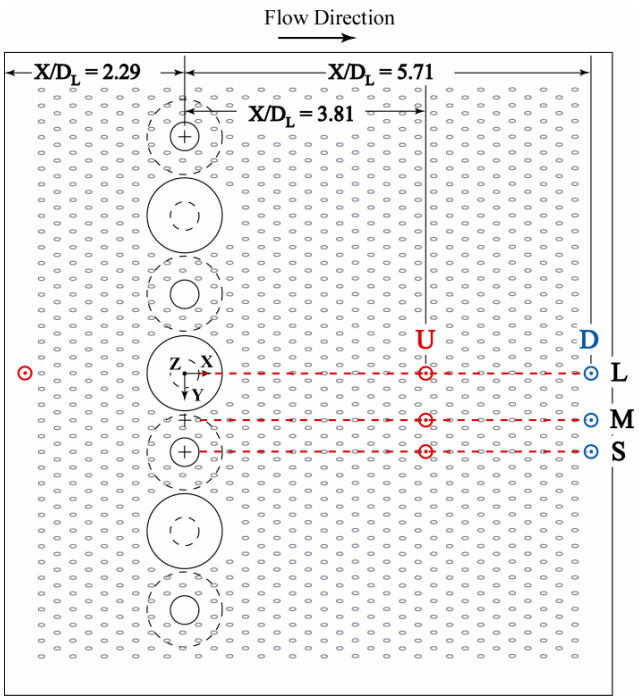

Figure 2.3. Illustration of the test plate where the dotted black circles signify locations of the opposing dilution holes on the top of the test section. The red and blue dots signify the measured profile locations.

20˚C. These conditions resulted in jet-to-mainstream density ratios of 1.0 for all of the unheated cases and 1.09 for all of the heated cases that were investigated.

For the cases presented in this paper, 62 to 68% of the total flow was directed through the secondary coolant passages for the effusion cooling and the dilution jets while the remaining flow was directed through the primary passage of the test section, depending on the coolant flow condition. The flow accelerated by a factor of 2.6 to 3.1 through the test section as a result of the mass addition. These flow conditions resulted in a test section exit Reynolds number from 1.8 to 2.2 x 10^5 based on the exit span of the combustor. The film cooling jet Reynolds number was based on the cooling hole diameter and it varied from 2.0 to 3.7 x 10^3.

Measurement Methods and Uncertainty

The velocity and the turbulence statistics of the flow were measured with a two-component laser Doppler velocimetry system. Two components of the flow velocity (streamwise and spanwise) were measured using a single fiber optic probe. The laser beam crossing had a measurement volume of 73 μm in diameter and 1.3 mm in length. Oil particles that were

nominally 1 μm were used to seed the air. Direct measurements of the streamwise velocity component, u, were possible because the probe was oriented perpendicular to the axial direction. However, in order to make measurement near the surface of the test plate, the probe was angled 8˚ to the surface. A trigonometric correction was used to shift the coordinate system to report the true radial velocity.

A sample of 10,000 data points was acquired for each component over an average period of 20 seconds. The probability of obtaining a sample was proportional to the speed of the flow. Therefore, statistical particle bias corrections were applied to the data by weighting each individual sample based on the residence time of a particle in the probe volume. The partial derivative uncertainty method, described by Moffat [12], was used to calculate the uncertainties of the measurements. The precision uncertainties for all of the measured values were calculated as $\pm 2\sigma$ which corresponded to 95% of the normal distribution. The uncertainty of the LDV measurements was ±1.66% in the freestream and ±3.35% in the more turbulent coolant layer.

The temperature field was reported as a non-dimensional temperature ranging from zero to unity, which corresponded to the freestream and coolant temperatures, respectively. The flow temperatures as well as the inlet and coolant temperatures were measured with 30-gage, type E thermocouples using a National Instruments SCXI 1000 data acquisition system sampling at a rate of 1,000 Hz for 20 seconds. The total uncertainty of the calculated non-dimensional temperature, θ, was ± 0.0095 at $\theta = 0.6$ and ± 0.011 at $\theta = 0.9$.

The pressure difference between the plenum and the liner surface was measured using 60,000 samples over 60 seconds with a 12.7 mmH_2O Setra pressure transducer. The pressure transducer had a bias uncertainty of ±0.079% of the full scale (or ±0.10 Pa). The total uncertainty of these measurements was ±1.24%.

Experimental Results

Prior to a discussion of the results of the flow and temperature measurements, inlet flow conditions and static pressure measurements will be presented. The flow velocity measurements are reported in terms of axial and radial components of velocity. The turbulence levels and Reynolds shear stress were calculated as functions of velocity statistics from both components. Radial temperature profiles are also discussed as they relate to how well the effusion liners perform in terms of surface and coolant layer temperatures.

Inlet Flow Conditions

The inlet conditions of the crossflow and dilution flow were interrogated to confirm the presence of uniform flow. The profiles shown in Figure 2.4 were measured approximately 6.5 cooling hole diameters downstream of the end of the contraction and 4.9 cooling hole diameters upstream of the first row of cooling holes on the large effusion/dilution plate. The dilution jet momentum flux ratio for these measurements was $I_D = 60$. The profiles show the increased near-wall velocity and turbulence associated with the coolant injection from the small inclined effusion plate, as well as negative velocity associated with flow separation due to the contraction. The 45° contraction created a novel combustor geometry that conformed to the decreasing area of the wind tunnel and caused the flow to separate which allowed for the study of how the film cooling and dilution jets would behave when injected into a separated crossflow. Velocity and turbulence measurements were made for both film cooling momentum flux ratios of $I_{fc} = 12$ and 25. The turbulence level of the crossflow at midspan was 2.0% for both cases.

The flow was also measured in the streamwise and pitchwise directions at both the small and large dilution jet exit planes, shown in Figure 2.5. The trends of the streamwise profiles indicate that the jet flow was skewed toward the trailing edge of the hole due to the influence of crossflow on the breakout plane pressure field and the resulting jet flow field. The pitchwise

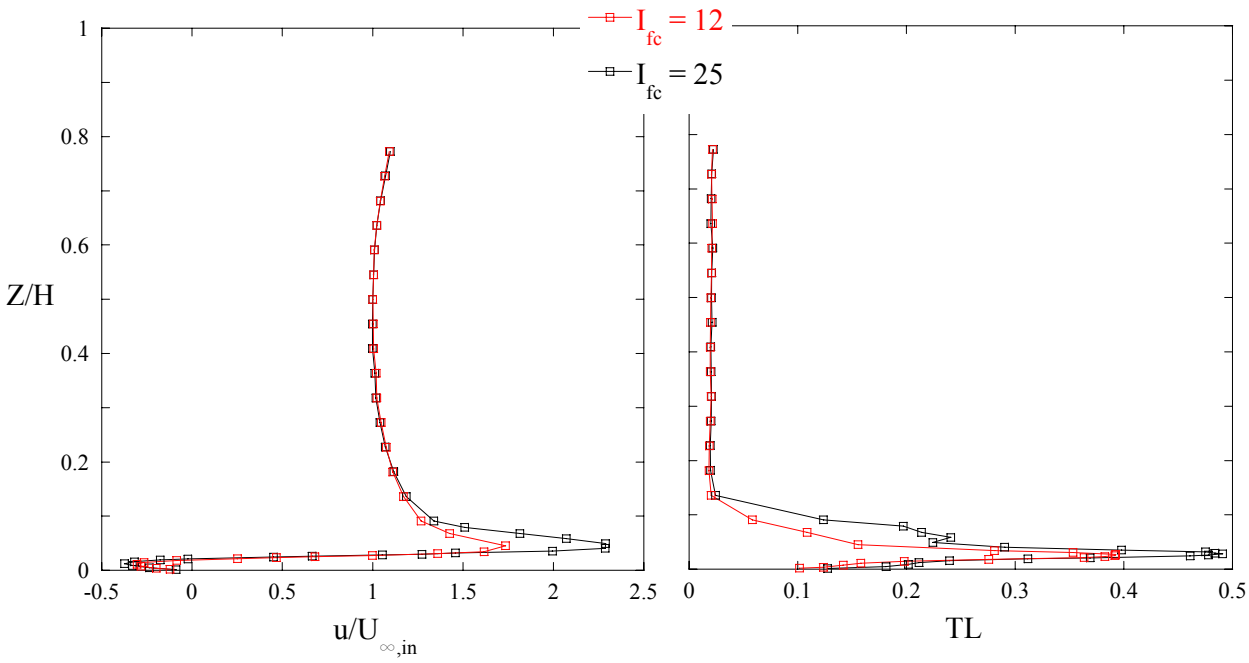

Figure 2.4. Streamwise velocity and turbulence level profiles measured at the liner leading edge $X/D_L = 2.1$ upstream of the dilution jet row.

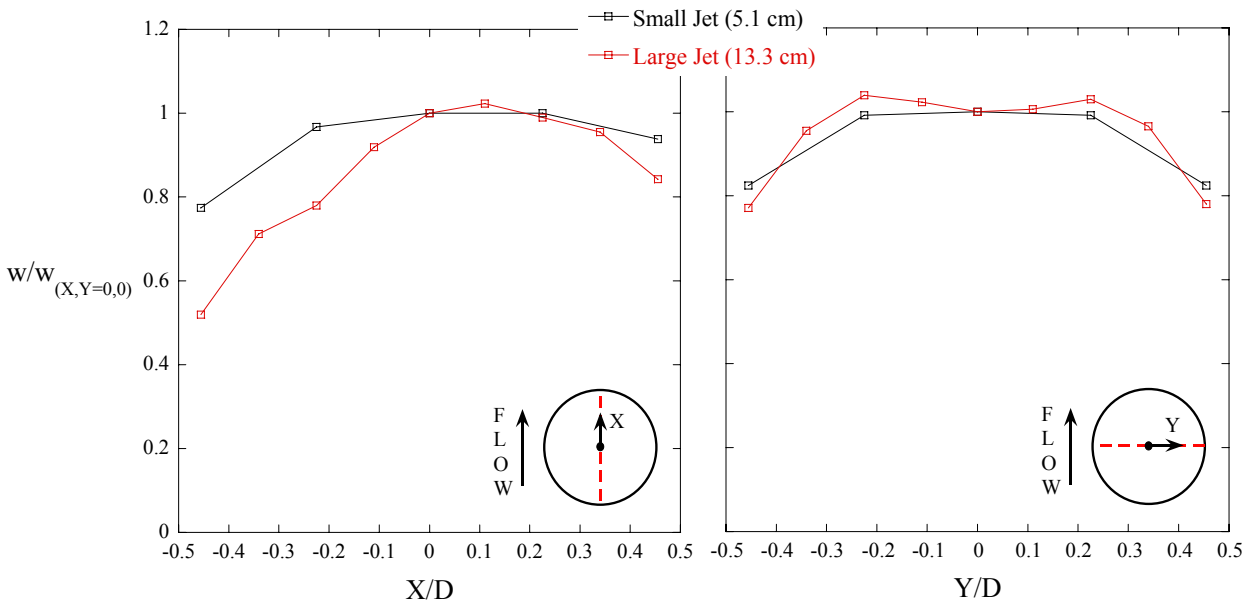

Figure 2.5. Streamwise and pitchwise velocity profiles measured at the dilution jet exit plane.

profiles indicate that the flow emanating from the small jet was more uniform due to the higher pipe length to diameter ratio resulting in a more fully developed flow. The maximum velocity is not located at the jet center for the large jet because the cone valves used to meter the jets created a circumferentially open area at the dilution pipe inlet. The turbulence intensity based on the dilution jet velocity was approximately 10%.

Static Pressure Measurements

The static pressure was measured at several locations along the surface of the combustor liner, especially near the dilution jet injection. These measurements were made to understand how the dilution jet injection affected the static pressure field which affected the film cooling velocity. The surface pressure measurements gave insight into how the film cooling momentum flux ratio varied in the dilution jet vicinity.

The static pressure was measured along the center line of the combustor. Measurements were also made along a streamwise line between the center dilution hole and the adjacent hole. The measurement locations are shown in Figure 2.6. These measurements were used to calculate the local film cooling momentum flux ratios at each row based on the mass averaged velocity which was calculated using the coolant mass addition at each hole row.

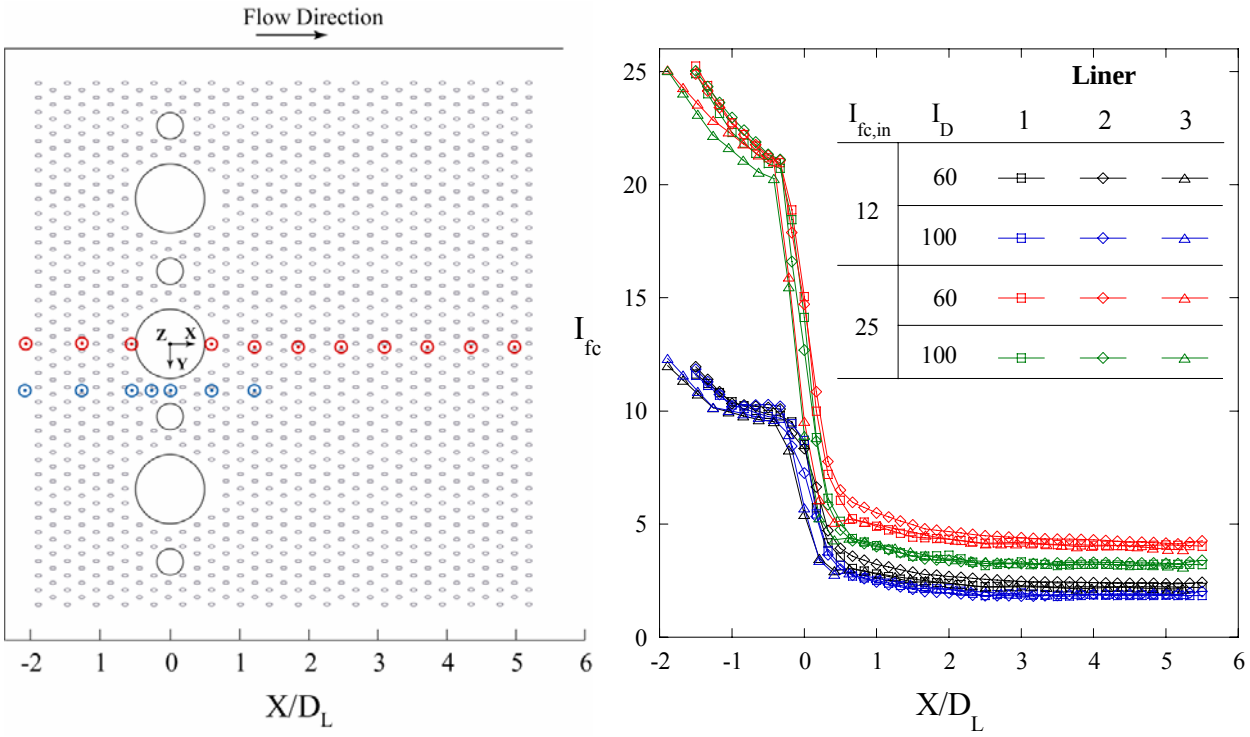

Figure 2.6. Film cooling momentum flux ratios calculated using measured surface static pressures for all liners and flow cases. Red and blue dots indicate centerline and dilution mid-pitch measurement locations, respectively.

These measurements indicate an increase in the static pressure of the flow approaching the dilution jet which corresponds to a 15 - 20% reduction of the film cooling momentum flux ratio from the first row to the seventh row. The static pressure increase was because the flow approached the dilution jet stagnation point and reattached from the separation caused by the 45˚ contraction, and both contributed to an increase in the static pressure.

A wake was generated downstream of the dilution jet injection which caused a low pressure region that persisted until it reached a steady value at $X/D_L \sim 3$. The jet wake resulted in a decrease in surface static pressure from the inlet value. However, the acceleration of the flow due to the dilution mass addition considerably reduced the local momentum flux ratio. Also, the flow approaching the dilution jets was either entrained by the jets or was redirected toward the area between adjacent jets due to the flow blockage. The flow blockage effectively acted like a nozzle and accelerated the flow, reducing the static pressure at that location. The flow acceleration was a stronger effect than the static pressure decrease resulting in a drastic decrease in the local film cooling momentum flux ratio. The static pressure upstream of the dilution jets was not affected by variations in dilution velocity. However, higher dilution jet velocity resulted

in a stronger wake and lower static pressure downstream of the injection.

The value that the film cooling momentum flux ratio asymptotically approached was only dependent on the film cooling and dilution flow rates and was independent of the cooling hole angle, spacing, and diameter. Recall that the velocity and temperature profiles were measured at X/D_L = 3.8 and 5.7. Between these two locations there was a 2% change of the average local momentum flux ratio. This was true for all four flow cases. The average local momentum flux ratios downstream of X/D_L = 3.8 were I_{fc} = 2.3, 1.9, 4.1 and 3.2 for $I_{fc,in}$,I_D = 12,60; 12,100; 25,60; and 25,100, respectively, and these values were irrespective of the liner. This trend indicates that the presence of additional dilution flow reduced the mass averaged film cooling momentum flux ratio despite the fact that the film cooling flow remained constant. Also, at the higher film cooling flow, variation of the dilution flow had a more pronounced effect on the mass averaged film cooling momentum flux ratio resulting in a difference of 24% as opposed to an 18% difference at the lower film cooling flow.

Flow Field Results

This section discusses radial velocity measurements made at several locations on the surface of the combustor liner. The purpose of these measurements was to determine the effect of several of the combustor flow and geometric parameters on the cooling layer thickness. These parameters include the dilution and film cooling jet momentum flux ratios, cooling hole spacing, diameter, and cooling hole surface angle. Flow velocity and turbulence statistics were measured at two streamwise locations and three pitchwise locations on the surface of the liner, illustrated in Figure 2.2.

The location of the X/D_L = 3.8 measurements dictated that they be made halfway between adjacent streamwise rows of cooling holes ($x/S_{s,d}$ = 0.5). However, at X/D_L = 5.7, measurements were made one full row spacing downstream of the last row of holes ($x/S_{s,d}$ = 1.0). This discrepancy in the measurement location with respect to the cooling hole made it challenging to directly compare these measurements because of the high streamwise gradient of the emanating cooling jet. The measurements were made a fixed distance of $x/S_{s,d}$ = 0.5 and 1.0 from the cooling hole center. The shallower 20˚ holes had a larger breakout area and therefore the measurement locations were closer to the downstream edge of the inclined hole, implying that the velocity and turbulence levels and gradients were higher.

The high streamwise velocity gradient was demonstrated via the axial development of the cooling flow in Figure 2.7 at location DL for an inlet film cooling and dilution momentum flux ratio of 25 and 60, respectively. These data indicate that there was a large gradient in the flow field downstream of the jet injection. At the downstream edge of the cooling hole the maximum streamwise velocity was approximately 2.1 times the mass-averaged velocity. The jet decelerated as the viscosity and turbulent nature of the flow diffused and transported the faster jet core to the slower surrounding flow. This resulted in a double peaked velocity profile at $x/S_{s,d}$ = 1.0, due to the entrainment of faster flow into the slower jet wake.

The Reynolds shear stress is important because it is a measurement of momentum transport due to turbulence which was more dominant in the film cooling layer rather than in the dilution dominated near-wall flow field at the locations U and D. Consequently, where the value of $\overline{u'w'}$ approached zero was a reliable indication of where momentum transport from the cooling layer

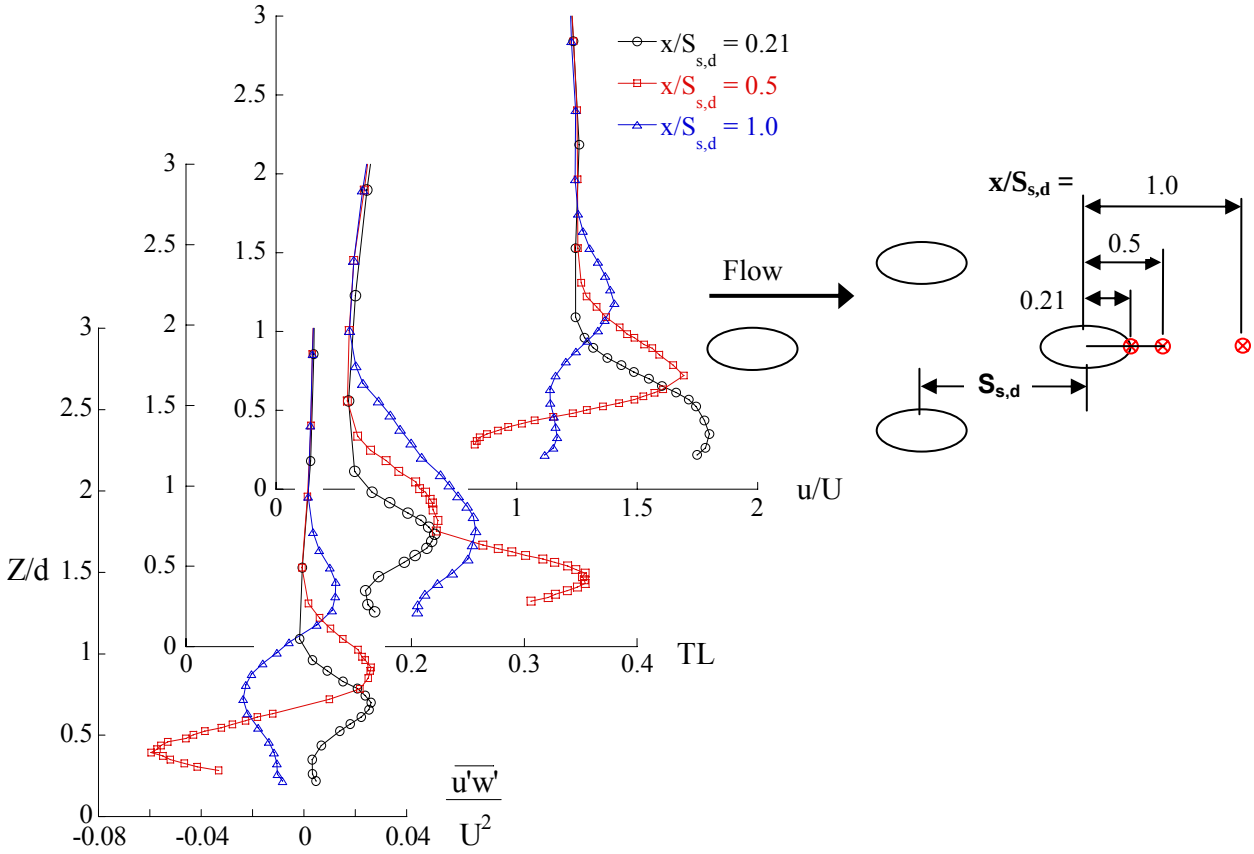

Figure 2.7. Streamwise development of streamwise velocity, turbulence level, and Reynolds shear stress at the cooling hole exit at location DL for $I_{fc,in}$ = 25, I_D = 60, α = 30˚, d = 0.46 cm.

had reduced. As shown in Figure 2.7, the $\overline{u'w'}$ product (normalized to the square of the mass-averaged velocity) was positive and had a maximum value coincident with the location of the shear layer between the jet and the mainstream. This suggests diffusion from the high speed jet to the lower speed mainstream.

As the jet penetrated higher and mixed with the mainstream, the positive $\overline{u'w'}$ product continued to correspond to the outer jet shear layer, and a negative $\overline{u'w'}$ region emerged which corresponded to the shear layer between the jet core and the wall. This implicates entrainment which is due in this case to vortical movement of flow in toward the cooling jet symmetry plane. The local minima and maxima of $\overline{u'w'}$ correspond to turbulence peaks in the film layer, where there consistently was shear stress reduction in the upper shear layer and shear stress augmentation beneath the jet core. As the simplified turbulent momentum equation suggests,

$$w\frac{\partial u}{\partial z} = \frac{1}{\rho}\frac{\partial}{\partial z}\left(\mu\frac{\partial u}{\partial z} - \rho\overline{u'w'}\right) \qquad (1)$$

a positive $\overline{u'w'}$ product reduced overall stress, which led to lower turbulent momentum transport in the radial direction. However, the high turbulence and strong entrainment that were evident at $x/S_{s,d} = 0.5$ in the lower shear layer quickly dissipated by $x/S_{s,d} = 1.0$. It should be noted that the Reynolds shear stress failed to predict the overall shear stress in a flow, as the viscous stress can play a major role in determining the overall shear. The flow characteristics were different depending on the distance the measurement was made from the hole.

The effect of film cooling and dilution momentum flux ratios on the flow in the near wall region was investigated. Figure 2.8 presents the streamwise velocity, turbulence levels, and $\overline{u'w'}$ product, all normalized to the mass averaged flow velocity as evaluated up to the test section mid-span. These profiles were all measured on liner 1 ($\alpha = 30^{\circ}$, d = 0.46 cm) at locations US and DS. Some differences in the measurements at US and DS ($x/S_{s,d} = 0.5$ and 1.0, respectively) have been mentioned previously, such as the double peaked velocity and a streamwise attenuation of the Reynolds shear stress. The turbulence level in the coolant layer and in the mainstream decreased as the flow progressed downstream. It is evident that at the low film cooling flow the mass averaged velocity scales the velocity, turbulence level, and Reynolds shear stress. However, at the high film cooling flow rate, especially for the measurements made

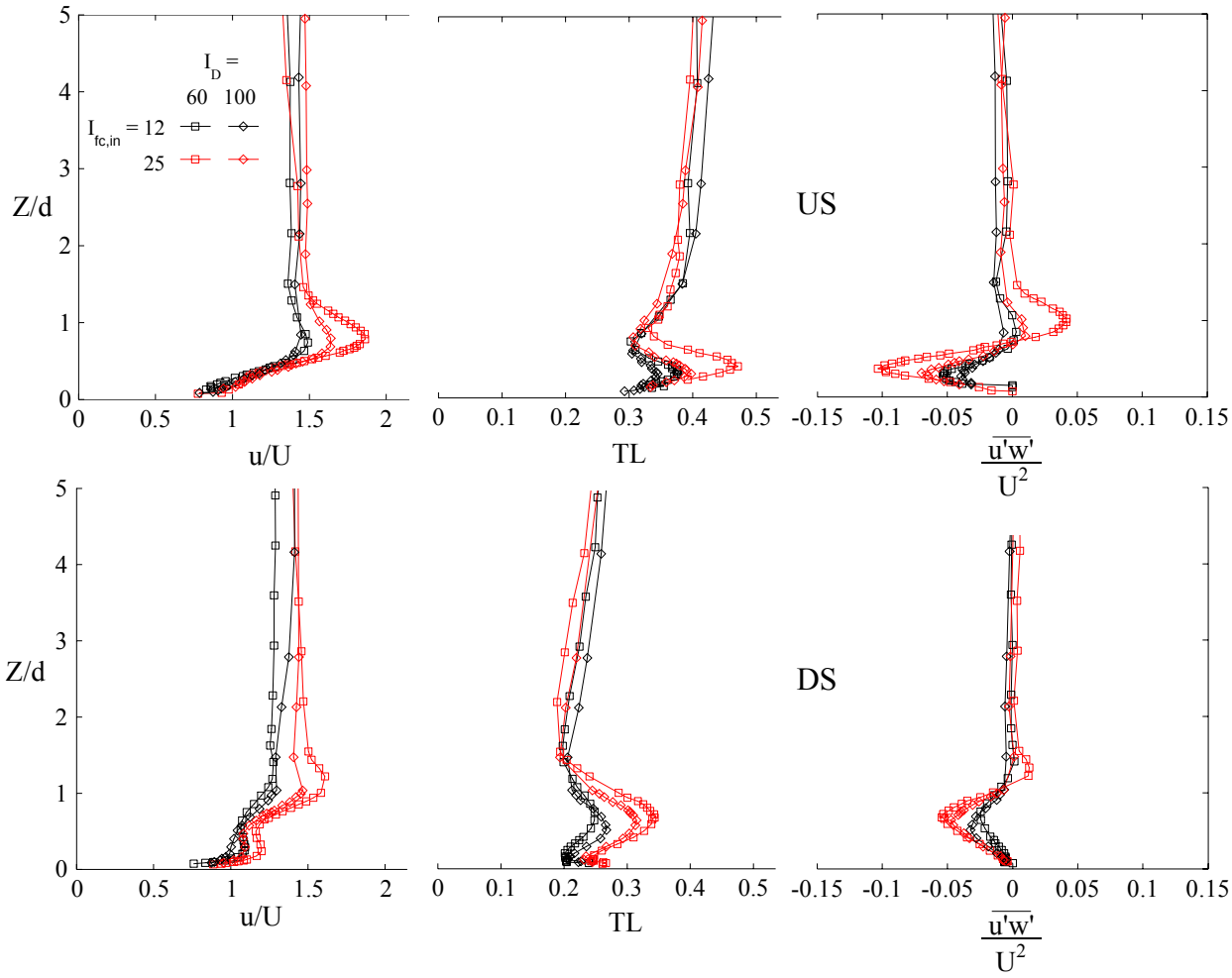

Figure 2.8. Comparison of velocity, turbulence level and Reynolds shear stress for locations US and DS on test liner 1 for all flow cases.

at X/D_L = 3.8 (Upstream), the mass averaged velocity does not effectively scale the data, resulting in different magnitudes in the coolant layer. This implies that an $I_{fc,in}$ = 12 coolant layer was more sensitive to high mainstream turbulence level effects created by dilution injection, whereas an $I_{fc,in}$ = 25 coolant layer acted as a better buffer.

A comparison of the characteristics of different cooling hole geometries in Figures 2.9 through 2.11 shows that the coolant flow field was sensitive to both the surface angle and diameter of the cooling holes. The shallower 20˚ effusion holes featured lower jet penetration, lower coolant layer turbulence levels and reduced momentum transport from the wake into the jet. It should be noted that the velocity, turbulence levels, and turbulent stress levels were largely independent of the upstream dilution jet diameter, i.e., there was little variation in the pitchwise direction.

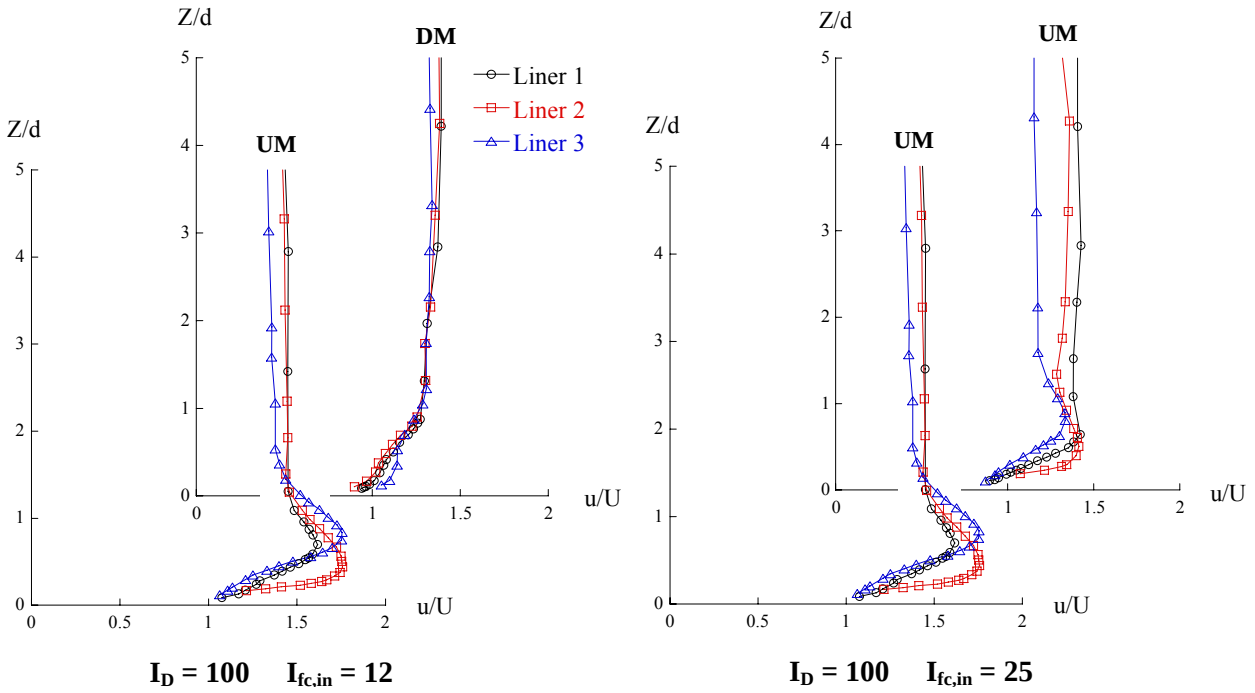

$I_D = 100$ $I_{fc,in} = 12$ $I_D = 100$ $I_{fc,in} = 25$

Figure 2.9. Streamwise velocity components at locations UM and DM for I_D = 100 and $I_{fc,in}$ = 12 (left) and $I_{fc,in}$ = 25 (right) for all liners.

The axial velocity components at UM and DM and $I_{fc,in}$ = 12 and 25 for I_D = 100 are compared in Figure 2.9. These profiles indicate that liner 2 (20˚ effusion holes) introduced lower jet penetration, exhibited by a velocity peak nearer to the liner wall at location UM. This result is expected because penetration height is generally a function of jet injection angle. At location DM, liners 1 and 2 produced very similar profiles suggesting that hole diameter is the dominant factor influencing the velocity profile. Liner 3 (α = 30˚, d = 0.57 cm) showed a different trend due to its larger diameter cooling holes. The velocity in the wake region below the jet core (Z/d < 1) was found to be faster due to the higher mass flow associated with the larger diameter cooling holes.

The Reynolds shear stress measurements in Figure 2.10 compare locations US and DS and the effect of dilution momentum flux ratio for liners 1 - 3. The Reynolds shear stress profiles reveal that at the location US (X/D_L = 3.8), liners 1 and 3 produced a positive and negative peak in the upper and lower cooling jet shear layers, respectively. The physical significance of this trend is turbulent transport of momentum away from the core of the jet which has been discussed previously.

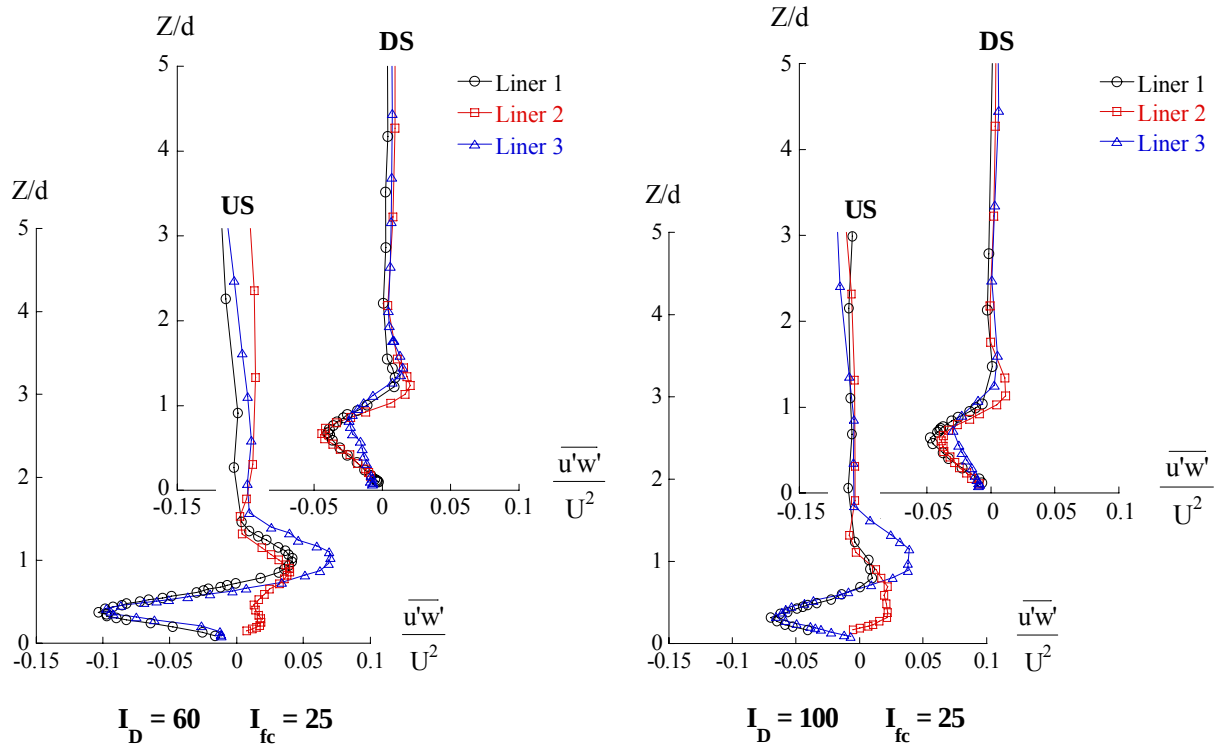

Figure 2.10. Nondimensional Reynolds shear stresses at locations US and DS for $I_{fc,in}$ = 25 and I_D = 60 (left) and I_D = 100 (right) for all liners.

Interestingly, liner 2 (α = 20˚, d = 0.46 cm) generated positive values of Reynolds shear stress in the shear layer between the jet core and the wall, which implies less momentum transport than the other liners. However, the 20˚ holes create a high velocity gradient resulting in high viscous shear stress in the shear layer below the jet. The Reynolds shear stress in the cooling layer did not change in the pitchwise direction, meaning there was little effect due to variations of the dilution jet size. The turbulent shear stresses produced by $I_{fc,in}$ = 12 show lower values than $I_{fc,in}$ = 25, but reveal similar trends.

The turbulence level is an important performance consideration because of its impact on cooling effectiveness and heat transfer. Mainstream flows with high turbulence levels tend to increase coolant mixing with the mainstream, spread coolant laterally, and diminish streamwise coolant coverage. Figure 2.11 shows the turbulence levels at locations UM and DM normalized to the mass-averaged velocity.

The turbulence levels were very similar at DM (X/D_L = 5.7) for all of the liners. However, at the upstream measurement location of UM (X/D_L = 3.8), liner 2 consistently generated less turbulence than the other liners. This was true for both film cooling momentum flux ratios. It is

believed that this effect is due to lower penetration of the coolant and less vortical entrainment and mixing by the 20˚ holes. The higher film cooling flow generally resulted in a slightly higher turbulence level in the coolant layer.

The turbulence level at UM was found to have two maxima corresponding to the shear layer above and below the cooling jet core. For liners 1 and 3 the turbulence level then began to decay below the bottom shear layer for the 30˚ cooling holes, yet this trend is not observed for the 20˚ holes. This is due to the adherence of the coolant to the wall which meant that the wake region (below the jet core) was dominated by the jet shear layer which prevented the relaxation of the turbulence in the region between the jet shear layer and the wall. The turbulence level at DM was found to have only one maximum corresponding to the bottom shear layer. A peak in turbulence was not seen at the upper shear layer because the DM location was located at a farther relative distance from the cooling hole ($x/S_{s,d}$ = 1.0 as opposed to $x/S_{s,d}$ = 0.5). This indicates that at this location the lower and upper jet shear layers have merged. This finding is consistent with the work of Scrittore et al. [7] who measured a coalescence of the elevated turbulence levels of the lower and upper shear layers approximately four hole diameters downstream of the hole. Note that in this study four hole diameters is equivalent to $x/S_{s,d}$ = 0.82.

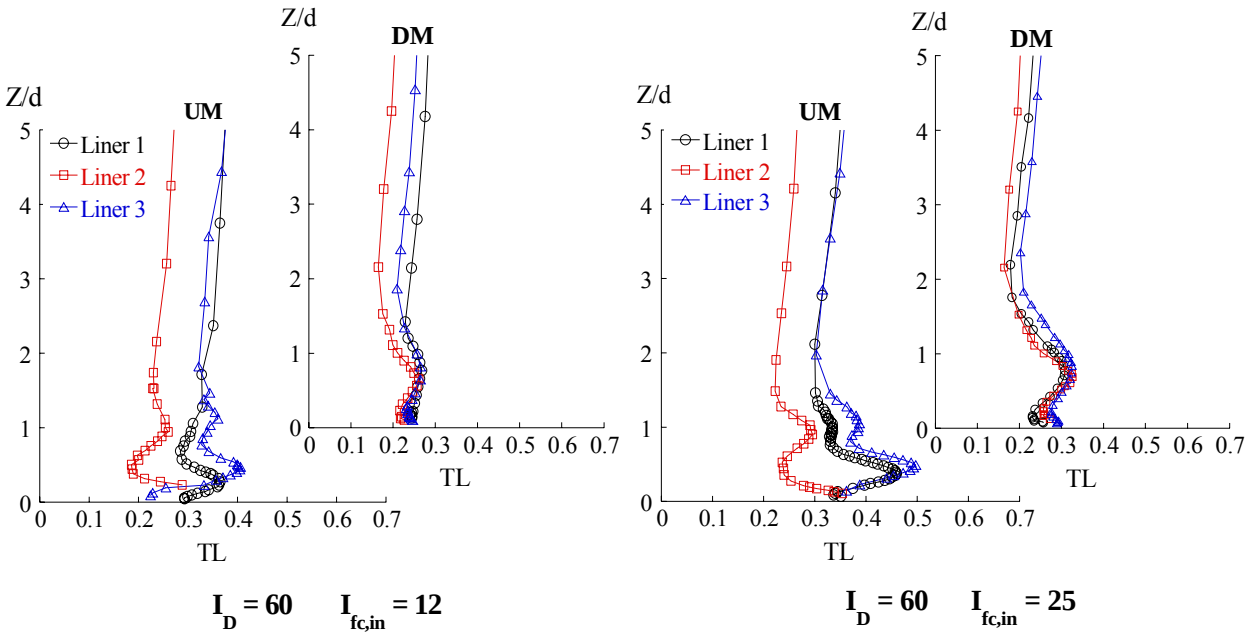

Figure 2.11. Turbulence level profiles at location UM and DM for I_D = 60 and $I_{fc,in}$ = 12 (left) and $I_{fc,in}$ = 25 (right).

The film cooling momentum flux ratio had an effect on the near-wall turbulence levels. At location UM for the flow condition $I_D = 60$ and $I_{fc,in} = 12$, the turbulence level reached values of TL = 0.37, 0.29, and 0.41 for liners 1 to 3, respectively, in the lower shear layer. With a film cooling momentum flux ratio of $I_{fc,in} = 25$, the turbulence level in the lower shear layer increased to TL = 0.46, 0.35, and 0.50, due to the higher velocity gradient. The mainstream turbulence varied with axial distance from the dilution jet injection. Turbulence levels of TL = 0.35 to 0.40 for $I_D = 60$ and 100, respectively, were observed at $X/D_L = 3.8$ which relaxed to levels of TL = 0.25 to 0.30 at $X/D_L = 5.7$. Thus, the variation in mainstream turbulence level was due to the dilution jet injection. It should be noted that the turbulence levels were lower downstream of the large dilution jet and higher downstream of the small jet by a maximum margin of 5%.

Thermal Field Results

This section discusses temperature measurements made on the surface of the combustor liner. The purpose of these measurements was to use the thermal characteristics of the near-wall flow to determine the coolant layer thickness and the surface cooling effectiveness. Similar to the velocity measurements, the goal was to characterize the effect of several of the combustor parameters such as dilution and film cooling jet momentum flux ratios, cooling hole spacing, diameter, and surface angle. The thermal profiles were measured at the same location as the velocity profiles, at two streamwise locations and three pitchwise locations on the liner surface illustrated in Figure 2.2.

The temperature profiles that are presented in Figure 2.12 were measured on liner 1 and offer a comparison of locations US and DS as well as a comparison of variations of the dilution and film cooling momentum flux ratios. Several observations can be made from an assessment of these temperature profiles. There is a large difference in the temperature trends in the near-wall region at location US compared to DS. An important reason was a discrepancy in the proximity of the measurement to the cooling hole between the two locations. As previously discussed, the profiles measured at $X/D_L = 3.8$ were closer to the cooling hole ($x/S_{s,d} = 0.5$) than the measurements made at $X/D_L = 5.7$ ($x/S_{s,d} = 1.0$). Further discussion is needed to explain why the near-wall temperature is sensitive to variations of the dilution jet momentum flux ratio.

Sensitivity of the near-wall temperature to the dilution momentum flux ratio at the US location can be attributed to the stronger turbulence and less developed coolant layer. At the DS

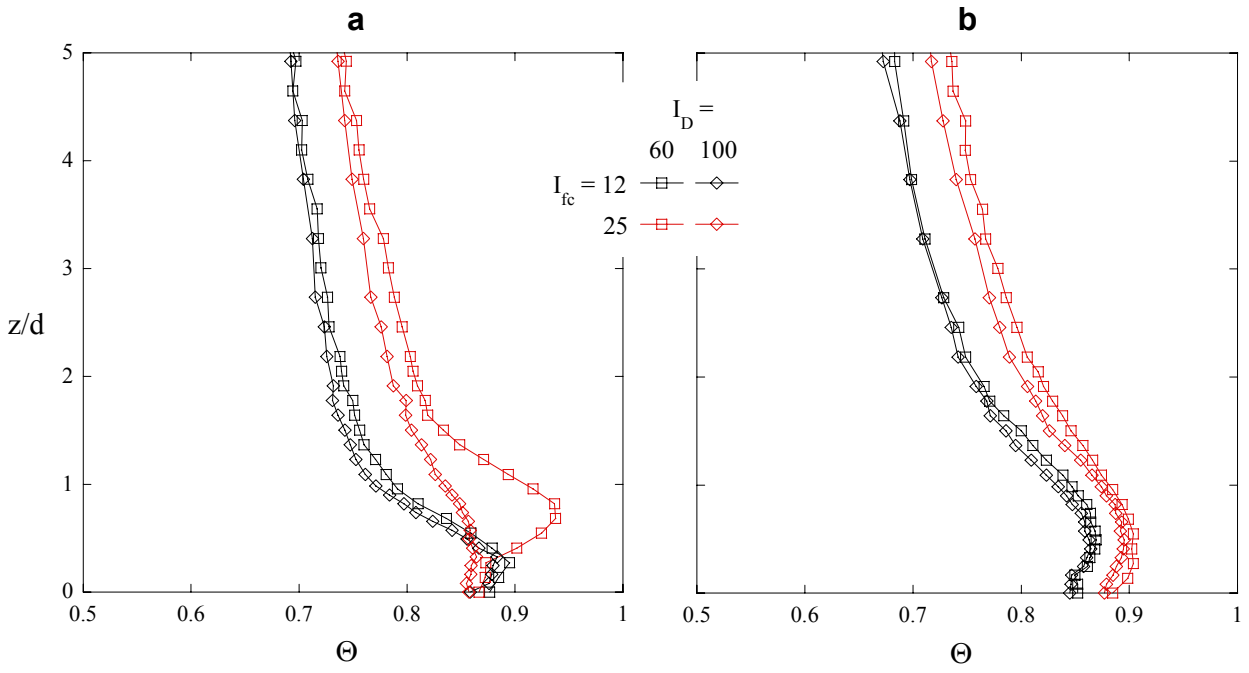

Figure 2.12. Temperature profiles on liner 1 at locations a) US and b) DS for all flow cases.

location the temperature profile was sensitive only to the film cooling flow rate, where the higher cooling flow resulted in a higher surface cooling effectiveness, $\Theta = 0.85$ and 0.88 for $I_{fc,in} = 12$ and 25, respectively. The temperature profiles at $X/D_L = 5.7$ were independent of the dilution jet momentum flux ratio because the mainstream turbulence relaxed to similar levels.

In the near-wall region at location US (Figure 2.12a) the higher film cooling flow ($I_{fc,in} = 25$) was more sensitive to the effect of the dilution jets. At that coolant flow rate the presence of additional cool air, via increased dilution jet injection, led to lower effectiveness in the region $Z/d < 1.7$, and the rest of the coolant layer was largely unaffected. The primary cause is that the mass-averaged coolant momentum flux ratio for $I_{fc,in} = 25$ was effectively higher for $I_D = 60$ ($I_{fc} = 4.1$) than $I_D = 100$ ($I_{fc} = 3.2$) at the thermal field measurement locations as established in Figure 2.6. In conclusion, the dilution jets with a higher momentum flux ratio reduced the local cooling jet momentum flux ratio and increased the production of turbulence which spread the coolant laterally and prevented it from accumulating. This resulted in decreased cooling downstream of the film cooling jet.

At the lower coolant flow ($I_{fc,in} = 12$) the cooling effectiveness was independent of the dilution jet momentum flux ratio. This is mostly due to the similarity of the local mass averaged

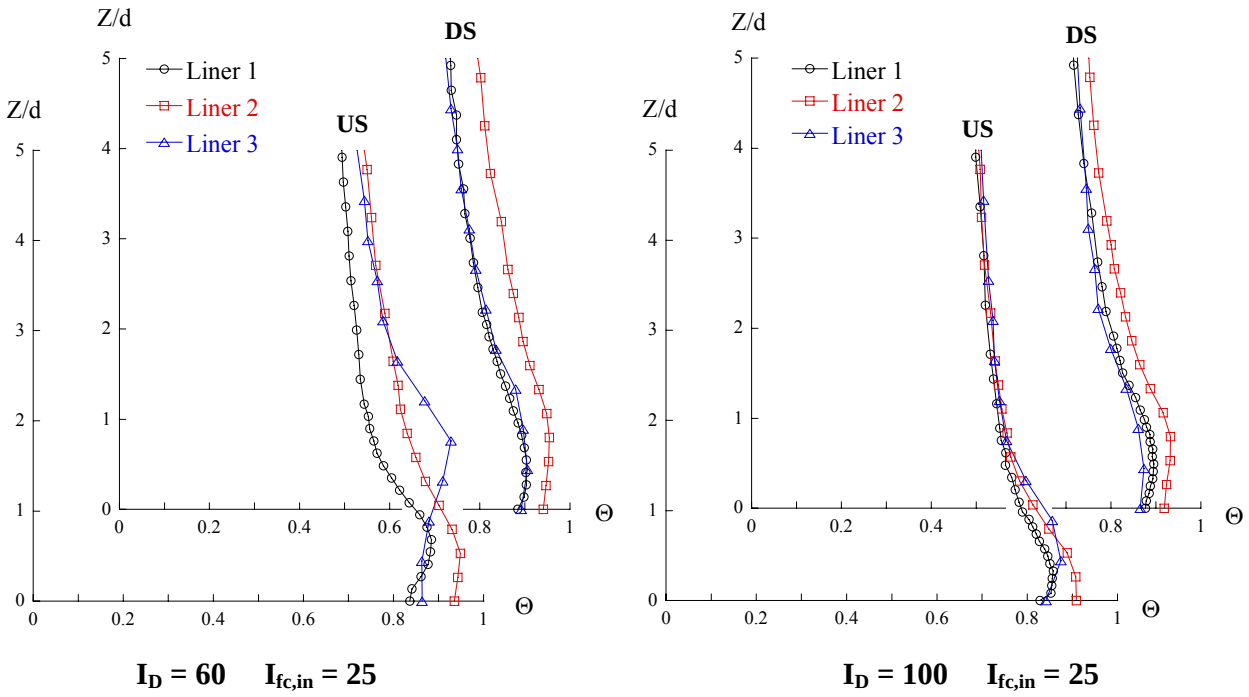

Figure 2.13. Temperature profiles for all liners at location US and DS for $I_{fc,in}$ = 25 and I_D = 60 (left) and I_D = 100 (right).

film cooling momentum flux ratios at the low and high dilution flows as shown in Figure 2.6. The temperatures are also similar because the spreading of the jet did not reduce cooling effectiveness because the temperature of the approaching coolant layer had effectively reached a steady value and is not changing in the axial direction.

Figure 2.13 presents the temperature profiles on all liners at the locations US and DS and compares the effect of the low and high dilution jet momentum flux ratios. These data show that the temperature profiles were sensitive to the cooling hole diameter and angle, the distance from the dilution jet injection, and the dilution jet momentum flux ratio. Liners 1 and 3 had similar surface cooling effectiveness values at all locations whereas liner 2 consistently had a higher value due to the shallower 20˚ cooling holes that inhibited turbulent mixing with the mainstream.

The temperature profiles measured at location US showed that the temperature trends were sensitive to the cooling hole diameter as well as the cooling hole angle. The minimum air temperature (maximum cooling air effectiveness, Θ) is a reliable identifier of the cooling jet core and it was used as a measure of the penetration height of the jets. Generally, it was observed that the cooling holes on liner 3 generated peaks in cooling effectiveness that were the highest from the liner surface, indicating that the jets from larger holes with constant spacing to diameter

ratios penetrated more into the crossflow. As previously mentioned, liners 1 and 3 produced similar surface effectiveness values which were as much as 11% lower than liner 2.

The temperature profiles that were measured at location DS revealed that the trends were very similar between all of the liners at that location. However, liner 2 shows higher cooling effectiveness below Z/d < 20. It is interesting to note that only the surface angle, not the number of cooling holes or the hole diameters, affected the surface cooling effectiveness at this location. These results agree with the findings of Lin et al. [13] who investigated a number of effusion cooling hole designs. They found that the hole injection angle and hole spacing are the primary parameters affecting adiabatic film cooling effectiveness. The measurements in Figure 2.13 made at location US for $I_D = 100$ and $I_{fc} = 25$ show that the temperature profiles were similar for all the liners above Z/d > 1.8 due to the presence of the higher turbulence from the $I_D = 100$ injection.

Conclusions

The durability of a gas turbine combustor requires that there is effective cooling of the component surfaces. The sensitivity of the coolant layer to the cooling hole diameter and angle and jet momentum flux ratio was investigated in this study. The effect of the dilution jet momentum flux ratio was also studied. The sensitivity of the cooling layer was determined through radial velocity and temperature profiles.

The results of this study indicate that the high mainstream turbulence and complex flow field created by the dilution jet injection strongly affected the behavior of the coolant layer. All of the effusion liners, featuring various cooling hole diameters and inclination angles, resulted in comparable cooling jet penetration heights. The penetration height was found to be about two cooling hole diameters based on the Reynolds shear stress magnitude. The Reynolds shear stress above the coolant layer in the mainstream depended on the proximity of the measurement to the dilution jet injection. It was found that at 3.8 dilution hole diameters downstream of the dilution jets the mainstream Reynolds shear stress magnitude was comparable to the value in the film cooling shear layer. At a downstream distance of 5.7 dilution hole diameters the turbulent transport in the mainstream relaxed and the Reynolds shear diminished to a negligible value.

It was found that film cooling liner 2 ($\alpha = 20^\circ$, d = 0.46 cm) consistently resulted in the lowest turbulence. This desirable characteristic is an outcome of the shallower cooling holes, as

they result in less entrainment of the crossflow into the jet wake. The velocity measurements taken at X/D_L = 3.8 (recall that these measurements were made x/d = 2.4 downstream of the cooling hole) indicated that there is a significant negative Reynolds shear stress component in the bottom film cooling jet shear layer for liners 1 and 3. This is attributed to jet lift-off and entrainment of lower speed flow in the wake region. This phenomenon was not seen on the 20˚ holes of liner 2, where only positive Reynolds stress values were observed, indicating that the jet core was diffusing which led to an overall reduction in shear stress. Based on the thermal profiles, liner 2 also resulted in the best surface cooling at all dilution and film cooling flows and at all locations.

Acknowledgments

The authors gratefully acknowledge United Technologies – Pratt & Whitney for their support of this work.

Nomenclature

d	film cooling hole diameter
D	downstream measurement location
D_S, D_L	small, large dilution hole diameter, respectively
H	combustor height
I	momentum flux ratio, $I = \rho_{fc} U_{fc}^2 / \rho_\infty U_\infty^2$
L	directly downstream of large dilution jet, film cooling hole length
$\dot{m}$	mass flowrate
M	mass flux ratio, $M = \rho_{fc} U_{fc} / \rho_\infty U_\infty$, downstream of midpoint between dilution jets
N	number of film cooling holes
S	directly downstream of small dilution jet
S_s, S_p	streamwise, pitchwise film cooling/dilution hole spacing, respectively
t	test plate wall thickness
T	temperature
TL	turbulence level, $TL = \sqrt{0.5\left((u_{rms}^2 + w_{rms}^2)\right)} / U_\infty$
u, v, w	mean velocity components corresponding to X, Y, and Z, respectively

U	upstream measurement location, mass-averaged freestream velocity
W	test section inlet width
X, Y, Z	global coordinate system shown in Figure 2.2
x, y, z	local coordinate system with provisional local origin

Greek

α	inclination angle of cooling hole
Θ	air cooling effectiveness, $\Theta = (T_\infty - T)/(T_\infty - T_{fc})$
ρ	density
μ	dynamic viscosity
ν	kinematic viscosity

Subscripts

1, 2, 3	film cooling test liners 1, 2, and 3, respectively
D	dilution
fc	film cooling
in	inlet
L	large dilution jet
p	pitchwise direction
rms	root mean square of fluctuating velocity
s	test plate surface, streamwise direction
S	small dilution jet
∞	mainstream (primary flow)

References

[1] Odgers, J. and Son, N. N., 1975, "Film Cooling - The Effect of a Cold Jet Normal to the Coolant Layer," Winter Annual Meeting, Houston, Texas.

[2] Button, B. L., 1983, "Effectiveness Measurements for a Cooling Film Disrupted by a Single Jet," ASME Paper No. 83-GT-250.

[3] Martiny, M., Schulz, A., Wittig, S. and Dilzer, M., 1997, “Influence of a Mixing-Jet on Film Cooling,” ASME Paper No. 97-GT-247.

[4] Köhler, J. and Beer, H., 1984, "Effectiveness Measurements for a Cooling Film Disrupted by a Row of Jets," *International Communications in Heat and Mass Transfer*, vol. 11, pp. 505-516.

[5] Gritsch, M., Martiny, M., Schulz, A., Kim, S., and Wittig, S., 1998, "Gas Turbine Heat Transfer: Newest Developments in Components Performance," Heat Transfer 1998: Proceedings of the 11th International Heat Transfer Conference (IHTC), Kyongju, Korea, August 23-28, 1998.

[6] Vakil, S. and Thole, K. A., 2003, “Flow and Thermal Field Measurements in a Combustor Simulator Relevant to a Gas Turbine Aero-Engine,” *Journal of Engineering for Gas Turbines and Power*, vol. 127, pp. 1-11.

[7] Scrittore, J. J., Thole, K. A., and Burd, S., 2007, “Investigation of Velocity Profiles for Effusion Cooling of a Combustor Liner,” *Journal of Turbomachinery*, vol. 129, pp. 518-526.

[8] Bons, J. P., MacArthur, C. S., and Rivir, R. B., 1996, "The Effect of High Free-Stream Turbulence on Film Cooling Effectiveness," *Journal of Turbomachinery,* vol. 118, pp. 814-825.

[9] Mayhew, J. E., Baughn, J. W., and Byerley, A. R., 2003, "The Effect of Freestream Turbulence on Film Cooling Adiabatic Effectiveness," *International Journal of Heat and Fluid Flow*, vol. 24, no. 5, pp. 669-679.

[10] Andrews, G. E., Asere, A. A., Gupta, M. L., and Mkpadi, M.C., 1985, “Full Coverage Discrete Hole Film Cooling: The Influence of Hole Size,” ASME Paper No. 85-GT-47.

[11] Barringer, M. D., Richard, O. T., Walter, J. P., Stitzel, S. M., and Thole, K. A., 2002, "Flow Field Simulations of a Gas Turbine Combustor," *Journal of Turbomachinery*, vol. 124, pp. 508-516.

[12] Moffat, J. R., 1988, "Describing the Uncertainties in Experimental Results," *Experimental Thermal and Fluid Science*, vol. 1, pp. 3-17.

[13] Lin, Y., Song, B., Li, B., Liu, G., and Wu, Z., 2003, "Investigation of Film Cooling Effectiveness of Full-Coverage Inclined Multihole Walls with Different Hole Arrangements," ASME GT2003-38881.

Paper 3:

The Effect of a Film Cooling Layer on the Flow and Thermal Fields in the Near-Region of an Array of Staggered Opposed Dilution Jets

Abstract

The gas turbine combustor flow and thermal fields are very complicated due to the interaction of the flows required in combustors to enhance mixing of the combustion effluent and those required to provide film cooling to the component surfaces. A better understanding of how full-coverage film cooling affects the flow and thermal fields near the dilution jets would be useful to combustor designers seeking improved knowledge about the turbulence levels in the dilution jet shear layer as well as how the flow behaves as it approaches and interacts with the dilution jet.

This paper discusses experimental results from a combustor simulator tested in a large scale low speed wind tunnel with engine representative dilution and film cooling jet momentum flux ratios. The results indicate that when the high momentum dilution jets are injected into the crossflow, a localized region in the flow of high vorticity and velocity was created. It was found that when film cooling air was injected the inlet flow field and the wake were fundamentally changed and the vortex diminished significantly. The temperature field downstream of the dilution jet showed evidence of a hot region which was moderated appreciably by film cooling flow. There was also a significant increase in surface cooling effectiveness due to the addition of the film coolant. It was found that differences in the temperature fields were nominal as the film cooling momentum flux ratio was varied from 12 to 25 compared to the large mass flow increase of the coolant.

Introduction

The design of gas turbine combustors is a significant engineering challenge due to an increasing exit temperature demand and rigorous durability requirements. These requirements are met by using advanced cooling methods, such as full-coverage discrete hole film cooling in conjunction with dilution air injection that mixes and cools the combustion products. However, these two different flows can have competing effects, leading to a reduction in cooling effectiveness due to the generation of vortices and secondary flows that are inherent to high momentum jets in crossflow.

Film cooling is often injected in a full-coverage arrangement initialized upstream of the row of dilution jets and extending downstream of the dilution jets. Full-coverage film cooling is a well documented technique used to create a buffer of relatively cooler air between the hotter core flow and the combustor liner. It is necessary to understand how the film cooling flow mixes with the crossflow and dilution jet to generate the resulting flow and thermal fields.

The objective of the work presented in this study is to spatially resolve velocity and thermal fields of the flow approaching and interacting with a row of dilution jets. The approaching flow in most combustor designs is comprised of combusted gases and a coolant layer created by full-coverage discrete film cooling injection. Of interest are the mechanics of how the dilution jets interrupt the film cooling layer.

This paper presents results from a non-reacting combustor simulator with engine representative dilution and film cooling jet geometries and momentum flux ratios. Laser Doppler velocimetry was used to measure the velocity and turbulence characteristics. The flow field was measured with and without the presence of film cooling, injected from full-coverage discrete holes. The effect of cooling air injection on the thermal fields was also measured. Prior to a discussion of the results, relevant past studies will be discussed followed by a description of the experimental facilities and methods.

Past Studies

Many researchers have studied model combustor flows featuring jet injection pertaining to aerodynamic and thermal field measurements. These studies are relevant particularly as a comparison regarding the effect of film cooling on mixing jets in crossflow. Odgers and Son [1] studied how a single normal jet interrupted a slot cooling flow and affected the film cooling efficiency. These researchers found that effectiveness changes were related to the dynamic pressure ratio of the normal jet to the hot crossflow, which is analogous to the dilution jet momentum flux ratio. Slot film cooling played only a minor role in affecting the behavior of the normal jet, where there was as much as a 10% reduction of downstream effectiveness for normal jet dynamic pressure ratios above unity. Similarly, measurements made by Button [2] indicated that a normal jet (I_D = 0.25 to 4) injected into slot flow will always reduce cooling effectiveness compared to the slot flow alone.

Martiny, Schulz, Wittig, and Dilzer [3] measured the effect of interrupting a slot film cooling by a single large jet at I_D = 7 and 10. They determined that the normal jet caused a change in the coolant flowfield downstream of the jet leading to weaker coolant coverage by as much as a 25% reduction in adiabatic effectiveness. A conclusion from these researchers is that the coolant disruption is more dramatic at higher jet momentum flux ratios. These studies differ from the data presented in this paper, which features much higher dilution jet dynamic pressure ratios, discrete full coverage film cooling injection, and a focus on the resolved aerodynamic and thermal behavior near the jet injection.

Köhler and Beer [4] studied the influence of a row of perpendicularly injected jets on slot coolant flow. These researchers also found that when the normal jet momentum flux ratio exceeded unity the cooling film was disturbed and the normal jets penetrated into the mainstream resulting in enhanced turbulent fluctuations that intensified momentum and heat transfer. This resulted in diminished cooling effectiveness downstream of the jet row. However, they found that an increase in the slot film cooling injection velocity increased cooling effectiveness due to an increase in coolant fluid mass. Their results showed that the cooling effectiveness depended strongly on the jet momentum flux ratio and the spacing of the jets in the row. It was concluded that a row of jets always generate a higher turbulence level than a single jet and more closely spaced jets significantly reduce cooling effectiveness in the near jet and downstream region.

Gritsch, Martiny, Schulz, Kim, and Wittig [5] measured the effects of high momentum

normal jets on slot cooling film. The purpose of their study was to determine the reasons for the weak cooling protection downstream of the jet injection. The coolant blowing ratios investigated were M = 1 and 2 with a mixing jet momentum flux ratio of I = 7 and 10. One of the most important findings was the identification of a suction effect due to the counter-rotating vortices downstream of the jet injection that augmented heat transfer as high as 100% for all operating conditions considered. The adiabatic effectiveness decreased between 15 and 25% in the downstream region. The detrimental effect of the normal jet with a high jet momentum ratio was the most severe for low film blowing ratios which corroborates the work of Scrittore, Thole, and Burd [6] who studied how cooling effectiveness on an film cooled combustor liner is affected by a high momentum dilution jet injected at I_D = 60 and 125. Scrittore et al. [6] concluded that the higher momentum jet resulted in lower laterally averaged surface cooling effectiveness downstream of the dilution hole, amounting to a 10% reduction at I_{fc} = 12 and a 3.5% reduction at I_{fc} = 25. A high-velocity, high-turbulence region of streamwise vorticity was identified at the lateral edge of the dilution jet.

The turbulence levels in a combustor resulting from the dilution jet injection can be extremely high, as reported by Vakil and Thole [7]. They measured highly anisotropic turbulence levels throughout the combustor as well as a much thicker film cooling layer downstream relative to upstream of the dilution jets. The spreading of the coolant off the liner wall was attributed to the mixing caused by the very high turbulence levels.

Holdeman and Walker [8] performed a study aimed at identifying orifice configurations with optimum mixing within a minimum combustor length. These researchers developed an empirical model for the temperature field downstream of jets mixing with confined crossflow and they found that the momentum flux ratio was the most important parameter influencing penetration and mixing.

Sykes, Lewellen, and Parker [9] performed a study computing the vorticity dynamics of a jet in crossflow. This study investigated the effect the velocity ratios of 2, 4 and 8. These researchers computed the flow and vorticity field and found that the flow around the jet is similar to a separated flow around a solid cylinder. They also found that there is significant entrainment into the wake of the jet, indicated by significant upward velocity in the lee of the jet.

In summary, there is little experimental data existing in the literature measuring the spatially resolved flow and thermal fields in the near dilution jet region, especially focusing on the effect

of full-coverage film cooling injection. The current study is unique because it investigates the effect of full-coverage discrete hole film cooling as opposed to slot injection on the combustor flow and thermal fields created by the dilution jets injected at realistic momentum flux ratio. This study also implements a systematic approach to understand why the flow and thermal fields are altered by the presence of film cooling.

Experimental Facilities and Measurement Methods

The following section describes the combustor simulator facilities where the measurements were made. This includes a description of the dilution hole pattern, cooling hole liner and air flow rates that were used in an effort to attain as realistic flow conditions as possible. The methods used to measure the flow fields, temperature fields, surface temperatures and surface pressures are described in terms of the instruments and procedures. Also described is the uncertainty associated with the measurement methods.

Experimental Test Section Design

The measurements reported in this paper were made in a large-scale low speed recirculating facility. The geometric scaling factor for the test section is approximately nine times that of an actual combustor, which permitted good measurement resolution in the experiments. Figure 3.1 illustrates the wind tunnel containing the test section and film cooling/dilution injection plate.

The wind tunnel facility had flow and thermal conditioning capabilities suitable to attain a uniform and periodic thermal and flow field at the inlet of the test section. The thermal conditioning also served to create a temperature difference between the core flow and bypass flow, simulating the heat release due to combustion. A 50 hp axial fan supplied flow through a primary heat exchanger used to cool the flow, to a transition section that divided the flow into three channels including a primary channel, representing the main gas path, and two symmetric secondary outer channels, representing the dilution and coolant flow paths. Within the transition section of the primary channel, the flow immediately passed through a perforated plate that provided the necessary pressure drop to control the flow splits between the primary and secondary passages. At a distance 2 m downstream of the perforated plate, the flow passed through a bank of heaters followed by a series of screens and flow straighteners. A maximum heat addition of 55 kW was possible from the heater section that was comprised of three

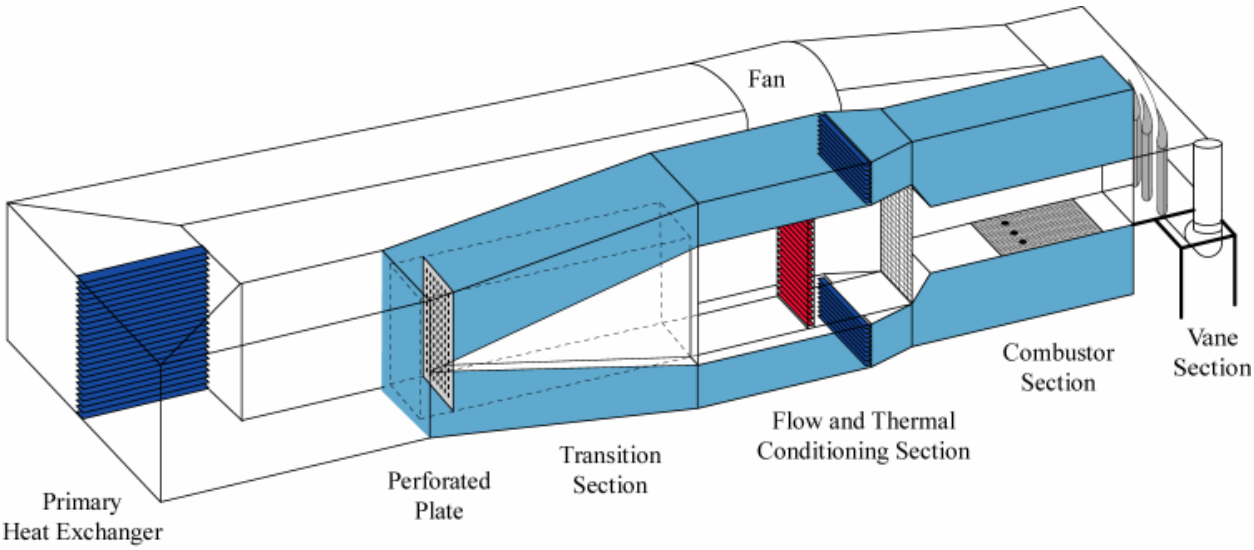

Figure 3.1. Illustration of the wind tunnel facility used for experiments.

individually controlled banks of electrically powered, finned bars. The flow passed through the screens and flow straighteners at the inlet of the test section.

In addition to heat being removed from the flow by a primary heat exchanger, the flow in the secondary passages passed through a second heat exchanger to further reduce the coolant flow temperature. The dilution flow was injected through one row of staggered, vertically opposed, normal jets from the top and bottom of the test section, which will be described further. The film cooling flow through the test plate was supplied from a plenum in the bottom secondary passage. An adjustable valve was used to meter the film cooling flow to ensure the correct mass flow was supplied to the plenum and, subsequently, to the combustor liner.

The inlet cross-sectional area of the test section was 1 m in height and 1.1 m in width. Immediately downstream of the flow straighteners, the primary channel flow was accelerated via a 45° contraction to a rectangular cross-section of 0.55 m in height (4.1 Z/D) and 1.1 m in width giving an exit to inlet cross-sectional area ratio of 0.55. The first row of film cooling holes was injected 1.3 m downstream of the contraction into the primary flow passage and the dilution jets were positioned 1.6 m downstream of the contraction.

Film Cooling and Dilution Hole Liner Design and Test Conditions

Flow and thermal planes were measured with and without film cooling injection. For cases without film cooling a solid bottom plate was installed and the dilution jets were injected into an

undisturbed crossflow. For the cases with film cooling, a full-coverage liner injected coolant upstream, between, and downstream of the dilution jets. The mass flow exiting the film cooling holes was set by applying the appropriate pressure ratio between the supply plenum total pressure and the exit surface static pressure. Using the appropriate discharge coefficient for the particular cooling hole and flow configuration based on the required ratio of coolant total supply pressure to surface static pressure, the mass flows through the test plate were established. The film cooling liner discharge coefficients were based on measurements made by Barringer [10]. The film cooling plate was constructed of 2.54 cm thick urethane foam with a low thermal conductivity (k = 0.029 W/mK) to allow for adiabatic surface temperature measurements. The dense pattern of 1197 streamwise oriented, cylindrical film cooling holes was cut into the urethane foam using a five-axis water jet. The holes were arranged into 35 rows in the streamwise direction. The hole pattern on the test plate is shown schematically in Figure 3.2.

Velocity and thermal planes were measured on the test plate as illustrated in Figure 3.3. There were seven total normal dilution jets, including three injected from the test section bottom and four from the top. These jets had diameters of 13.3 cm and were aligned in a staggered manner, illustrated in Figure 3.3. The pitchwise spacing of adjacent jets was 28.6 cm ($S_{p,D}/D$ = 2.14). Note that the reported coordinate distances were normalized by three parameters: the combustor height, H, the cooling hole diameter, d, and the dilution hole diameter, D. The dilution jet flow was controlled using cone valves and the jet velocity was measured directly using a pitot probe at the center of the jet. Streamwise and pitchwise profiles through the hole center were measured to qualify the flow and are reported in a later section.

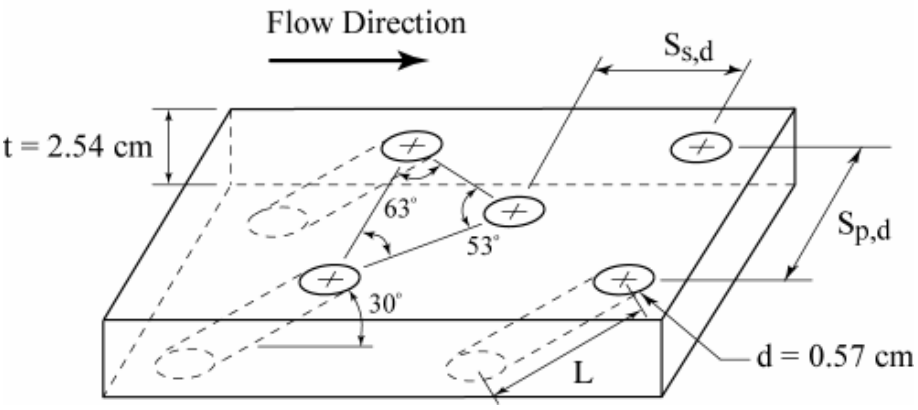

N	1197
d	0.57 cm
α	30°
L/d	8.9
t/d	4.44
$S_{s,d}/d$ $S_{p,d}/d$	4.86

Figure 3.2. Illustration of the film cooling holes detailing the layout and geometric parameters.

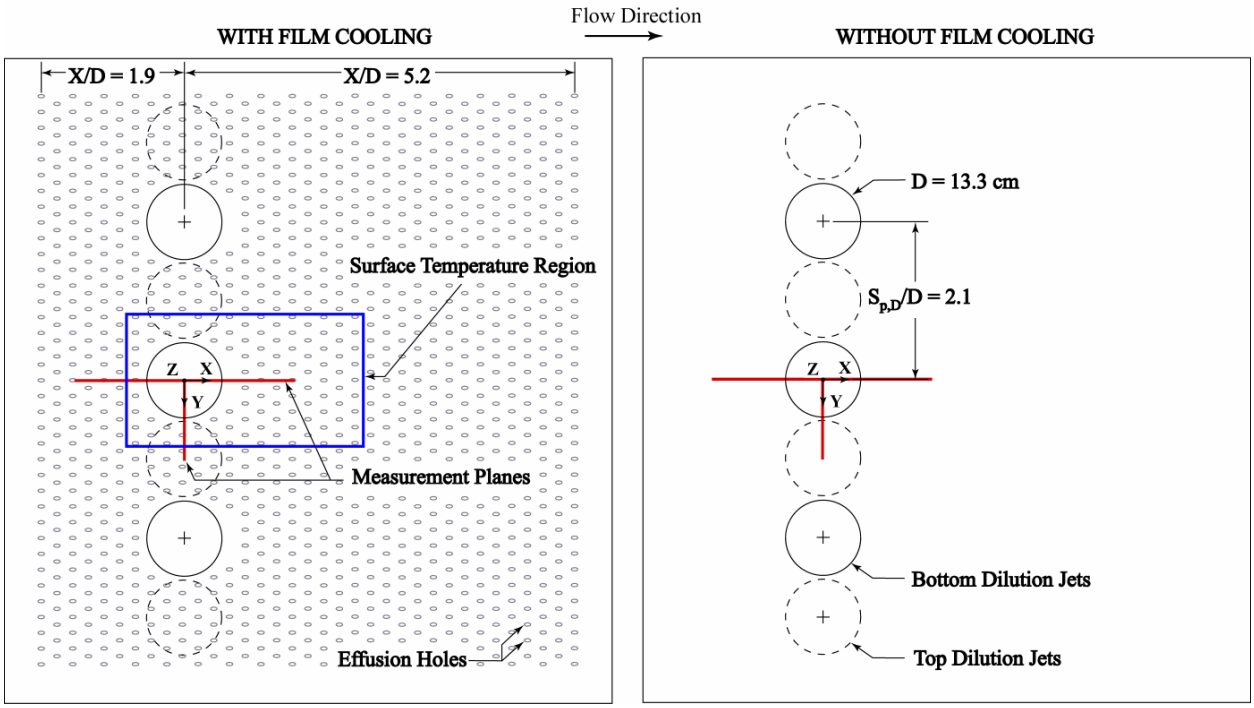

Figure 3.3. Illustration of the test plates highlighting the measurement planes.

For all of the data presented in this study, the dilution momentum flux ratio was I_D = 100. Two film cooling momentum flux ratios of $I_{fc,in}$ = 12 and 25 were tested that describe the cooling flow from the first row of cooling holes. This is an important distinction because the mainstream air flow accelerated in the streamwise direction which resulted in a decrease of the local film cooling momentum flux ratio. This trend will be discussed further and is shown in Figure 3.7.

Typical operating conditions for the flow tests consisted of a matched coolant and mainstream temperature of 30˚C. For the temperature field measurements, the mainstream and coolant temperatures were 50˚C and 20˚C, respectively. These conditions resulted in a coolant-to-mainstream density ratio of 1.0 for all of the unheated cases and 1.1 for all of the heated cases. The density ratios are not representative of realistic combustors, which have density ratios two to three times higher; however, the momentum flux ratios are consistent with realistic combustors. For the cases with film cooling, 65% of the total flow was directed through the secondary coolant passages with 9% for the film cooling and 56% for the dilution jets. The flow accelerated by a factor of 2.9 through the test section as a result of the mass addition. These flow conditions resulted in a test section inlet and exit Reynolds number of 5.6 x 10^4 and 1.6 x 10^5, based on the combustor inlet and exit heights, respectively. The average film cooling jet

Reynolds number was 2.1 x 10^3 and 3.1 x 10^3 for $I_{fc,in}$ = 12 and 25, respectively. The dilution jet Reynolds number was 1.36 x 10^5 based on the dilution hole diameter.

Measurement Methods and Uncertainty

Laser Doppler velocimetry (LDV) was used to make the flow measurements. The LDV system was equipped with two fiber optic probes capable of measuring three-components. To allow the measurement volume of the probes to reach the center of the test section, data was taken with a 750 mm focusing lens equipped with a 2.6 magnification beam expander. This configuration had a measurement volume of 73 μm in diameter and 1.3 mm in length. The flow was seeded with olive oil particles that were nominally 1 μm in diameter. The data was acquired with each probe angled 20˚ from perpendicular to the flow direction. In order to take measurements near the surface of the liner panel, the probes were tilted at 8˚ from the bottom surface. A trigonometric algorithm previously used by Vakil et al. [7] was used to calculate the true streamwise, pitchwise, and spanwise velocity components based on the non-orthogonal data captured from the three laser beam pairs. The nominal sampling time for each measurement location was 20 seconds and 10,000 data points were acquired for each of the three components. The probability of obtaining a sample was proportional to the speed of the flow; therefore, statistical particle bias corrections were applied to the data by weighting each individual sample based on the residence time of a particle in the probe volume.

A Flir EX320 infrared camera was used to take images of the adiabatic surface. Using thermocouples to calibrate the images, the camera captured the radiative heat flux emitted from the black painted panels. The infrared image was an average of five pictures which reduced the measurement uncertainty. Thermocouples were used in monitoring inlet and coolant temperatures and all of the temperature measurements were made using 30-gage, type E thermocouples that were connected to a data acquisition system through 20-gage thermocouple extension wire.

The partial derivative method, described by Moffat [11], was used to estimate the uncertainties of the measured values. The precision uncertainties for all of the measured values were calculated as ±2σ which corresponded to a 95% confidence interval of the normal distribution. The pressure difference between the plenum and the liner surface was measured using 60,000 samples with a 12.7 mmH_2O Setra pressure transducer, which had a bias

uncertainty of ±0.079% of the full scale (or ±0.10 Pa). The total uncertainty of the differential coolant pressure measurements was ±4.5% of the measured value.

The precision uncertainty for the streamwise velocities measured by the LDV was ±3.8% while the bias uncertainty for the mean velocity measurements was ±1% resulting in a total uncertainty of ±3.9%. The thermocouple measurements used to quantify the temperature planes and surface temperatures had a maximum precision and bias uncertainty of ±0.32°C and ±0.2°C, respectively, leading to a total uncertainty of ±0.38°C. The total uncertainty in the calculation of the non-dimensional temperature, θ, was ±0.019 at $\theta = 0.9$ and ±0.023 at $\theta = 0.3$. Uncertainty in surface cooling effectiveness, η, was found to be ±0.022 at $\eta = 0.4$ and ±0.021 at $\eta = 0.9$.

Experimental Results

Prior to a discussion of the results of the flow and thermal fields, the inlet flow conditions will be presented. Surface static pressures were measured on the combustor liner and are reported with an emphasis on how the dilution jet injection affected the flow field and consequently the film cooling momentum flux ratio. Static pressures were also measured on the solid plate in order to isolate the effects of the dilution injection. The flow measurements are reported in terms of streamwise, pitchwise, and spanwise components of velocity as well as turbulence levels. Temperature plane measurements are also discussed as they indicate how the flow transport affected the flow temperature and surface temperature.

Inlet and Coolant Flow Conditions

The inlet flow conditions were measured to ensure a uniform and periodic inlet flow. At the inlet to the test section, the flow accelerated through the 45˚ contraction and the straight channel began 7.75 dilution hole diameters upstream of the dilution injection. Velocity measurements at the channel mid-span shown in Figure 3.4 indicate that the flow velocity increased by 53% before it began to decelerate as it approached the dilution jet stagnation point. The velocity decreased by 18% from its maximum value at X/D = -6 to the value at X/D = -1. The mid-span velocity reached its maximum value at X/D = -6, and that value only changed by 1.1% between X/D = -6 to -4, suggesting that the velocity at X/D = -5 remained relatively unaffected by the contraction or the dilution jet injection. These measurements were made with a dilution jet momentum flux ratio of $I_D = 100$.

Based on the information from the measurements of Figure 3.4, inlet velocity profiles at X/D = -5 were measured at the channel mid-pitch (Y/W = 0, directly upstream of the center hole) and at Y/W = 0.25 which is directly upstream of the adjacent dilution hole ($Y/S_{p,D} = 1$). These inlet measurements were important because they ensured consistency when the film cooling momentum flux ratio was changed. Figure 3.5 presents the inlet flow and thermal profiles which were measured five dilution hole diameters upstream of the dilution jet row. A comparison of the streamwise velocity and turbulence levels of two inlet profiles in Figure 3.5a shows good agreement and, consequently, good uniformity. Flow profiles measured at Y/W = 0 with and without film cooling also agreed well. The turbulence level was 2.2% in the freestream, but there was a region of high turbulence in the near wall region (Z/H < 0.2) that was attributed to turbulence generation due to the wall. The non-dimensional temperature profiles of Figure 3.5a consisted of a vertical profile measured at mid-pitch and a pitchwise profile measured at mid-span. These profiles were somewhat affected by the test section side-walls.

The exit plane of the dilution jet was interrogated to ensure that the flow was reasonably uniform as shown in Figure 3.6. The streamwise profile through the hole center (Figure 3.6a)

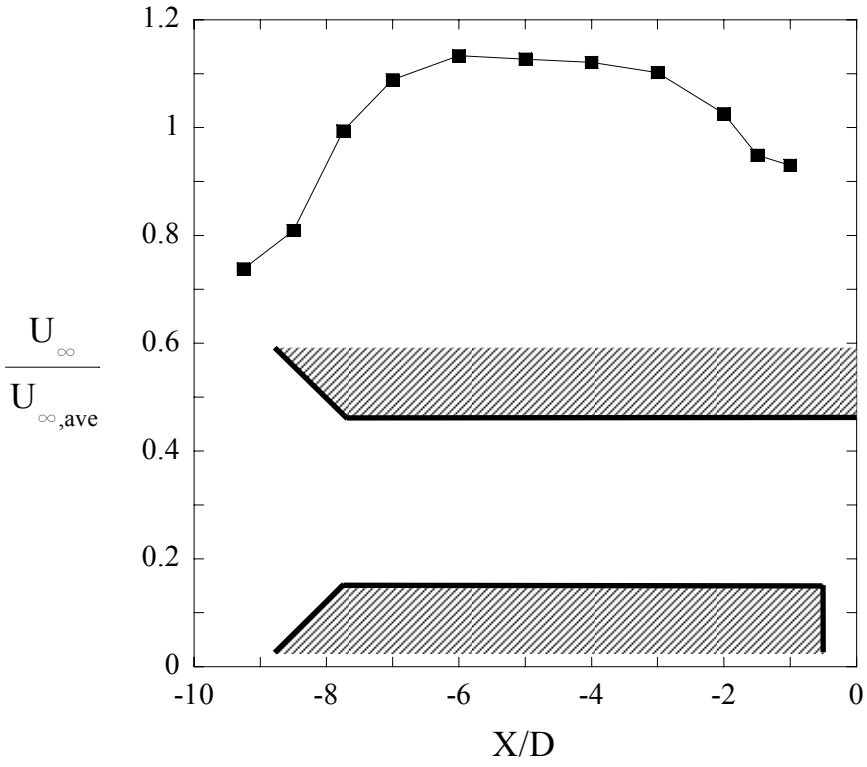

Figure 3.4. Flow velocity at center of the channel upstream of l_D = 100 jet injection.

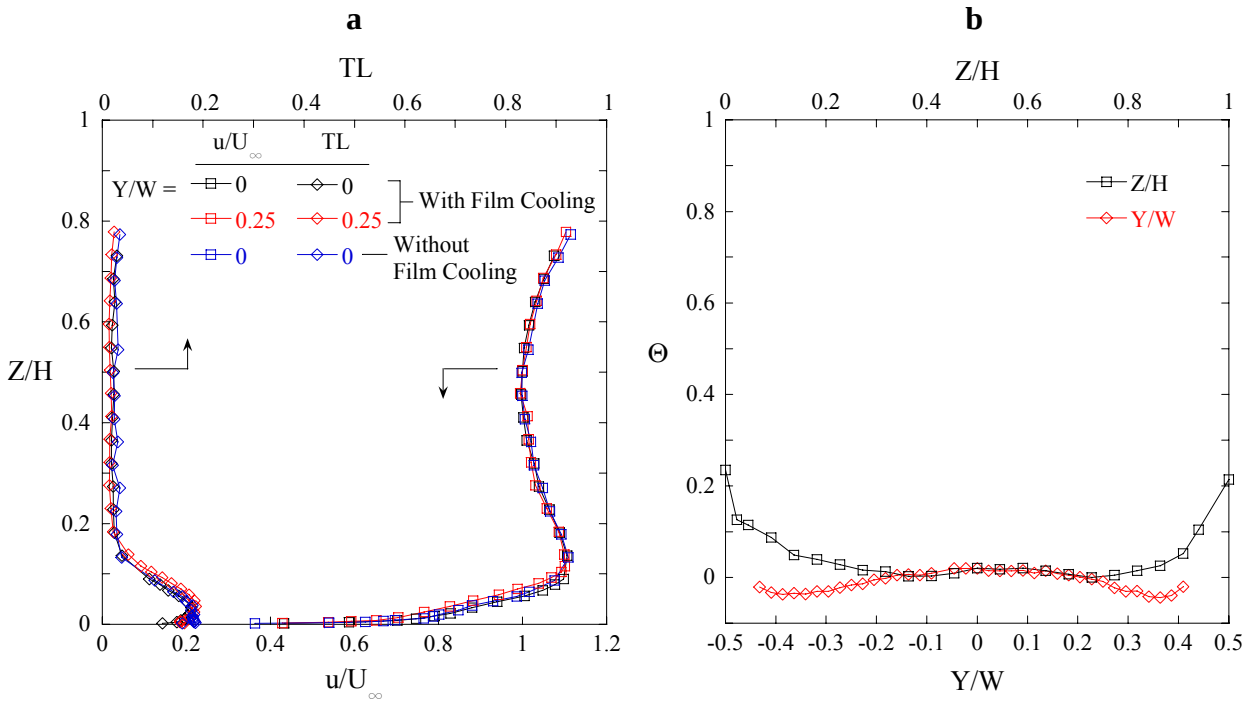

Figure 3.5. a) Spanwise velocity and turbulence level profiles and b) spanwise and pitchwise temperature profiles at the mid-pitch and mid-span, respectively. Measurements were made at X/D = -5 for I_D = 100.

revealed that the exit velocity was skewed toward the trailing edge, which is explained by the approaching crossflow partially interfering with the jet at the leading edge, which altered the pressure distribution of the dilution jet exit plane. The velocity across the hole was sufficiently uniform (Figure 3.6b), where the standard deviation was 1% of the average velocity. The average turbulence intensity based on the dilution jet velocity was 8%.

Static Pressure Measurements

The static pressure was measured on the surface of the combustor liner for the dilution jet momentum flux ratio of I_D = 100 to understand how the dilution injection affected the static pressure field for the flow cases with and without film cooling. Because the film cooling momentum flux ratio was set based on the inlet surface static pressure, the surface pressure measurements gave insight into how the film cooling velocity and, consequently, the momentum flux ratio varied in the dilution jet vicinity.

Figure 3.7 details the film cooling momentum flux ratios at each row based on the surface static pressure measurements. The mass averaged freestream velocity was calculated using the

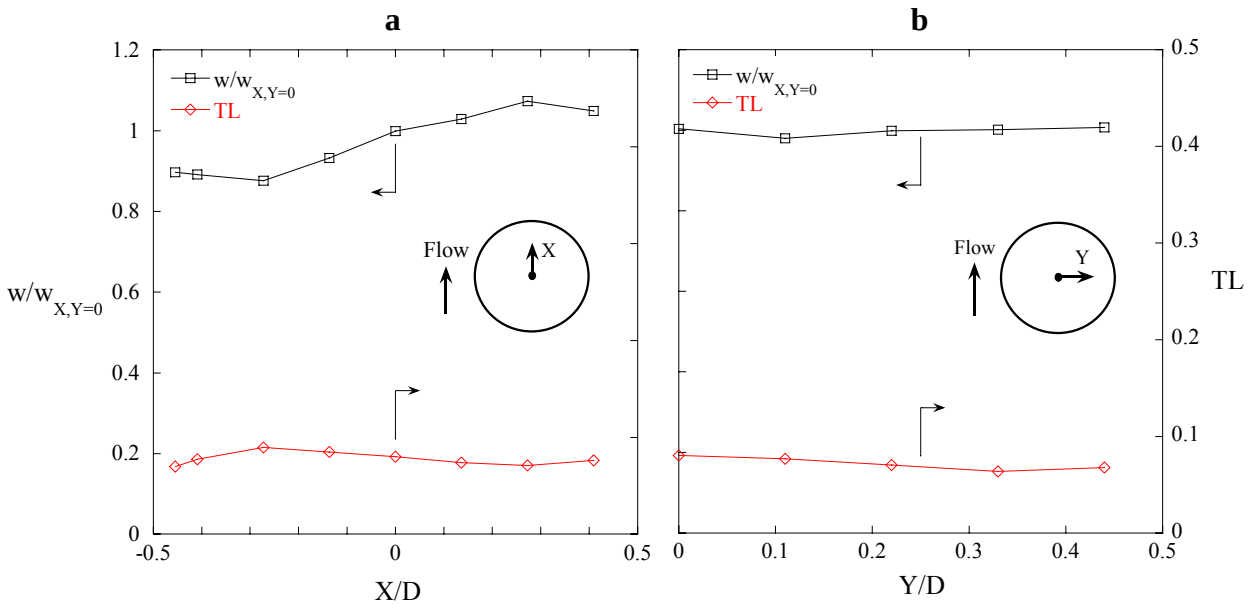

Figure 3.6. a) Streamwise and b) pitchwise profiles of the dilution jet velocity measured at the dilution jet exit plane for I_D = 100.

inlet velocity and mass addition of coolant from each row. The mass averaged momentum flux ratio for the film cooling jets was averaged over all of the cooling holes and was I_{fc} = 4.7 and 8.9 for the two film cooling flows of $I_{fc,in}$ = 12 and 25, respectively. At those film cooling flows, the pressure increase associated with the crossflow approaching the dilution jet corresponded to a 1.5% and 8.6% film cooling momentum flux ratio reduction, respectively.

On the solid plate (without film cooling) pressure taps were placed along the dilution jet circumference to measure the surface pressure variation around the dilution jet. The crossflow was either entrained or forced to accelerate between the adjacent jets. The accelerated crossflow created a large static pressure drop from the stagnation point to the lateral edge of the dilution hole as shown in Figure 3.8. The lowest static pressure was measured at φ = 113˚ where the pressure coefficient dropped to approximately C_p = -200. The location of minimum pressure signified the location of the fastest near-wall flow velocity. The near-wall flow velocity then decreased as it approached the wake of the jet. The static pressure at the downstream edge of the dilution hole was lower than upstream of the jet which was indicative of the separated flow of the jet wake.

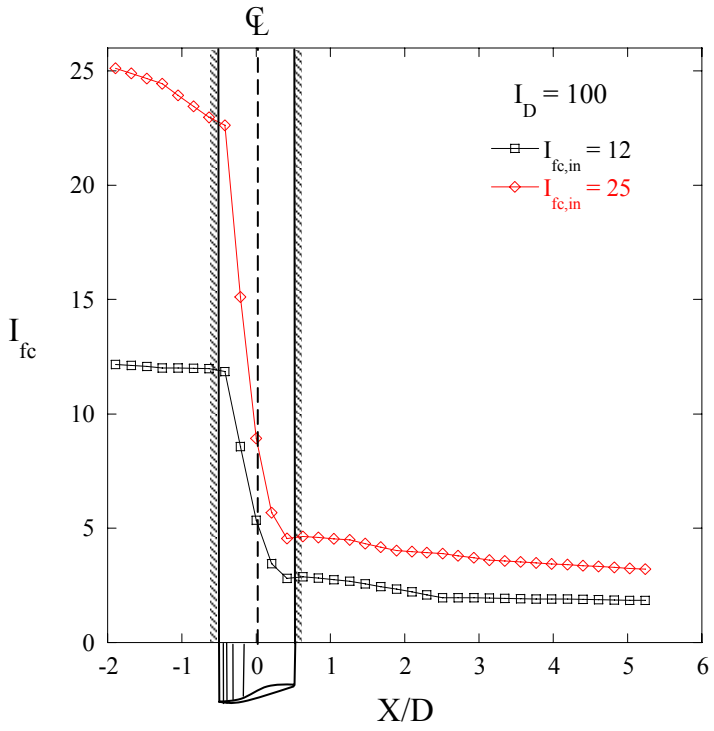

Figure 3.7. Local film cooling momentum flux ratios for I_D = 100.

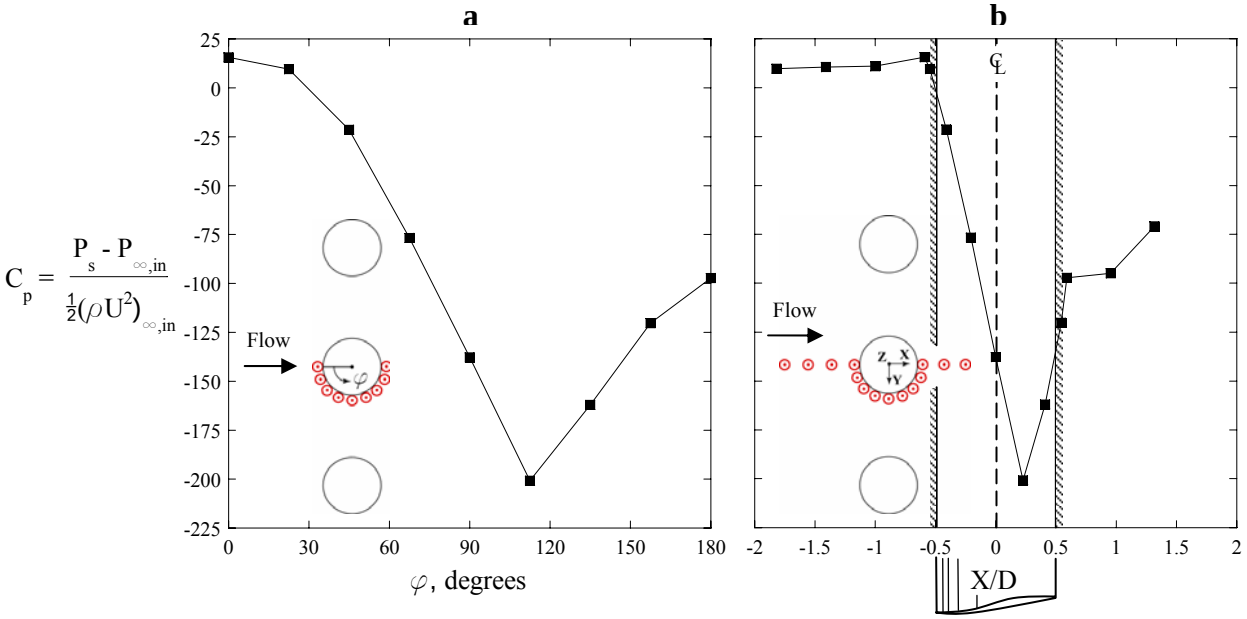

Figure 3.8. Pressure coefficient measured without film cooling as a function of a) the angular coordinate, φ, and b) the streamwise coordinate for I_D = 100. Red dots indicate static tap locations.

Flow Field Results

This section discusses velocity measurements measured at the two planes shown in Figure 3.3. The purpose of these measurements was to determine how the presence of film cooling flow affected high momentum normal jet injection into crossflow. Of interest was how the addition of film flow changed flow patterns, altered turbulence levels, and affected vortices. All flow measurements were normalized to the midspan velocity at X/D = -5.

The data shown in Figure 3.9 represent the flow patterns produced by a high momentum normal jet (I_D = 100, VR = 10) emanating into a crossflow Reynolds number 5.6 x 10^4 based on the inlet height. There was the presence of a region of very high streamwise velocity that reached a value of $u/U_{\infty,in}$ = 6.3 that was located very near the lateral edge of the dilution jet. This high velocity region will be discussed in more detail. The flow in the dilution jet wake was directed primarily upward until nearly midspan because the jet momentum was sufficiently high to outweigh the dilution jet bending influence by the crossflow pressure drag. At the near wall in the wake region, there was a negative velocity near the jet trailing edge that was comparable to separated flow in the wake of a solid cylinder.

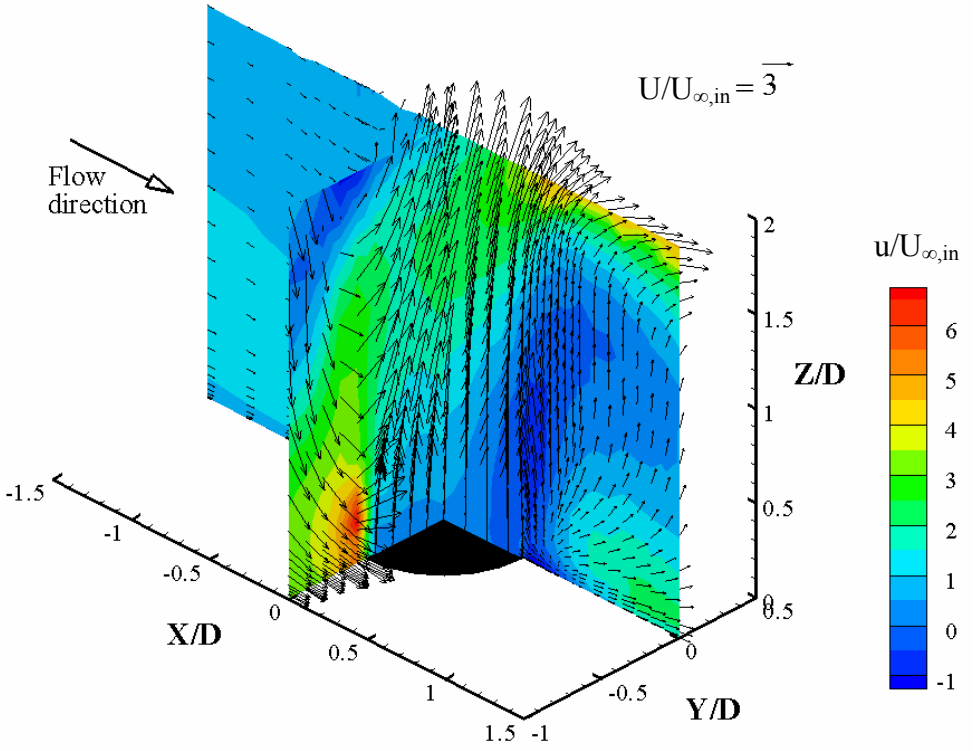

Figure 3.9. Streamwise and pitchwise flow planes showing flow velocity vectors and streamwise velocity component contours for a dilution momentum flux ratio of 100.

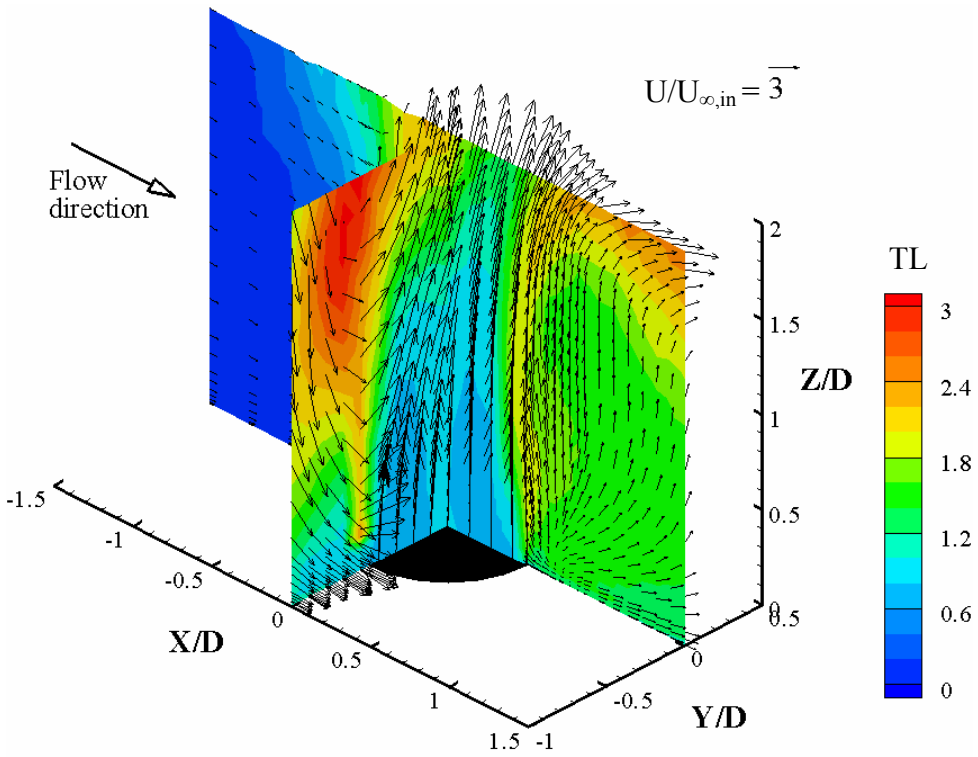

Figure 3.10. Streamwise and pitchwise flow planes showing flow velocity vectors and turbulence level contours for a dilution momentum flux ratio of 100.

A vortex was identified at the lateral edge of the dilution jet, centered where the flow attained its maximum streamwise velocity. This so-called bound vortex has been described by Moussa et al. [12] who found that the maximum streamwise and total vorticity in the cross-sectional plane was always found at the lateral edge of the jet at the near-wall. The measured vortex evolved from the shear layer vorticity of the jet, with the ultimate source from the pressure gradient at the interface between the jet and crossflow. Also, Aavani et al. [13] reasoned that the vorticity generated on the front and back walls in the jet passage, though not initially aligned in the streamwise direction, can be turned such that they are manifested as streamwise vortices.

A flow reversal was measured near mid-span where the bottom and top staggered jets interacted. The negative streamwise velocity reached $u/U_{\infty,in} = -1.1$. It should be reiterated that the top and bottom jets were not aligned, but staggered as shown in Figure 3.3. This implies that the opposing jets did not directly impinge, but instead interacted via a different mechanism. As the dilution jet penetrated, it also expanded laterally as it moved through the crossflow and formed a counter-rotating kidney-shaped vortex. Consequently, there was a negative streamwise velocity where the staggered jets interacted.

The highest turbulence level in both planes was measured at the location where the staggered jets coalesced as shown in Figure 3.10. The fluctuating velocity reached a maximum value of 2.8 times the local velocity and the turbulence intensity of the jet at the exit plane was 8% of the jet velocity. The turbulence was elevated because of the shear layer at the edges of the jet as it injected into the crossflow. It is interesting to note that at the lateral edge of the hole, the turbulence levels were not elevated until Z/D > 0.2, corresponding to where the lateral edge vortex was located. The entire wake region had a relatively uniform turbulence level of about 160%. At the midspan location where the flow from the jet developed a more predominant streamwise component (X/D, Y/D, Z/D = 1.0, 0, 2.0), the turbulence intensity reached a value of about 80% based on the local velocity magnitude. In conclusion, the majority of the turbulence was generated due to interaction of the staggered dilution jets.

Higher resolution measurements were made to better characterize the lateral edge vortex. Figure 3.11 shows a magnification of the vortex from the insets highlighted by the black boxes. A very strong rotational flow about the location of maximum streamwise velocity was measured. The vortex was at a location of very high velocity gradient due to the high speed flow of the

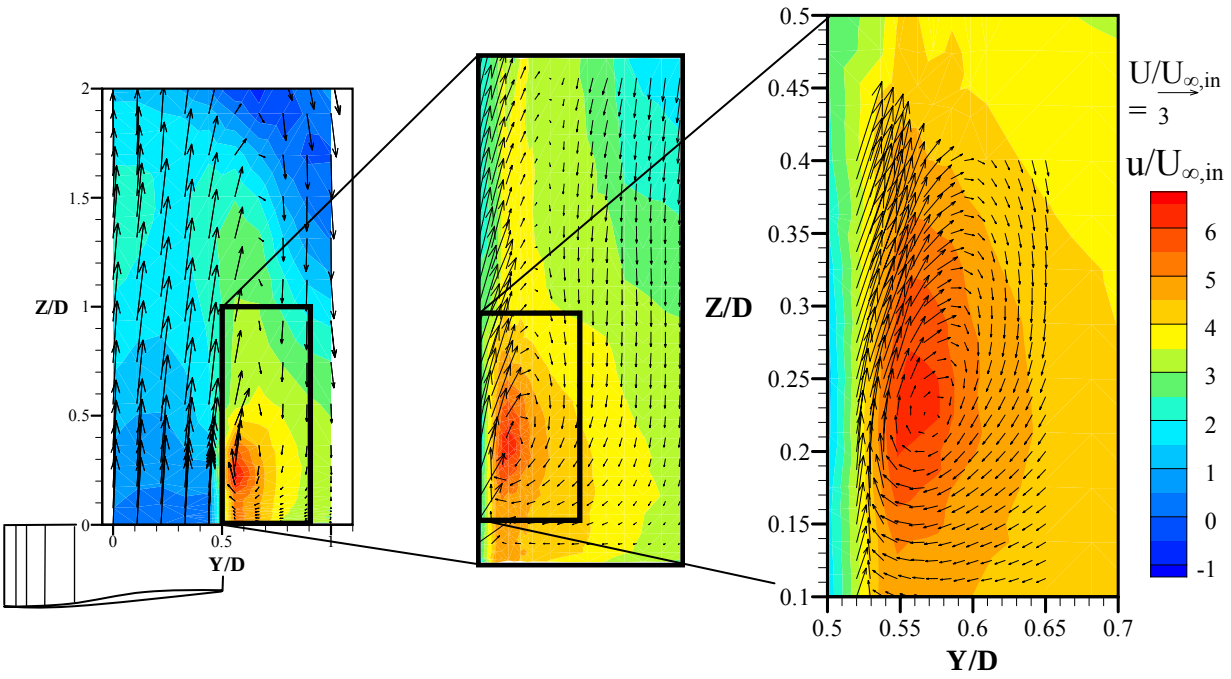

Figure 3.11. Pitchwise flow planes of velocity vectors and streamwise velocity contours for I_D = 100 without film cooling. Inset graphs identify a vortex centered at Y/D, Z/D = 0.57, 0.23, respectively.

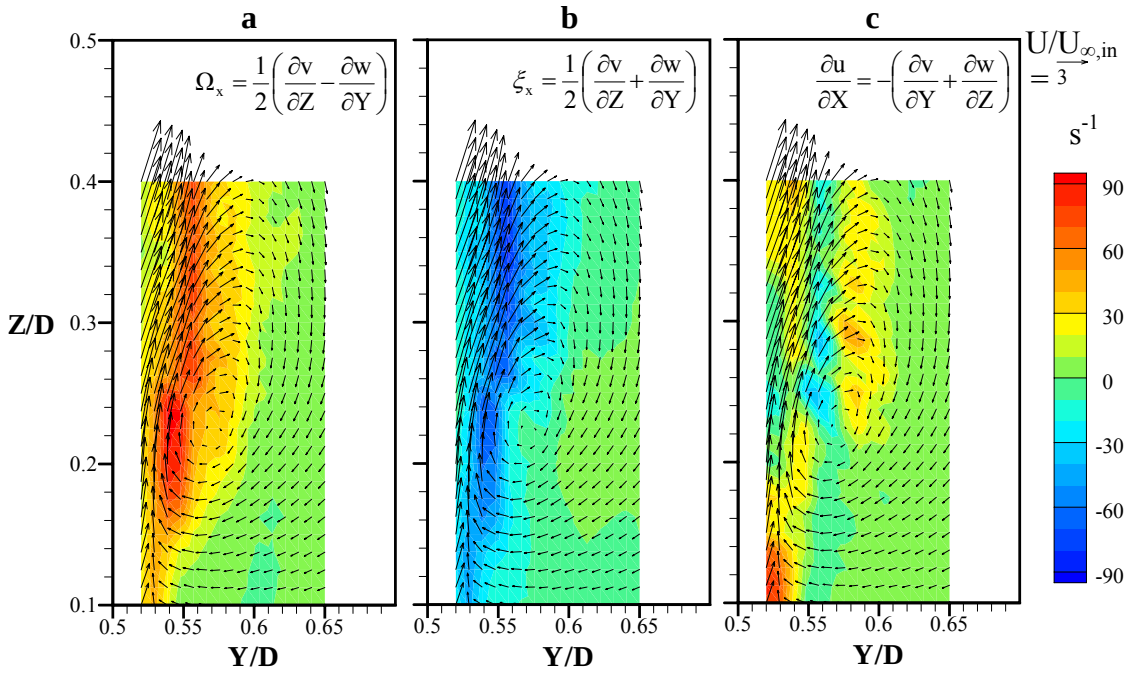

Figure 3.12. Pitchwise plane for I_D = 100 showing contours of a) rotation rate, b) rate of angular fluid distortion about an axis parallel to the x-axis and c) rate of change of streamwise velocity.

dilution jet. The lateral edge vortex was sustained by the crossflow that was directed downward toward the surface. The flow was induced downward toward the wall between adjacent dilution jets due to the high momentum from the staggered and opposed jets interacting and causing a flow blockage at the center of the test section.

It can be insightful to characterize the state of motion of the fluid by calculating the fluid element translation and rotation along with the various distortion mechanisms that can act on the fluid. The vorticity is a measure of the rate of rotation of the fluid element which does not result in a fluid stress. However, angular distortion of the fluid element is proportional to the shear strain. In the cross-sectional plane of Figure 3.12 (YZ-plane) the rate of angular distortion describes how the fluid is distorted about the X-axis. The angular distortion rate differs with the shear stress in the YZ-plane only by the absolute viscosity term. Considering that the flow is incompressible and has a constant temperature and density, the rate of change of the streamwise velocity in the streamwise direction ($\partial u/\partial X$) can then be calculated using continuity. Calculations of the flow field kinematics are useful in characterizing the viscous shear stresses in the flow given by $\tau_{YZ} = 2\mu\xi_X$.

The high positive values of average rotation rate, Ω_x, signify a strong clockwise rotation. The uniform rotation that this calculation quantifies cannot result in any stress in the flow. However, it is interesting to observe that the high rotation rate was primarily due to the high speed flow from the dilution jet that also caused a severe angular distortion of the flow. The rest of the flow field (Y/D > 0.6) resulted in a negligible rotation and distortion rate. The rate of change of the streamwise velocity was also only affected in the jet shear layer. The streamwise gradient was relatively isotropic apart from some locations in the jet shear layer. There was a negative streamwise velocity gradient at the center of the vortex. This suggests that the flow reached the maximum velocity at this location which is consistent with the fact that the smallest cross-sectional area of the space between adjacent dilution jets should be concurrent with the maximum crossflow velocity.

When film cooling was injected, the vortex was not present in the flow field at the lateral edge of the dilution jet as shown in Figure 3.13. Correspondingly, the maximum streamwise velocity was reduced from $u/U_{\infty,in}$ = 6.3 to 3.6 and the fastest crossflow was pushed further from the surface (Z/D > 0.7). For both cases the crossflow accelerated as it passed between the

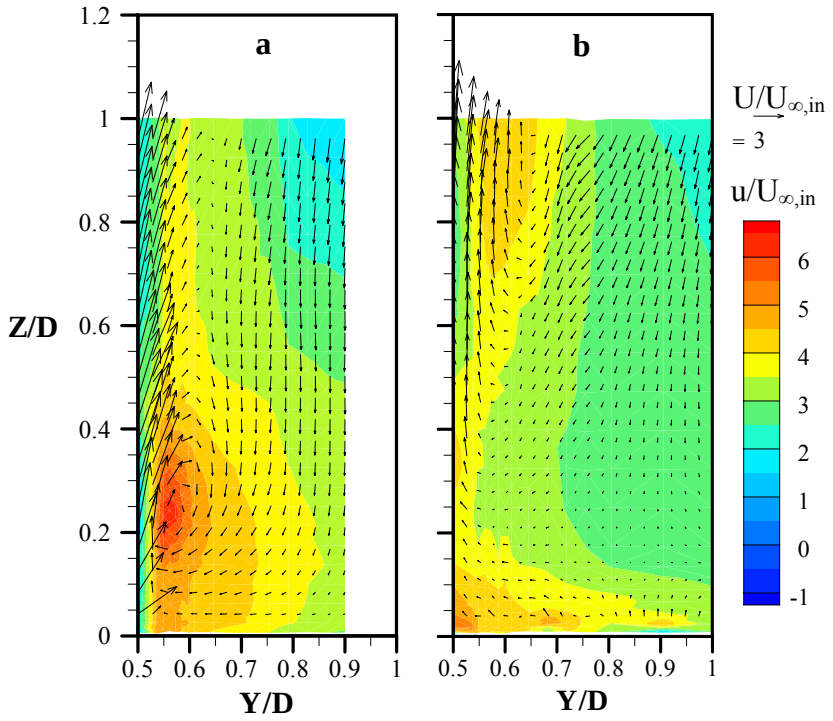

Figure 3.13. Comparison of streamwise velocity in the pitchwise flow plane for I_D = 100 a) without film cooling and b) with film cooling ($I_{fc,in}$ = 25).

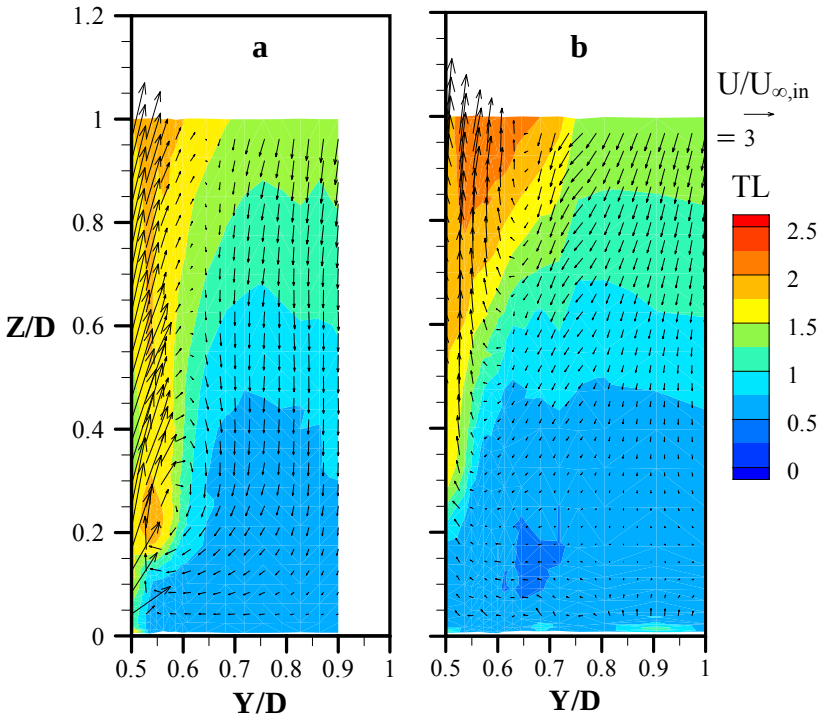

Figure 3.14. Comparison of turbulence level in the pitchwise flow plane for I_D = 100 a) without film cooling and b) with film cooling ($I_{fc,in}$ = 25).

dilution jets. There was also a lower overall streamwise velocity with film flow, especially in the region 0.1 < Z/D < 0.7, where the average velocity was approximately $u/U_{\infty,in}$ = 3. An explanation for the attenuation of the vortex will be given after an analysis of how film cooling affected the behavior of the flow field at the upstream edge of the dilution hole.

The effect of film cooling flow on the turbulence levels are compared in Figure 3.14. These measurements show that with film cooling, the high turbulence associated with the vortex disappeared and there was only shear layer turbulence. There was, however, an increase in turbulence at 0.7 < Z/D < 1.0, due to a combination of the shear layer and the relocation of the high speed streamwise flow. The turbulence level reached TL = 227% (Tu = 38%) at Z/D = 1 in the jet shear layer. Aside from turbulence level differences in the jet shear layer, a comparison of the remainder of the measurement region showed similar trends.

The increased flow velocity and increased turbulence levels away from the bottom wall with film cooling were due to a less negative spanwise crossflow velocity approaching the dilution jets. A consequence of this fact was that less flow was directed toward the bottom wall resulting in predominantly streamwise-directed flow in the region Z/D < 0.4 shown in Figure 3.13b. The

high streamwise velocity when no film cooling was injected was a consequence of the formation of the lateral edge vortex that was likely strongest at the lateral edges of the dilution jet.

Velocity profiles measured at three streamwise locations approaching the dilution hole stagnation point further highlight this phenomenon, shown in Figure 3.15. When film cooling air was injected beginning at X/D = -1.9 the core flow had a less negative spanwise component, meaning that the effect of the cooling air, even though required to have minimal penetration height into the mainstream flow for cooling purposes, influenced the upstream flow pattern up to mid-span (Z/D ≤ 2). This flow situation changed the crossflow pattern approaching the dilution jet which explains differences shown in Figures 3.13a and 3.13b. The film cooling injection created positive vertical w-momentum that permeated into the mainstream flow.

Detailed measurements of the dilution hole leading edge allow insight into how the crossflow and film flow interact with the dilution jet. Figure 3.16 presents these measurements, comparing the flow field without and with film flow injected at $I_{fc,in}$ = 25. The flow vectors are superimposed on turbulence level contours which indicate an elevated turbulence at the leading edge shear layer for both cases. The turbulence was higher in the leading edge shear layer when there was no film cooling flow. The turbulence reached a value of TL = 1.54 and TL = 1.42

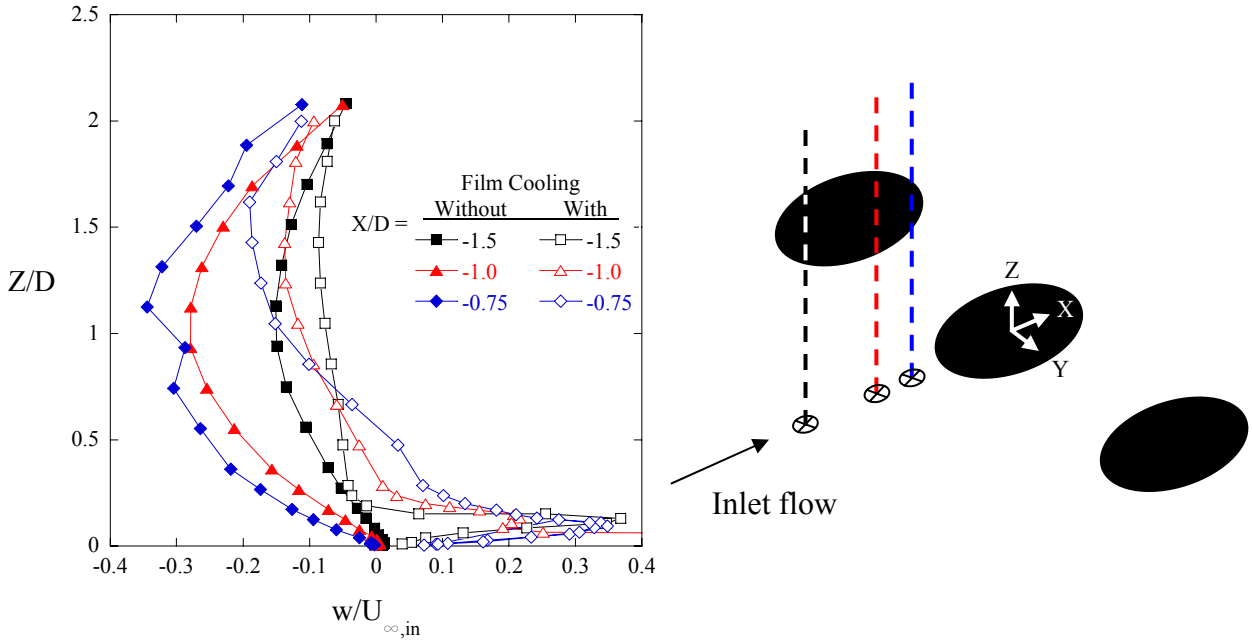

Figure 3.15. Spanwise velocity component profiles with and without film cooling flow at three streamwise locations upstream of the dilution hole for I_D = 100. For cases with film cooling $I_{fc,in}$ = 25.

without and with coolant, respectively. The generated turbulence was lower with film flow because the film reduced the velocity gradient at the shear layer. It should be noted that without film cooling there was no flow reversal at the near-wall indicating there was no vortex (see Figure 3.16a). However, there was a small flow reversal observed below the film cooling jet as it approached the upstream edge of the dilution jet. The vortex established by the flow reversal likely propagated vertical structures around the circumference of the dilution hole, which is a situation that was observed by Fric and Roshko [14] and Andreopoulos [15], and diminished the lateral edge vortex.

Another effect of the film cooling was the streamwise location of the maximum turbulence. Without film cooling the highest TL was located at X/D = -0.5. With film cooling the highest turbulence level was located further downstream at X/D = -0.45. This was because turbulence was transported along with the cooling flow and the turbulence was spread as it interacted and mixed with the dilution jet. The dilution jet vectors showed a slight downstream component when influenced by the film flow which suggests that the film momentum displaced the shear layer slightly downstream.

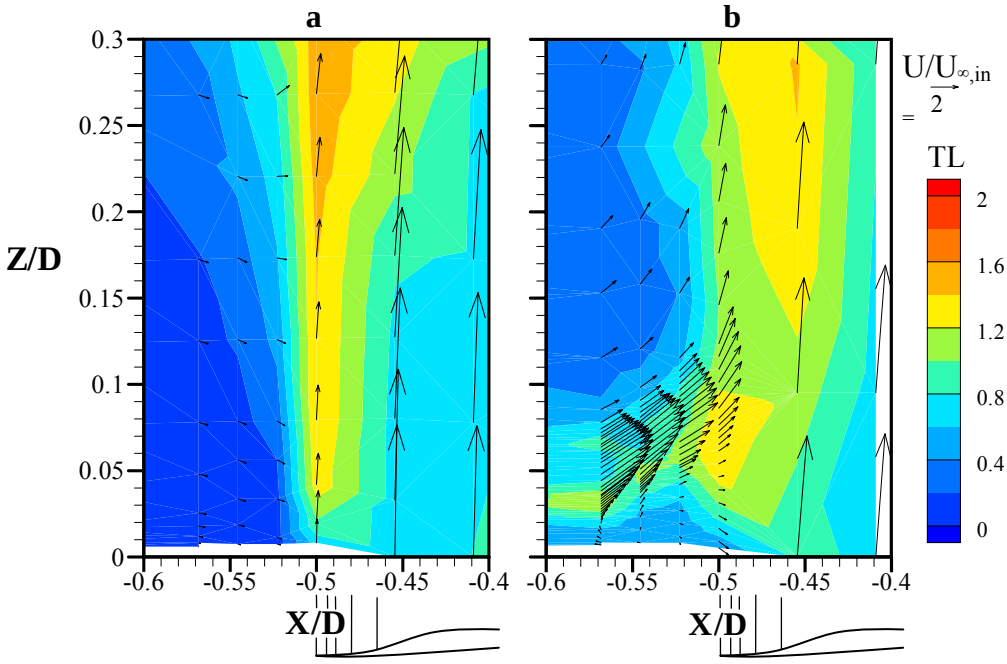

Figure 3.16. Comparison of turbulence level and flow vectors near the dilution hole leading edge (X/D = -0.5) for I_D = 100 a) without film cooling and b) with film cooling ($I_{fc,in}$ = 25).

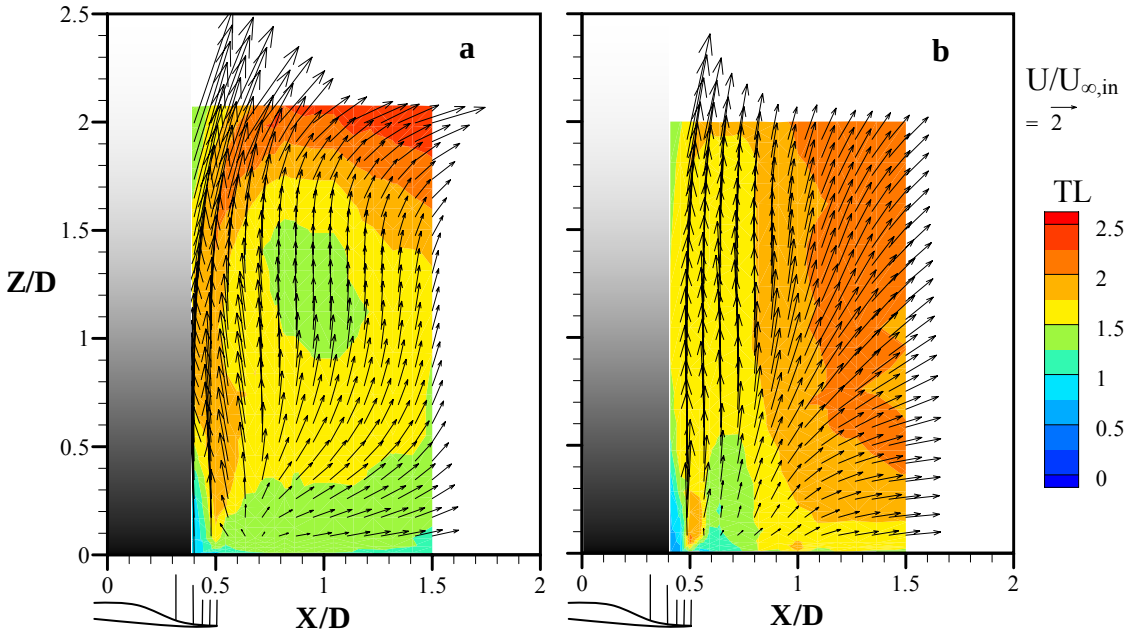

Figure 3.17. Comparison of turbulence level and flow vectors near the dilution hole trailing edge (X/D = 0.5) for l_D = 100 a) without film cooling and b) with film cooling ($l_{fc,in}$ = 25).

The flow field in the jet wake was very sensitive to the presence of film cooling flow. Velocity vectors of the XZ-plane were measured from the dilution hole trailing edge to X/D = 1.5 and these measurements illustrate the behavior in the dilution jet wake as shown in Figure 3.17. Near the wall there was a point at X/D = 0.7 where the velocity was nearly zero. The computations of Sykes et al. [9] revealed a zero-velocity point in the near-wall region at X/D = 1.5 which was further downstream as compared to this study. It is interesting to note that in the center of the plane where the turbulence level was lowest (1.0 < Z/D < 1.5) the directions of the velocity vector changed minimally. The presence of film cooling caused changes in the flow field such as 1) a more uniform spanwise velocity profile at X/D = 1.5, 2) less spanwise and more streamwise directed flow at mid-span and 3) very different turbulence level trends. The more uniform velocity profile at X/D = 1.5 with film cooling resulted in a more uniform turbulence level profile due to the more uniform velocity gradient.

Fric and Roshko [14] studied the wake of a transverse jet issuing into crossflow at velocity ratios in the range from 2 to 10. They found that the wake vorticity originated from the crossflow boundary layer fluid and not from the jet fluid, which is important when considering the mixing of the wake flow. Their results indicated that the wake contained essentially no jet

fluid suggesting that there was no substantial mixing of the crossflow and jet fluid within the wake. The film cooling flow would thus have a larger influence on the wake flow field than the dilution jet flow.

Thermal Field and Adiabatic Cooling Effectiveness Results

This section discusses temperature measurements made in a streamwise and pitchwise plane intersecting at the dilution hole center illustrated in Figure 3.3. These measurements were made to determine how well the addition of cooling flow in the highly turbulent environment near the dilution jet reduced the air and surface temperatures. The presented temperature data are in terms of the non-dimensional temperature term, Θ, a measure of the cooling capability of the flow where a value of unity represents the coolant temperature and zero designates the mid-span inlet temperature.

The temperature measurements in Figure 3.18 compare the thermal field of jet injection into a crossflow a) without film cooling and b) with film cooling. The thermal field of Figure 3.18a corroborates the velocity plane measurements, reinforcing the conclusion that the dilution jet had

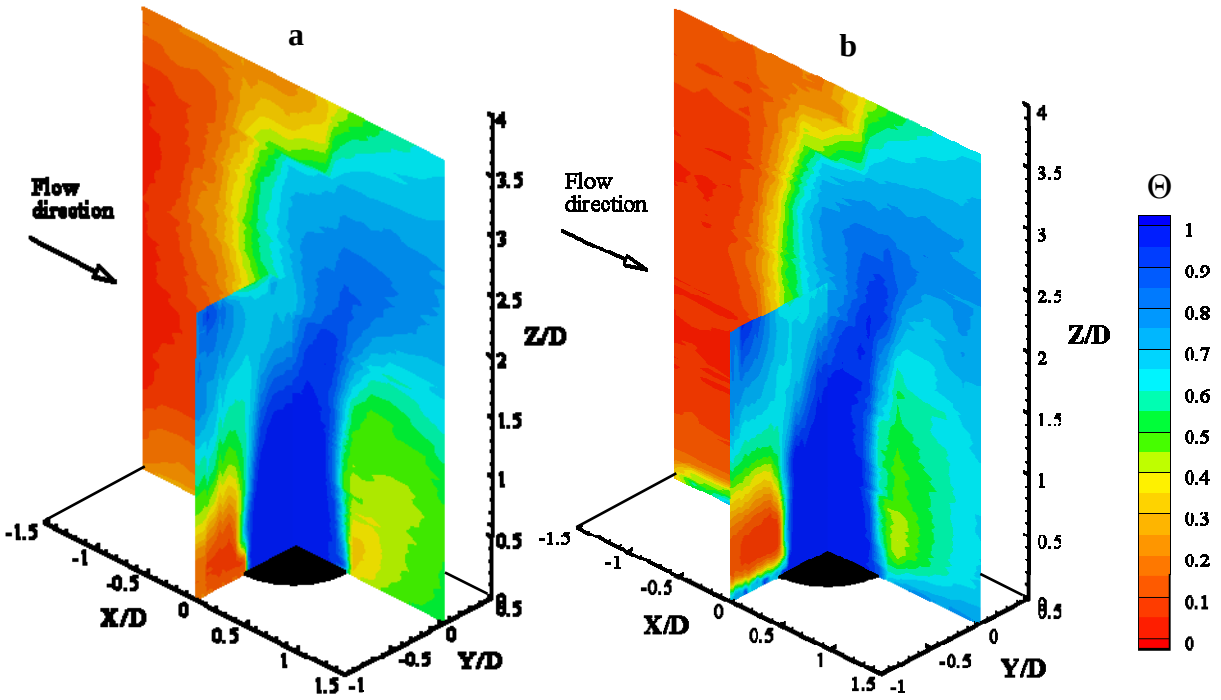

Figure 3.18. Comparison of temperature planes showing non-dimensional temperature contours for I_D = 100 a) without film cooling and b) with film cooling ($I_{fc,in}$ = 25).

a high penetration depth and produced a flow blockage that resulted in some cooler air being directed upstream at Z/D = 2.5. The dilution jet core, defined as a temperature of Θ = 0.95, penetrated up to Z/D = 1.5. These measurements also showed a region of high temperature in the near wall region adjacent to the dilution jet. Some of this hot flow was directed into the dilution jet wake and resulted in a warm region at the near-wall of the dilution hole trailing edge. The introduction of film cooling flow resulted in differences in the thermal field at the lateral edge and in the wake of the dilution jet. Film cooling provided an effective buffer between the hot flow and the surface, where all of the coolant remained below Z/D < 0.15 (Z/d < 3.5). The most drastic effect of the film cooling was observed in the dilution jet wake which was cooler relative to the wake with no film cooling.

When film cooling was injected, there was a cooling benefit in the jet wake on and off the surface. In order to quantify how sensitive the cooling benefit was to the film cooling momentum flux ratio, Figure 3.19 shows a comparison of the thermal field at a) $I_{fc,in}$ = 12 and b) $I_{fc,in}$ = 25. There was very little difference in the cooling effectiveness upstream of the jet, and the larger impact was in the wake region. Specifically, the largest effect of the film cooling

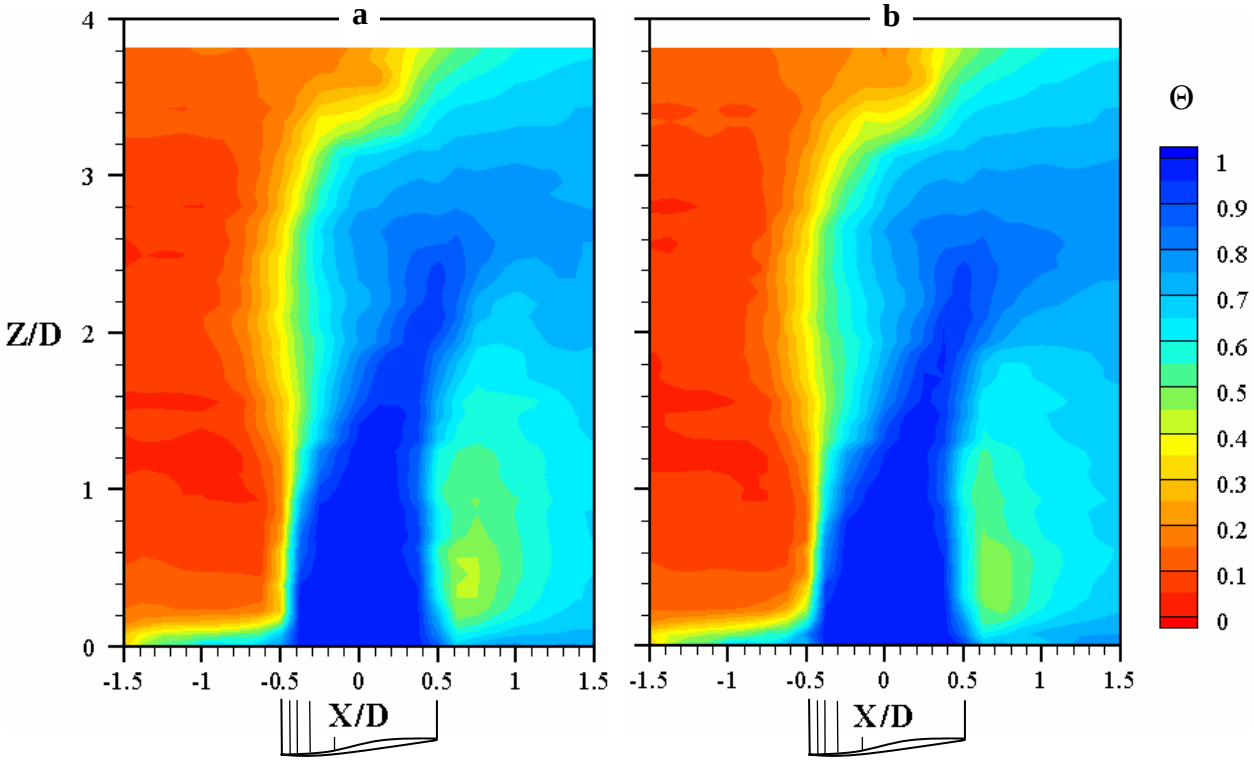

Figure 3.19. Streamwise temperature planes showing non-dimensional temperature contours at the dilution injection location for I_D = 100 in the presence of film cooling at a) $I_{fc,in}$ = 12 and b) $I_{fc,in}$ = 25.

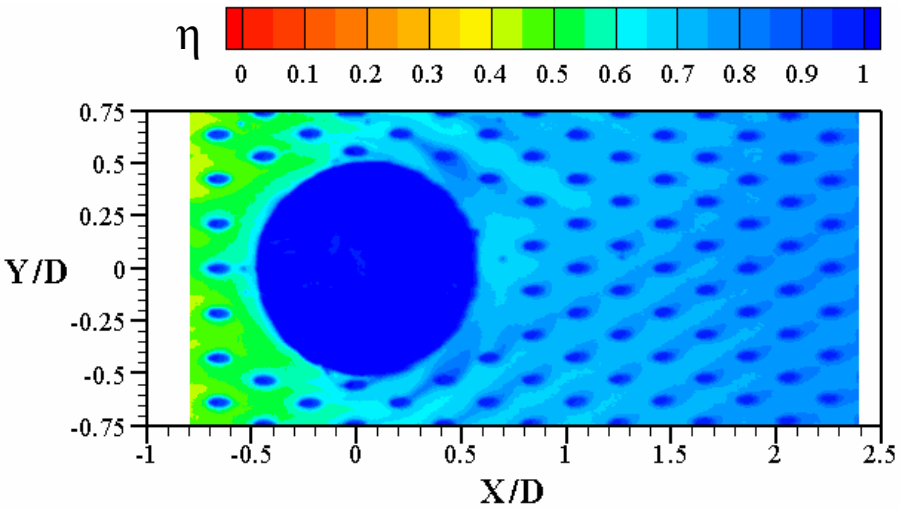

Figure 3.20. Adiabatic surface temperature measurements made on film cooling liner at flow conditions $I_{fc,in}$ = 25 and I_D = 100.

variation was on the warm region of the wake, causing a reduction in temperature. Additionally, a proportional relationship existed between the downstream surface cooling effectiveness and the momentum flux ratio. The high momentum flux ratio caused a temperature decrease resulting in a 5% increase in surface cooling effectiveness. The net benefit was nominal though compared to the 44% increase in coolant mass flow from $I_{fc,in}$ = 12 to 25.

Surface temperature measurements are shown in Figure 3.20. It should be noted that there were six rows of cooling holes upstream of this measurement region. These surface temperature measurements are valuable because they reveal how the cooling jets are being directed toward the downstream side of the dilution jet, mimicking the curvature of the dilution hole. It is evident that upstream of the dilution jet there were no coolant trails from the discrete holes, meaning that the cooling jets lifted off the surface due to the high momentum flux ratio created by the low velocity crossflow. However, the cooling jets in the region between adjacent dilution jets (-0.5 < X/D < 0.5) had a much lower local momentum flux ratio due to the faster crossflow (see Figure 3.7) and the jets stayed attached to the surface more effectively.

Conclusions

The flow and thermal fields created by staggered, vertically opposed dilution jet injecting into a low speed crossflow were investigated in this study. Special emphasis was made on how the film cooling injected from discrete cooling holes altered the velocity and temperature

characteristics at the near dilution region. The effect of the film cooling momentum flux ratio on the temperature field near the dilution jet was also quantified.

The results of this study indicate that there was a localized region of very high streamwise velocity and strong vortical rotation in the near-wall region at the dilution jet lateral edge produced by the shear layer vorticity between the dilution jet and crossflow. Further analysis of the kinematics of the vortex shows that there was a high rotation rate and high angular distortion rate. When film cooling was present, which is necessary to cool combustor surfaces, the vorticity was reduced and the high speed flow was pushed higher from the liner surface. This was caused by a change to the flow field upstream of the dilution jets whereby the injection of the film layer promoted vertical velocity up to midspan. The propagation of the horseshoe vortex in the presence of film cooling likely diminished the lateral edge vortex. The velocity and turbulence field in the dilution jet wake was also significantly altered in the presence of film cooling flow due to entrainment of the higher vertical momentum flow generated by the film cooling.

The cooling film played a role in determining the thermal field, such as in the wake immediately downstream of the dilution jet. Compared to no film cooling, film cooling flow injected at $I_{fc,in} = 25$ decreased the temperature at the hottest location with a corresponding increase in the surface cooling, η. However, there was little change to the thermal field as the film flow was varied from $I_{fc,in} = 25$ to $I_{fc,in} = 12$. The film flow was very effective at remaining near the wall in the region between adjacent dilution jets, where there was little penetration. This observation was consistent with static pressure and flow field measurements, as the crossflow was accelerated at that location resulting in a much lower film cooling momentum flux ratio. The surface temperature measurements corroborated the observation that the coolant stayed attached to the surface and was directed around the jet circumference toward the lee of the dilution jet.

Acknowledgments

The authors gratefully acknowledge United Technologies – Pratt & Whitney for their support of this work.

Nomenclature

C_d	discharge coefficient
C_p	pressure coefficient, $C_p = \left(P_s - P_{\infty,in}\right) \Big/ \frac{1}{2}\rho U_{\infty,in}^2$
d	film cooling hole diameter
D	dilution hole diameter
fc	film cooling
H	combustor height
I	momentum flux ratio, $I = \rho_c U_c^2 / \rho_\infty U_\infty^2$
L	film cooling hole length
$\dot{m}$	mass flowrate
M	mass flux ratio, $M = \rho_c U_c / \rho_\infty U_\infty$
N	number of film cooling holes
S_s, S_p	streamwise, pitchwise film cooling/dilution hole spacing
t	test plate wall thickness
T	temperature
TL	turbulence level, $TL = \sqrt{0.33\left((u_{rms}^2 + v_{rms}^2 + w_{rms}^2)\right)} \Big/ U_{m-a,in}$
Tu	turbulence intensity, $Tu = \sqrt{0.33\left((u_{rms}^2 + v_{rms}^2 + w_{rms}^2)\right)} \Big/ U_{local}$
u, v, w	local, mean velocity components corresponding to X, Y, and Z
U	total velocity magnitude
VR	velocity ratio, $VR = U_c / U_\infty$
W	test section inlet width
X, Y, Z	global coordinate system shown in Figure 3.2

Greek

α	inclination angle of cooling hole
β	compound angle of cooling hole
η	adiabatic surface cooling effectiveness, $\eta = \frac{T_{\infty,in} - T_{adiabatic}}{T_{\infty,in} - T_c}$

Θ	non-dimensional temperature, $\Theta = \frac{T_{\infty,in} - T}{T_{\infty,in} - T_c}$, dilation of the velocity vector
μ	dynamic viscosity
ν	kinematic viscosity
ξ	rate of angular distortion
ρ	density
σ	standard deviation
τ	shear stress
φ	rotational angle about dilution hole center from hole leading edge
Ω	rate of rotation of fluid element

Subscripts

adiabatic	adiabatic surface
ave	average
c	coolant (secondary flow)
fc	film cooling
in	combustor inlet
m-a	mass-averaged
p	pitchwise direction
rms	root mean square of fluctuating velocity
s	test plate surface, streamwise direction
x	about the x-axis
YZ	in the YZ-plane
∞	freestream (primary flow)

References

[1] Odgers, J. and Son, N. N., 1975, "Film Cooling - The Effect of a Cold Jet Normal to the Coolant Layer," Winter Annual Meeting, Houston, Texas.

[2] Button, B. L., 1983, "Effectiveness Measurements for a Cooling Film Disrupted by a Single Jet," ASME Paper No. 83-GT-250.

[3] Martiny, M., Schulz, A., Wittig, S. and Dilzer, M., 1997, “Influence of a Mixing-Jet on Film Cooling,” ASME Paper No. 97-GT-247.

[4] Köhler, J. and Beer, H., 1984, "Effectiveness Measurements for a Cooling Film Disrupted by a Row of Jets," *International Communications in Heat and Mass Transfer*, Vol. 11, pp. 505-516.

[5] Gritsch, M., Martiny, M., Schulz, A., Kim, S., and Wittig, S., 1998, "Gas Turbine Heat Transfer: Newest Developments in Components Performance," Heat Transfer 1998: Proceedings of the 11th International Heat Transfer Conference (IHTC), Kyongju, Korea, August 23-28, 1998.

[6] Scrittore, J. J., Thole, K. A., Burd, S. W., 2005, “Experimental Characterization of Film-Cooling Effectiveness Near Combustor Dilution Holes,” ASME Paper No. GT2005-68704.

[7] Vakil, S. and Thole, K. A., 2003, “Flow and Thermal Field Measurements in a Combustor Simulator Relevant to a Gas Turbine Aero-Engine,” *Journal of Engineering for Gas Turbines and Power*, Vol. 127, pp. 1-11.

[8] Holdeman, J. D. and Walker, R. E., 1977, “Mixing of a Row of Jets with a Confined Crossflow,” *AIAA Journal*, Vol. 15, No. 2, pp. 243-249.

[9] Sykes, R. I., Lewellen, W. S., and Parker, S. F., 1986, "On the Vorticity Dynamics of a Turbulent Jet in a Crossflow," *Journal of Fluid Mechanics*, Vol. 168, pp. 393-413.

[10] Barringer, M. D., Richard, O. T., Walter, J. P., Stitzel, S. M., and Thole, K. A., 2002, “Flow Field Simulations of a Gas Turbine Combustor,” *Journal of Turbomachinery*, Vol. 124, pp. 508-516.

[11] Moffat, J. R., 1988, “Describing the Uncertainties in Experimental Results,” *Experimental Thermal and Fluid Science*, Vol. 1, pp. 3-17.

[12] Moussa, Z. M., Trischka, J. W., and Eskinazi, S., 1977, "The Near Field in the Mixing of a Round Jet with a Cross-Stream," *Journal of Fluid Mechanics*, Vol. 80, pp. 49-80.

[13] Aavani, K., Taeibi-Rahni, M., and Soltani, M. R., 2006, "Experiments in Near-Field of Turbulent Jets into a Crossflow," *Scientia Iranica*, Vol. 13, No. 2, pp. 134-151

[14] Fric, T. F. and Roshko, A., 1989, "Structure in the Near Field of the Transverse Jet," *7th Symposium of Turbulent Shear Flows*, pp. 6.4.1-6.4.6.

[15] Andreopoulos, J., 1985, "On the Structure of Jets in a Crossflow," *Journal of Fluid Mechanics*, Vol. 157, pp. 163-197.

Paper 4:
Investigation of Velocity Profiles for Effusion Cooling of a Combustor Liner

Accepted for publication in the *ASME Journal of Turbomachinery**

Abstract

Effusion cooling of combustor liners for gas turbine engines is quite challenging and necessary to prevent thermal distress of the combustor liner walls. The flow and thermal patterns in the cooling layer are affected by the closely spaced film-cooling holes. It is important to fully document how the film layer behaves with a full-coverage cooling scheme to gain an understanding into surface cooling phenomena.

This paper discusses experimental results from a combustor simulator tested in a low-speed wind tunnel. Engine representative, non-dimensional coolant flows were tested for a full-coverage effusion plate. Laser Doppler velocimetry was used to measure the flow characteristics of the cooling layer.

These experiments indicate that the full-coverage film cooling flow has unique and scaleable velocity profiles that result from the closely spaced effusion holes. A parametric study of the cooling flow behavior illustrates the complex nature of the film flow and how it affects cooling performance.

*Co-authors: Dr. Karen A. Thole, Mechanical and Nuclear Engineering Department, Pennsylvania State University
Dr. Steven W. Burd, Pratt & Whitney

Introduction

Component cooling technologies play an increasingly important role as the firing temperatures of gas turbine combustors are raised higher than ever to meet the demand for higher turbine power. As combustor gas temperatures are well above the incipient melting temperature of the component metal, methods such as coating applications, film cooling (also referred to as effusion cooling), slot cooling, backside impingement, and backside pin fin cooling become necessary. Effusion cooling, which contains an array of closely spaced discrete film cooling holes, is widely used to cool the liner walls of gas turbine combustors. This cooling method forms a layer of cooling flow on the combustor liner to isolate the component metal from the hot mainstream flow. As such, high mass flow with little mixing is desired.

A large-scale re-circulating wind tunnel was used to simulate a typical combustor where full-coverage film-cooling flows were tested. The film cooling blowing ratios used in this study were typically higher than those presented for turbine applications and higher than most found in the open literature. The study presented in this paper did not include reacting flow; thereby effects attributed to the heat release due to combustion were not represented in this study. From these large scale tests, however, it was possible to understand the effects of film flow on combustor liner cooling.

The objective for the work reported in this paper was to compare the development of the film-cooling effectiveness to the developing flow field. A prediction of the cooling effectiveness based on the behavior of the film cooling flow would allow insight as to where a full-coverage cooling scheme becomes fully developed as defined by self-similar velocity profiles. After describing the characteristics of the combustor simulator facility, this paper describes results from the experiments conducted using the effusion plate.

Past Studies

Many studies have documented both experimental and computational data for film cooling flows. The large number prevents a full discussion of all of the results in our paper, but rather a subset will be discussed that is relevant to full-coverage, high momentum-flux ratio cooling flows.

A series of papers by Andrews et al. [1,2,3] have compared the influence of cooling hole size, pitch, and inclination angle through a number of experimental studies. In combustor

designs, the amount of coolant flow per surface area is considered in the selection of the cooling hole diameter and pattern to ensure that the intended pressure loss across the combustor is met. Andrews et al. [1] investigated normal (90°) cooling holes for a number of different arrays and found that there was a significant improvement in the overall cooling effectiveness for a larger hole relative to a smaller hole, which they attributed primarily to the fact that there were lower external heat transfer coefficients for the larger holes. Since they conducted these tests at high temperatures, they also found significant radiation effects. Andrews et al. [2] found that the heat transfer coefficients scaled well using a Nusselt number based on distance along the externally film-cooled plate and Reynolds number based on the cooling hole characteristics (diameter and jet velocity). Andrews et al. [3] also compared normal (90°) and inclined film holes (30° and 150°) for an array of effusion holes and found that cooling effectiveness improved with inclined holes. The counterflow holes (150°) resulted in reverse flow and good cooling performance at low coolant flows but not at high coolant flows. Lin et al. [4] also investigated a number of effusion cooling hole designs. They found that the hole injection angle and hole spacing are the primary parameters affecting adiabatic film cooling effectiveness. Interestingly, they also found that for co-flowing jet injection there was little effect of blowing ratio, but for counter-flow injection they found that blowing ratio had a large effect. This is consistent with work cited by Andrews et al. [3].

Martiny et al. [5] used a very low injection angle of 17° for an effusion, film-cooled plate in which they measured adiabatic effectiveness levels for a range of blowing ratios. Their results indicated significantly different flow patterns depending on the cooling jet blowing ratio. It is important to recognize that their study used only four rows of cooling holes and as will be shown in this paper, this small number of rows did not allow for a fully developed condition to occur.

Sasaki et al. [6] examined if it were possible to use a superposition method with a full-coverage film-cooling array. They found that, in fact, there was an additive nature of multi-row film-cooling that allowed the use of the superposition method. In a later study, however, Harrington et al. [7], who also studied a full-coverage film cooling array with normal jet injection, found that the superposition prediction of the full-coverage cooling effectiveness based on single row measurements tended to overpredict adiabatic effectiveness. They found that eight rows of cooling holes were required to reach an asymptotic "fully developed" adiabatic effectiveness level. These researchers also measured jet separations for their normal (90°) holes

at blowing ratios greater than 0.65.

Fric et al. [8] used flow visualization techniques to detect cooling jet separations and coalescence as a function of blowing ratio. They found that the film coverage is minimum for the blowing ratios from 1.7 to 3.3 and film coverage improves above this range. Bazdidi-Tehrani et al. [9] found that there was little effect of the density ratio on the film heat transfer coefficient for a given coolant mass flow per unit surface area, which was similar to their cooling effectiveness results. Pietrzyk et al. [10] found that higher density jets had higher penetration distances and lower velocities in the near wall region. It was also found that high and low density jets had similar maximum turbulence values, but there was a significantly lower turbulence relaxation rate for the high-density jets.

In summary, there is little data presented in the literature studying full-coverage, high momentum flux ratio cooling focusing on flow fields related to cooling effectiveness. While there is a wealth of film-cooling literature, much of this data is not applicable because of the high blowing ratios and densely spaced cooling holes required for most aero-engine combustors.

Experimental Facilities and Measurement Methods

The focus of this study was to obtain flow field measurements for a densely-spaced full-coverage array of film cooling holes. The characteristics of the flow and how they relate to the adiabatic cooling effectiveness for a realistic combustor cooling design are of interest to designers and a focus of this work. To achieve good spatial resolution, it was beneficial to use large-scale models while matching the relevant non-dimensional parameters. The primary measurement techniques used were laser Doppler velocimetry to quantify the flow field and an infrared camera to measure surface temperatures. This section describes the experimental facility in which these measurements were made, the instrumentation that was used, and the corresponding estimates of measurement uncertainty.

Experimental Facilities

The geometric scaling factor for the test section is approximately nine times that of an actual combustor, which permitted good measurement resolution in the experiments. The wind tunnel is illustrated in Figure 4.1 which contained the test section and effusion plate. Flow was supplied by a 50 hp axial fan. A transition section was downstream of a primary heat exchanger that

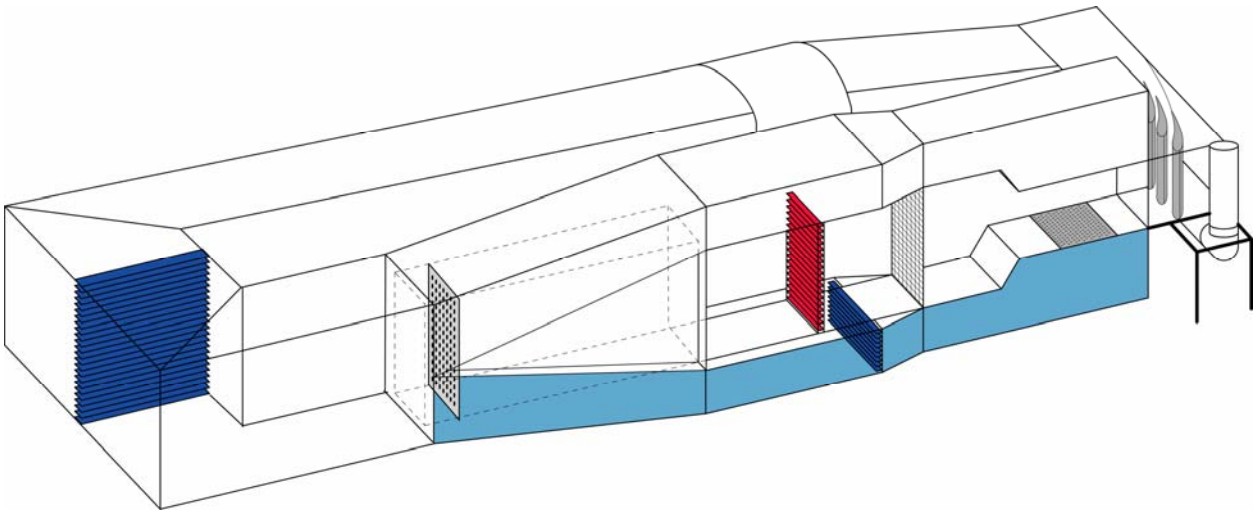

Figure 4.1. Illustration of the wind tunnel facility used for film cooling experiments.

divided the flow into three channels including a heated primary channel, representing the main gas path and two symmetric secondary outer channels, representing the coolant flow paths. Within the transition section of the primary channel, the flow immediately passes through a perforated plate that provides the necessary pressure drop to control the flow splits between the primary and secondary passages. At a distance 2 m downstream of the perforated plate, the flow passes through a bank of heaters followed by a series of screens and flow straighteners. The heater section comprises three individually controlled banks of electrically powered, finned bars supplying a maximum total heat addition of 55 kW.

The cross-sectional area of the test section at this location is 1 m in height (H_{in}) and 1.1 m in width (W). At a distance of 0.85 m downstream of the flow straighteners, the heated primary flow is accelerated via a reduction in the flow area due to a 45° contraction. At a distance 0.46 m downstream of the contraction the secondary coolant flow is injected into the primary flow passage through film-cooling holes in the effusion plate located on the bottom wall of the test section. At this location, the cross-sectional area is 0.55 m in height (96 z/d) and 1.1 m in width giving an inlet to exit area ratio of 1.8.

In addition to heat being removed from the flow by a primary heat exchanger, the flow in the secondary passages passes through a second heat exchanger to further reduce the coolant flow temperature. The flow in the secondary passages is then directed into a 0.61 m^3 plenum that supplies the test plate coolant. To ensure the correct coolant flow is supplied to the coolant plenum, an adjustable valve was used to meter the flow. The mass flow exiting the film-cooling

holes was set by applying the appropriate pressure ratio between the total supply plenum pressure and the exit static pressure. Using the documented discharge coefficient $C_d = 0.73$ for this particular cooling hole and flow configuration where the ratio of coolant total supply pressure to mainstream static pressure is 1.0015 (Barringer et al. [11]), the mass flows through the test plate were established. The effusion plate was constructed of 2.54 cm thick urethane foam with a low thermal conductivity (k = 0.029 W/mK resulting in a maximum conduction loss of 1.1×10^{-3} W/ cm^2) to allow for adiabatic surface temperature measurements. The dense pattern of 730 cylindrical film-cooling holes was cut into the urethane foam using a five-axis water jet. The holes were arranged into 20 rows in the streamwise direction. The cooling hole pattern on the test plate is described in Table 4.1 and shown schematically in Figure 4.2.

For this study, the film cooling characteristics were studied at four different blowing ratios: M = 3.2, 3.8, 4.4, and 5.0. One parameter that is not representative is the coolant-to-mainstream density ratio, which is typically quite high in combustors. Typical operating conditions for the film cooling flow tests consisted of a matched coolant and mainstream temperature of 30˚C. For the cooling effectiveness measurements, the mainstream temperature was nominally 45˚C with a coolant flow temperature of 26˚C. These conditions resulted in density ratios for all of the unheated cases of 1.0 (jet-to-mainstream) and 1.08 for all of the heated cases that were studied.

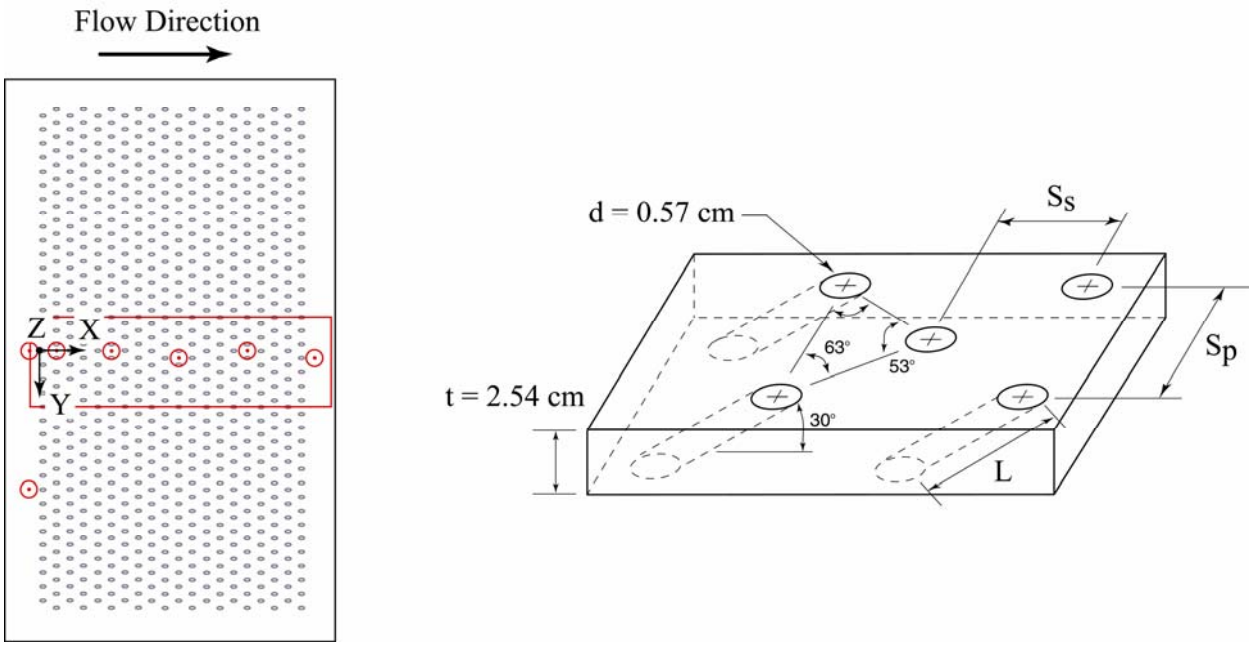

Figure 4.2. Illustration of the test plate showing the surface temperature measurement region and velocity profile measurement locations.

Table 4.1. Description of effusion plate geometry

D	5.7 mm
L/d	8.9
t/d	4.4
S_S/d S_p/d	4.9
α	30°
β	0°

Adiabatic effectiveness data were taken for the blowing ratios: M = 3.2 and 5.0. For the cases presented in this paper, 9-13% of the total flow was directed through the secondary coolant passages for the effusion cooling while the remaining flow was directed through the primary passage of the test section. The flow accelerated 9 to 15% through the test section as a result of the mass flow addition. These flow conditions resulted in a test section exit Reynolds number of 8.2 to 8.6 x 10^4. The film cooling jet Reynolds number varied from 2.4 to 3.8 x 10^3.

Measurement Methods and Uncertainty

A single fiber optic laser Doppler velocimeter (LDV) probe capable of measuring two-components was used to take flow measurements. To allow the measurement volume of the probes to reach the center of the test plate, data was taken with a 750 mm focusing lens equipped with a 2.6 magnification beam expander. This set-up had a measurement volume of 73 μm in diameter and 1.3 mm in length. The flow was seeded with olive oil particles that had an average diameter of 1 μm. The plane was acquired with the probe perpendicular to the flow direction. This allowed for the direct measurement of the local streamwise velocity component, *u*. However, in order to take measurements near the surface of the liner panel, the probe was slightly tilted at 8˚, whereby there was little effect on the true wall-normal component measurements. The sampling time for each measurement location was 20 seconds whereby 10,000 data points were acquired for each component. The probability of obtaining a sample was proportional to the speed of the flow; therefore, statistical particle bias corrections were applied to the data by weighting each individual sample based on the residence time of a particle in the

probe volume. Multiple flow measurements at different locations showed good repeatability.

A Flir Systems P20 infrared camera was used to take measurements of the effusion test plate to calculate the adiabatic effectiveness at the plate surface. The camera captured the temperature of the surface at each image pixel location by measuring the total electromagnetic radiation emitted from the black painted foam plate surface. Two type E thermocouples measuring temperatures at the surface of the plate were used to calibrate the images to assure that the correct surface emissivity and ambient temperatures were being used to report the actual surface temperatures. Five pictures were averaged at each image location to reduce uncertainty in the measurements. The infrared camera was mounted above the top endwall of the test section 0.53 m from the test plate. The proximity of the camera to the test plate allowed a spatial resolution of 0.49 mm^2/pixel, with a maximum image size of 410 square centimeters. However, the size of the test plate required five image locations and the additional step of assembling the infrared images into a correctly dimensioned composite image. Thermocouples were used in monitoring inlet and coolant temperatures. All of the temperature measurements were made using 30-gage, type E thermocouples that were connected to a data acquisition system through 20-gage thermocouple extension wire.

The partial derivative and sequential perturbation methods, described by Moffat [12], were used to estimate the uncertainties of the measured values. The precision uncertainty for the highest streamwise velocities was 0.8% based on a 95% confidence interval while the bias uncertainty for the mean velocity measurements was 1%. Precision uncertainties were calculated using the deviation of five images for each of the five measurement sets of IR camera images. The precision uncertainty of the measurements was ±0.086°C. The bias uncertainty was ±0.47°C based on the calibration of the image. The bias uncertainty of the thermocouples was ±0.2°C. The total uncertainty was then calculated as ±0.47°C for the images and ±0.22°C for the thermocouples. Uncertainty in effectiveness, η, was found based on the partial derivative of η with respect to each temperature in the definition and the total uncertainty in the measurements. An uncertainty of $\partial\eta = \pm 0.017$ at $\eta = 0.5$ and $\partial\eta = \pm 0.019$ at $\eta = 0.9$ were calculated. The precision uncertainty for the highest streamwise velocities was 0.77% while the bias uncertainty for the mean velocity measurements was 1%.

Experimental Results

As was discussed, one of the objectives of this work was to determine how the film cooling flowfield develops for an effusion film-cooled plate. Prior to measuring this flow development, the incoming boundary layer was measured to characterize the inlet conditions. Static pressure measurements were also made along the plate to determine the local momentum flux ratios as a function of streamwise distance along the plate. To determine the flow field development, velocity profiles were acquired at a number of locations, as indicated in Figure 4.2. These locations were chosen to chart the development of the film flow as it progressed down the test plate for the flow conditions I = 10.6 and 25.5 (M = 3.2 and 5.0) and a density ratio of 1.0. Velocity profiles were also measured downstream of row 20 for I = 10.6, 14.8, 19.7, and 25.5 to understand the effect of the momentum flux ratio. After it was found that the film flow became fully developed after the 15th row of cooling holes, lateral and streamwise planes were measured at row 15 to describe how the film cooling was interacting with mainstream and upstream film flow.

The following section will describe the results of this study by first describing the inlet flow conditions approaching the first row of cooling holes, results of the flow field measurements and then adiabatic effectiveness results for the entire streamwise extent of the test plate.

Inlet and Cooling Flow Conditions

The inlet conditions were measured at two locations upstream of the first row of cooling holes. To ensure inlet flow uniformity, the measurements were located at the center of the test plate and at 25% of the width as shown in Figure 4.2. These measurements were made five cooling hole diameters upstream of the first row of cooling holes. Note that all profiles are normalized to the local mainstream velocity. The maximum percent difference based on the mainstream velocity between the two inlet locations was 1.6% for the streamwise component and 0.29% for the turbulence level. The inlet mainstream streamwise velocity was 2.3 m/s with a freestream turbulence level of 1.3%. The displacement thickness of the inlet boundary layer was found to be 0.86 Z/d with a momentum thickness Reynolds number of 451. Figure 4.3 shows the two boundary layer profiles at the two different pitchwise locations that were measured. As can be seen from Figure 4.3, there was good pitchwise uniformity at the start of the plate.

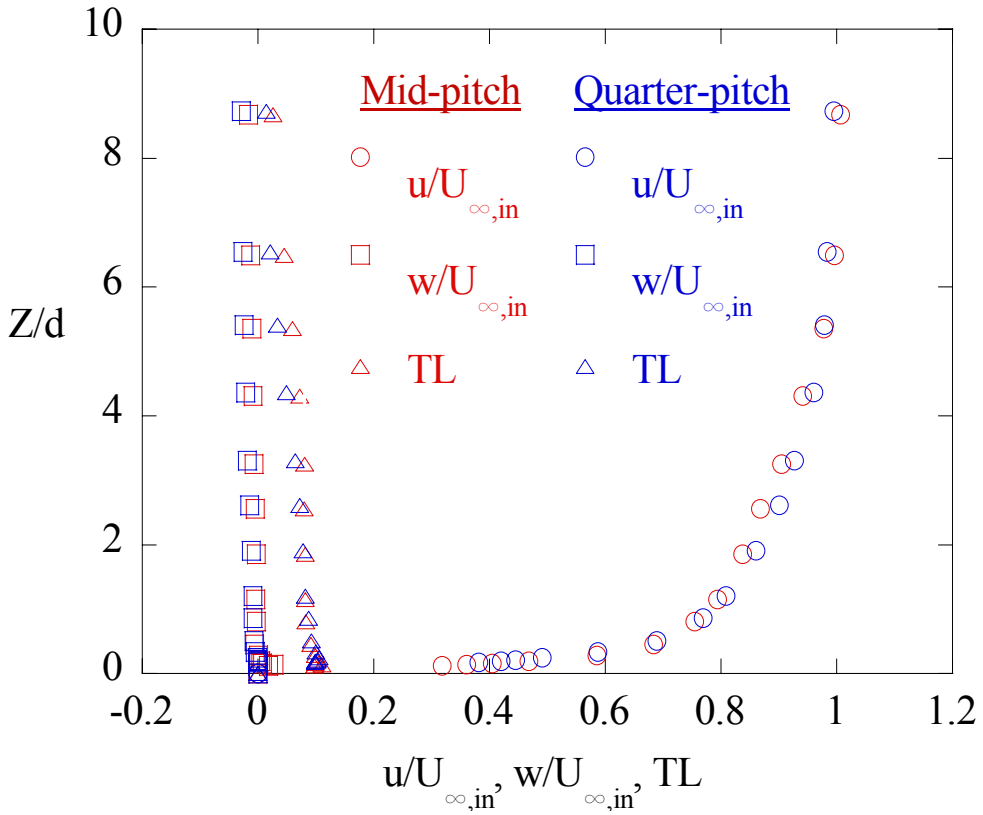

Figure 4.3. Inlet flow conditions measured at mid-pitch and quarter-pitch.

The film cooling flow was established using the discharge coefficient and an inviscid calculation with a knowledge of the cooling plenum's total pressure with respect to the static pressure at the hole exits. The static pressures were measured at the test plate centerline between every other row of cooling holes to accurately deduce the coolant discharge rate and local momentum flux ratios. It was found that the coolant plenum total pressure and surface static pressure difference remained constant within 3% indicating that there was a constant coolant supply in the streamwise direction. However, the accumulation of cooling flow increased the local freestream velocity, thereby decreasing the local momentum-flux ratio as shown in Figure 4.4. The local momentum-flux ratio of the cooling jets was found to decrease by about 20% from the first to 20th hole row.

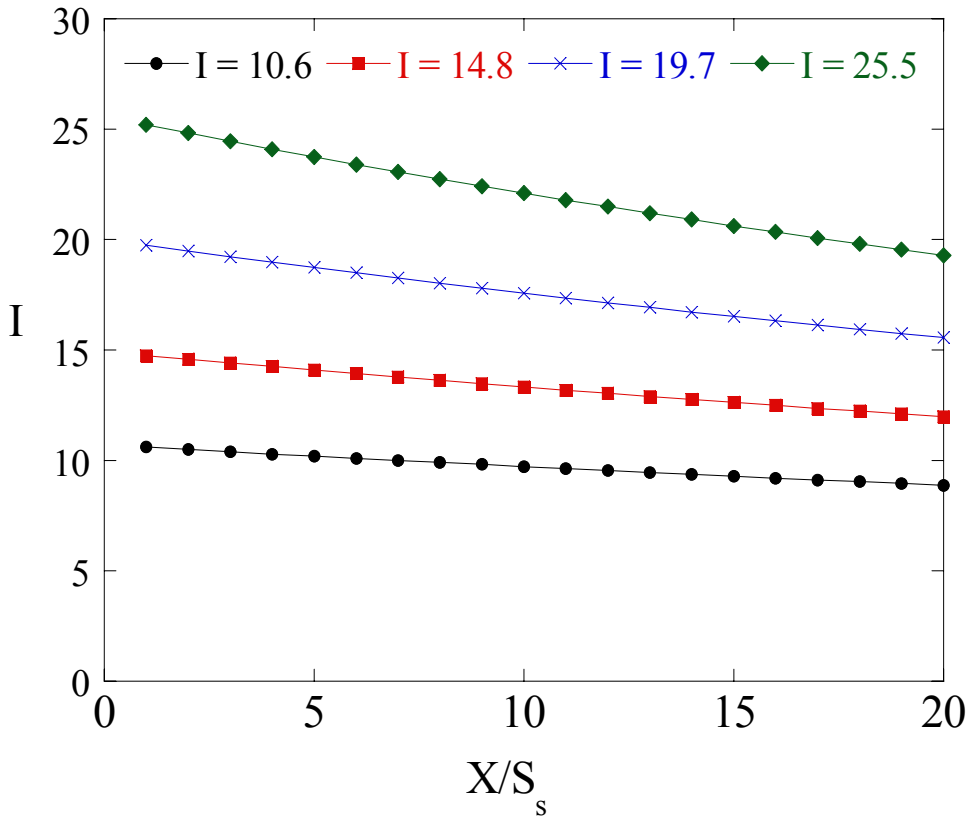

Figure 4.4. Streamwise dependence on the local film cooling momentum-flux ratios.

Development of the Velocity Profiles

Velocity profiles were measured downstream of cooling hole rows 1, 5, 10, 15, and 20 to determine how the film-cooling effusion flow develops and whether the flow becomes fully developed. These profiles were taken one cooling row downstream of the respective hole rows as shown in Figure 4.2. Measurements were made for the blowing ratios M = 3.2 and 5.0 (I = 10.6 and 25.5).

Figure 4.5 shows the mean velocity profiles as the flow develops along the effusion plate for the lowest momentum flux ratio case. As the flow is injected from the first row to the 15th row, there is a continual decrease in the penetration height of the jet, as defined by the maximum streamwise velocity. The peak occurs at 2.4 d for row 1 and at 1.4 d for row 15 and row 20. It is also interesting to note that the continuous injection results in an increase in velocity for the outer portion of the flow (above the peak velocity).

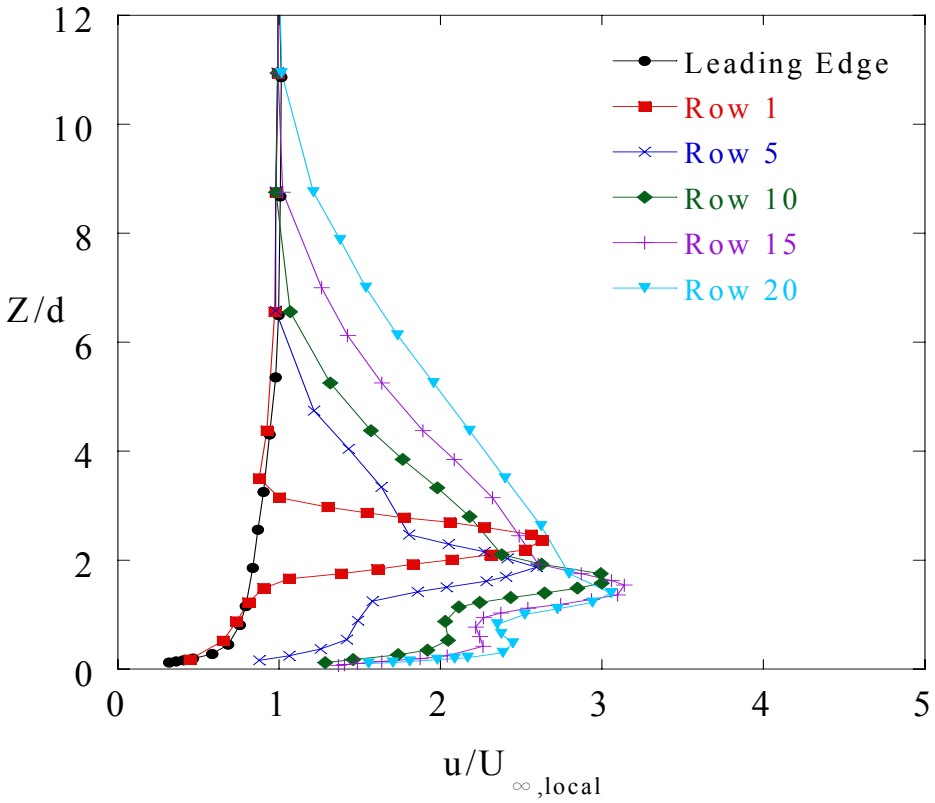

Figure 4.5. Streamwise velocity profiles measured for I = 10.6.

Figure 4.6 also shows that the streamwise velocities have two distinct local velocity maxima that emerge at row 10 and remain further downstream. This phenomenon was consistent at both high and low blowing ratios, as will be discussed. The most important information that can be gleaned from Figures 4.5 and 4.6 is that for both momentum flux ratios the data indicate that the flow becomes fully developed at nominally row 15 in terms of a peak velocity, while the outer portion of the flow continues to accelerate from the mass addition.

Pietrzyk [13] formulated a physical model describing the flow field behind a high velocity ratio jet (V_{jet}/U_{∞}=0.5). This researcher identified a wall-jet layer generated by longitudinal vortexes created at the lateral edges of the cooling hole. This layer was attributed to generating the secondary velocity peak at the near-wall. It was concluded that the longitudinal vortices were the most detrimental flow structures affecting film cooling performance. Pietrzyk et al. [14] found that there was an influx of higher speed fluid into the wake region below the jet core causing a negative velocity gradient near the wall. It was also found that the strength of the longitudinal vortices scaled with the velocity ratio, which was essentially the main scaling

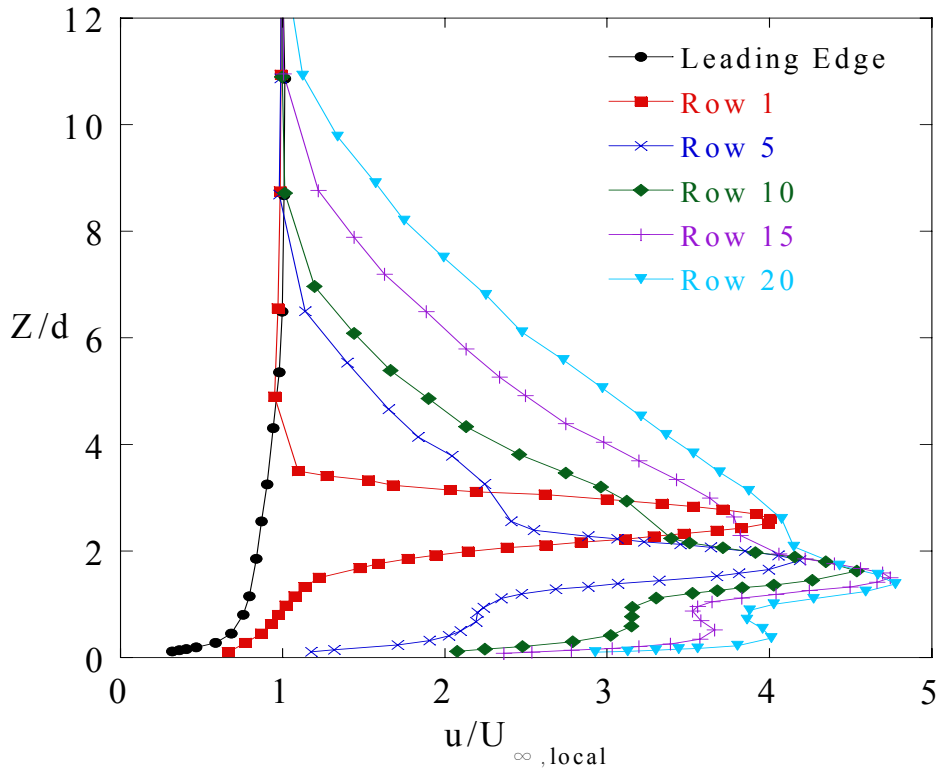

Figure 4.6. Streamwise velocity profiles measured for I = 25.5.

parameter in this study. Lee et al [15] also measured double peaked streamwise velocity profiles in the flowfield downstream of streamwise inclined jets in crossflow. These researchers found that inclined jets induce a much higher wall-normal velocity in the jet wake region than normal jets, due to stronger secondary motion and a larger pressure drop gradient. Both of these studies considered only a single row of holes.

As was discussed, the location of the peak streamwise velocity was found to be dependent on the hole row as shown in Figure 4.5 for I = 10.6. A similar result occurred as shown in Figure 4.6 for I = 25.5. For row 1, the peak velocity occurred only slightly further off the wall for the I = 25.5 case relative to the I = 10.6 case. As the flow further developed, the location of the peak for the two flow cases occurred at nearly the same vertical location at Z/d = 1.4. But, the velocity values for the I = 25.5 case were much higher than for the I = 10.6 case.

Turbulence levels were also compared for the two momentum flux ratios and can be seen in Figures 4.7 and 4.8. Note that these turbulence levels are the root mean square (rms) of the streamwise and wall-normal velocity fluctuations normalized by the local mean velocities external to the film-cooled layer. The data in Figures 4.7 and 4.8 indicate that higher turbulence

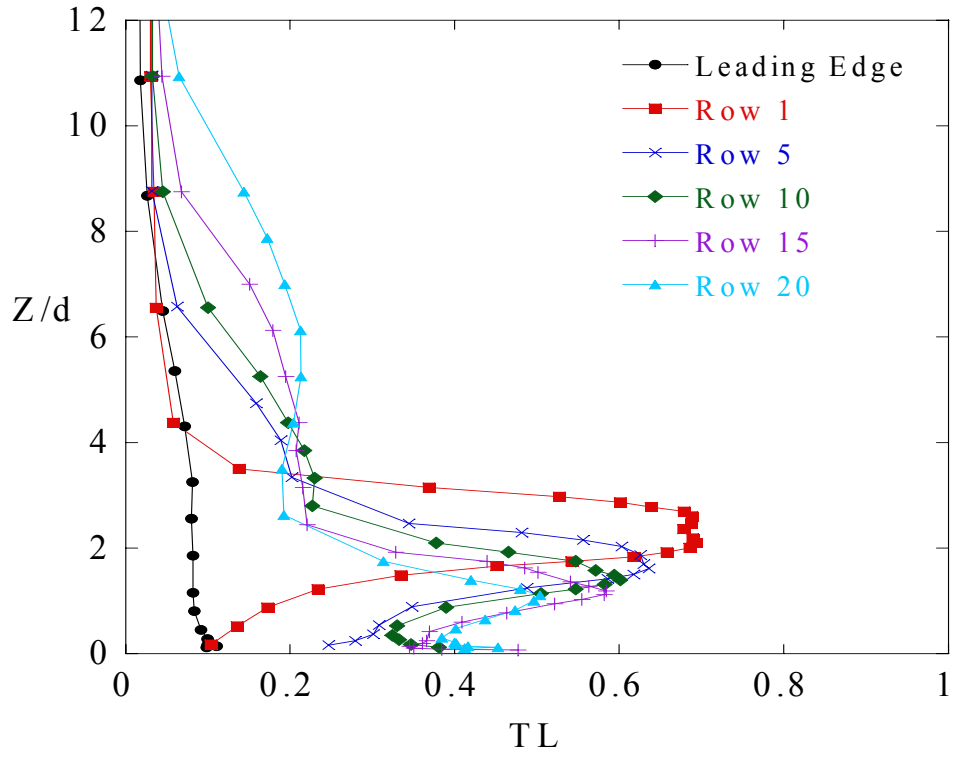

Figure 4.7. Turbulence level profiles for I = 10.6.

levels occur at higher momentum flux ratios, which is expected given the larger shear in the boundary layer. Similar to the mean velocities, however, the wall-normal location of the peak turbulence levels is relatively insensitive to the momentum flux ratio.

Similar to the mean velocities that were shown in Figures 4.5 and 4.6, the turbulence profiles become self-similar in terms of peak values downstream of the 15th row. In the near wall region, the peak turbulence levels for both cases decrease with increasing streamwise distance while the levels continue to increase with downstream distance in the outer flow region (above the peak). The turbulence levels in the near wall region also start to increase very close to the wall and become self-similar at nominally the 15th cooling row.

It is evident that both the mean velocity profiles and the turbulence levels at a given film cooling hole row scaled with the injection levels. As a result, an attempt was made to analyze the results by using the momentum flux and the mass flux ratios as scaling parameters in plotting the profiles. Figures 4.9 and 4.10 show several row locations whereby the mass flux ratio was placed in the denominator of the velocity scaling parameter. These figures indicate a very good scaling of the velocity profiles using the mass flux ratio at each row considered. Momentum flux

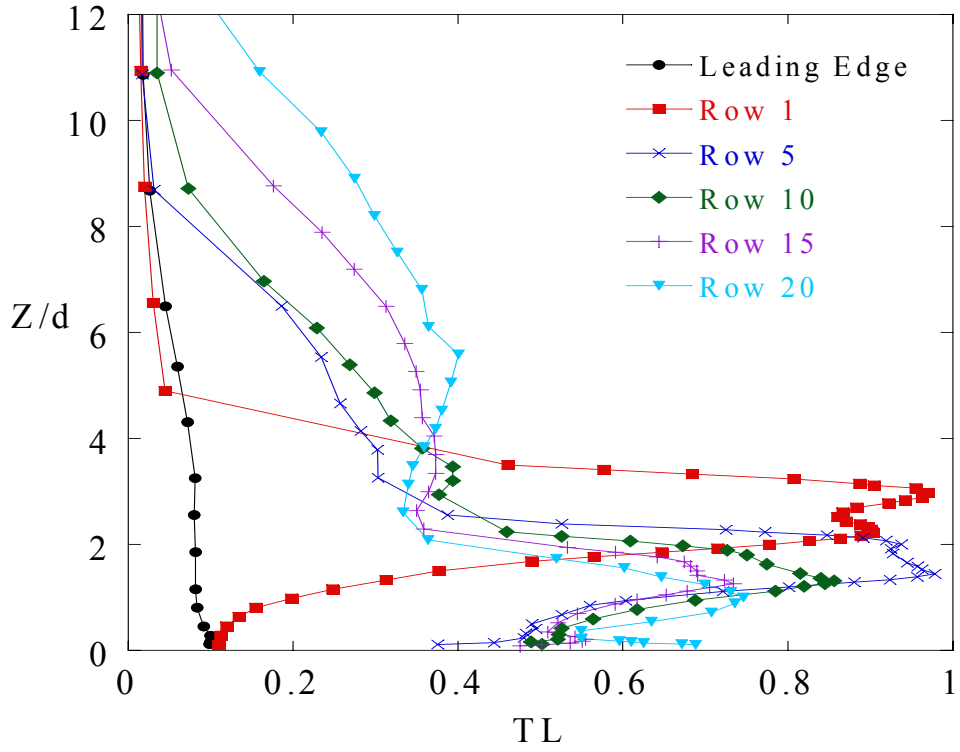

Figure 4.8. Turbulence level profiles for I = 25.5.

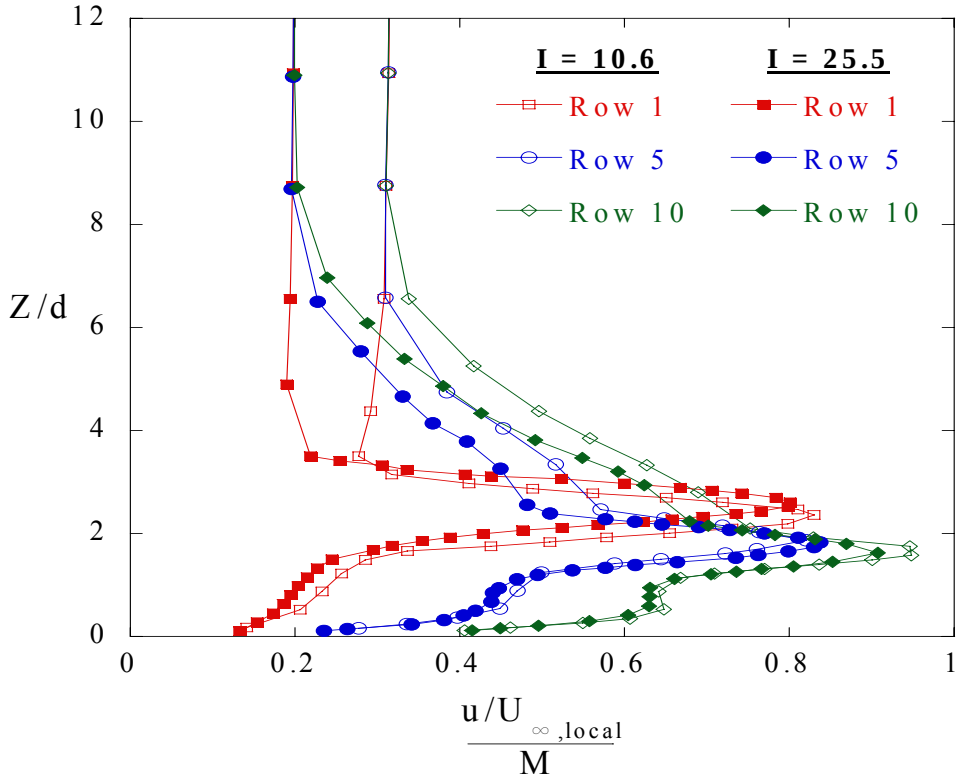

Figure 4.9. Streamwise velocity profiles measured one row downstream of rows 1, 5, and 10 for I = 10.6 and 25.5 using the blowing ratio, M, to normalize the profiles.

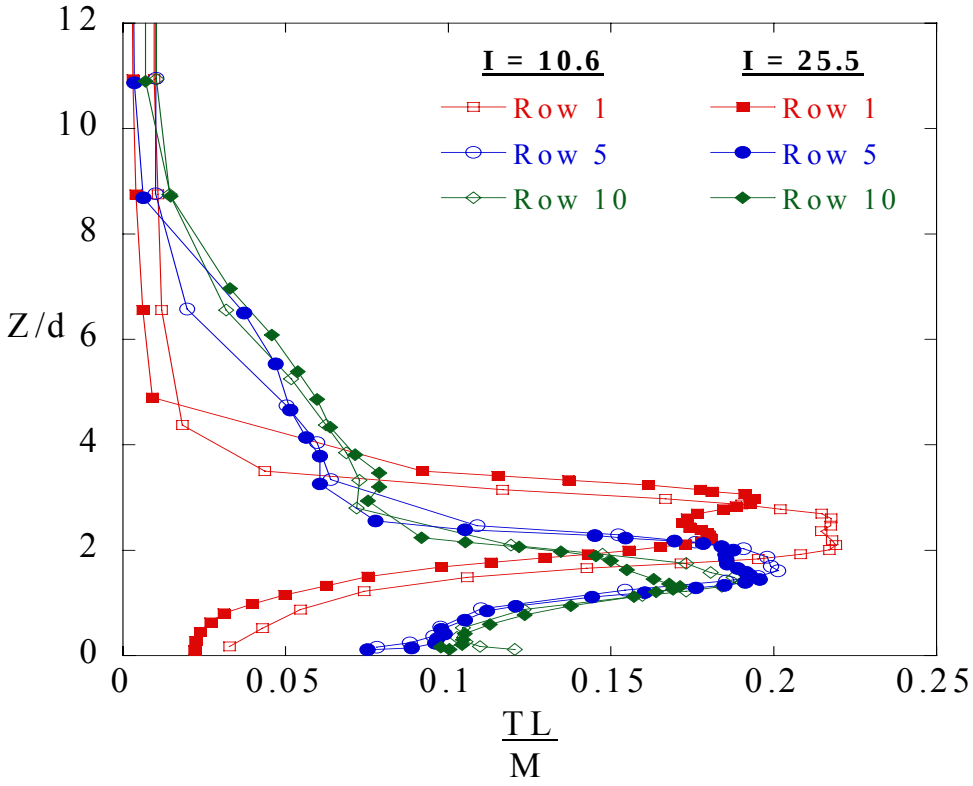

Figure 4.10. Turbulence level profiles measured one row downstream of row 1, 5 and 10 for I = 10.6 and 25.5. Profiles normalized to blowing ratio, M.

ratios were also used to scale the velocity fields, but did not indicate good scaling characteristics.

To further evaluate whether the mass flux ratio was a good scaling parameter, a number of velocity profiles were measured one hole row spacing downstream of the last row of cooling holes to gain an understanding of how the blowing ratio affects the accumulated flow characteristics. The motivation was to establish if the flow profile retained its shape, if the thickness of the film was affected and how the different flow rates affected turbulence transport.

Profiles for a range of momentum flux ratios are shown in Figure 4.11 with the corresponding turbulence levels shown in Figure 4.12. These profiles were measured downstream of the 20th row of holes, which was considered to be in the fully developed region. The streamwise velocity and turbulence levels scale very well to the mass flux ratio as shown in Figures 4.13 and 4.14 for both the mean velocity as well as for the turbulence levels. Progressing from the wall, the velocity profiles begin to diverge, because of effects due to interactions with the freestream.

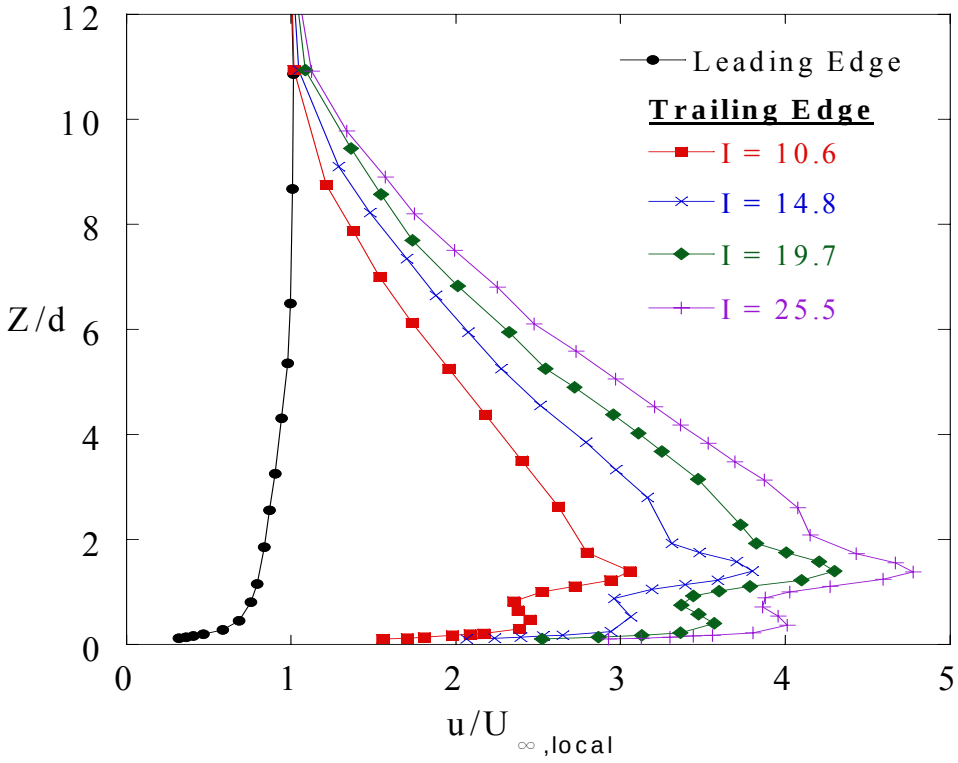

Figure 4.11. Streamwise velocity profiles measured one row downstream of row 20.

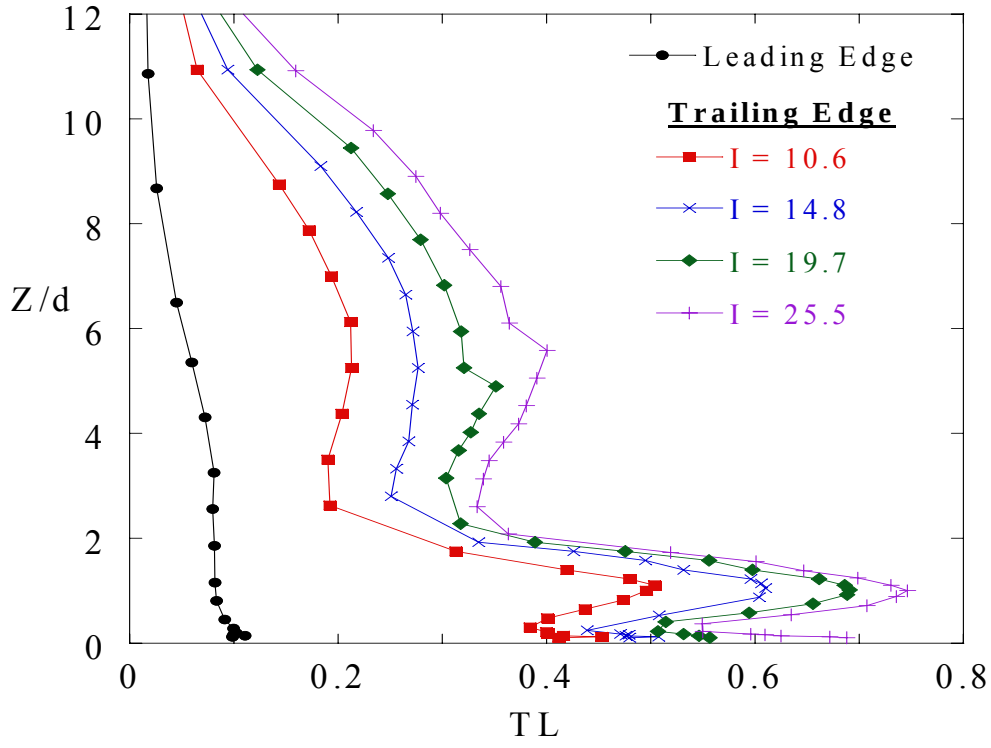

Figure 4.12. Turbulence level profiles measured one row downstream of row 20.

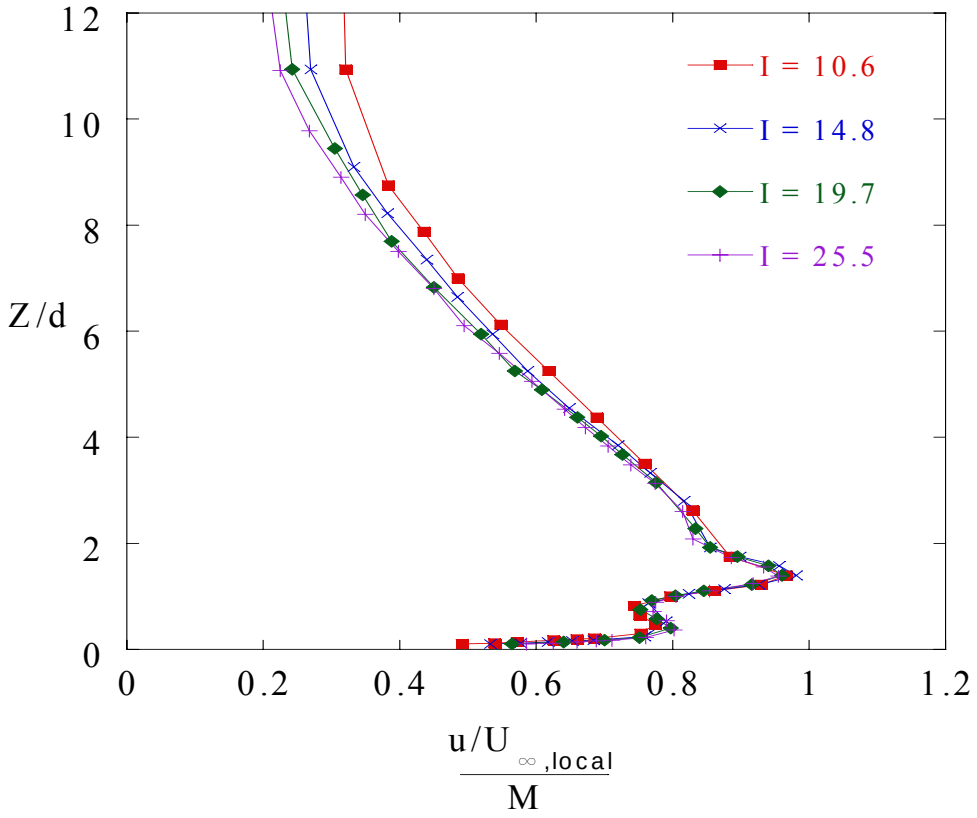

Figure 4.13. Streamwise velocities profiles measured one row downstream of row 20. Profiles normalized to blowing ratio, M.

Forth et al. [16] studied film cooling heat transfer parameter scaling for different geometries and flow and thermal conditions. They found that the cooling flow could be divided into "weak injection" and "strong injection" regimes. Strong injection indicated the presence of jet liftoff occurring at I ≈ 0.1. These researchers found that the velocity ratio best scales heat transfer data in the strong injection regime. The velocity ratio directly corresponds to mass flux ratio with unity density ratio and agrees with the results presented in this paper.

Each blowing ratio creates a velocity profile with a double-peaked nature that the authors believe is an inherent characteristic of the full-coverage effusion plate operating at high blowing ratios. However, this profile shape is highly dependent on the measurement location with respect to the cooling hole. The double-peaked profile is seen most readily in the range from X/d = 3 to 5 downstream of the hole center.

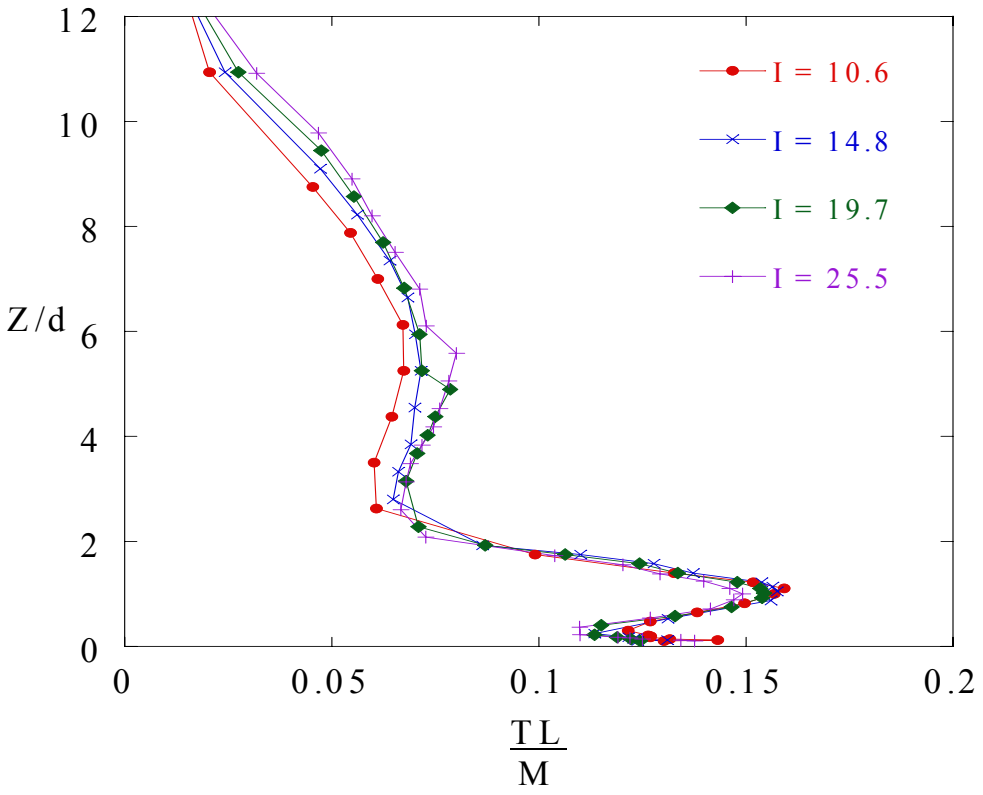

Figure 4.14. Turbulence level profiles measured one row downstream of row 20. Profiles normalized to blowing ratio, M.

The turbulence level profiles indicate complex trends that correspond to distinct regions with respect to the cooling jet. Three peaks in turbulence level can be observed between two adjacent minima. The minima that occurs at Z/d = 3 corresponds to a near-zero streamwise velocity gradient at that location. The peak in turbulence level at Z/d = 1 is consistent with the shear layer at the bottom of the coolant jet and the drop in turbulence in the near wall region at Z/d = 0.37 corresponds to the secondary velocity peak at that location.

Two planes of velocities were measured downstream of the fifteenth row of cooling holes for I = 25.5. The streamwise velocity plane shown in Figure 4.15 gives u and w velocity vectors superimposed on a streamwise velocity contours. Figure 4.15 shows good streamwise periodicity evidenced by the Z/d = 2 jet penetration height of the row 15 jet as well as the upstream (row 13) jet. It is clear that the cooling jet separated from the test plate surface as it created a recirculation zone extending no farther than one hole diameter from the cooling hole trailing edge. The flow quickly reattached to the wall which caused the second velocity peak that appears in the mean velocity profiles shown in Figure 4.13.

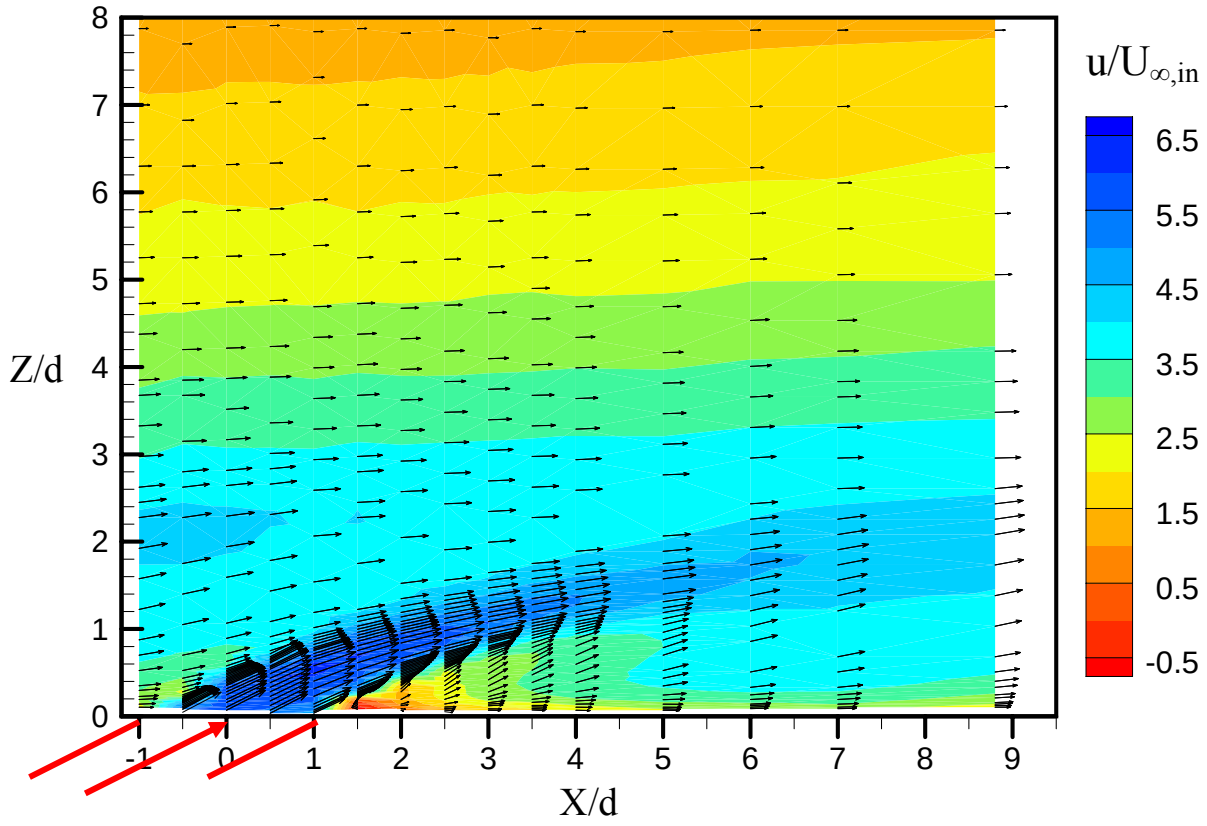

Figure 4.15. Streamwise velocity contours downstream of row fifteen for I = 25.5. Vectors show streamwise and wall-normal velocity components. Arrow indicates row 15 cooling hole.

Shown in Figure 4.16, the highest turbulence level in the flow field was 115%, found downstream of the location in the jet shear layer where the local velocity was 3.2 times the local mainstream velocity. It should be noted that the extremely high turbulence levels were due to the higher streamwise mean and fluctuating velocities in the cooling layer being normalized to the much lower local freestream velocity. As shown in Figure 4.16, the turbulence levels in the bottom shear layer of the jet were generally higher than the top shear layer indicating higher velocity gradients near the wall and increased turbulence generation. The coolant jet core exiting the hole had turbulence levels between 45 and 50%.

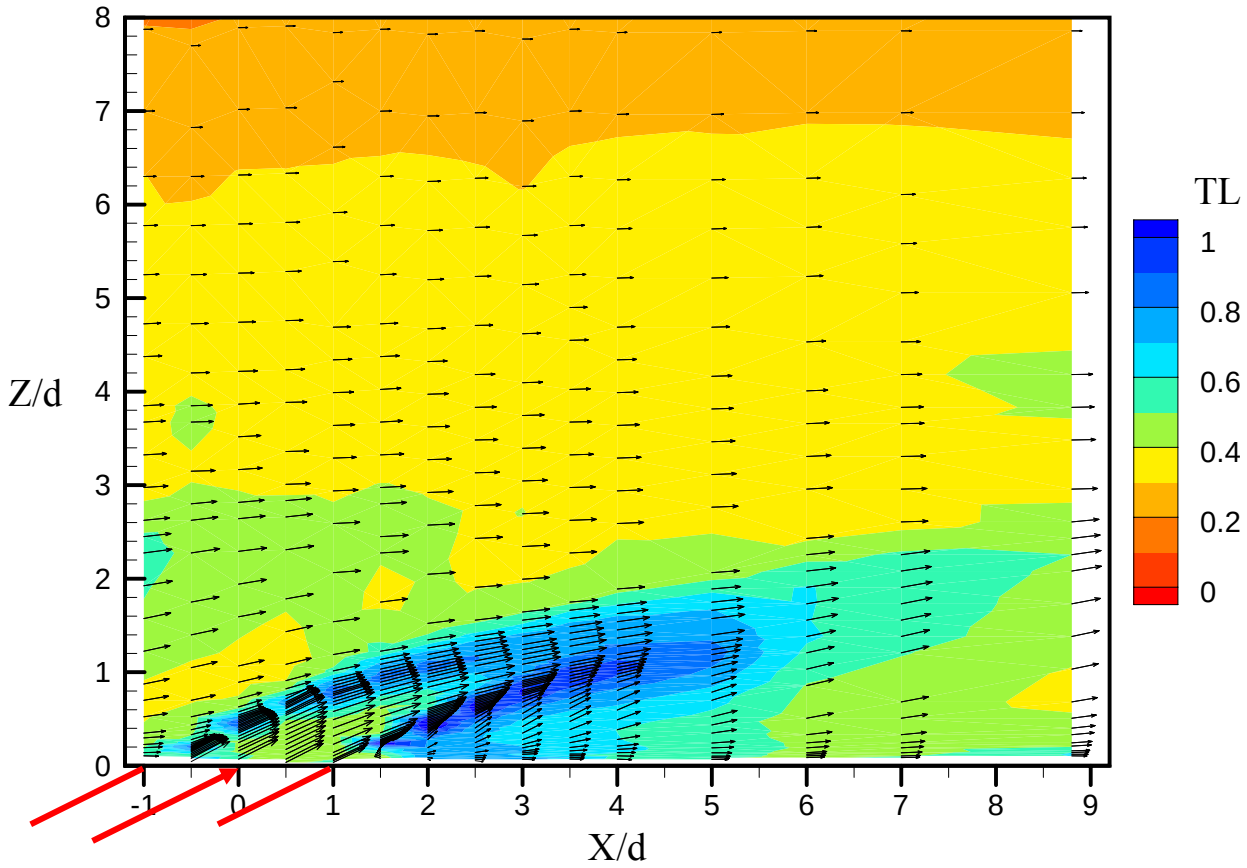

Figure 4.16. Turbulence levels with flow field vectors for I = 25.5 showing streamwise and wall-normal velocity components. Arrow indicates row 15 cooling hole.

Figures 4.17a-c show a plane normal to the streamwise direction with contours of streamwise velocity, wall-normal velocity, and turbulence levels. The appearance of a counter-rotating vortex is shown through the contours of the streamwise and wall-normal velocities. The primary peak in the streamwise velocity is formed into a kidney shape near the outer edges of the jet. Figure 4.17c clearly shows that the peak turbulence is located below the highest streamwise velocity gradients. Also seen in Figure 4.17c is the turbulence transport from the adjacent upstream cooling hole.

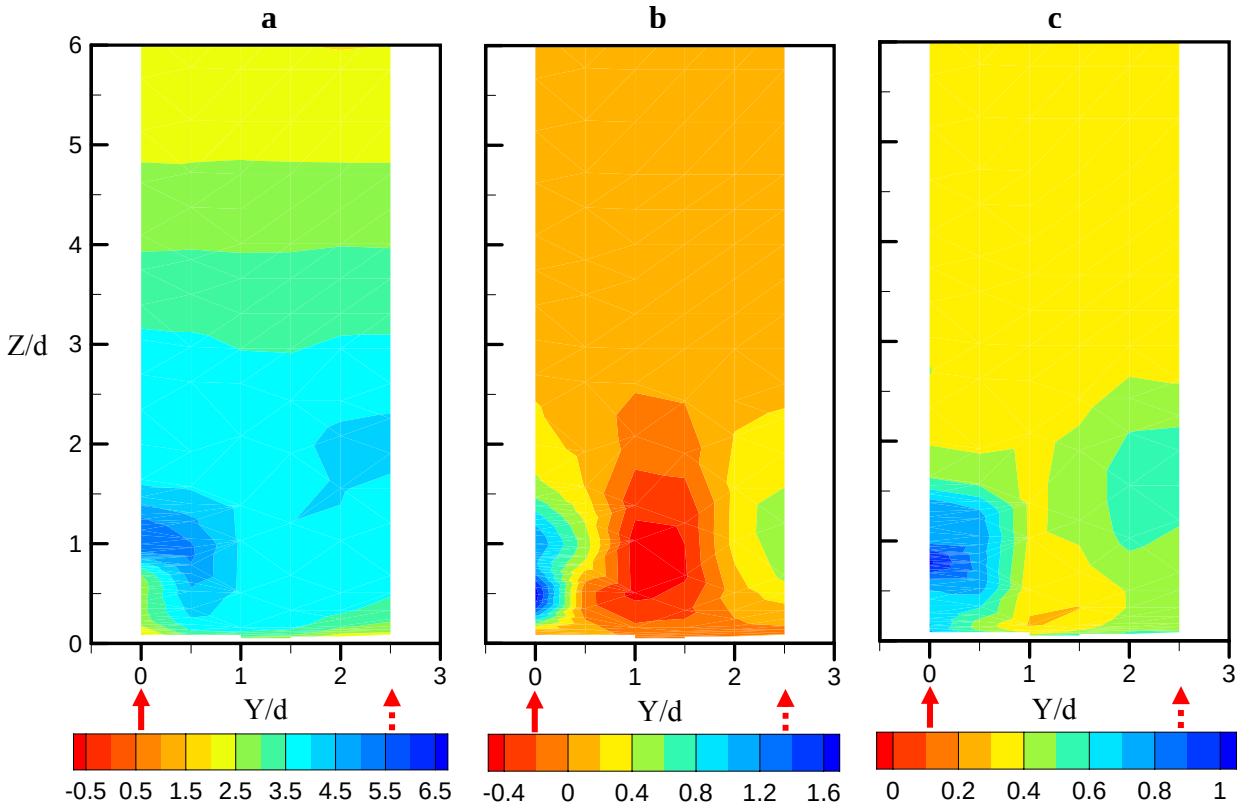

Figure 4.17. Cross-sectional plane X/d = 3 downstream of row 15 showing (a) streamwise velocity, $u/U_{\infty,in}$, (b) wall-normal velocity, $w/U_{\infty,in}$, and (c) turbulence levels. Solid arrows indicate row 15 hole location and dashed arrows indicate row 14 hole location.

Cooling Effectiveness Results

Adiabatic effectiveness measurements were made on the effusion test plate for the cases I = 10.6 and 25.5 in the region shown in Figure 4.2. This region was chosen to capture the cooling characteristics of all twenty rows of cooling holes. The measurement region captured six columns of cooling holes located at the mid-pitch of the test plate. Conditions were found to be pitchwise periodic over the measurement region as shown in Figure 4.18.

Contours of the adiabatic effectiveness shown in Figure 4.18 show a slight improvement in cooling effectiveness at I = 25.5 relative to I = 10.6. The cooling effectiveness trends showed similarities to the film flow profiles. Since there was a difference in effectiveness levels at the 19th and 20th rows, however, it is evident that a thermally fully-developed condition is not reached at the same location the velocity field becomes fully developed. This is in spite of the asymptotic behavior of the adiabatic effectiveness for both blowing ratios.

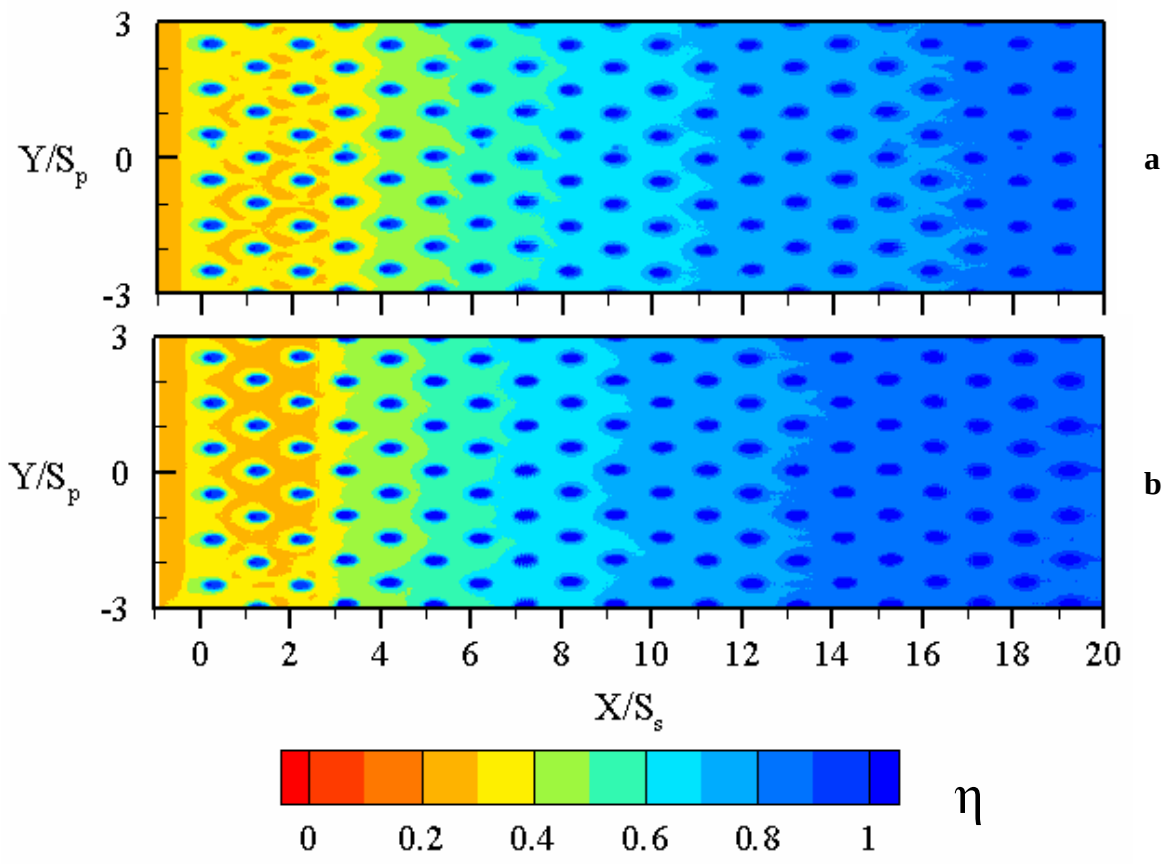

Figure 4.18. Adiabatic effectiveness contours of the effusion panel from rows 1 to 20 for (a) I = 10.6 and (b) I = 25.5.

Lateral averages of the adiabatic effectiveness show the same cooling behavior for the first three rows of holes. Similar trends for both blowing ratios were seen downstream of the third cooling row, with a slightly improved cooling effectiveness at I = 25.5, shown in Figure 4.19. It can also be seen from the contours and the lateral averages that there is conduction upstream of the test plate, evidenced by the non-zero effectiveness levels at the leading edge. This conduction can be explained by the fact that the cooling holes are cooling the plate through convection within the holes. Also interesting about the contours and the lateral averages is the fact that there is an actual decrease in the adiabatic effectiveness levels to $X/S_s = 2$ before an increase can be seen. The reason for this decrease is because the jet penetration heights were very high at the leading edge of the plate, as was indicated by the velocity profiles. Moreover, these jets entrained hot mainstream flow to the surface by the longitudinal vortices, resulting in negative wall-normal velocities, revealed in Figure 4.17b. Furthermore, the rate of hot

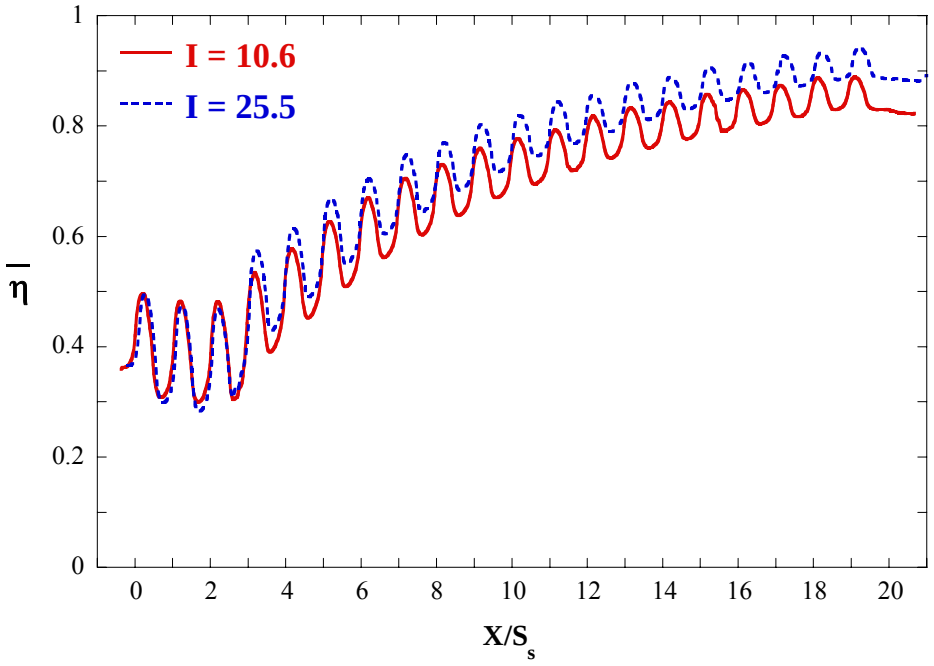

Figure 4.19. Lateral average of adiabatic effectiveness of the effusion panel from rows 1 to 20 for I = 10.6 and I = 25.5. Note that $X/S_s = 0$ is the leading edge of the first hole row.

mainstream entrainment for the first three hole rows was the same for both blowing ratios, indicated by the identical cooling behavior shown in Figure 4.19. The penetration heights at the leading edge did not allow the coolant to effectively cool the plate until further downstream where the velocity peaks moved closer to the wall.

Conclusions

An effusion cooling scheme was investigated through flow-field measurements and adiabatic wall temperatures. A range of blowing ratios were considered for the given cooling scheme for a design that contained twenty rows of cooling holes with equally spaced holes in both the streamwise and pitchwise directions.

The results of this study indicate that full-coverage effusion cooling develops into a fully-developed velocity profile at a nominal location of 15 film-cooling hole rows. The jet penetration for the first few rows of film-cooling holes was much higher than that which occurred for the fully-developed condition. The penetration height for the cooling hole rows was independent of the momentum flux ratio for the range that was considered at the fully-developed

condition.

The most interesting aspect of the results was the indication that for an effusion cooling hole design, such as that considered in these tests, the streamwise velocity and turbulence level profiles scale exactly with blowing ratio. This scaling effect was found to hold at all measurement locations and all blowing ratios. This finding allows the profile shape and magnitude to be readily determined.

The velocity planes that were measured indicated jet separation just downstream of the hole trailing edge and the existence of the commonly reported counter-rotating vortex which serves to entrain hot mainstream flow toward the surface at the plate leading edge. Downstream, however, this effect serves to mix the accumulated coolant flow and provide a more uniform surface temperature across the pitch.

The cooling effectiveness of the film layer increased asymptotically at the same rate for both blowing ratios with only little improvement for the higher blowing ratio relative to the lower blowing ratio.

Acknowledgements

The authors gratefully acknowledge United Technologies – Pratt & Whitney for their support of this work.

Nomenclature

d	film cooling hole diameter
H_{in}	combustor inlet height
I	momentum flux ratio, $I = \rho U^2 / \rho_\infty U_\infty^2$
L	film cooling hole length
$\dot{m}$	mass flowrate
M	mass flux ratio, $M = \rho_c U_c / \rho_\infty U_\infty$
S_s, S_p	streamwise, pitchwise film cooling hole spacing
t	test plate wall thickness
T	temperature
TL	turbulence level, $TL = \sqrt{0.5\left((u_{rms}^2 + w_{rms}^2)\right)} / U_{local}$

u, v, w	local, mean velocity components corresponding to X,Y, Z
X, Y, Z	coordinate system shown in Figure 4.2
W	test section inlet width

Greek

α	inclination angle of cooling hole
∂	uncertainty
ρ	density
ν	kinematic viscosity
η	adiabatic effectiveness, $\eta=(T_\infty - T_{adiabatic})/(T_\infty - T_c)$

Subscripts

c	coolant conditions (secondary flow)
in	inlet conditions
local	local conditions
p	pitchwise direction
rms	root mean square of fluctuating velocity
s	test plate surface, streamwise direction
∞	freestream conditions (primary flow)

Superscripts

$\bar{}$	lateral average

References

[1] Andrews, G. E., Asere, A. A., Gupta, M. L., and Mkpadi, M.C., "Full Coverage Discrete Hole Film Cooling: The Influence of Hole Size," ASME 85-GT-47.

[2] Andrews, G. E., Alikhanizadeh, M., Tehrani, F. B., Hussain, C. I., and Azari, M. S. K., "Small Diameter Film Cooling Holes: Influence of Hole Size and Pitch," ASME 87-HT-28.

[3] Andrews, G. E., Khalifa, I. M., Asere, A. A., and Bazdidi-Tehrani, F., “Full Coverage Effusion Film Cooling with Inclined Holes,” ASME 95-GT-274.

[4] Lin, Y., Song, B., Li, B., Liu, G., and Wu, Z., “Investigation of Film Cooling Effectiveness of Full-Coverage Inclined Multihole Walls with Different Hole Arrangements,” ASME GT2003-38881.

[5] Martiny, M., Schulz, A., and Witting, S., “Full-Coverage Film Cooling Investigations: Adiabatic Wall Temperatures and Flow Visualization,” ASME 95-WA/HT-4.

[6] Sasaki, M., Takahara, K., Kumagai, T., and Hamano, M., 1979, "Film Cooling Effectiveness for Injection from Multirow Holes," ASME *Journal of Engineering for Power*, vol. 101, pp. 101-108.

[7] Harrington, M., McWaters, M., Bogard, D., Lemmon, C., and Thole, K. A., 2001, “Full-Coverage Film Cooling with Short Normal Injection Holes,” *Journal of Turbomachinery*, vol. 123, pp. 798-805.

[8] Fric, T., Campbell, R., and Rettig, M., “Quantitative Visualization of Full-Coverage Discrete-Hole Film Cooling,” ASME 97-GT-328.

[9] Bazdidi-Tehrani, F., and Andrews, G., “Full Coverage Discrete Hole Film Cooling: Investigation of the Effect of Variable Density Ratio (Part II),” ASME 97-GT-341.

[10] Pietrzyk, J. R., Bogard, D. G., and Crawford, M. E., 1990, “Effects of Density Ratio on the Hydrodynamics of Film Cooling,” *Journal of Turbomachinery*, vol. 112, pp. 437-443.

[11] Barringer, M. D., Richard, O. T., Walter, J. P., Stitzel, S. M., And Thole, K. A., 2002, “Flow Field Simulations of a Gas Turbine Combustor,” *Journal of Turbomachinery*, vol. 124, pp. 508-516.

[12] Moffat, J. R., 1988, "Describing the Uncertainties in Experimental Results," *Experimental Thermal and Fluid Science*, vol. 1, pp. 3-17.

[13] Pietrzyk, J. R., 1989, "Experimental Study of the Interaction of Dense Jets With a Crossflow for Gas Turbine Applications," Ph.D. Dissertation, Univ. of Texas at Austin.

[14] Pietrzyk, J. R., Bogard, D. G., and Crawford, M. E., 1989, "Hydrodynamics Measurements of Jets in Crossflow for Gas Turbine Film Cooling Applications," *Journal of Turbomachinery*, vol. 111, No. 2, pp. 139-145.

[15] Lee, S. W., Lee, J. S., Ro, S. T., 1994, "Experimental Study on the Flow Characteristics of Streamwise Inclined Jets in Crossflow on Flat Plate," *Journal of Turbomachinery*, vol. 116, pp. 97-105.

[16] Forth, C. J. P., and Jones, T. V., 1986, "Scaling Parameters in Film-Cooling," Proc. 8th Int. Heat Transfer Conference, pp. 1271-1276.

Paper 5:

Investigation of the Velocity and Thermal Development of Cooling Film Created by Compound Angle Effusion Holes

Abstract

Gas turbine combustors contain extreme thermal environments that are produced by the combustion process. When these flow temperatures exceed the melting temperature of the combustor metal, effective surface cooling strategies are necessary. Effusion film cooling is used in gas turbines to meet the cooling requirements and cooling holes with compound angles are used to enhance the surface coverage of the coolant. The present study discusses the penetration height of the coolant injected from compound angle cooling holes.

This paper discusses experimental results of compound angle effusion film cooling injection in a gas turbine combustor model with engine representative film cooling jet momentum flux ratios. Experiments were performed with and without crossflow in an effort to model the conditions found in a gas turbine combustor. Velocity and temperature measurements were made at several streamwise locations in order to determine the growth of the coolant layer. The effect of the film cooling momentum flux ratio and the influence of the presence of crossflow on the growth of the coolant layer are investigated.

Results indicate that there were significant differences between the flow field created with and without crossflow. For the cases with crossflow, the penetration height of the jet based on the turbulence was found to be relatively independent of the film cooling momentum flux ratio. It was found from the angle of the velocity vectors that the cooling film layer grew nearly linearly in the streamwise direction. The turbulence levels without crossflow were found to be higher than the turbulence levels with crossflow because there was a larger shear stress due to a larger velocity difference between the coolant and crossflow. The film cooling penetration heights based on the temperature and velocity measurements were similar for all film cooling momentum flux ratios. The combustor liner surface temperature decreased in uniform increments in the streamwise direction for the lowest coolant flow and decreased in reducing increments for the highest coolant flow.

Introduction

As the demand for higher gas turbine power continually grows, the firing temperature of turbine combustors necessarily increases to meet the requirement. The higher combustor temperatures require increasingly aggressive component cooling strategies to abate the effects of the hotter environment. Effusion film cooling is an effective surface cooling method, especially when the holes are angled to the surface, because it creates a buffer of relatively cooler air between the hot combustor gases and the combustor liner. Compound angle cooling holes inject laterally into the crossflow which has the further advantage of increasing exposure of the coolant to the surface. For effusion cooling to be most effective, the turbulence and coolant penetration must be minimal to prevent mixing of the film cooling with the hot crossflow.

Combustor effusion cooling was simulated in a large-scale, closed loop wind tunnel combustor model. The large scale of the test section permitted high resolution measurements of the velocity and temperature fields. Upstream of the film cooling injection, the mainstream passed through a contraction that simulated separated flow similar to the wake created by dilution jet injection. The absolute flow and temperature conditions were not met, and the density ratio was not matched in this study but the film cooling momentum flux ratios included values that were representative of those found in combustors.

The objective of this work was to quantify the penetration height of compound angle effusion cooling. Because the flow field in combustors is very complex, the penetration characteristics were studied with injection both into crossflow and into quiescent flow. The penetration height was measured at three momentum flux ratios. The penetration of the coolant was important to be able to improve the modeling of the turbine inlet flow and thermal fields. Profiles of velocity, turbulence level, and temperature were measured at several streamwise locations to determine the additive effect of the film cooling flow on the penetration of the coolant into the freestream. After a review of relevant past studies and a description of the characteristics of the combustor simulator facility, this paper will describe results from the experiments conducted using the compound angle effusion plate.

Past Studies

Many compound angle flow studies available in the open literature focus on the behavior of a single film cooling hole or a single row of film cooling holes. The literature also offers many studies on the behavior of the flow and temperature fields that have been measured and modeled for effusion film cooling jets aligned with the mainstream flow. The present study is unique because it reports detailed flow and thermal field measurements of the film layer created by multiple rows of compound angle jets.

The present study is closely related to experiments by Scrittore, Thole, and Burd [1] who characterized the flow and thermal behavior along an effusion film cooling liner with streamwise injection (no compound angle). Their goal was to make detailed profile measurements of the coolant layer. This past work found that the blowing ratio of the effusion jets did not significantly contribute to the penetration height of the coolant layer. They also found that the velocity and turbulence profiles measured at the same location with different conditions had a similarity property when they were normalized with the blowing ratio. This implies that the vertical location of the maximum velocity and turbulence is independent of the blowing ratio in the tested range from $3.2 \leq M \leq 5.0$. Moreover, the maximum velocity and turbulence in the profiles were found to be linearly dependent on the blowing ratio.

The current study aims to analyze how film cooling jets behave in an effusion array, injecting at a lateral angle to the mainstream flow direction. It is useful, however, to review the simpler case of only one row of jets injecting into the crossflow. Honami, Shizawa, and Uchiyama [2] measured the velocity and thermal fields created by compound angle film cooling injection ($\beta = 90°$) and they studied the effect of an asymmetric vortex created as a result of the compound angle injection. They reasoned that the absence of the vortex pair (observed in the flow field created by streamwise injection) was due to the strong curvature of the jet that created a skewed boundary layer whose vorticity was canceled by the rolling up of the primary stream. They also recognized that suppression of the asymmetric vortex can lead to higher film cooling effectiveness and wider spreading of the jet onto the surface.

In an effort to better explain the flow mechanisms created by the lateral jet injection McGovern and Leylek [3] computationally studied the dominant flow mechanisms responsible for compound angle film cooling performance. They found that as the compound angle was increased ($\beta = 0°$, 45°, 60°, and 90°), the vortex structure downstream of the hole changed from

symmetric counter-rotating vortices to a large single vortex structure. In contrast to the conclusions of Honami et al. [2], these researchers concluded that the cooling jet trajectory and the behavior of the near-field flow characteristics were primarily influenced by the static pressure at the film hole breakout plane which was found to be heavily dependent on the compound angle of the cooling hole.

The findings of McGovern and Leylek [3] agreed with the work of Lee, Kim, and Lee [4] who documented compound angle injection with velocity field measurements, pressure losses, and surface flow visualization. Along with identifying the shift from counter-rotating vortices to a single large vortex with increasing orientation angle (β = 15° to 90°), they found that an increase in the orientation angle results in better film coverage but creates a greater flow disturbance that leads to increased secondary flows and aerodynamic losses. They also proposed a flow model that identified regions with distinct differences in the near-wall flow pattern that can explain the vortex generation and has possible implications for explaining the downstream penetration height of the jet flow.

Schmidt et al. [5] measured the adiabatic effectiveness associated with a single row of β = 60° compound angle film cooling holes. The momentum flux ratio of the film cooling jets ranged from $0.16 \leq I \leq 3.9$. They found that compound angle injection had significantly greater cooling effectiveness than streamwise injection only at larger momentum flux ratios. Sen et al. [6] measured the heat transfer coefficients corresponding to the same experimental compound angle film cooling hole geometries as Schmidt et al. [5]. Their results indicate that at low momentum flux ratios, holes with a large compound angle had little effect on both the adiabatic effectiveness and the heat transfer rates. However, at high momentum flux ratios, the compound angle cooling injection significantly increased the heat transfer levels. They concluded that it is critical to know the heat transfer coefficient to effectively evaluate the film cooling performance with compound angle injection, especially at high momentum flux ratios, because the adiabatic effectiveness alone cannot determine the performance. Compound angle injection at high momentum flux ratios produced higher effectiveness values than streamwise injection, but the higher heat transfer levels resulted in poorer overall performance.

These studies serve to describe the origin of the near-field flow behavior and the performance of single row injection, but they do not illuminate how the flow field is affected by multiple row coolant injection. In an effusion film cooling scheme the influence of upstream rows can be

significant on all of the subsequent downstream rows. Ligrani and Mitchell [7] examined this phenomenon by measuring the effect of an embedded vortex (intentionally produced upstream longitudinal vortex) on the flow field and heat transfer downstream of two rows of laterally injected holes ($\beta = 50.5°$). They concluded that if the rotation orientation of the embedded vortex and cooling jet vortices was co-rotational then the film injectant is more readily swept beneath the vortex cores and into vortex upwash regions. This results in reduced coolant protection by the injectant due to the motion of the secondary flow as well as higher heat transfer over larger portions of the test surface. The contrary situation where the embedded vortex and the cooling jet vortices had opposite rotation resulted in a situation where the secondary flow vectors near the wall are directed opposite to the direction of the lateral components of the injectant velocity. In this case the injectant is less likely to be rearranged by vortex secondary flows.

Ligrani and Mitchell [7] also studied the alignment of the embedded vortex with respect to the two rows of staggered coolant injection. Varying the location of the embedded vortex with respect to the injection hole will result in some qualitative similarity, but the embedded vortex/jet arrangement with the most applicability to the current study were co-rotating vortices where the embedded vortex was aligned with a second row hole which is the flow arrangement that resulted in the highest local Stanton number maxima, occurring at the hole center line. The interaction of an embedded vortex with jet vortices has implications on multiple row compound angle jet injection.

In a study with a similar experimental design, Ligrani, Ciriello, and Bishop [8] studied how 1) the number of rows, 2) the angular orientation, and 3) the hole spacing influenced the temperature field downstream of the coolant injection. They found that the hole spacing is important in regard to injection coalescence and injectant coverage along the test surface and the momentum flux ratio has important consequences in regard to jet lift-off.

In summary, past research has been performed to study the near-field flow behavior of single compound film cooling holes or a single row of holes with few investigations on the effect of the laterally injecting hole(s) on the near-region heat transfer. However, these studies fail to examine the flow and thermal field created by film cooling injection from several rows of compound angle holes.

Experimental Facilities and Measurement Methods

The purpose of this study was to obtain high resolution flow and thermal field measurements for a densely-spaced effusion array of compound film cooling holes. To achieve good spatial resolution, it was beneficial to use a large-scale model while matching the relevant non-dimensional parameters such as the momentum flux ratio. This section describes the experimental facility in which these measurements were made, the instrumentation that was used, and the corresponding estimates of measurement uncertainty.

Experimental Facilities

The experiments were conducted in a closed-loop, low-speed wind tunnel equipped with a combustor simulator test section. The geometric scaling factor for the test section was approximately nine times that of a realistic combustor, allowing for good experimental measurement resolution. Figure 5.1 illustrates the wind tunnel and identifies the important components such as the supply fan, the flow and thermal conditioning, and the combustor test section.

A 50 hp axial fan supplied air flow in the closed-loop circuit. The flow was passed through a primary heat exchanger to maintain a steady temperature of the working air. A transition section then divided the air path into three channels including a primary channel, representing the core flow (crossflow), and two secondary channels which supplied the effusion air. Only the bottom secondary channel was activated and was used to supply coolant flow to the combustor section.

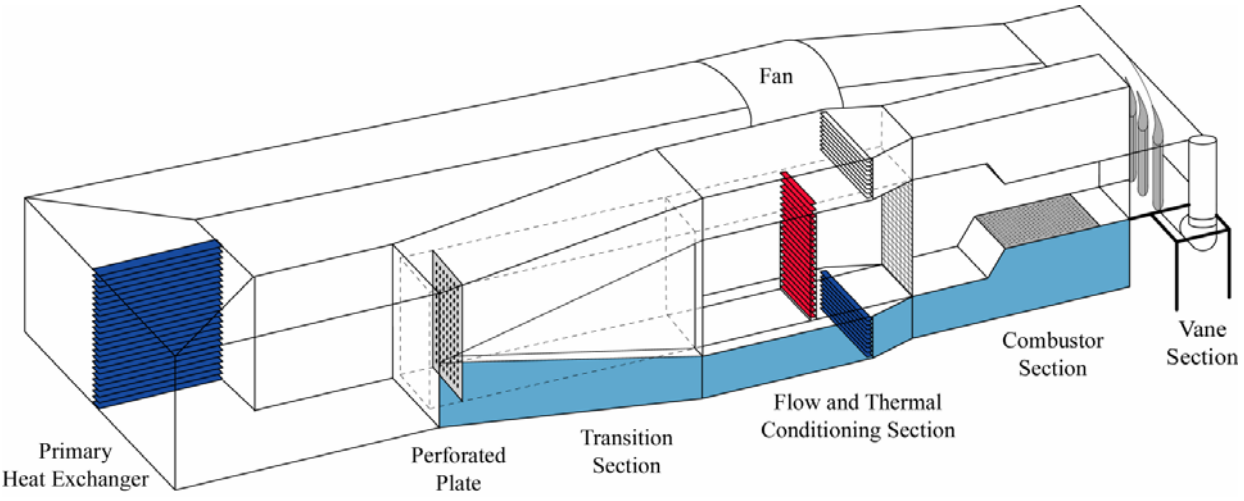

Figure 5.1. Illustration of the wind tunnel facility used for experiments.

To gain the effusion flows necessary to meet the requirements of the experiments, a perforated plate was used to control the mass flow ratio between the primary and secondary channels by creating a pressure drop in the primary channel.

At a distance 2 m downstream of the perforated plate, the flow in the primary passage passed through a bank of heaters followed by a series of screens and flow straighteners. The heater section consists of three individually controlled banks of electrically powered, finned bars supplying a maximum total heat addition of 55 kW. The flow in the secondary passage passed through another heat exchanger to further reduce the temperature of the air that supplied the effusion test plate. The heaters and heat exchanger were only used for measurements of the temperature field.

The combustor test section began immediately downstream of the screens and flow straighteners. The primary flow path of the test section at this location had a height of 1 m and a width of 1.1 m, which was further reduced by a 45° contraction to dimensions of 0.55 m x 1.1 m, creating an inlet to exit area ratio of 1.8. The compound angle effusion was injected from the bottom wall immediately after the contraction, which was at the start of the straight channel leading to the turning vane section.

The flow in the secondary passage that supplied the effusion plate was directed into a 0.61 m^3 plenum and the inlet flow to the plenum was metered via an adjustable valve. The ideal effusion jet velocity was calculated based on an inviscid analysis using the difference between the adjustable total plenum supply pressure and the exit static pressure. The actual effusion jet velocity corresponding to the required momentum flux ratio was taken as the product of the ideal velocity (found from the inviscid analysis) and the appropriate discharge coefficient for this particular effusion geometry and flow configuration. The discharge coefficient measurements will be discussed later in this paper.

Effusion Plate Design and Measurement Locations

The effusion plate was constructed of 2.54 cm thick urethane foam with a low thermal conductivity of k = 0.029 W/mK to allow for adiabatic surface temperature measurements. The three-dimensional coordinates were designated as X, Y, and Z which corresponded to the streamwise, pitchwise, and spanwise directions of the combustor test section, respectively. The dense pattern of 1208 cylindrical film-cooling holes was cut into the urethane foam using a five-

axis water jet. The holes were arranged into 35 rows in the streamwise direction.

The presence of the compound angle injection in the confined crossflow produced an accumulation of flow at the sidewall in the direction where the jets were angled (positive Y-direction). It was necessary that the measurements be made on a location on the effusion liner where the flow field was not influenced by the sidewalls. This implied that the measurements should be made where there was a velocity and temperature gradient of zero in the pitchwise direction at all locations along the streamwise extent of the liner as shown in Figure 5.2. This location was found to be at $Y/W = 0.3$ ($Y/S_P = 12$) at all coolant flow rates and will be discussed further in detail.

Velocity and temperature profile measurements were measured at $X/S_S = -1, 0, 5, 11, 17, 23, 29$, and 35 to understand the development of the flow and thermal fields at different streamwise locations on the compound angle effusion liner. Velocity and temperature profiles were measured with and without crossflow. The momentum flux ratio is meaningless with a zero crossflow velocity, so the Reynolds number of the first row effusion jets was used to identify

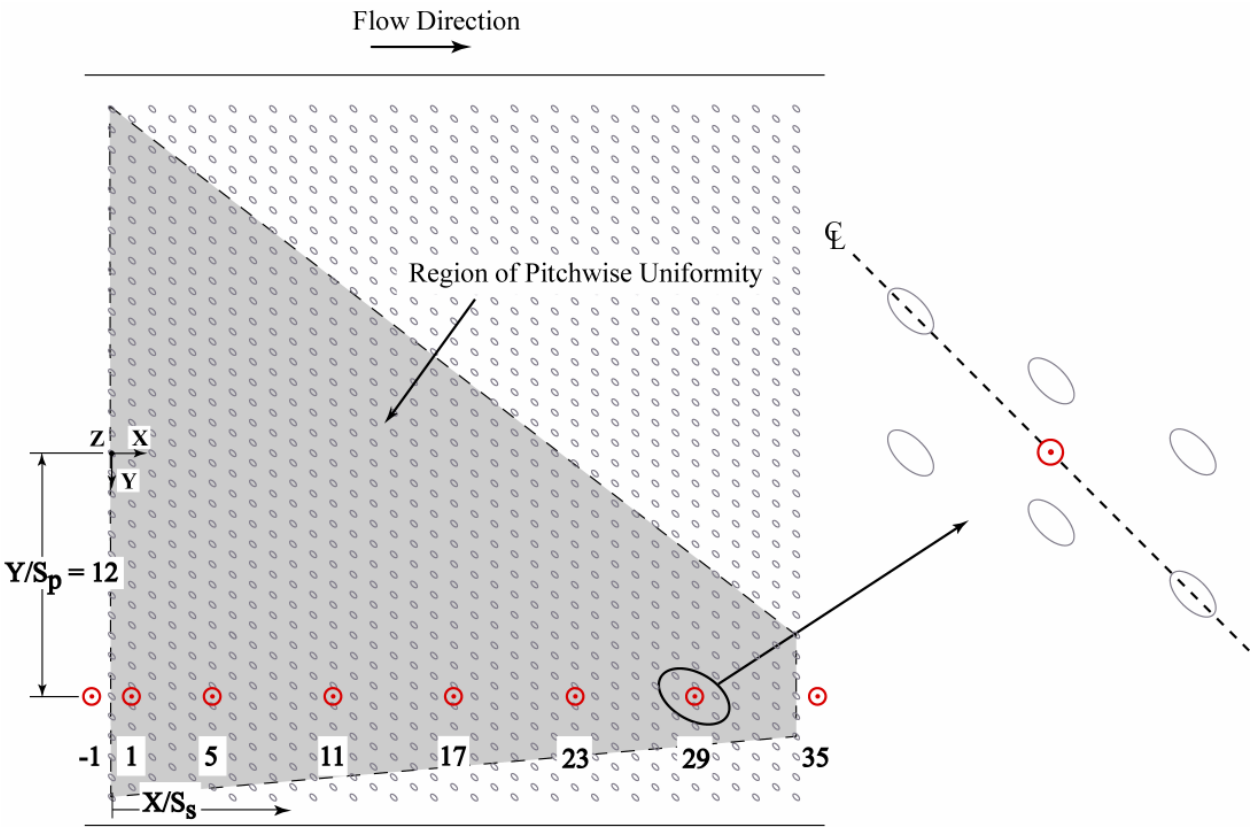

Figure 5.2. Illustration of the effusion liner and measurement locations.

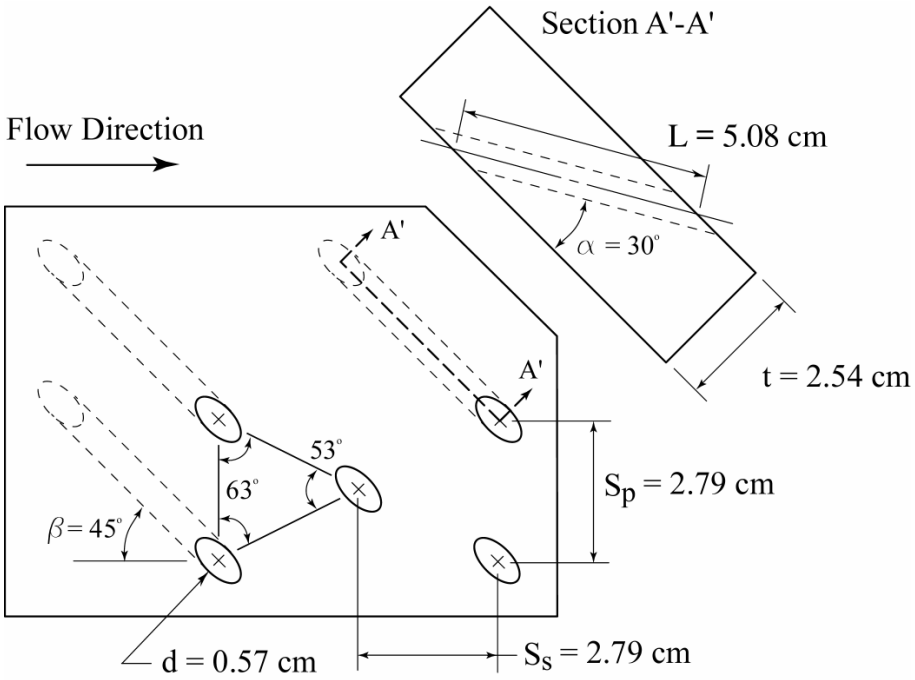

N	1208
d	0.57 cm
α	30°
β	45°
L/d	8.9
t/d	4.5
S_s/d S_p/d	4.9

Figure 5.3. Illustration of the effusion hole geometry and tabulated parameters.

cases with and without crossflow to make an effective comparison. The cooling jet Reynolds numbers investigated in this study were Re_j = 791, 3200, and 4082. The Reynolds numbers were based on the hole diameter of 0.57 cm. The spacing to diameter ratio was 4.86 and the cooling hole pattern on the test plate is described in Figure 5.3. With a crossflow velocity of 2.3 m/s the Reynolds numbers of the film cooling jets corresponded to film cooling momentum flux ratios of I = 1.0, 15.3, and 25.1.

Typical operating conditions for the experiments consisted of a matched coolant and mainstream temperature of 30˚C. For the temperature field measurements, the mainstream temperature was 55˚C with a coolant flow temperature of 13˚C. These conditions resulted in density ratios of 1.0 for all of the unheated cases and 1.14 for all of the heated cases.

Because the wind tunnel supplied the flow through a closed-loop circuit the total flow was divided to supply the mainstream and coolant flow. Of the total flow between 4% and 20%, depending on the coolant flow rate, was directed through the secondary coolant passages for the effusion cooling while the remaining flow was directed through the primary passage of the test section. The core flow accelerated by a factor of 1.04, 1.19, and 1.25 for the coolant flows of I = 1.0, 15.3, and 25.1, respectively, through the test section as a result of the coolant mass addition. These flow conditions resulted in a test section inlet Reynolds number of $Re_{\infty,inlet} = 8.0 \times 10^4$,

based on the channel height. The exit Reynolds number was $Re_{\infty,exit}$ = 8.1 x 10^4, 9.5 x 10^4, and 1.0 x 10^5, depending on the coolant flow rate.

Discharge Coefficient Measurements

The compound angle effusion liner discharge coefficients were measured over a range of absolute pressure ratios. The absolute pressure ratio is defined as the ratio of the total absolute pressure in the coolant supply plenum to the static absolute pressure at the effusion hole exit. The measured value at each pressure ratio was based on the average discharge coefficient of 319 cooling holes arranged in 22 rows. The actual jet velocity was calculated based on the total coolant mass flow measured with a laminar flow element. The ideal effusion jet velocity was calculated based on an inviscid analysis using the difference between the total plenum supply pressure and the exit static pressure. It is an ideal analysis because it neglected losses as the flow passed through the cooling holes.

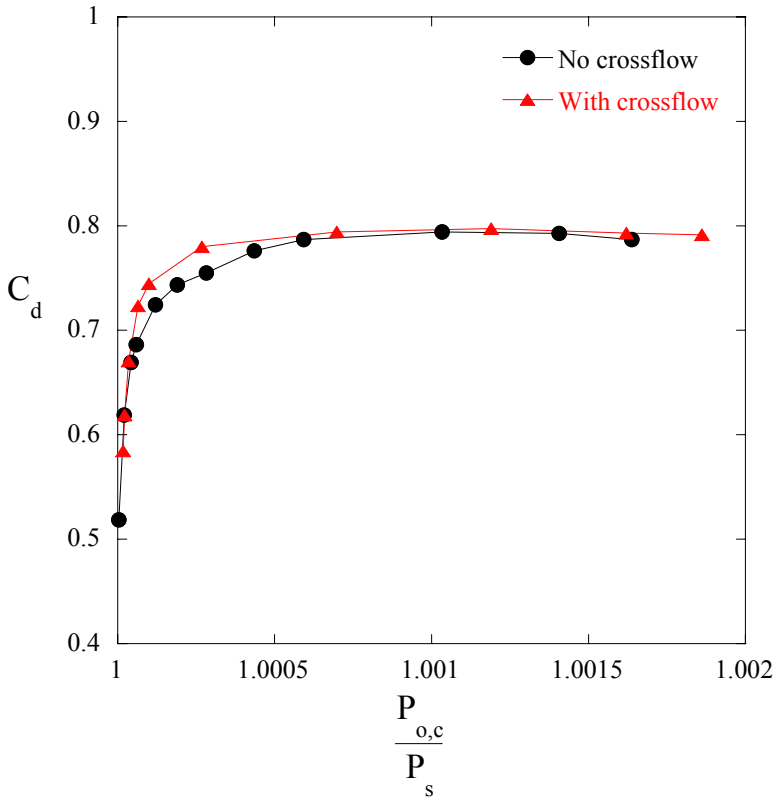

Figure 5.4. Discharge coefficients of the compound angle effusion holes based on absolute pressure ratio.

The discharge coefficients for the array were measured with and without external crossflow

to gain an understanding of how sensitive the discharge coefficients were to the crossflow conditions. These measurements are reported in Figure 5.4. With no external crossflow the discharge coefficient approached a value of $C_d = 0.8$ as the absolute pressure ratio was increased. The discharge coefficient with external crossflow also reached a value of $C_d = 0.8$ at the higher pressure ratios. At pressure ratios in the range $1.00003 \leq P_{o,c}/P_s \leq 1.0007$, the discharge coefficients with external crossflow were higher. This range of pressure ratios corresponded to the blowing ratios $0.4 \leq M \leq 2$.

The external crossflow slightly affected the hole exit pressure plane, and consequently the behavior of the jet flow within the hole, in the range $1.00003 \leq P_{o,c}/P_s \leq 1.0007$, resulting in increased discharge coefficients. The work of Crabb et al. [9], Thole et al. [10], Burd and Simon [11, 12], Walters and Leylek [13], and Rowbury et al. [14] corroborated these discharge coefficient results in that external crossflow enhanced the discharge coefficient because the crossflow was accelerated due to blockage by the coolant injection thereby reducing the static pressure at the hole exit. Burd and Simon [12] found that larger compound angles ($\beta \sim 60°$) increased the flow blockage compared to streamwise injection, which exacerbating the effect of the crossflow on the hole exit plane static pressure and increased the discharge coefficient.

Measurement Methods and Uncertainty

The velocity and turbulent statistics were measured with a three-component laser Doppler velocimetry (LDV) system. The system used two back-scatter probes that were capable of measuring all three spatial components of the velocity: the streamwise, pitchwise, and spanwise components in the annular sector. The probe was equipped with a 750 mm focusing lens with a 2.6 magnification beam expander. The probes were angled toward each other at 17˚ from their symmetry plane, which was orthogonal to the streamwise direction. This arrangement resulted in a measurement volume at the beam crossing of 73 μm in diameter and 1.3 mm in length. In order to take measurements near the surface the entire arrangement was tilted toward the surface at an 8˚ angle. A geometrical conversion previously used by Vakil et al. [15] was used to transform the measured values of the non-orthogonal coordinate system of the LDV to the coordinate system relevant to the combustor simulator.

The air flow was seeded with olive oil particles that had an average diameter of 1 μm. At each measurement location 10,000 data points were acquired for each component over a sample

time of approximately 20 seconds. The probability of obtaining a sample was proportional to the speed of the flow, therefore statistical particle bias corrections were applied to the data by weighting each individual sample based on the residence time of a particle in the probe volume. The partial derivative method, described by Moffat [16], was used to estimate the uncertainties of the measured values. The precision uncertainties for all of the measured values were calculated as $\pm 2\sigma$ which corresponded to 95% of the normal distribution. The uncertainty associated with the streamwise velocities measured by the LDV was ±2.5% and the uncertainty of the rms of the velocity fluctuations normalized to the mainstream velocity was ±2.0%.

The non-dimensional temperatures reported in this study indicated how effective the coolant air was at preventing mixing leading to the reduction of its cooling capacity. The effectiveness is necessarily a combination of the local flow temperature as well as the inlet and coolant temperatures. All of the temperatures were measured using 30-gage, type E thermocouples that were connected to a National Instruments SCXI data acquisition system through 20-gage thermocouple extension wire. Each temperature value was measured at 1 kHz over a period of 20 seconds. The thermocouple measurements used to quantify the temperature field had a bias uncertainty of ±0.2°C.

The pressure difference between the plenum and the liner surface that was used to set the flow rate through the effusion holes was measured with a 12.7 mmH_2O Setra pressure transducer which had a bias uncertainty of ±0.079% of the full scale (or ±0.10 Pa). The pressure difference was measured at 1 kHz over a period of 60 seconds using an SCXI DAQ system. The injectant flow for the discharge coefficient measurements was measured using a laminar flow element (LFE) that had a bias uncertainty of ±0.86% of the actual reading. The LFE pressure drop was measured using a 127 mmH_2O Setra pressure transducer, which had a bias uncertainty of ±0.019% of the full scale (or ±0.24 Pa).

The uncertainty of the discharge coefficient measurements, C_d, was ±1.56%. The uncertainty of the cooling jet velocities and the cooling jet momentum flux ratios reported for the field measurements was ±1.6% and ±3.2%, respectively. The uncertainty of the flow velocities normalized to the freestream velocity and jet velocity was ±3.3% and ±3.0%, respectively. The uncertainty of the calculated non-dimensional temperature, θ, was ±0.007, ±0.0084, ±0.011 at θ = 0, 0.26, and 0.65, respectively.

Experimental Results

This section discusses the results of the velocity and thermal fields measured on the compound angle effusion liner. Surface static pressures were measured along the streamwise extent of the liner to determine how the effusion jet velocity changed in the streamwise direction, especially due to the upstream flow contraction. Due to the compound angle nature of the effusion injection in the confined test section, it was important to find where the flow field was uniform in the pitchwise direction, i.e., where the flow field was not influenced by the test section side-walls.

Static Pressure Measurements

The static pressure on the surface of the effusion liner was measured along the streamwise coordinate of the test section. The purpose of these measurements was to determine how the effusion jet velocity was varying due to the external influences such as the 45° contraction and effusion flow accumulation. These results include measurements that were made with crossflow as well as measurements of the surface pressure without crossflow.

The local jet momentum flux ratio (based on the local mass-averaged mainstream flow velocity) was normalized to the momentum flux ratio of the first row of jets in order to compare the trends of each coolant flow along the streamwise direction. As shown in Figure 5.5 there

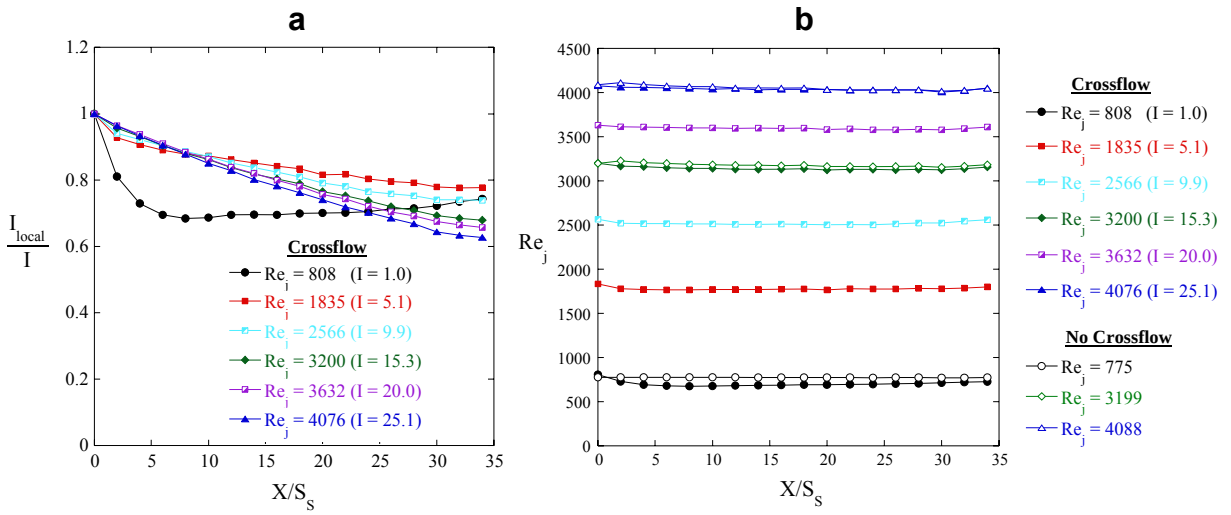

Figure 5.5. a) Local effusion jet momentum flux ratio normalized to the momentum flux ratio of the first row of jets and b) the local film cooling Reynolds numbers with and without crossflow.

were six film cooling cases with crossflow and three cases with no crossflow. For the sake of

consistency and clarity the film cooling cases were identified using the Reynolds number and momentum flux ratio of the first row of film cooling jets. The three effusion flows with no crossflow have no momentum flux ratio by definition and were not included in Figure 5.5a. However, the Reynolds number can represent film cooling flow with and without crossflow and these data are shown in Figure 5.5b.

For all film cooling Reynolds numbers above 1835, the ratio of the local to inlet momentum flux ratio followed an expected trend as it decreased for all cases, at larger slopes for higher film cooling Reynolds numbers. These trends are due to the increased air flow from the effusion jets increasing the mass-averaged mainstream channel flow velocity and consequently reducing the local momentum flux ratio. The crossflow separated at the exit of the contraction and created a region of lower pressure that resulted in a high film cooling momentum flux ratio at the first row of jets. The crossflow then reattached resulting in a decreasing local momentum flux ratio. Figure 5.5b shows that the reattaching mainstream flow caused a momentum flux ratio decrease for $Re_j = 808$ because the coolant injected at $Re_j = 775$ without crossflow resulted in very little streamwise variation of the local momentum flux ratio.

Determination of Measurement Locations

The compound angle effusion coolant was injected into a confined low speed crossflow. Due to the nature of the compound angle injection in the annular test section, the flow inevitably interacted with the sidewalls. The effect was exacerbated at higher effusion flow rates; therefore, it was necessary to determine where the velocity and thermal fields were uniform in the pitchwise direction. Uniformity was defined in a location with a zero gradient of the velocity and temperature in the pitchwise direction.

Velocity and temperature measurements were made across the pitch of the test section five cooling hole diameters from the surface ($Z/d = 5$). This specific vertical distance was chosen because it was above the jet core of the upstream film cooling jet, yet it demonstrated the behavior of the coolant velocity and temperature because it remained within the film layer. These measurements were made at several streamwise locations and included the pitchwise region from $Y/W = -0.1$ to 0.45. Figure 5.6 shows where the flow was fully developed, establishing that the velocity and temperature profiles be measured at $Y/W = 0.3$ ($Y/S_P = 12$).

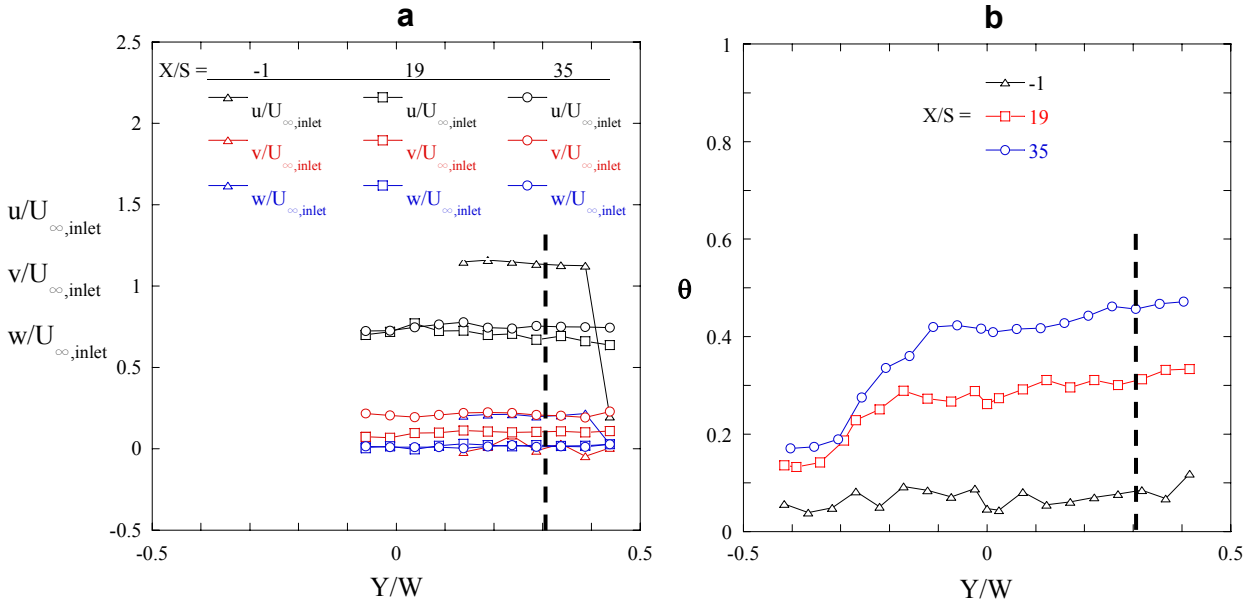

Figure 5.6. Pitchwise measurements showing a) three components of velocity and b) non-dimensional temperature at the positions X/S_S = -1, 19, and 35 for I = 1.0.

At pitchwise values below Y/W < -0.1 the non-dimensional temperature (θ) was non-uniform which highlighted the dependence of the uniformity on the number of upstream cooling holes along the compound angle coordinate (β = 45°). The significance of this observation is that for the pitchwise profile made at X/S_S = 19, the location Y/W = 0.25 has nineteen upstream cooling hole rows aligned toward it. However, the location Y/W = -0.25 only has seven rows of holes aligned toward it due to the compound angle. This implies that the pitchwise region of velocity and temperature uniformity became smaller in the streamwise direction.

Flow Field Results

Once it was determined where the pitchwise velocity and thermal fields were uniform, velocity profiles were measured at X/S_S = -1, 1, 5, 11, 17, 23, 29, and 35 to focus on how the coolant layer developed in the streamwise direction. The three components of velocity were measured at all streamwise locations for I = 1.0, 15.3, and 25.1.

Effusion Injection With Crossflow. Measurements with crossflow were non-dimensionalized to the local mainstream velocity. The streamwise component of the velocity with crossflow is shown in Figure 5.7. These plots show the development of the streamwise velocity and suggest

that when the coolant is injected at I = 1.0 (Figure 5.7a) the local flow velocity in the region above Z/d > 5 decreases along the liner. This is a counter-intuitive observation because effusion injection normally accelerates the flow due to the mass addition. Incidentally Z/d = 5 coincides with the location of peak velocity at X/S_S = -1 due to the flow passing through the contraction (see Figure 5.1). In contrast, the flow is accelerating in the region between the peak velocity and the wall. This suggests that the flow non-uniformity created by the contraction was redistributed due to the coolant addition leading to a more uniform profile.

The higher momentum injectant (Figures 5.7b and 5.7c) showed different trends than Figure 5.7a, revealing that there was sufficient coolant injection to initiate flow acceleration at all locations of the flow field. The maximum velocity for I = 15.3 and 25.1 at X/S_S = 35 was u/U_∞ = 1.8 and 2.2, respectively, and at these momentum flux ratios there was a 9% difference in their penetration heights at X/S_S = 35.

Computations made by McGovern and Leylek [3] indicate that there is a single large vortex downstream of each cooling hole that remains intact until a distance of X/d = 6 downstream of the coolant injection. Because the spacing of the holes in the current study is S_S/d = 4.9, it can be reasoned that the vortices created by the first row are intact at the second row and correspondingly for each subsequent row.

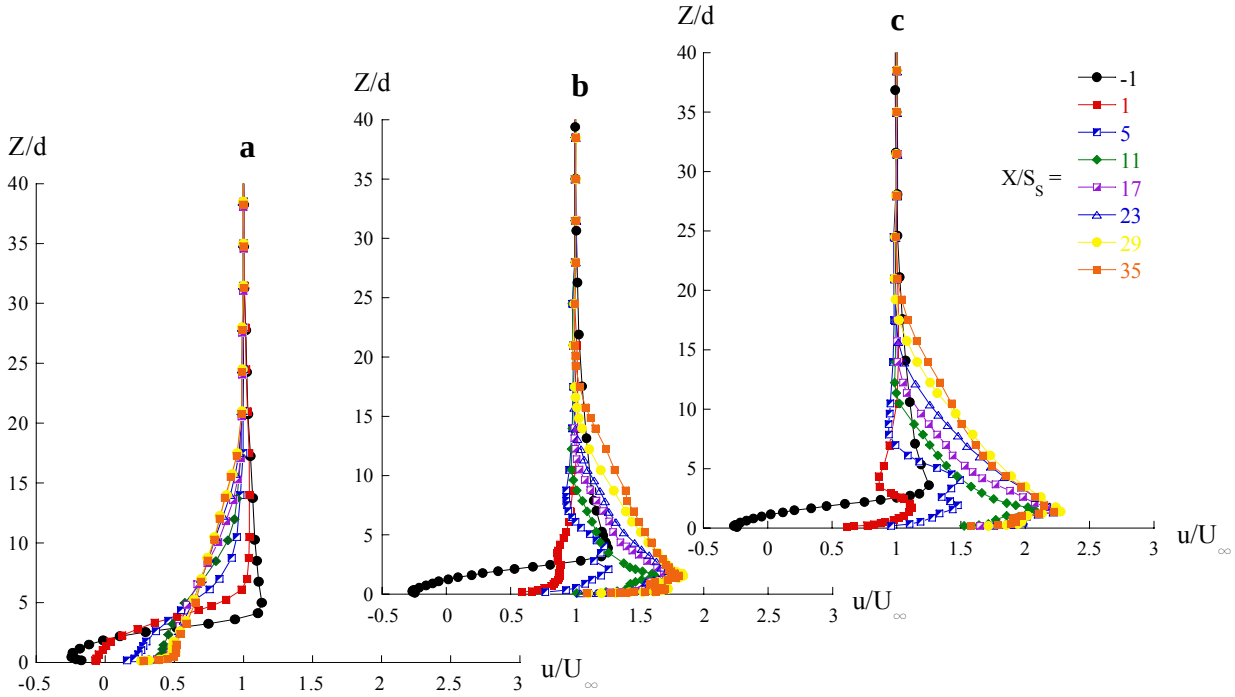

Figure 5.7. Profiles of the streamwise velocity components with crossflow for a) I = 1.0, b) I = 15.3, and c) I = 25.1 measured at the streamwise positions shown.

The pitchwise and spanwise velocity component measurements are given in Figures 5.8 and 5.9, respectively. These measurements indicated that the effusion flow of I = 1.0 did not strongly affect the pitchwise velocity component. The pitchwise velocity reached a maximum value of $v/U_\infty = 0.32$ at $X/S_S = 35$ (at $Z/d = 1.17$) that was about 40% lower than the streamwise velocity component of $u/U_\infty = 0.51$. This is in contrast to I = 15.3 and 25.1 where the pitchwise velocities were about 10% higher than the streamwise component. This was in part due to the higher momentum of the cooling jets providing a more effective buffer from the crossflow. The penetration height as measured by the streamwise velocity component was found to increase linearly as a function of the streamwise position.

It is interesting to note that for the coolant injection of I = 15.3 and 25.1 the film flow develops in such a way that the maximum streamwise and pitchwise velocities only increase by 8% and 11%, respectively, from $X/S_S = 11$ to 35. This small increase suggests that the local crossflow velocity (external to the coolant layer) is accelerating at a similar rate to the coolant velocity. Most of the flow acceleration occurs between $1.4 < Z/d < 20$. However, at $X/S_S = 35$ the coolant layer velocity remains constant while the local mainstream continues to increase, resulting in lower u/U_∞ and v/U_∞ values at that location.

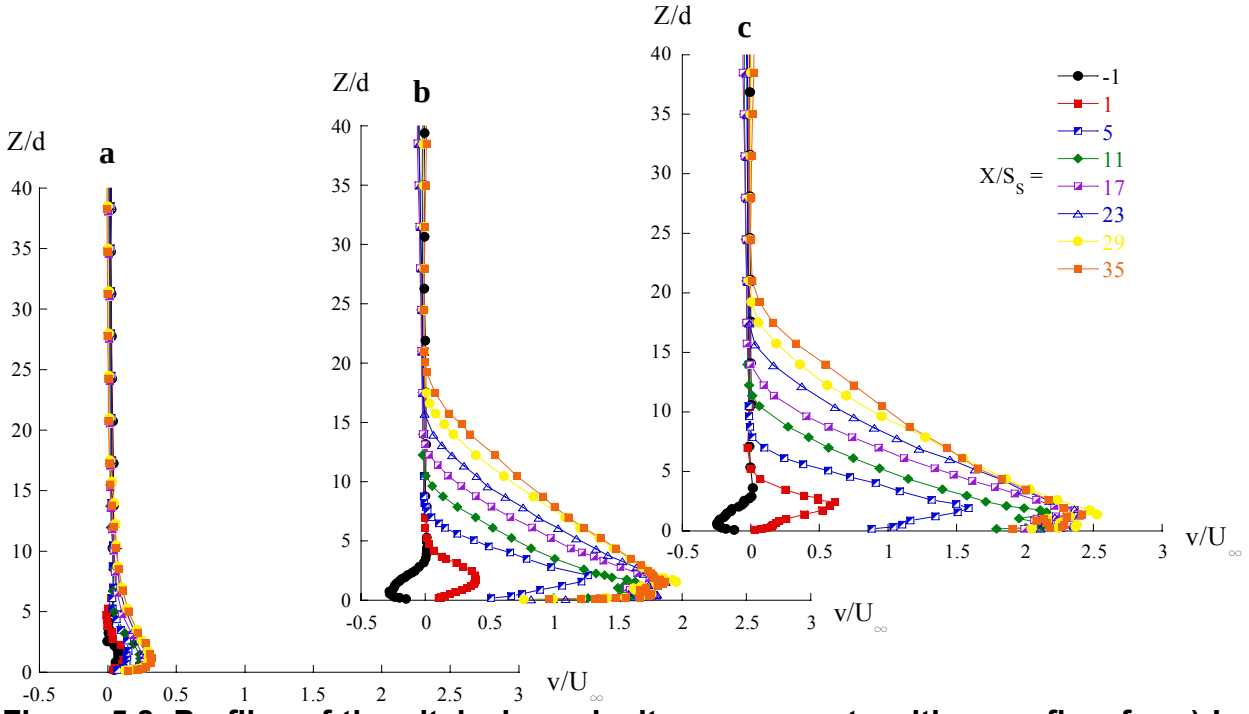

Figure 5.8. Profiles of the pitchwise velocity components with crossflow for a) I = 1.0, b) I = 15.3, and c) I = 25.1.

To explain why the coolant layer velocity remained constant at $X/S_S = 35$ while the local mainstream continued to increase, it is revealing to compare the flow development at the streamwise positions $X/S_S = 29$ and 35. The factors that are necessary to understand the flow development are the numbers of upstream hole rows along both the streamwise coordinate and along the compound angle coordinate aligned with the effusion jets ($\beta = 45°$). The last two measurement locations shared the same amount of rows along the compound angle coordinate (aligned with the hole centerlines), but differed in the number of upstream holes in the streamwise direction, suggesting that the development of the coolant layer flow field depended mostly on the number of upstream rows along the compound angle coordinate. The development of the local crossflow velocity was affected by the diffusion of coolant and the accumulation of flow along the streamwise direction which was influenced by the number of upstream rows.

The velocity component profiles of Figure 5.9 showed interesting trends based on the streamwise location. The lowest coolant flow rate of Figure 5.9a reveals that there was very little flow transport in the spanwise direction except for at the first few rows of cooling holes. The higher flow rates produced an effect at the first row of holes that directed crossflow toward the surface and will be discussed in further detail. The velocity profiles at $X/S_S = -1$ and 1 were altered as a result of strong entrainment of the flow toward the surface. The flow field created by

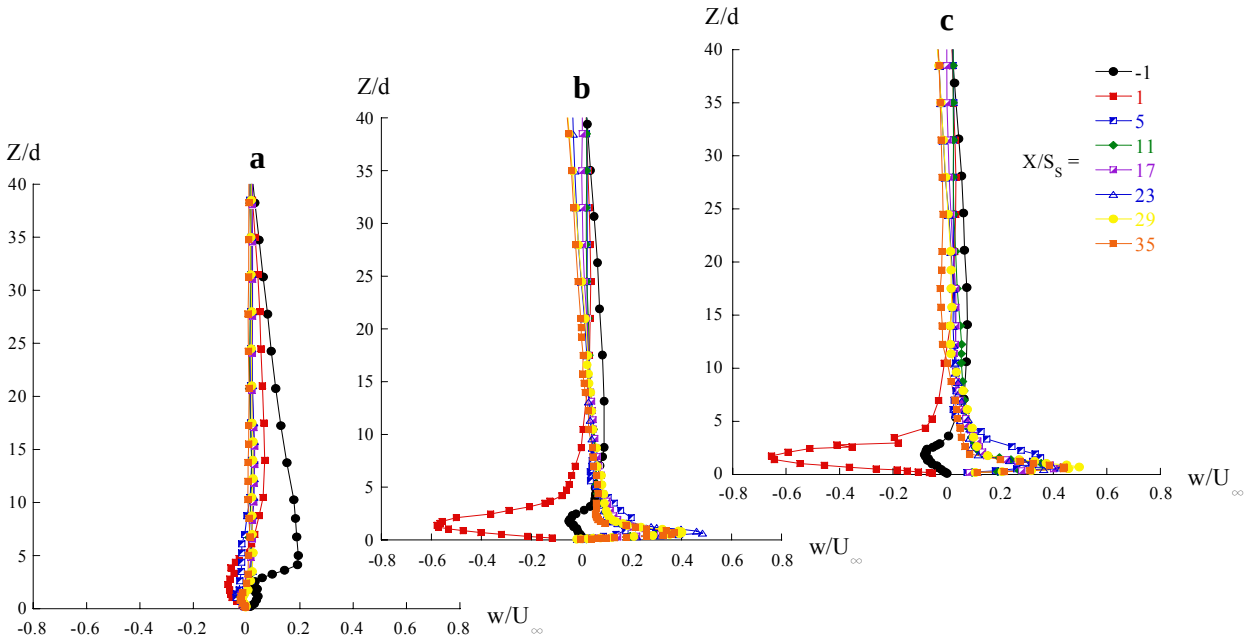

Figure 5.9. Profiles of the spanwise velocity components with crossflow for a) I = 1.0, b) I = 15.3, and c) I = 25.1.

the higher momentum jets reversed the spanwise velocity and created positive spanwise flow at $X/S_S \geq 5$. Similar spanwise velocity values were measured at both of the higher coolant flows.

To determine the coolant penetration height the flow angles were calculated in the plane made by the streamwise and pitchwise (X and Y) axes. The flow angles shown in Figure 5.10 are important because they combine the information from the u and v velocity components to determine how much influence the injectant has on the flow field. This information includes the direction of the flow and the penetration of the coolant.

The coolant injection of I = 15.3 and 25.1 resulted in a maximum flow angle of approximately $\varphi = 45°$ for the near-wall film downstream of $X/S_S = 5$ and coolant injected at I = 1.0 reached a maximum flow angle of $\varphi = 32°$. Upstream of the injection and at the first row the flow angle is negative for I = 1.0 because of negative near-wall streamwise velocity produced by recirculation due to the test section contraction. The flow angle is negative for I = 15.3 and 25.1 because the pressure field produced by compound angle injection directed the inlet crossflow toward the lower pressure side of the jets. The penetration height was based on the deviation of the local flow angle from the inlet flow angle and was determined where the flow angle difference was reduced to a value of 1% of $\varphi = 90°$ or 0.9°. At $X/S_S = 29$ these locations were

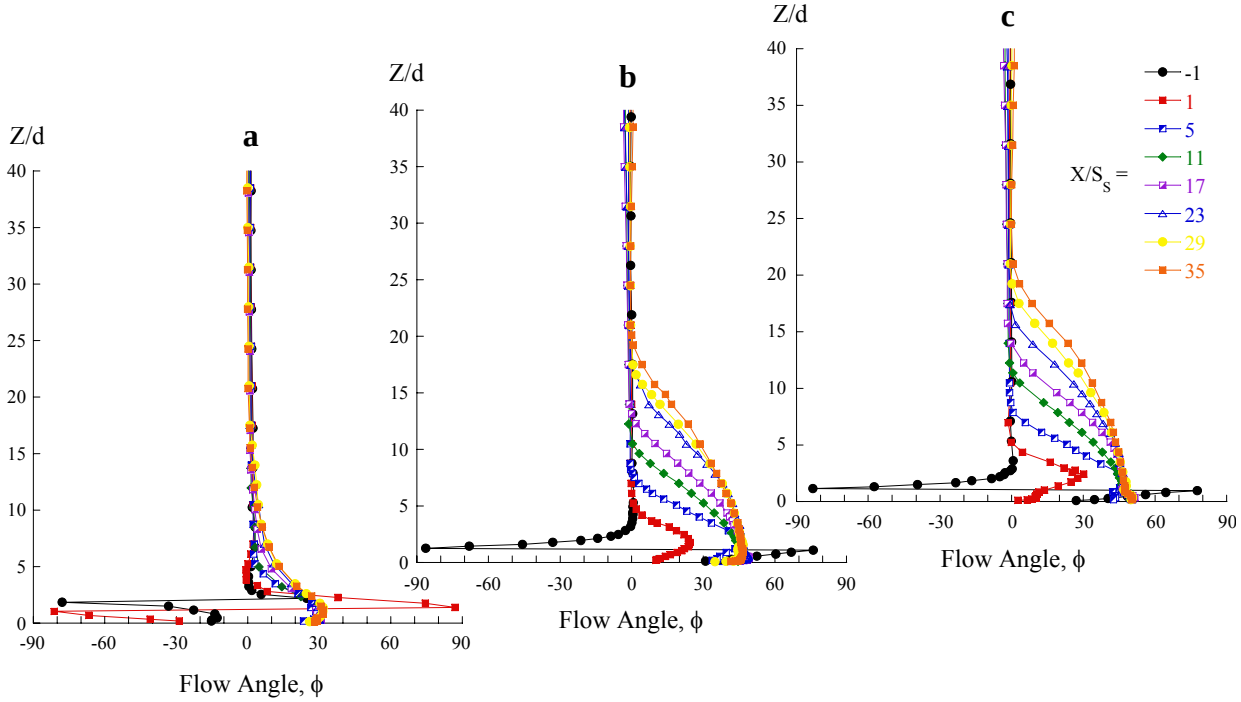

Figure 5.10. Profiles of the XY-plane flow angle, φ, with crossflow for a) I = 1.0, b) I = 15.3, and c) I = 25.1.

found to be Z/d = 13.5, 17.0, and 18.9 for I = 1.0, 15.3, and 25.1, respectively, with a linear penetration height increase for I = 15.3 and 25.1.

The turbulence levels created by the jets in crossflow are shown in Figure 5.11. The elevated levels of turbulence throughout the flow field imply redistribution of turbulence (diffusion) and also signify a shear layer between two dissimilar layers of fluid leading to the production of turbulence. Interestingly, the turbulence penetrated to similar heights for each film cooling momentum flux ratio, implying that the rate of turbulence diffusion is independent of the momentum flux ratio. However, the value of the turbulence levels varied depending on the film cooling momentum flux ratio. Note that for measurements with crossflow, the turbulence levels were normalized to the freestream velocities at the locations of the velocity measurements.

The turbulence field created by I = 1.0 injection is shown in Figure 5.11a. The inlet turbulence level at X/S_S = -1 reached a maximum value of 27% at Z/d = 2.9 when normalized by the inlet freestream velocity of $U_{\infty,in}$ = 2.3. The maximum turbulence level continued to decrease in the streamwise direction suggesting that the high turbulence level at X/S_S = -1 was due to the separation of the mainstream at the exit of the contraction. The turbulence continued to penetrate higher into the crossflow due to injection of the coolant which generated turbulence that diffused into the mainstream. By X/S_S = 35 the turbulence level was maintained at a level of TL_∞ = 8.9% at Z/d = 2.9 (spanwise location of maximum inlet turbulence level).

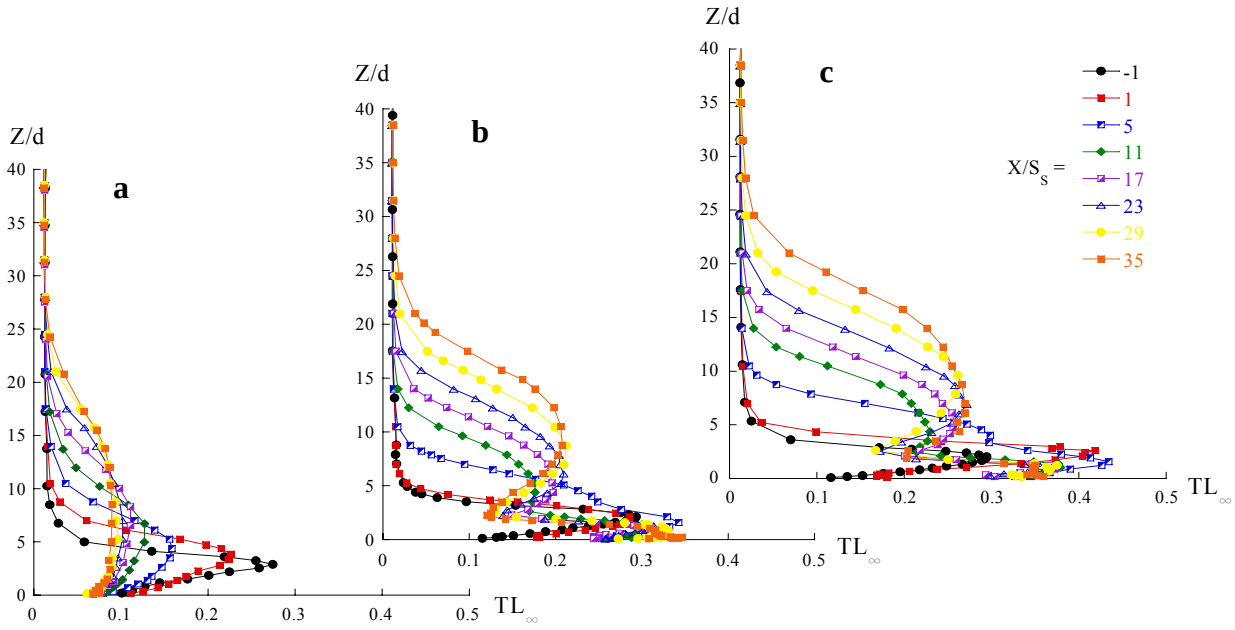

Figure 5.11. Turbulence level profiles (normalized by U_∞) with crossflow for a) I = 1.0, b) I = 15.3, and c) I = 25.1.

The data of Figures 5.11b and 5.11c reveal that the turbulence has different trends in different regions of the flow field. These regions can be categorized into (1) the coolant layer outer region between the jet upper shear layer and the crossflow and (2) the region from the jet upper shear layer to the wall (which includes the lower and upper jet shear layer, the jet core, and the wake region between the lower shear layer and the wall). The turbulence level in the outer regions of the coolant layer steadily increased in the streamwise direction as the layer continued to expand and as the turbulence was generated from the jet shear layer. It was observed that at any streamwise location the turbulent fluctuations produced by the diffusing coolant layer were detected at larger vertical distances into the crossflow than changes to the velocity field.

In Figures 5.11b and 5.11c the turbulence level upstream of the cooling holes at $X/S_S = -1$ reached a maximum value of 29% which was due to (1) the mainstream air flowing through the contraction and (2) flow acceleration due to a low pressure effect caused by the coolant injection. Progressing in the streamwise direction, the turbulence level throughout the entire flow field increased to a maximum value of 34% and 43% at $X/S_S = 5$ for I = 15.3 and 25.1, respectively. Similar to the streamwise velocity, the turbulence continued to increase in the outer region, yet it decreased in the inner region until it reached an asymptotic value at $X/S_S = 23$.

Qualitative flow visualization allowed for an explanation of the behavior of the flow, especially for the interaction of the approaching crossflow and injectant at the first row of holes. The crossflow was observed to accelerate toward the first row of cooling jets, becoming entrained by the high speed jets. The manifestation of the entrainment and resulting acceleration was marked by the crossflow flowing toward the wall (corroborated by Figures 5.9b and 5.9c, $X/S_S = 1$) as well as a negative pitchwise velocity (opposite to the transverse angle of the jet). Higher pressure at the exit of the first row of laterally injecting jets directed the crossflow toward the lower pressure side of the jet and conferred a negative pitchwise component to the velocity.

Lee, Kim, and Lee [4] proposed a flow model to describe the behavior of the crossflow as it approaches and passes the compound angle jet. They measured a similar negative pitchwise velocity approaching the compound angle jets. The behavior of the flow in their model was based on the pressure field at the jet breakout plane. They established the model to explain how the asymmetric pressure distribution can direct the flow in the pitchwise direction. In the present study, the jet injection increased the near-wall turbulence and augmented the existing turbulence created by the flow separation due to the contraction.

Effusion Injection Without Crossflow. The velocity and turbulence profiles without crossflow are presented in Figures 5.12 through 5.15. It should be reiterated that injection into quiescent air precluded the use of the crossflow velocity as a normalization parameter. These measurements were normalized to the jet velocity. In order to make an effective quantitative comparison between the flow field measurements made with and without crossflow, the measurements made with crossflow have been re-normalized with the film cooling jet velocity and have been re-plotted.

Measurements of the velocity components reveal that there was a comparable split between the streamwise and pitchwise velocity components (within 8% for both flow rates with crossflow) suggesting that the coolant flow was directed at nearly a 45° to the streamwise coordinate. The velocity profiles measured at X/S_S = 29 and 35 showed similarities because the same number of jets were directed toward each location along the compound angle coordinate (β = 45°). The velocity components shared a similarity between the shape of each velocity profile and the penetration height based on the component. For the cases shown in Figure 5.12, the maximum velocity vector magnitude as a percentage of the jet velocity at X/S_S = 35 was about 85%. The average maximum streamwise velocity of all of the flow cases in Figure 5.12 at X/S_S = 35 was u/U_j = 0.56. For the cases with crossflow the velocity above the cooling layer increased incrementally at each streamwise location due to the film cooling injection.

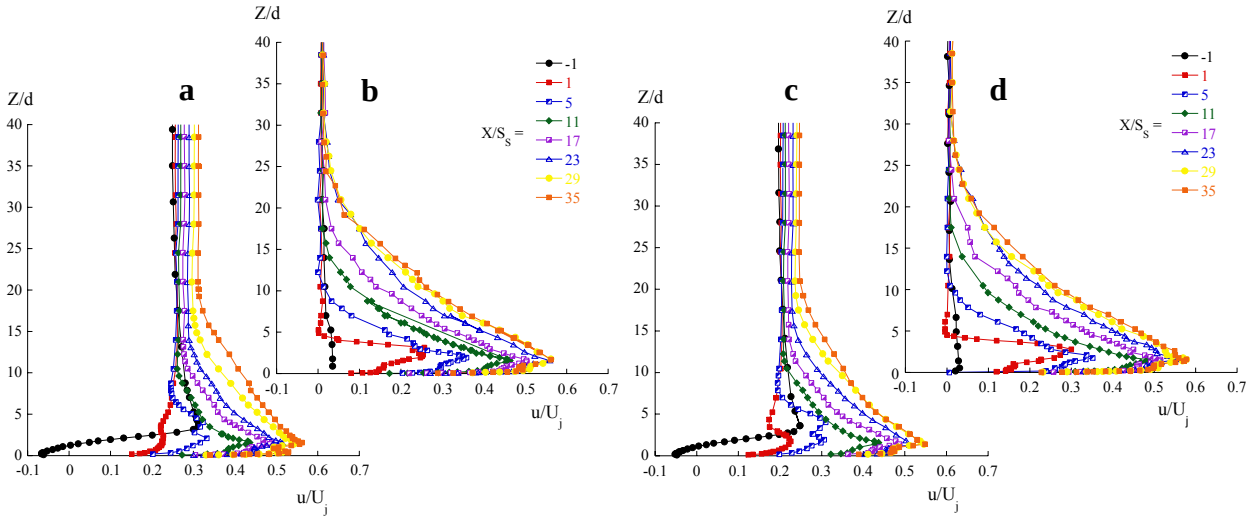

Figure 5.12. Profiles of the streamwise velocity for Re_j = 3199 (a) with crossflow and (b) without crossflow and Re_j = 4088 (c) with crossflow and (d) without crossflow.

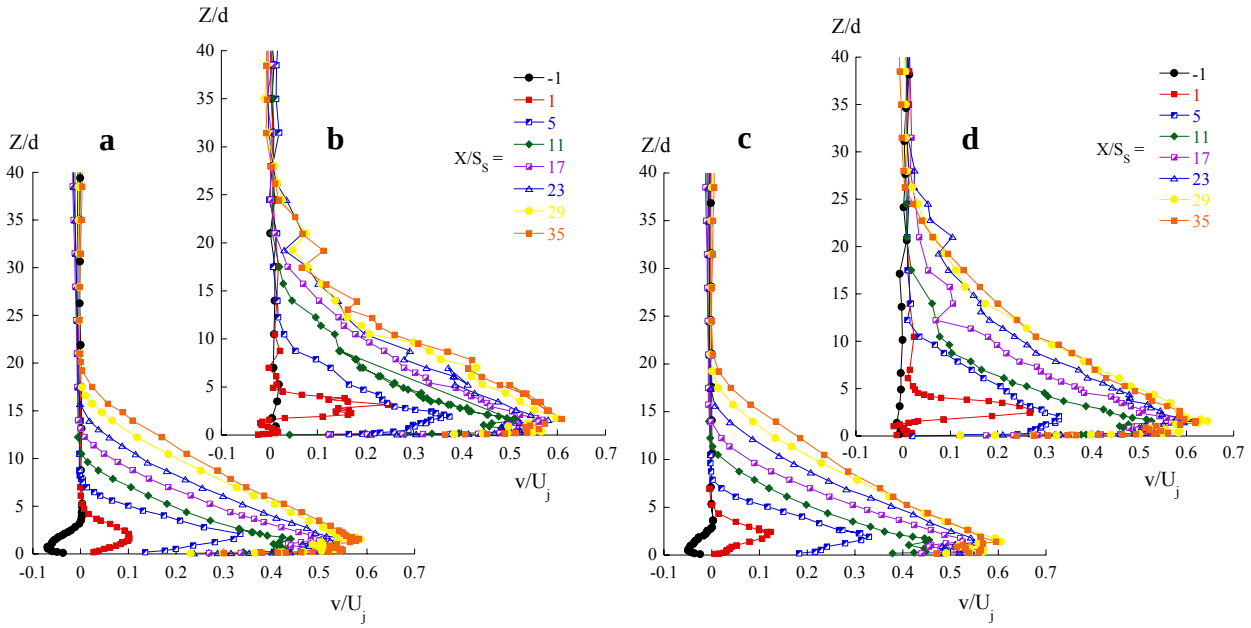

Figure 5.13. Profiles of the pitchwise velocity for Re_j = 3199 (a) with crossflow and (b) without crossflow and Re_j = 4088 (c) with crossflow and (d) without crossflow.

It is interesting to note that without crossflow the height of the coolant layer stopped developing after X/S_S = 23 which contrasts to the nearly linear increase of the cooling layer height at all streamwise locations for film cooling with crossflow. This difference was attributed to the ability of the crossflow to induce the coolant to flow streamwise. Without the influence of the crossflow the height of the coolant layer only depended on the number of upstream cooling holes along the compound angle coordinate. It should be noted that the flow angle is not a reliable indicator of the penetration height of the coolant layer without crossflow because the flow was directed at φ = 45° at almost all locations in the flow field because there was no crossflow forcing the coolant to flow streamwise.

The pitchwise velocities normalized to the velocities of the film cooling jets are shown in Figure 5.13. The maximum pitchwise velocity at X/S_S = 35 for all of the flow cases shown in Figure 5.13 was approximately v/U_j = 0.60. The maximum pitchwise velocities at each streamwise location were similar for all of the cases with and without crossflow. The maximum pitchwise velocities at X/S_S = 1, however, are not comparable between the cases with and without crossflow. This is because the crossflow influenced the coolant to flow in the streamwise direction which reduced the pitchwise velocity.

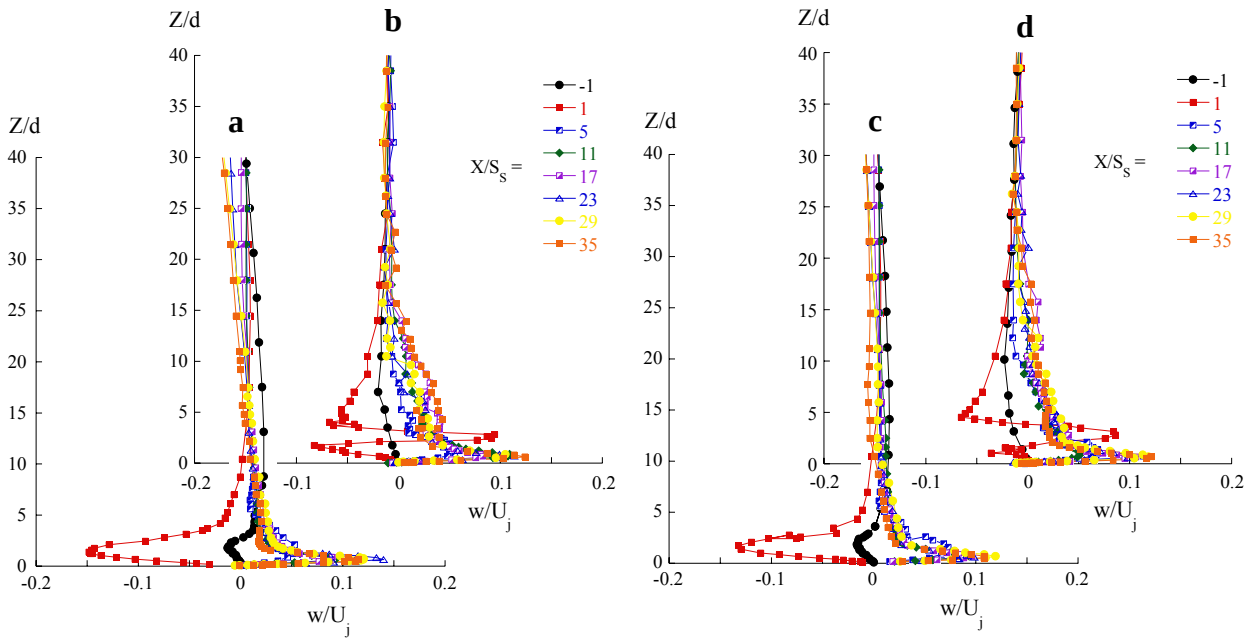

Figure 5.14. Profiles of the spanwise velocity for Re_j = 3199 (a) with crossflow and (b) without crossflow and for Re_j = 4088 (c) with crossflow and (d) without crossflow.

The spanwise velocities at the film cooling flows of Re_j = 3199 and 4088 were also very similar as shown in Figure 5.14. Similar to the measurements with crossflow, there was a negative spanwise velocity due to flow entrainment. However, unlike the measurements with crossflow, the coolant injection without crossflow showed a positive spanwise velocity at X/S_S = 1 (at Z/d = 3) that is due to injection from the first row of jets (the measurement location is aligned with the centerline of the upstream hole). The high spanwise velocity was not present for cases with crossflow because the jets in the first row were bent toward the streamwise direction by the crossflow, and the jets eluded the measurement location as a result. Without crossflow, the jets are unaffected by external flow and their compound angle is preserved in the trajectory of the jet.

There are subtle differences between the turbulence level trends in the flow field with and without crossflow. The turbulence levels along the test plate with and without crossflow are shown in Figure 5.15. Note that the turbulence levels were normalized to the cooling jet velocity. It was found that the turbulence level was higher without crossflow at all locations in the film layer at all streamwise positions except X/S_S = -1. Increased turbulence without crossflow was observed further from the liner surface because the crossflow dampened the

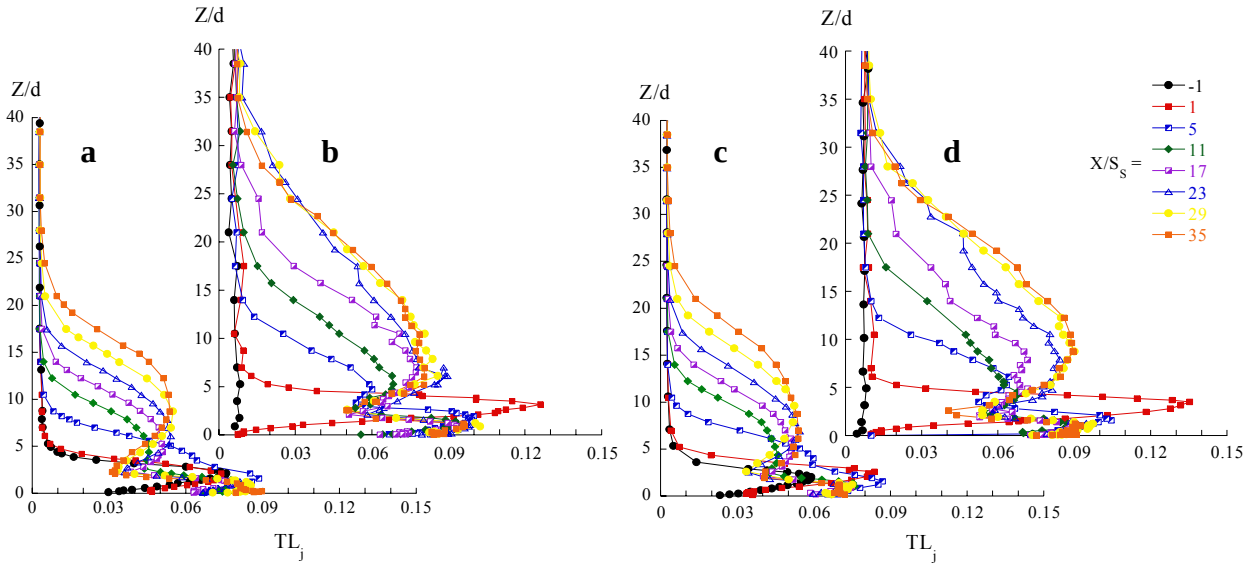

Figure 5.15. Turbulence level profiles (normalized to U_j) of Re_j = 3199 (a) with crossflow and (b) without crossflow and Re_j = 4088 (c) with crossflow and (d) without crossflow.

velocity fluctuations and constrained the coolant injectant to a smaller region. The higher Reynolds number injection of Re_j = 4088 compared to 3199 resulted in a 7% higher peak turbulence level at X/S_S = 1 and an 11% higher turbulence level in the outer coolant region at X/S_S = 35, which was not proportional to the nearly 28% increase in Reynolds number.

It is interesting to note that for all cases and crossflow conditions the turbulence level does not have an additive nature in the jet core, meaning that the turbulence does not increase with additional jet rows. This trend is in contrast to the increase of turbulence with streamwise distance in the region above the jet core, which is a trend also observed for the streamwise velocity. The highest turbulence levels without crossflow were TL_j = 12.6% and 13.5% for Re_j = 3199 and 4088, respectively, and were reached at X/S_S = 1. The absence of crossflow increased the turbulence at that location because the larger velocity gradient between the quiescent flow and coolant jets generated higher turbulence.

Thermal Field Results

Temperature profiles were measured to compare how the momentum flux ratio of the injectant influenced the development of the temperature characteristics of the coolant layer. Temperature profiles were measured at the same locations on the liner surface as the velocity measurements for I = 1.0 and 25.1 and are shown in Figure 5.16. The temperature measurements

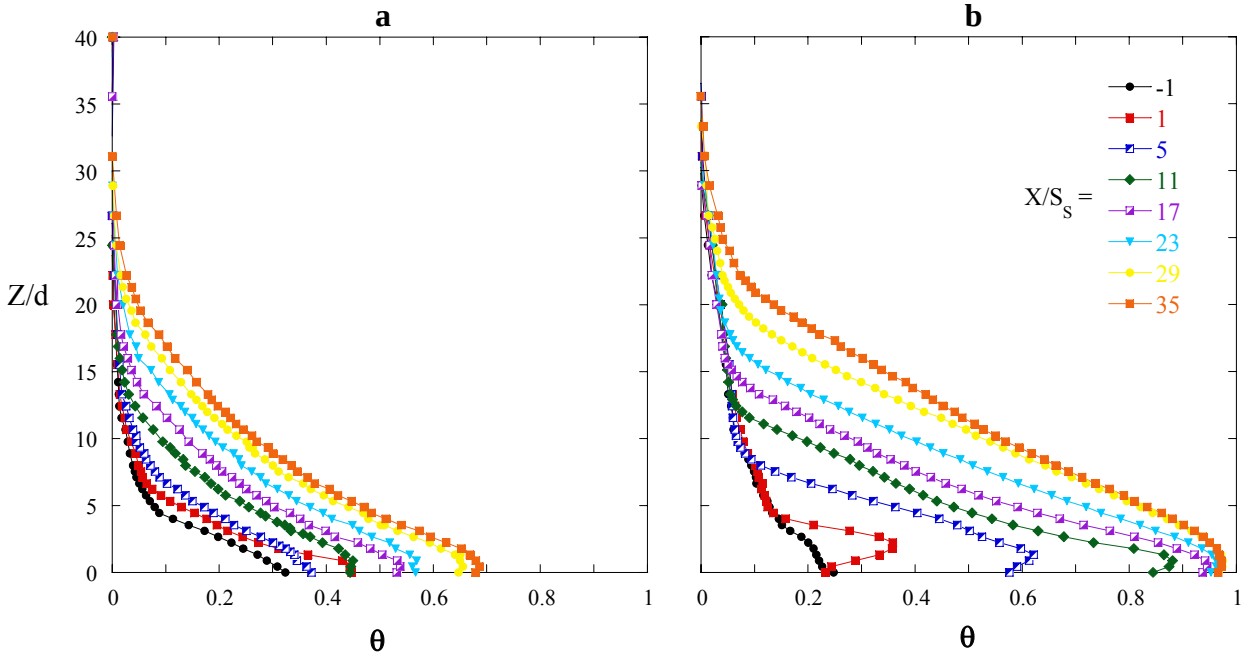

Figure 5.16. Profiles of the non-dimensional temperature, θ, with crossflow for a) I = 1.0 and b) I = 25.1.

were non-dimensionalized as θ to the mainstream air temperature and coolant temperature.

It should be noted that there a temperature profile developed upstream of the film cooling liner with a lower temperature at the liner surface than at mid-span. The freestream temperature that was used to calculate the non-dimensional temperature was measured at Z/H = 0.5 resulting in a non-zero wall temperature at X/S_S = -1. There was a lower non-dimensional surface temperature at I = 25.1 (Figure 5.16b) because film cooling injected at I = 25.1 separated and produced an increased flow rate of hot freestream air toward the wall (see Figure 5.9c).

The surface temperature at each row of holes and the penetration height based on the temperature were different for each coolant flow rate. Film cooling injected at I = 1.0 resulted in a relatively uniform incremental increase of θ at the surface as a function of streamwise distance, with a penetration height of Z/d = 23.7 at X/S_S = 29. The penetration height based on the non-dimensional temperature increased an average of two hole diameters per row (2 d/S_S) for I = 1.0. The progression of the surface temperature for I = 25.1 was more non-linear and decreased much more rapidly for the first eleven rows. However, the surface temperature at X/S_S = 17 was θ = 0.94 and remained within 3% of that value for the remainder of the liner. The penetration height of the coolant reached Z/d = 26.7 at X/S_S = 29 for I = 25.1. The penetration height of the coolant increased at a similar linear rate when based on both the temperature field and the velocity field.

The temperature penetration height was higher than the velocity penetration height by about ten cooling hole diameters at both I = 1.0 and 25.1.

Conclusions

The velocity and thermal fields produced by a compound angle effusion film cooling liner were studied. The penetration height of the coolant as well as the surface temperature development in the streamwise direction was of interest. The details of the velocity and thermal fields were analyzed at incremental streamwise locations among the thirty five rows of coolant injection on the test plate.

It was found that the presence of crossflow affected the discharge coefficients of the effusion holes in a certain range of absolute coolant pressure ratios. The jet was influenced by changes in the hole breakout plane pressure distribution with crossflow that lead to favorable changes to the jet flow. However, jets with a low momentum flux ratio created an exit plane pressure distribution that negated any positive effect of the crossflow on the discharge coefficients.

The development of the local momentum flux ratio was analyzed based on surface static pressure measurements as well as a calculation of the mass-averaged velocity at each row. In the presence of crossflow, it was found that the static pressure variations created by mainstream flow separation due to the contraction caused a reduction of the film cooling momentum flux ratio. Jet injection into quiescent air resulted in a constant streamwise film cooling Reynolds number because it removed the effect that the contraction had on the pressure variation.

Since the holes were oriented laterally at 45°, the determination of the pitchwise region where the flow was uniform and was free from side-wall influence was found to be centered at Y/W = 0.3. A factor affecting the uniformity was the pitchwise variation of the number of jets that were upstream along the compound angle coordinate ($\beta = 45°$).

Measurements of the velocity and thermal fields indicate that the coolant layer grew linearly along the streamwise coordinate, in agreement with the linear nature of the coolant mass addition. The velocity field created by I = 1.0 injection was the exception because it did not produce streamwise flow acceleration above the jet core. However, the turbulent fluctuations did propagate into the crossflow to a height similar to that observed at I = 15.3 and 25.1.

It was found that jet injection without crossflow resulted in higher penetration heights than injection with crossflow. The inertia of the crossflow prevented the coolant from growing

unrestrained. Also, film cooling injection without crossflow had an increased velocity gradient and intensified shear between the coolant and the mainstream resulting in higher turbulence. The turbulence levels were higher without crossflow than with crossflow at all locations in the flow field. The increased turbulence without crossflow promoted turbulent mixing and coolant diffusion into the quiescent air.

The coolant layer penetration heights based on the temperature measurements were similar for the two cases tested, I = 1.0 and 25.1, and were found to increase an average of two hole diameters per row. The temperature profiles were nearly linear from lowest temperature near the surface to the highest temperature in the freestream. The surface temperature decreased in the streamwise direction due to the coolant injection. The decrease was linear for the low coolant flow and asymptotic for the higher coolant flow. Coolant injected at I = 25.1 was much more effective at cooling the surface than I = 1.0.

Acknowledgements

The authors gratefully acknowledge United Technologies – Pratt & Whitney for their support of this work.

Nomenclature

C_d	discharge coefficient
d	film cooling hole diameter
H	test section height
I	momentum flux ratio, $I = \rho_j U_j^2 / \rho_\infty U_\infty^2$
k	thermal conductivity
L	film cooling hole length
M	mass flux ratio, $M = \rho_j U_j / \rho_\infty U_\infty$
N	number of cooling holes
Re	Reynolds number, $Re = Ud/\nu$
S_s, S_p	streamwise, pitchwise film cooling hole spacing
t	test plate wall thickness
T	temperature

TL_∞	turbulence level, $TL = \sqrt{0.33\left((u_{rms}^2 + v_{rms}^2 + w_{rms}^2)\right)}\Big/U_{\infty,local}$
TL_j	turbulence level, $TL = \sqrt{0.33\left((u_{rms}^2 + v_{rms}^2 + w_{rms}^2)\right)}\Big/U_{jet}$
u, v, w	local, mean velocity components corresponding to X, Y, Z
X, Y, Z	streamwise, pitchwise, and spanwise coordinates, respectively
W	test section width

Greek

α	surface inclination angle of cooling holes
β	compound angle of cooling holes
ρ	density
φ	XY-plane flow angle, $\varphi = \tan^{-1}(v/u)$
σ	statistical standard deviation
θ	$\theta = (T_\infty - T)/(T_\infty - T_c)$
ν	kinematic viscosity

Subscripts

c	plenum coolant conditions (secondary flow)
exit	test section exit conditions
j	film cooling jets, normalized to jet velocity
inlet	test section inlet conditions
local	local conditions (same streamwise position)
0	stagnation pressure
p	pitchwise direction
rms	root mean square of fluctuating velocity
s	static pressure at test plate surface, streamwise direction
∞	mainstream (primary) flow, normalized to mainstream flow velocity

References

[1] Scrittore, J. J., Thole, K. A., Burd, S. W., 2007, “Investigation of Velocity Profiles for Effusion Cooling of a Combustor Liner,” *Journal of Turbomachinery*, vol. 129, pp. 518-526.

[2] Honami, S., Shizawa, T., and Uchiyama, A., 1994, “Behavior of the Laterally Injected Jet in Film Cooling: Measurements of Surface Temperature and Velocity/Temperature Field Within the Jet,” *Journal of Turbomachinery*, vol. 116, pp. 106-112.

[3] McGovern, K. T., Leylek, J. H., 2000, “A Detailed Analysis of Film Cooling Physics: Part II – Compound-Angle Injection with Cylindrical Holes,” *Journal of Turbomachinery*, vol. 122, pp. 113-121.

[4] Lee, S., Kim, Y., and Lee, J., 1997, “Flow Characteristics and Aerodynamic Losses of Film-Cooling Jets with Compound Angle Orientations,” *Journal of Turbomachinery*, vol. 119, pp. 310-319.

[5] Schmidt, D. L., Sen, B., and Bogard, D. G., 1996, "Film Cooling With Compound Angle Holes: Adiabatic Effectiveness," *Journal of Turbomachinery*, vol. 118, pp. 807-813.

[6] Sen, B., Schmidt, D. L., and Bogard, D. G., 1996, "Film Cooling With Compound Angle Holes: Heat Transfer," *Journal of Turbomachinery*, vol. 118, pp. 800-806.

[7] Ligrani, P. M. and Mitchell, S. W., 1994, “Interactions Between Embedded Vortices and Injectant from Film Cooling Holes with Compound Angle Orientations in a Turbulent Boundary Layer,” *Journal of Turbomachinery*, vol. 116, pp. 80-91.

[8] Ligrani, P. M., Ciriello, S., and Bishop, D. T., 1992, “Heat Transfer, Adiabatic Effectiveness, and Injectant Distributions Downstream of a Single Row and Two Staggered Rows of Compound Angle Film-Cooling Holes,” *Journal of Turbomachinery*, vol. 114, pp. 687-700.

[9] Crabb, D., Durao, D. F. G, and Whitelaw, J. H., 1981, "A Round Hole Normal to a Crossflow," *Trans. ASME*, vol. 103, pp. 142-153.

[10] Thole, K. A., Gritsch, M., Schulz, A., and Wittig, S., 1997, "Effect of a Crossflow at the Entrance to a Film-Cooling Hole," *Journal of Fluids Engineering*, vol. 119, pp. 553-541.

[11] Burd, S. W. and Simon, T. W., 1999, "Measurement of Discharge Coefficients in Film Cooling," *Journal of Turbomachinery*, vol. 121, pp. 243-248.

[12] Burd, S. W. and Simon, T. W., 1997, "The Influence of Coolant Supply Geometry on Film Coolant Exit Flow and Surface Adiabatic Effectiveness," ASME Paper No. 97-GT-25.

[13] Walters, D. K. and Leylek, J. H., 2000, "A Detailed Analysis of Film-Cooling Physics: Part 1 – Streamwise Injection With Cylindrical Holes," *Journal of Turbomachinery*, vol. 122, pp. 102-112.

[14] Rowbury, D. A., Oldfield, M. L. G, and Lock, G. D., 2001, "Large-Scale Testing to Validate the Influence of External Crossflow on the Discharge Coefficients of Film Cooling Holes," *Journal of Turbomachinery*, vol. 123, pp. 593-600.

[15] Vakil, S. and Thole, K. A., 2005, "Flow and Thermal Field Measurements in a Combustor Simulator Relevant to a Gas Turbine Aero-Engine," *Journal of Engineering for Gas Turbines and Power*, vol. 127, pp. 1-11.

[16] Moffat, J. R., 1988, "Describing the Uncertainties in Experimental Results," *Experimental Thermal and Fluid Science*, vol. 1, pp. 3-17.

Summary and Recommendations for Future Work

This research evaluated the influence that dilution jets have on the film cooling effectiveness and how the flow and thermal fields in a combustor are affected by both the dilution flow and the closely spaced film cooling holes. Three papers captured the effects of the dilution jet injection, while two papers involved only film cooling injection. The dilution jet results were split into surface cooling effectiveness measurements, discussed in the first paper, far-dilution flow and thermal field measurements discussed in the second paper, and a near-dilution study on the effect of film cooling on the complex flow field produced by dilution injection discussed in the third paper. The fourth and fifth papers characterized the flow fields produced by streamwise injected and compound angle effusion film cooling, respectively.

The first paper presented high resolution measurements of the adiabatic cooling effectiveness on the combustor liner as it was affected by the dilution and film cooling air injection. Increasing dilution jet velocity had a negative effect on the surface cooling effectiveness downstream of the dilution jet injection. This was because the coolant layer was disrupted more by the higher speed jets and entrained off the surface. Surface cooling effectiveness measurements along with thermal field measurements indicated the presence of warm fluid between the distinct film cooling jets upstream of the dilution holes. Downstream of the dilution holes, the turbulence levels were quite high resulting in good spreading of the film cooling jets. For the same film cooling flows, lower momentum dilution jet injection resulted in better surface cooling in the near-dilution region due to the additional cooling resulting from the interaction of the dilution jets with the combustor liner. The film cooling fluid stagnated as it approached the dilution jets and was convected around the jets resulting in high streamwise velocities adjacent to the dilution jets. Localized turbulent regions were generated in the shear layer between the crossflow and dilution jets that partially extended into the jet cores.

The second paper sought to capture the effect of several parameters on the far-dilution flow and thermal fields. These parameters included the dilution and film cooling injection velocities and the angle and diameter of the film cooling hole. Film cooling holes inclined at 20˚ generated lower turbulence than 30˚ cooling holes. This desirable characteristic was an outcome of the shallower cooling holes, as they resulted in less entrainment of the crossflow into the jet wake. The penetration height of the coolant was found to be insensitive to the angle and diameter of the

cooling hole in the region downstream of the dilution jets and was found to be about two cooling hole diameters based on the Reynolds shear stress magnitude. Velocity measurements showed that there was a significant negative Reynolds shear stress component in the bottom film cooling jet shear layer created by 30˚ holes. This was attributed to jet lift-off and entrainment of lower speed flow in the wake region. This phenomenon was not created by 20˚ holes, where only positive Reynolds stress values were observed, indicating that the jet core was diffusing which led to an overall reduction in shear stress. Based on the thermal profiles, liner 2 also resulted in the best surface cooling at all dilution and film cooling flows and at all locations.

The third paper studied how the complex flow field produced by the dilution jet injection was affected by the presence of effusion film cooling flow. The flow field produced by the staggered opposed dilution jets was found to be significantly altered by the injection of effusion film cooling flow. When the high momentum dilution jets are injected into the crossflow, a localized region in the flow of high vorticity and velocity was created. When film cooling air was injected the inlet flow field and the wake were fundamentally changed and the vortex diminished significantly. The temperature field downstream of the dilution jet showed evidence of a hot region which was moderated appreciably by film cooling flow, but variation of the film cooling momentum flux ratio from 12 to 25 had a nominal effect on the thermal field compared to the large coolant mass flow increase. There was also a significant increase in surface cooling effectiveness due to the addition of the film coolant.

The fourth paper discussed the streamwise progression of the flow field produced by streamwise aligned injection of effusion film cooling. The effusion cooling developed into a fully-developed velocity profile after fifteen film cooling hole rows. The cooling jet penetration was much higher for the first few rows of cooling holes than the downstream jets. The penetration height of the cooling jets was independent of the momentum flux ratio and the streamwise velocity and turbulence level profiles were found to scale with the blowing ratio. This scaling effect was valid at all measurement locations and all tested blowing ratios allowing the profile shape and magnitude to be readily determined for these ranges. Jet separation at the hole trailing edge was measured as well as the commonly reported counter-rotating vortex which entrained hot mainstream flow toward the surface at the plate leading edge. Downstream, however, this effect served to mix the accumulated coolant flow and provide a more uniform surface temperature.

The fifth and final paper presented the streamwise progression of the flow and thermal fields produced by compound angle injection of effusion film cooling. This paper offered a supplement to the data presented in the fourth paper. There were significant differences between the flow field created with and without crossflow. For the cases with crossflow, the penetration of the turbulence was found to be relatively independent of the film cooling momentum flux ratio. It was found from the angle of the flow field velocity vectors that the cooling film layer grew nearly linearly in the streamwise direction. The turbulence levels without crossflow were found to be higher than the turbulence levels with crossflow because there was a larger shear stress due to a larger velocity difference between the coolant and crossflow. The film cooling penetration heights based on the temperature and velocity measurements were similar for all film cooling momentum flux ratios.

Recommendations for Future Work

Although this study offered a thorough examination of the effects of dilution and film cooling flow in the gas turbine combustor, there is still a significant amount of work that could be done to better understand the implications for the flow behavior and surface cooling. Further studies on many aspects of this research are possible such as quantification of the heat transfer as a result of the complex flow field created by the dilution and film cooling injection.

Heat transfer measurements in the near-dilution jet region would be a beneficial extension of this research because the net heat flux benefit or detriment due to flow features (such as the film cooling and dilution jets) must include knowledge of how the heat transfer coefficient is affected. Measurement of the surface heat transfer coefficient would allow for calculation of the Net Heat Flux Reduction (NHFR) which would account for changes in both the adiabatic cooling effectiveness and the heat transfer coefficient.

Highly resolved flow and temperature measurements were captured at deliberately chosen planes in the flow field in this research program. A possible improvement on this measurement scheme would be to use a spatially comprehensive measurement method to be able to gain a more global understanding of how the entire flow field is behaving. An interesting research avenue would be time-resolved measurements of the flow field created by the dilution jet injection into crossflow.